

Investigations of Cross Section Model and Near Detector Choices

Jake Calcutt¹, Joshua Hignight¹, and Kendall Mahn¹

¹Michigan State University

1 Overview

The Deep Underground Neutrino Experiment (DUNE) is a next-generation Long Baseline neutrino experiment designed to search for CP violation and establish the mass hierarchy. It consists of both a Near and Far Detector separated by 1300km and uses a neutrino beam created at Fermilab.[1]. While the design of the Liquid Argon Far Detector has been finalized, there is still ongoing effort in deciding the configuration of the Near Detector. The main near detector design includes a Fine-Grained Tracker (FGT) with possible inclusion of additional detectors. Under consideration are a Liquid (LArTPC) or High Pressure Gaseous Argon TPC (GArTPC). DUNE's physics goals require systematic uncertainties in the interaction model to be below the 2% limit after a near-to-far extrapolation[2]. The focus of this document is to quantify how the neutrino interaction model could affect DUNE's goals. This work was done concurrent with the DUNE ND Taskforce (NDTF), and so the studies investigate possible weaknesses and limitations of the current parameterization of neutrino interaction uncertainties. The studies also explore how different interaction models - used as proxies for variations in a given model - couple to the different NDs and the FD.

Below is a list of the studies we have conducted for this work.

- Choice of parameterization.
 - The sufficiency of a pure- Q^2 parameterization in a Near to Far extrapolation.
 - * Are variations in CCQE and 2p2h models covered in this parameterization?
 - Does the Q^2 parameterization ignore additional physics as represented as variations in q_0 - q_3 ?
- The different abilities of the 3 ND configurations to reconstruct the neutrino energy.

- Variations in neutron multiplicities and energy lost to neutrons.
 - * Do the detectors need to be sensitive to neutrons?
- How do different ND configurations couple to model differences in variations in proton & pion multiplicity and momentum.
- Difference from true neutrino energy.
 - * How do the above effects couple to reconstructed energy?

2 Methods

2.1 Monte Carlo Generators

Neutrino interaction modeling is of great interest to current and future oscillation experiments. Currently, there are a few different neutrino interaction software packages, referred to here as "generators". While it is not guaranteed that the physics of nature corresponds to any of these software packages, the different choices made by the generators can act as a proxy for possible variations in the neutrino interaction model. The models considered span a range of different 'vertex-level' interaction models (e.g. CCQE, 2p2h, Resonant) and Final State Interaction (FSI) models. These are given in Table 1

2.2 Generating Events

Sets of ν and $\bar{\nu}$ events with an Argon-40 target are produced with these generators according to the 2015 DUNE CDR fluxes, shown in Figure 1 for ν_μ at the ND and FD. The oscillation parameters used for the FD fluxes are included in Table 2. Note that the ν_μ and $\bar{\nu}_\mu$ flux correspond to the Forward and Reverse Horn Current (FHC and RHC) modes respectively. No 'wrong-sign' studies, where the $\bar{\nu}_\mu$ flux is that within the primary ν_μ beam, are considered in this work. The various data sets are then passed through the NUISANCE[6] software to reduce the outputs to a common format, in turn saving all final state particle information for each event.

Generator	Version	Model
GENIE[3]	2.10	RFG
NEUT[4]	5.3.6	Nieves et. al RPA+2p2h/MEC ($M_A = 1.01$)
NuWro[5]	11	LFG + RPA + Nieves et. al

Table 1: The various Monte Carlo event generators used for this work.

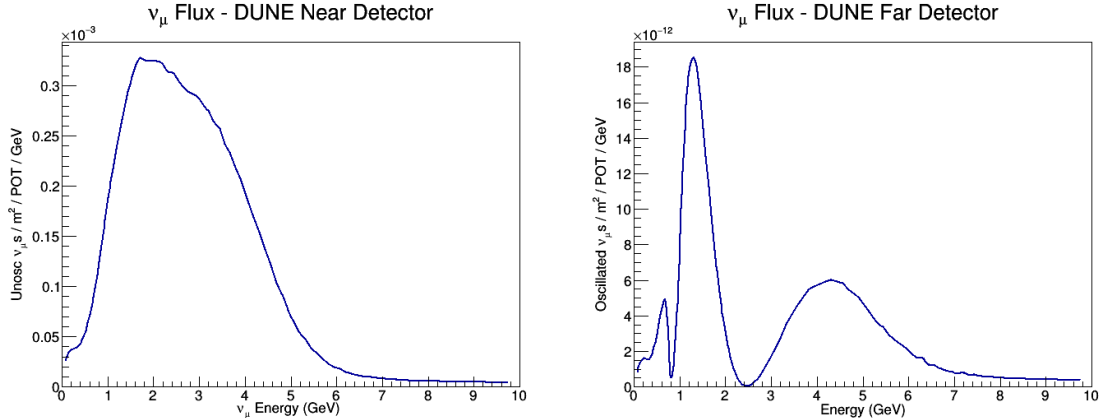


Figure 1: ν_μ flux at DUNE ND (Left) and FD (Right)

Parameter	Central Value	Relative Uncertainty
θ_{12}	0.5843	2.3%
θ_{23} (NH)	0.738	5.9%
θ_{23} (IH)	0.864	4.9%
θ_{13}	0.148	2.5%
Δm_{21}^2	$7.5 \times 10^{-5} \text{ eV}^2$	2.4%
Δm_{31}^2 (NH)	$2.457 \times 10^{-3} \text{ eV}^2$	2.0%
Δm_{31}^2 (IH)	$-2.449 \times 10^{-3} \text{ eV}^2$	1.9%

Table 2: The various Monte Carlo event generators used for this work.

2.3 How We Study a Near to Far Extrapolation

The various studies regarding near to far extrapolations are explored using the following procedure. Ratios of either NEUT or NuWro to GENIE - referred to as 'single ratios' - separately at the ND and FD are taken. NEUT and NuWro are both normalized to GENIE to highlight shape differences rather than overall normalization effects. These offer insight into model variations in and how the dependence of ND configuration couple to these variations. The effect of a near to far extrapolation is approximated by taking a 'double ratio' between the near and far single ratios. To be explicit, these are defined in Equations 1 and 2, where 'Other MC' refers to either NEUT or NuWro and 'Near' can be replaced by 'Far' in the single ratio. We note this is a crude approximation to give intuition about the problem for just a single reaction process; a fit to the ND spectrum will have multiple reactions in a given topology which can complicate the determination of physics effects for a single reaction.

$$\text{ND Single Ratio} = \frac{(\text{Other MC} @ \text{Near Detector})}{(\text{GENIE} @ \text{Near Detector})} \quad (1)$$

$$\text{Double Ratio} = \frac{(\text{ND Single Ratio})}{(\text{FD Single Ratio})} \quad (2)$$

2.4 Detector Configurations and Efficiencies

These studies highlight the effect of the different efficiencies of the various detectors. We first consider a 'perfect' ND and FD without any efficiencies applied, and then look what changes as we consider the 3 different configurations of the ND and a simple LAr efficiency in the FD.

Efficiency information is included with the following procedure. Each particle is randomly accepted or rejected by throwing a random number and checking against the efficiency according to the particle's momentum. No angular efficiencies have yet been taken into account for this work. At time of this writing, only a full description of the FGT efficiency according to NDTF samples is available, but other configurations will be added to subsequent versions of this note. An example of the efficiency for protons in the FGT is given in Figure 2, FGT efficiencies for other particles are included in Appendix ???. We also lack knowledge of the efficiencies for π^0 in the FGT, so we accept all of these in this configuration. Because we do not have the efficiency's for the LAr and GAr, simple thresholds for protons are applied for the GAr - 100 MeV/c - and LAr ND and FD - 200 MeV/c. We also make no assumptions for the efficiencies of μ , $\pi^{+,-}$, and π^0 in the simple descriptions, and so all of these types of particles are accepted in the LAr and GAr.

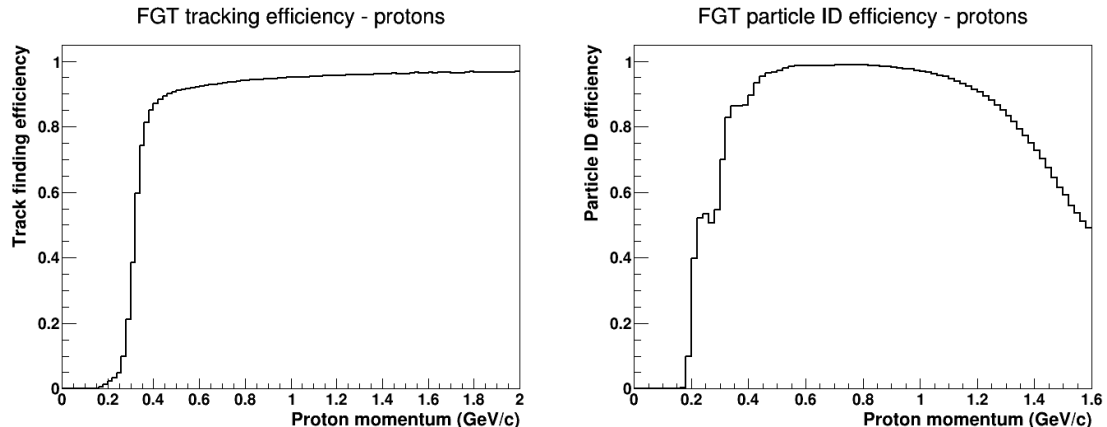


Figure 2: Left: Tracking efficiency for protons in FGT. Right: PID efficiency for protons in FGT. Total efficiency for a given proton momentum is given by the product of the two efficiencies.

3 Parameterization

The VALOR software package has been used on multiple T2K oscillation analyses, and has recently been used to study the DUNE near detector configurations. (((The group uses MC templates to map between reconstructed and true information for various reactions.))) Uncertainties in interaction models are parameterized by model variations as a function of Q^2 . Currently, Q^2 parameterizations are defined for neutrinos and antineutrinos as:

- CCQE ν_μ with Q^2 bins $\{0 - 0.20, 0.20 - 0.55, >0.55\}$ GeV 2
- CCQE $\bar{\nu}_\mu$ with Q^2 bins $\{0 - 0.20, 0.20 - 0.55, >0.55\}$ GeV 2
- 2p2h ν_μ with 1 Q^2 bin
- 2p2h $\bar{\nu}_\mu$ with 1 Q^2 bin

This portion of the work seeks to determine if variations in CCQE and 2p2h models are well represented by these parameterizations in Q^2 . It also serves to highlight the behavior of the models as they couple to FSI and detector effect as we use a reconstructed Q^2 when efficiencies are applied.

3.1 Q^2 Parameterization

The single and double ratio procedure described in Section 2.3 is conducted using events created by all three generators at the ND and FD and distributed according to Q^2 . This is done separately with and without efficiencies, for both ν_μ and $\bar{\nu}_\mu$, and for true-CCQE and true-2p2h. Applying efficiencies allows us to investigate how the interaction model can couple to detector effects. For distributions without efficiencies, the MC-level Q^2 quantity is used, giving us insight into the interaction model uncertainties. However, when including efficiencies, Q^2 becomes a reconstructed quantity, as it is calculated from the final state particles that are accepted after efficiencies are applied. This is highlighted in Equations 3 - 6. Though we call it 'reconstructed', it is calculated using the true energies and momentums without smearing applied, so it is not truly reconstructed in the usual sense of the word. Using this reconstructed quantity reveals how interaction/FSI variations, and detector effects couple together.

$$Q^2 = |q_0^2 - q_3^2|, \quad (3)$$

$$q_0^2 = (E_{reco} - E_{lep})^2, \quad (4)$$

$$q_3^2 = (\vec{P}_{reco} - \vec{P}_{lep})^2 \quad (5)$$

$$E_{reco} = E_{lep} + \Sigma E_\pi + \Sigma (E_{prot} - M_{prot}) \quad (6)$$

Conclusions are drawn from the double ratios according to the following prescription. We look for if the ratio is flat - i.e. if a horizontal line is within the statistical error bars - in a given bin of the parameterization. Flatness in that bin is a crude estimation for model-dependent shape uncertainties canceling out in a near-to-far extrapolation, and shows that a reweighting of that whole bin is sufficient to cover uncertainties. Again, we stress that this is a crude approximation to the near-to-far extrapolation.

For ν_μ CCQE events, both NEUT's and NuWro's models differ significantly from GENIE' model in Q^2 distributions, as seen in the single ratios in Figure 3. Despite this, the double ratios for both NEUT and NuWro to GENIE remain relatively flat and close to 1, with small amounts of variation in the higher Q^2 region.

For double ratios with FGT efficiencies applied to the ND and simple LAr efficiencies applied to the FD, shape variations are greater above 1.25 GeV^2 as seen in Figure 4. This suggests an additional bin in the region .55 to 1.25 GeV^2 should be included. These studies will be expanded in the future to increase statistics and determine the origin of the variation in this region, one possible source being the rejection of low-momentum muons after we apply efficiencies.

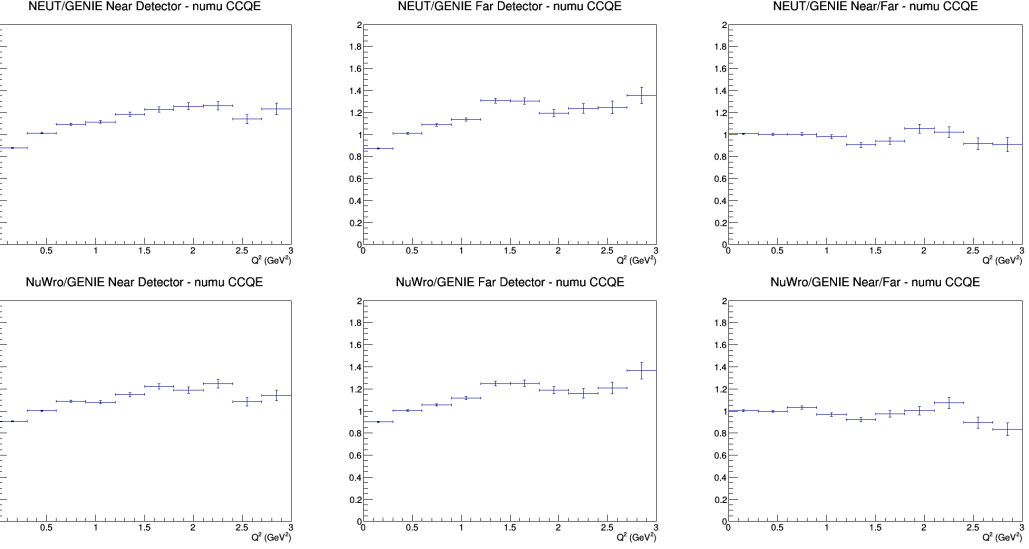


Figure 3: MC-level Q^2 distributed ν_μ events using DUNE flux, no efficiencies applied to ND or FD. Top: Ratios of NEUT to GENIE. Bottom: Ratios of NuWro to GENIE. Left to Right: Single ratio at ND, single ratio at FD, double ratio Near/Far. Of note is the relative flatness throughout the double ratio compared to the single ratio at the ND. Note that the VALOR binning is separated by lower bin edges of (0, 0.20, and 0.55) GeV^2

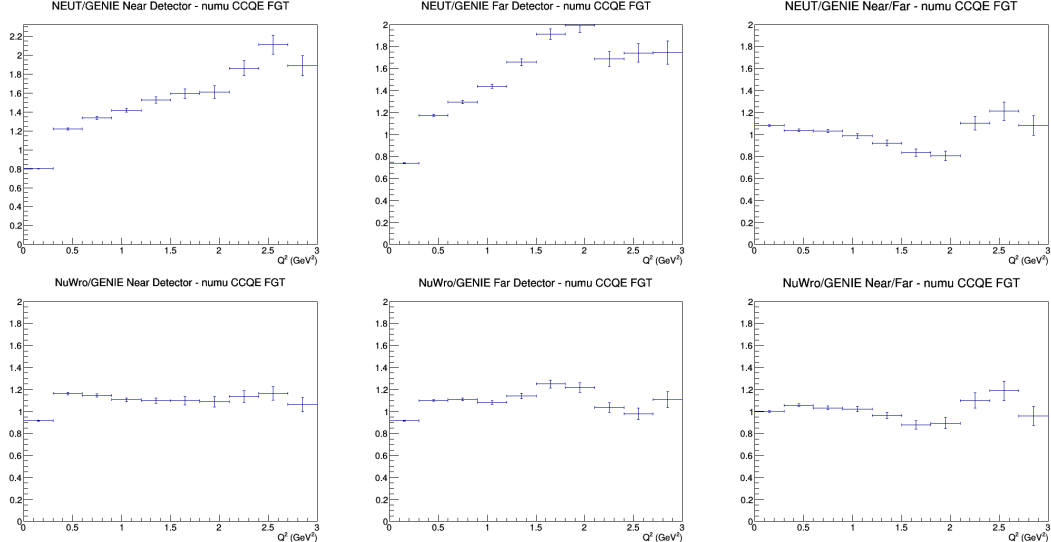


Figure 4: Reconstructed Q^2 distributed ν_μ events using DUNE flux, FGT efficiencies applied to ND and simple LAr efficiencies applied to FD. Top: Ratios of NEUT to GENIE. Bottom: Ratios of NuWro to GENIE. Left to Right: Single ratio at ND, single ratio at FD, double ratio Near/Far. More shape variations do arise above around 1.25 GeV^2 in the double ratios. This suggests another bin should encompass the region between $.55$ and 1.25 GeV^2 . Note that the current VALOR binning is separated by lower bin edges of $(0, 0.20, \text{ and } 0.55) \text{ GeV}^2$

However, for $\bar{\nu}_\mu$ CCQE events, we observe distortions in the Q^2 distribution even in the double ratios. This is true without efficiencies for both NEUT to GENIE and NuWro to GENIE ratios. This is displayed in Figure 5. The variations again arise above 1.5 GeV^2 for the double ratios, supporting the addition of a bin between $.55$ and 1.25 GeV^2 . This appears without efficiencies, and points to variations in the CCQE interaction model being responsible for this effect rather than FSI variations or detector effects.

We run into trouble extending the $\bar{\nu}_\mu$ CCQE study with efficiencies applied, as this leaves the high Q^2 region with very low statistics, preventing us from drawing any meaningful conclusions. These plots are included in Appendix A for completeness. The studies will be continued once we have higher statistics, and with more complete descriptions of the LAr and GAr as this information becomes available.

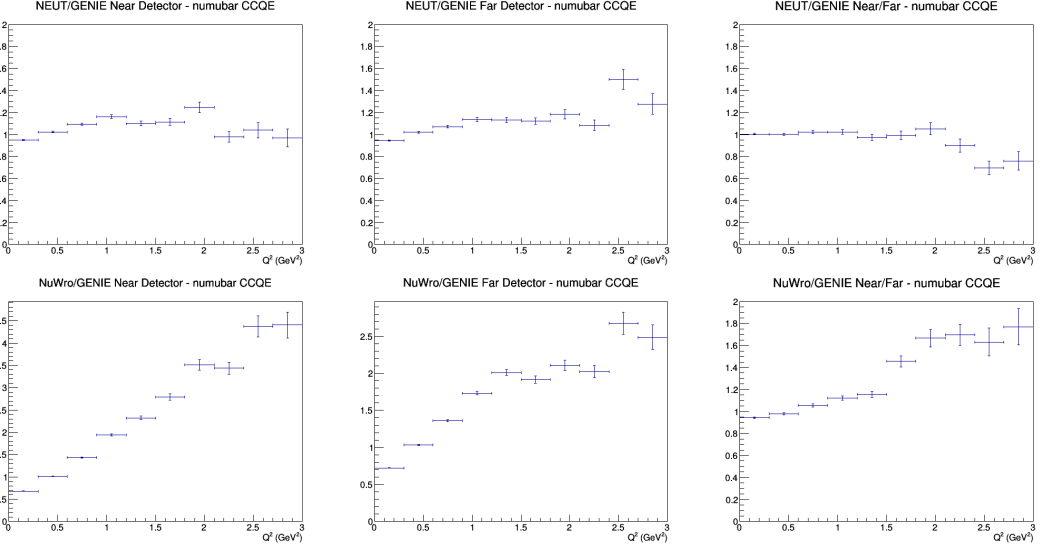


Figure 5: MC-level Q^2 distributed $\bar{\nu}_\mu$ CCQE events using DUNE flux. Top: Ratios of NEUT to GENIE. Bottom: Ratios of NuWro to GENIE. Left to Right: Single ratio at ND, single ratio at FD, double ratio Near/Far. Large amounts of variations in the region above 1.5 GeV^2 in both double ratios. This differs from ν_μ CCQE, where this arose in the ratios after efficiencies are added. Here, it exists without any efficiencies, pointing to variations in the CCQE model, rather than FSI or detector effects, not being covered by the parameterization. An additional bin between .55 and 1.25 GeV^2 is suggested. Note that the VALOR binning is separated by lower bin edges of $(0, 0.20, \text{ and } 0.55) \text{ GeV}^2$.

For 2p2h ν_μ and $\bar{\nu}_\mu$ events, the double ratios from both NEUT and NuWro remain centered close to or around 1 below about 1 GeV^2 without efficiencies applied, as seen in Figure 6 and 7. Above 1 GeV^2 , the statistics are again low. At this moment, the currently-proposed 1-bin normalization appears sufficient in the region below 1 GeV^2 . The low statistics prevent us from making conclusions in the high Q^2 region as well as drawing conclusions from applying efficiencies. These will be revisited in later iterations of this work.

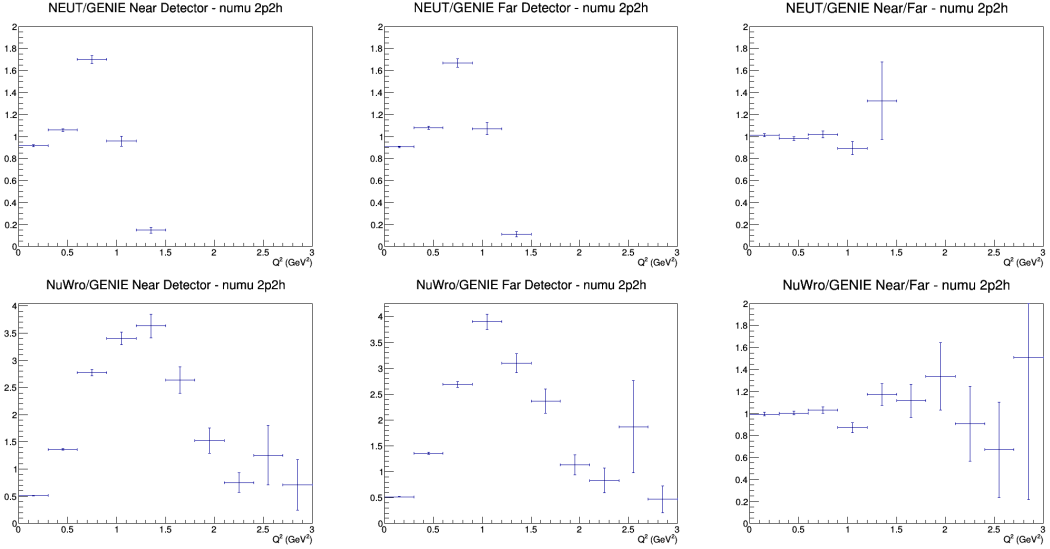


Figure 6: Q^2 distributed $\bar{\nu}_\mu$ 2p2h events using DUNE flux. Top: Ratios of NEUT to GENIE. Bottom: Ratios of NuWro to GENIE. Left to Right: Single ratio at ND, single ratio at FD, double ratio Near/Far. Large amounts of variations are present resulting from low statistics in the higher end of all distributions, but the lower end holds close to 1. Note that the VALOR binning is separated by lower bin edges of (0, 0.20, and 0.55) GeV^2 .

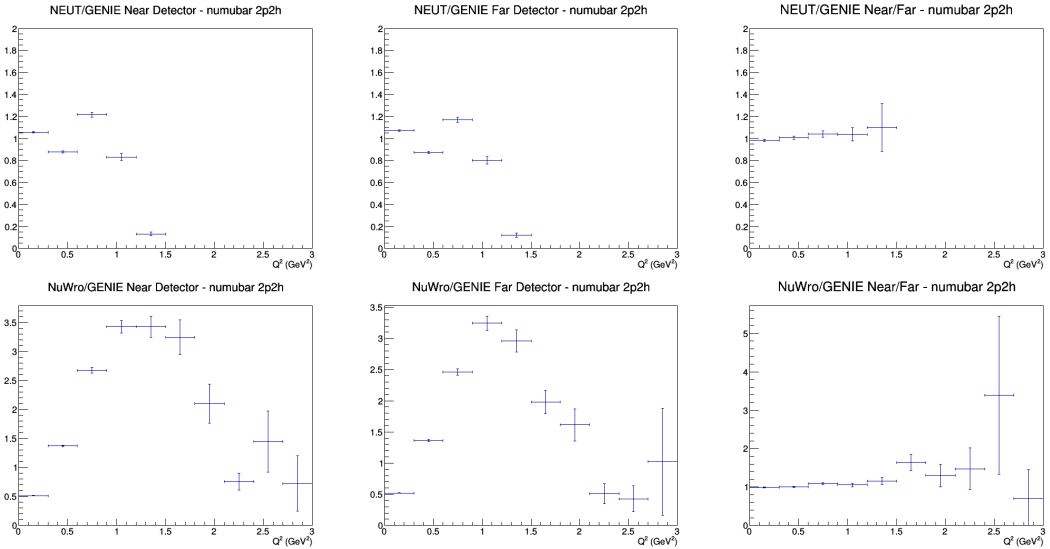


Figure 7: Q^2 distributed $\bar{\nu}_\mu$ 2p2h events using DUNE flux. Top: No efficiencies, Bottom: FGT efficiencies applied to ND, LAr efficiencies applied to FD. Left to right: NEUT to GENIE double ratio, NuWro to GENIE double ratio. Large amounts of deviations from 1 throughout distributions with efficiencies applied. Note that the VALOR binning is separated by lower bin edges of (0, 0.20, and 0.55) GeV^2 .

We currently find an additional bin in the region (.55, 1.25) will account for uncertainties in both ν_μ and $\bar{\nu}_\mu$ CCQE. For ν_μ and $\bar{\nu}_\mu$ 2p2h, the overall normalization currently appears sufficient from these studies. Investigations into the origin of the variation in the high Q^2 region of CCQE will be conducted as this work is furthered. Additional statistics and more complete efficiency descriptions for the LAr and GAr are required, and will be conducted at a later date.

3.2 q_0 vs. q_3 Variations

In addition to studying the Q^2 ratios, the ratios in $q_0 - q_3$ were also investigated to explore the possibility that variations arise when changing the parameterization from Q^2 to $q_0 - q_3$. The Q^2 parameterization assumes the variations are purely functions of Q^2 . Under this assumption, the double ratios should be flat in $q_0 - q_3$ regions corresponding to the Q^2 -binned parameterization. If this is not the case, a pure- Q^2 parameterization cannot sufficiently account for CCQE and 2p2h variations.

These studies were done in the exact same way as those in the previous section, only with the events and ratios distributed in $q_0 - q_3$ bins. Note: to be symmetric around 1, the scale extends from 0 to 2, but the variations in those bins can actually be greater than 2. Again, the quantities are MC-level truth information in the distributions without efficiencies, but are reconstructed in those with efficiencies applied, as described in Equations 3 - 6.

For ν_μ CCQE, the double ratios without efficiencies appear flat for both NEUT to GENIE and NuWro to GENIE double ratios, as seen in Figure 8. There is distortion in the upper right region, consistent with the high Q^2 regions in Figure 3. This binning proves to be a problem for creating reliable conclusions once efficiencies are applied, as statistics for each individual bin become quite low. These are included in Appendix ???. Higher statistics will be achieved for future work.

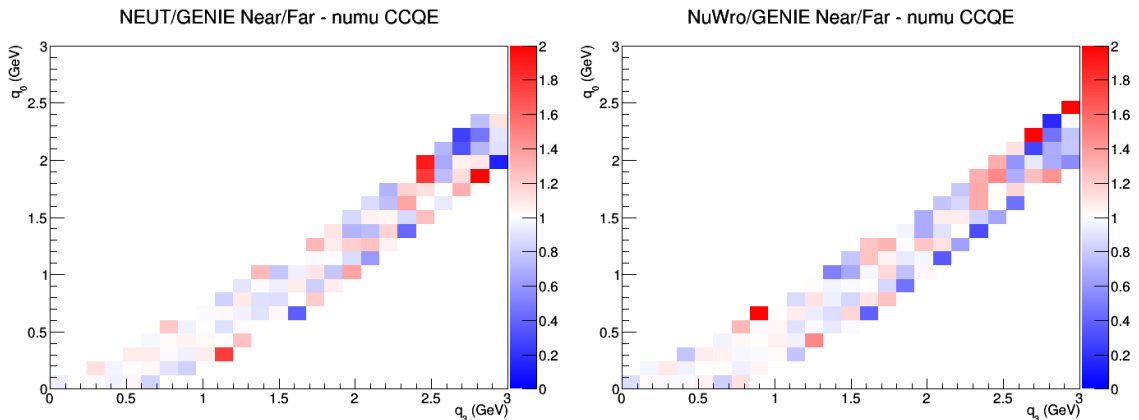


Figure 8: MC-level $q_0 - q_3$ distributed ν_μ CCQE events using DUNE flux without efficiencies applied. Left: Double ratio of NEUT to GENIE, Right: Double ratio of NuWro to GENIE. Relatively flat distributions, but with bin-to-bin variations arising from low statistics. Consistent with corresponding Q^2 ratios

For $\bar{\nu}_\mu$ CCQE, the large variations in the high Q^2 region are present in the

corresponding $q_0 - q_3$ region. As shown in Figure 9, the upper right region of both double ratios are consistent with the corresponding double ratios in Figure 5. Here again, the NuWro to GENIE double ratio is consistently higher in this region, while the NEUT to GENIE double ratio is slightly lower.

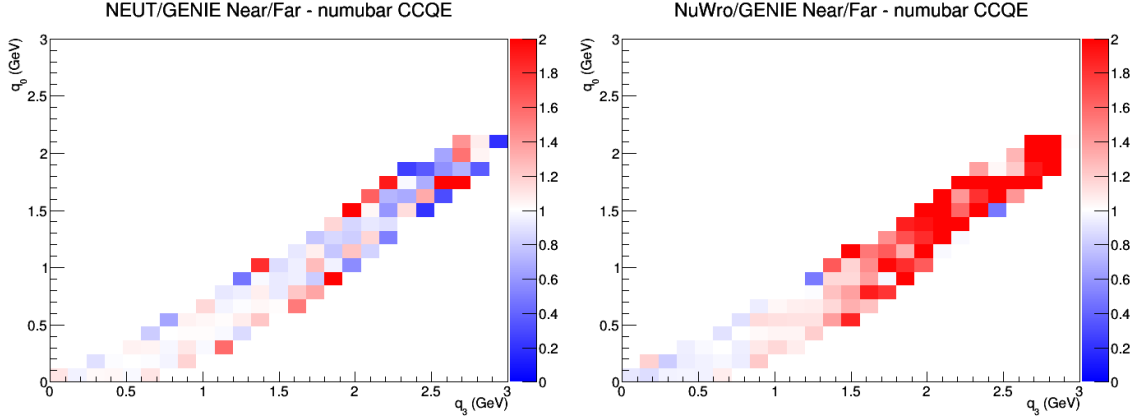


Figure 9: $q_0 - q_3$ distributed $\bar{\nu}_\mu$ CCQE events using DUNE flux without efficiencies applied. Left: Double ratio of NEUT to GENIE, Right: Double ratio of NuWro to GENIE. Variations in upper right region. Consistent with corresponding Q^2 ratios.

Each of the three generators have very different behavior for 2p2h ν_μ and $\bar{\nu}_\mu$ events with no efficiencies applied, as can be seen in Figure 10. This contains the raw event rate for 2p2h, and is shown to highlight the drastic shape difference. This causes very restricted phase space in the double ratios in $q_0 - q_3$, and so double ratios are not shown here - however they are included in B. The shape differences suggest that an overall binning in Q^2 cannot cover uncertainties, and reweighting events according to $q_0 - q_3$ shape should be used instead.

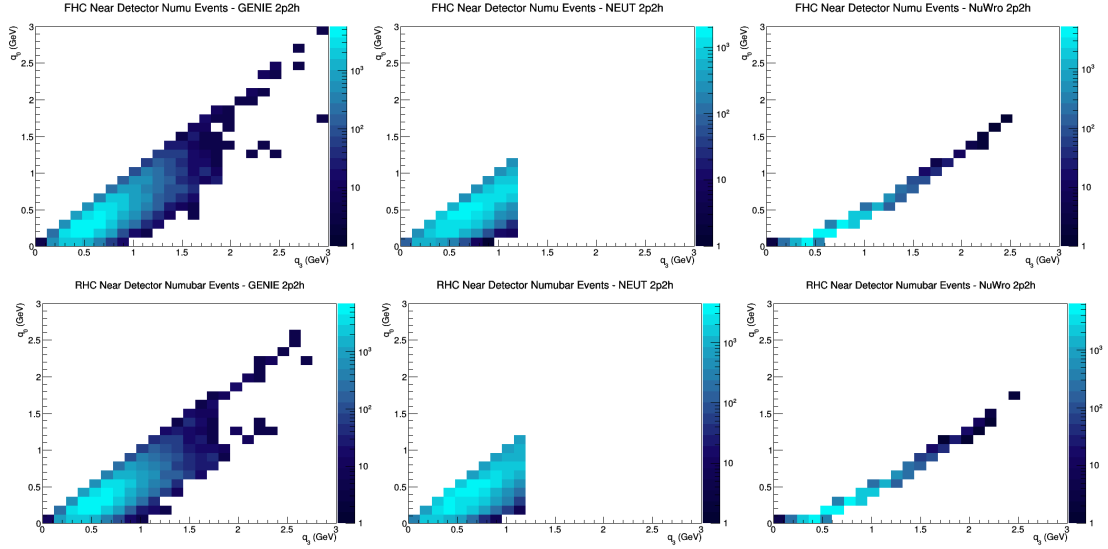


Figure 10: MC-level q_0 - q_3 distributed 2p2h events using DUNE flux with no efficiencies applied. Top: ν_μ events, Bottom: $\bar{\nu}_\mu$ events. Right to Left: GENIE events distribution, NEUT events distribution, NuWro events distribution. The phase spaces are very different without efficiencies, and restrict the coverage of the double ratios in q_0 - q_3 . Suggest use of 1 Q^2 bin to cover uncertainties.

3.3 Parameterization - Conclusions

It appears as though the pure- Q^2 parameterization and the binning developed by VALOR would cover model variations for ν_μ and $\bar{\nu}_\mu$ CCQE events, but slight modifications are suggested. The near-to-far extrapolation plots - the double ratios - appear relatively flat in the regions of the individual bins in the low Q^2 region. This changes above 1.25 GeV^2 , so placing another bin between 0.55 and 1.25 GeV^2 should suffice. The q_0 - q_3 double ratios are consistent with this conclusion. Future work will be focused on improving statistics and implementing full LAr and GAr efficiencies as that information becomes available, as well as investigating the origin of the high- Q^2 variations which possibly arise from proton or - more-likely - muon acceptance effects.

The low- Q^2 ν_μ and $\bar{\nu}_\mu$ 2p2h events appear to be covered by the current 1-bin parameterization when only looking at the Q^2 distribution. However, the shape differences in q_0 - q_3 show that a pure- Q^2 parameterization should not be used. Future work will continue with improving statistics, as well as implementing all efficiencies.

4 Reconstructed Energy

A framework for investigating variations in reconstructed energy calculations between different generators and ND configurations has been developed. Currently, the estimate for the incident neutrino energy is calculated by summing the total energy from final state leptons and pions (all charges) and the kinetic energy of final state

Generator & Interaction	$N_{neutron} > 3(\%)$	$E_{neutron} > 600MeV/c(\%)$ ND	FD	
			ND	FD
GENIE-CCQE	13	2	13	2
GENIE-2p2h	28	1	29	2
GENIE-CC1 π	17	21	18	25
GENIE-CCOther	24	17	24	19
NEUT-CCQE	1	0.8	1	0.7
NEUT-2p2h	8	4	8	4
NEUT-CC1 π	9	21	9	23
NEUT-CCOther	9	18	11	21
NuWro-CCQE	4	2	3	2
NuWro-2p2h	3	0.3	3	0.2
NuWro-CC1 π	30	22	34	27
NuWro-CCOther	33	20	38	26

Table 3: Percentage of events $N_{neutron} > 3$ and $E_{neutron} > 600MeV/c$, broken down by generator and event type. These cut offs were chosen to encompass most of the GENIE

protons after passing efficiencies through the data sets. All neutrons are assumed undetectable. This can be summed up in Equation 6: where E_{lep} is the energy of the outgoing lepton, E_π is the energy of the pion, and E_{prot} and M_{prot} are the energy and mass of the proton.

4.1 Neutron Multiplicities & Energy

Differences between models in the number of final state neutrons and the total energy into FS neutrons can largely affect reconstruction of neutrino energy. Large variations in reconstructed energy can arise due to missing energy caused by the inability to detect neutrons in the various models.

To investigate this, we have looked at GENIE, NEUT, and NUWRO to see if the different models showed a large difference in the neutron energy and multiplicity. This was done for CCQE-like, CC1 π , 2p2h, and everything else (“Other”) interactions and neutrinos as well as anti-neutrinos. In all cases, the generators agreed rather well with each other even though there were some differences in the neutron multiplicity. These differences account for a small fraction of the events, generally less than 10%, as can be seen in Table 3. Figure 11 shows an example of this for 2p2h neutrino events, while the other interaction modes can be found in Appendix C

Further more, the difference in the multiplicities between the generators becomes irrelevant after a ND to FD extraction, as can be seen in Figure 12. Here, the region where the most energy is lost agrees very well between the ND and FD for all generators and interaction types. The areas with low statistics do show a disagreement, but very few events fall into this area.

Care should still be taken when calculating the neutrino energy of the event if only a calorimetric approach is used, as is the case in this document. This is because

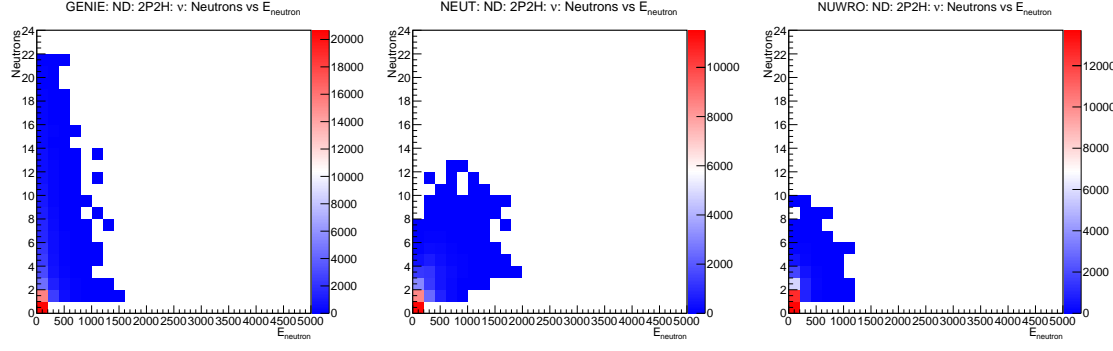


Figure 11: The neutron multiplicity vs total neutron energy for 2p2h interactions for GENIE, NEUT, and NUWRO, respectively. Even though they do show a different phase-space for the neutron multiplicity, they all agree where most of the energy lost to neutrons should be. This is similar for other interaction types as well.

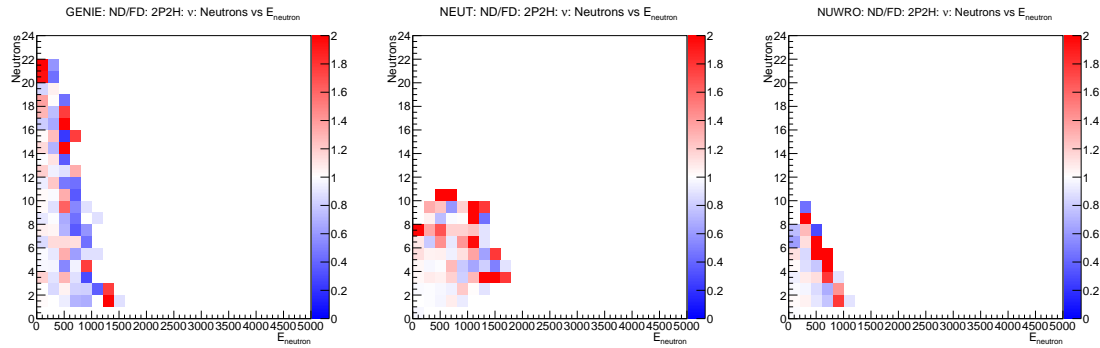


Figure 12: The ratio of the ND to the FD for neutron multiplicity vs total neutron energy for 2p2h interactions for GENIE, NEUT, and NUWRO, respectively. In the area where the largest amount of energy is lost to neutrons, low multiplicity and low energy, the agreement between the ND and FD is almost perfect.

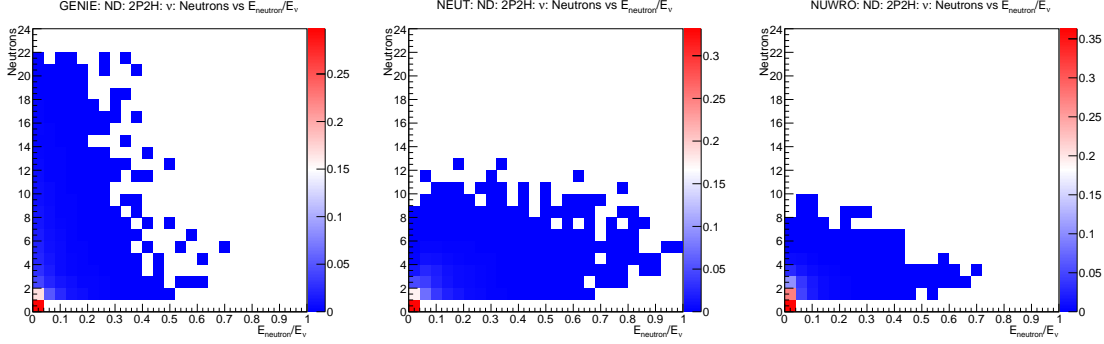


Figure 13: Neutron multiplicity vs total neutron energy divide by the neutrino energy for 2p2h interactions from GENIE, NEUT, and NUWRO, respectively. For low multiplicity, the neutron carries away a significant fraction of the neutrino energy.

as much as 50% of the energy can be taken away by the neutron in CCQE-like events. Even for 2p2h events, as shown in Figure 13, it can be as high as 30%. The other interaction modes and anti-neutrino events can also be found in Appendix C and have a smaller fraction.

Missing neutrons can effect the neutrino energy reconstruction, which is especially important for neutrino oscillation studies which require an exact energy. However, much of the effect of these missing neutrons can be taken into account with the near to far extrapolation. At the moment the difference between the models seem to be OK for these analyses given a near to far ratio. Future investigations will include the ability for errors in GENIE to cover the differences between the models.

4.2 Proton/Pion Multiplicity and Momentum

Similar to the neutron multiplicity and energy studies, proton and pion multiplicities offer insight into the coupling of the detector configurations with variations in FSI models as well as the energy reconstruction capabilities of the different detector configurations. The total momentum of the particles gives us a proxy for the energy into the FS protons or pions as well as a direct link to detector efficiency effects. For these studies, the 3-momentum of the final state protons are summed. The magnitude is then plotted against the multiplicity for the specific particle type. This was done for the FS particles in true-CCQE, true-2p2h, CC0 π , CC1 π , and CCOther, with no efficiencies applied so we can look at the effects of the FSI models, as well with all 3 ND configuration efficiencies and the LAr FD efficiencies, so we can investigate the effects of the different ND and how the couple to the FD.. As the efficiencies for pions are currently unknown for the LAr and GAr, we will only consider the protons in the current iteration of this note.

To show the difference in the FSI models, Figure 14 shows the proton multiplicity vs total proton momentum for 2p2h interactions. 2p2h models where chosen as they have the smallest phase space in this projection and therefore show the differences the best, but all interaction types have been investigated and can be found in Appendix ???. From this, one can see that there is a difference between the FSI models.

Particularly, GENIE prefers to have more proton multiplicity compared to NEUT and NuWro. It also has lower total momentum for these protons when compared to the other two.

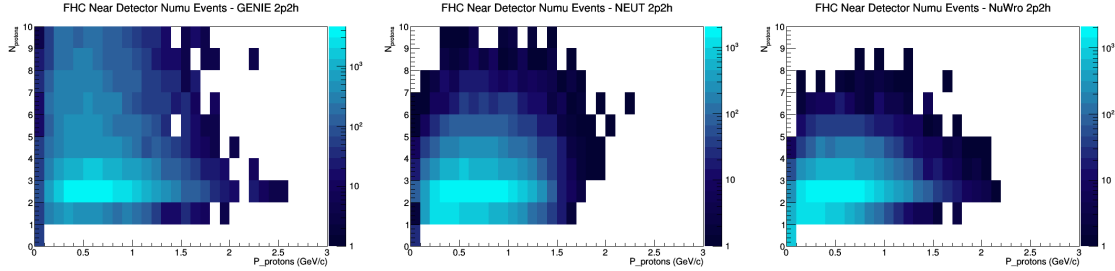


Figure 14: The proton multiplicity as a function of total proton momentum for 2p2h interaction in GENIE, NEUT, and NuWro, respectively. There is a clear difference in phase space with GENIE having both higher proton multiplicity and lower total momentum.

Unlike with the neutron multiplicity, the differences between the models is important as the near to far extrapolation does not hold. Figure ?? shows this with variations of 20-30% in the regions where the most events are. The exact reason for this discrepancy is unclear. It could be attributed to the plot only includes the total momentum of all protons, with it being possible that one or two protons take away the most energy and the highest momentum protons would agree between the two detectors. This is something that needs to be investigated further in future works.

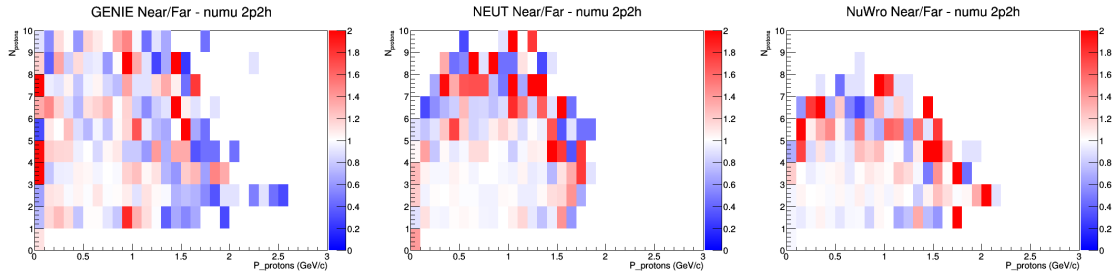


Figure 15: The ND/FD of proton multiplicity as a function of total proton momentum for 2p2h interaction in GENIE, NEUT, and NuWro, respectively. In the region with the most events, there are variations of up to 20%

Once detector efficiencies are added in, there is even a greater difference in the near to far ratio. Figure 16 shows these striking differences. The top row shows the near to far ratio for the FGT to a LAr far detector. In the region of interest the differences are 100% and greater. The middle row shows the high pressure GAr TPC, with differences again ranging from 20-100%. The last row shows the LAr TPC, and unsurprisingly, gives the best agreement. Event then though, differences of up to 20% exist, arising most likely due to the different flux at each detector.

These plots show the importance of not just the FSI model in use but also the detector's threshold to measure protons. The FGT, which has the most realistic

thresholds and therefore the ones most unlike the LAr far detector, shows just how important this can be. It is expected pions will have an even larger impact than the protons due to there re-interactions with the nucleus. This needs to be confirmed and will be shown in updates to this document.

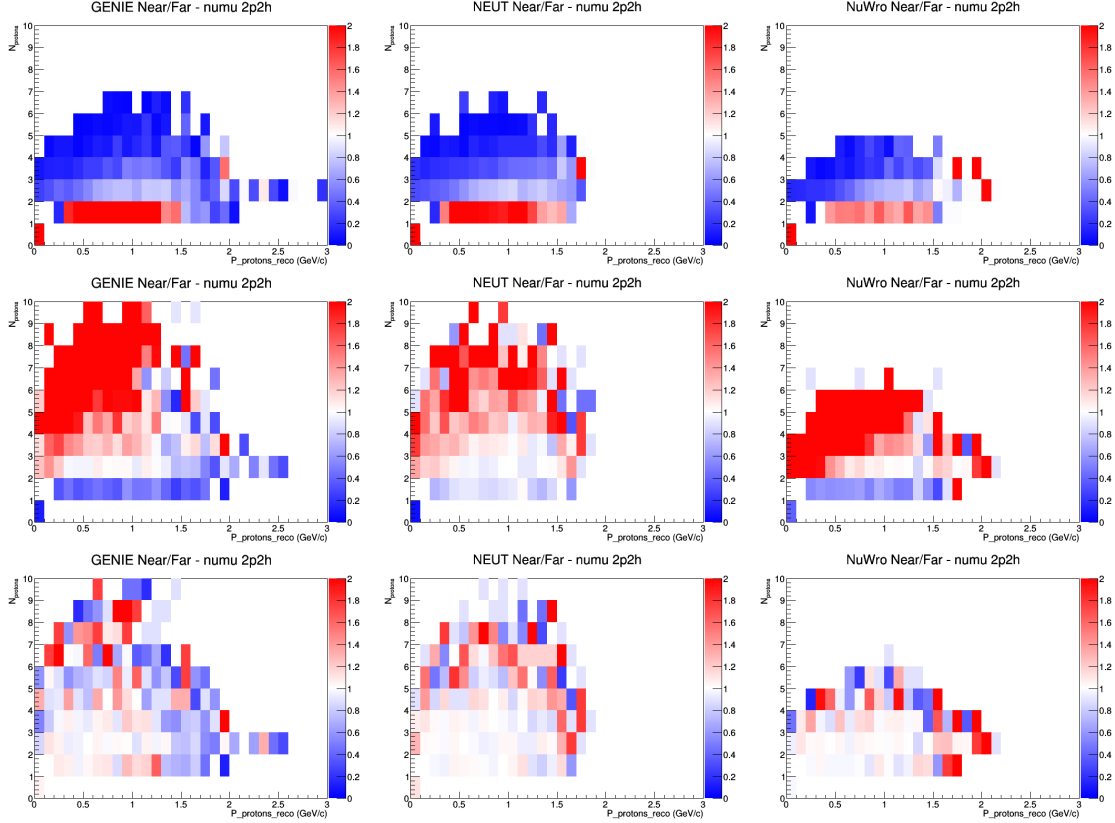


Figure 16: The ND/FD of proton multiplicity as a function of total proton momentum for 2p2h interactions. The left hand columns show GENIE, and middle column shows NEUT, and the right hand column shows NuWro. The top row has the FGT efficiencies applied for the ND, the middle row has the high pressure GAr TPC efficiencies, while the last row has the LAr TPC efficiencies for the ND. All of these use LAr efficiencies for the FD.

4.3 Difference from True Neutrino Energy

The studies in Sections 4.1 and 4.2 highlight the differences in the generators in reproducing the true neutrino energy, as well as the differences in the abilities of the different detector configurations to reconstruct this energy. This section studies the overall change we see to E_{reco} as we apply detector efficiencies. To do this, the difference between true and reconstructed neutrino energy from each generator is plotted. Each distribution is normalized to 1 so the y-axis serves as the relative event rate. This is done separately for a 'perfect' near detector - one in which we assume no particles except neutrons are rejected - and each near detector configuration and

the far detector with simple LAr thresholds for protons, as well for each interaction type: true-CCQE, true-2p2h, CC0 π , CC1 π , and CCOther. True-CCQE and true-2p2h are both defined as MC-level CCQE/2p2h interaction with 1 reconstructed lepton if efficiencies are applied. CC0 π is defined as 0 π^\pm , 1 lepton, and any number of protons and π^0 after reconstruction. CC1 π is defined as 1 π^\pm , 1 lepton, and any number of protons and π^0 after reconstruction. Finally, CCOther is defined as any final state with 1 lepton and any number of hadrons reconstructed.

In ν_μ mode: for all reaction types except CCOther, all three generators seem to have similar differences in all detector configurations. This is evident in Figure 17 - which includes CCQE and CCOther interactions in the ND with FGT efficiencies - and the figures in Appendix E. For CCOther, all three generators appear to have a long tail extending to high discrepancy regions - well past that of CCQE for example - though NuWro has a higher amount of events in the $\Delta E = 0.5$ GeV to 2 GeV region.

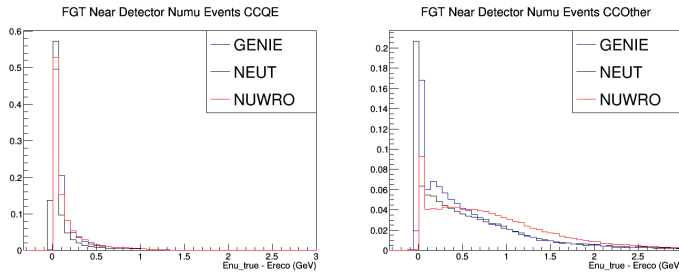


Figure 17: Difference between true and reconstructed Neutrino Energy in the FGT ND. CCQE events seem to have similar discrepancies, while CCOther mode has large tails in all three generators with NuWro having more events with higher discrepancy than the other two.

Meanwhile, for $\overline{\nu_\mu}$ CCQE, 2p2h, and CC0 π events NuWro consistently has ΔE closer to 0 than the other generators as shown in Figure 18. In CC1 π and CCOther NuWro again has more events where true neutrino energy is underestimated by reconstruction, shown in Figure 19. Additionally, there exists a large difference in the distribution of events from NEUT and NuWro between the FGT and LAr FD. This is slightly better in the LAr ND - as expected due to our naive LAr efficiencies. This can be seen in Figure 20.

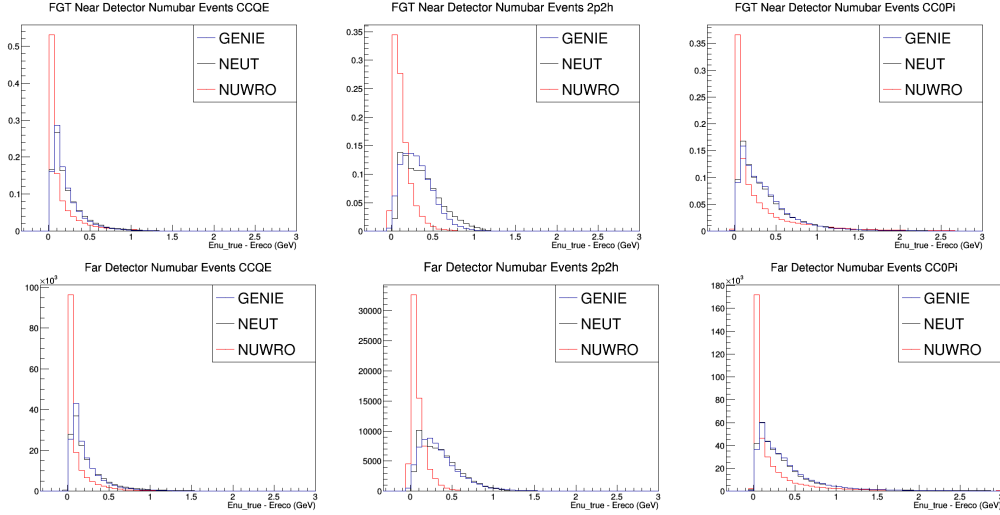


Figure 18: Difference between true and reconstructed E_ν . Top: At Near Detector with FGT efficiencies. Bottom: Far Detector with LAr efficiencies. Left to Right: CCQE, 2p2h, CC0 π . NuWro can be seen to have consistently less discrepancy in reconstructed energy than NEUT and GENIE in CCQE, 2p2h, and CC0 π .

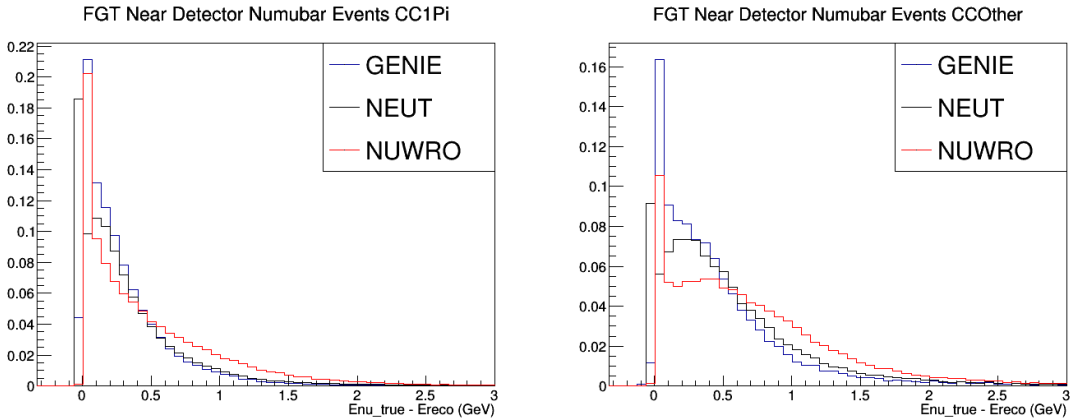


Figure 19: NuWro has higher discrepancy in reconstructed energy than NEUT and GENIE in both CC1 π and CCOther.

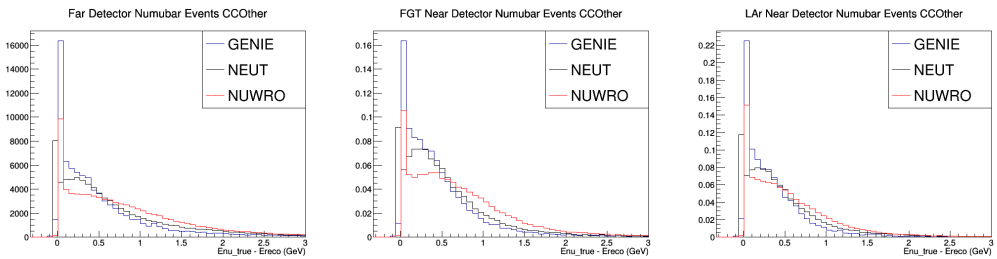


Figure 20: NuWro CCOther events have differences in shape between the Far Detector and LAr FD. The LAr ND matches more closely, though this is expected because of our current naive efficiency assumptions.

5 Future Work

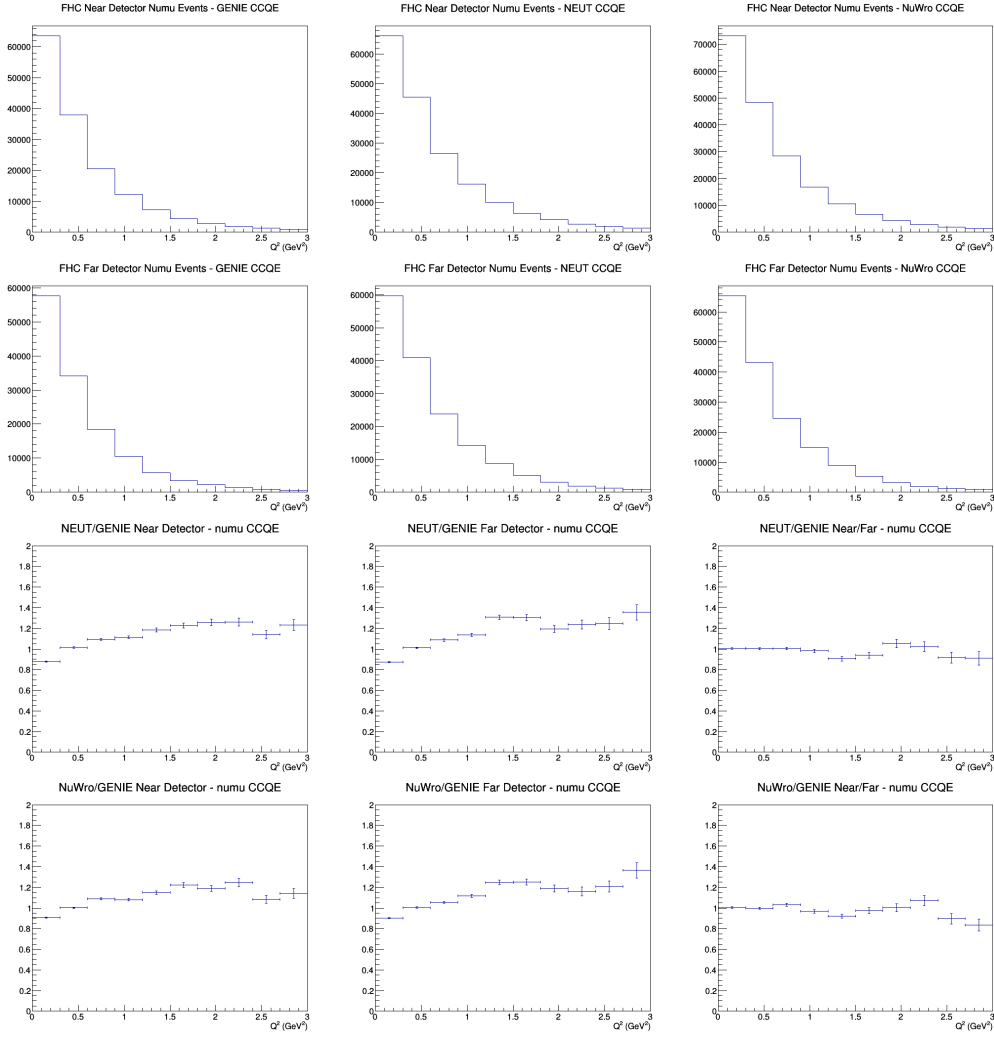
The above studies need to be furthered and expanded upon to successfully arrive at useful conclusions on ND configuration choice.

- Improved statistics.
 - This can be easily and quickly achieved.
- Investigate origins of high- Q^2 variations
 - Is this FSI or detector effects?
- Extend studies to include LAr and GAr efficiency and acceptance information when available.
- Extend final state studies into proton multiplicity vs. energy, and include pions when efficiencies are available.

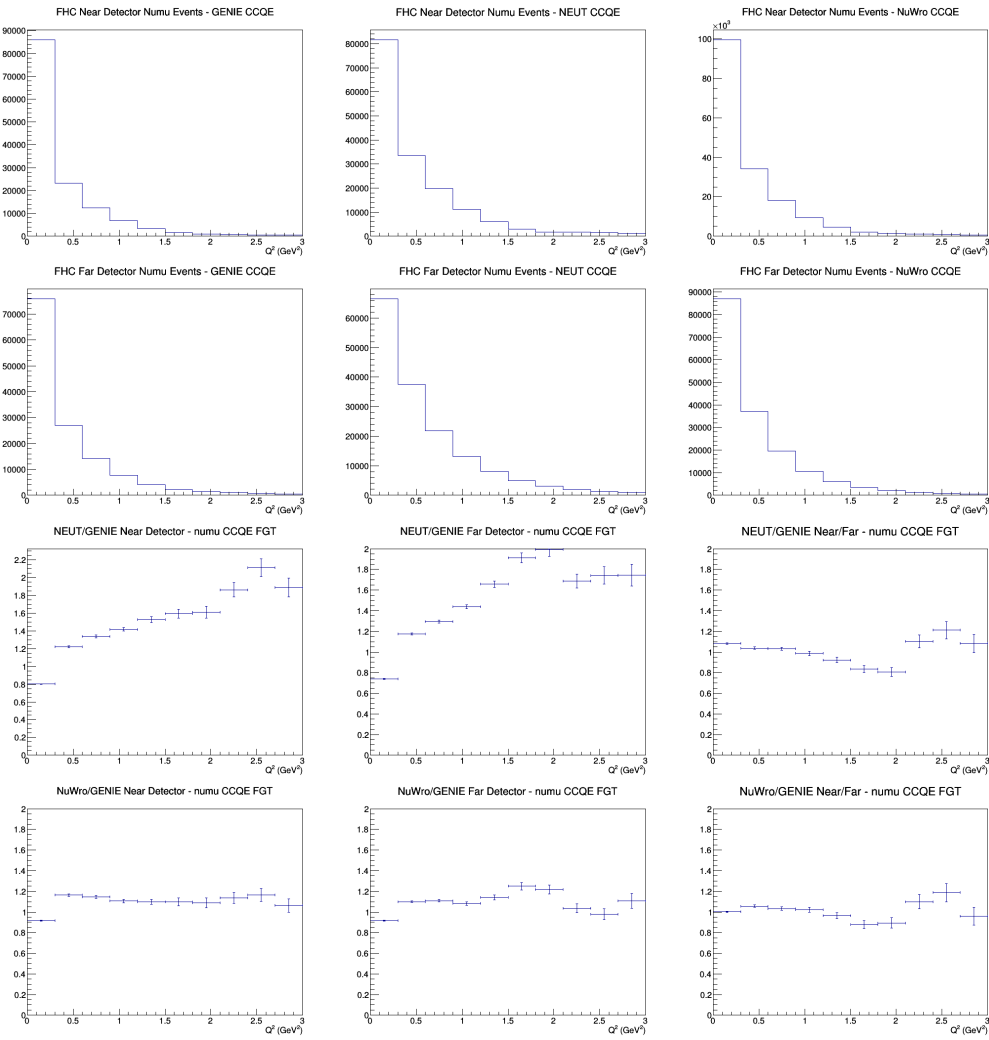
A Q^2 Plots

This appendix includes all the plots not show in Section 3.1. For full description of the files, please make reference to that section. The plots will be put in the same order as before.

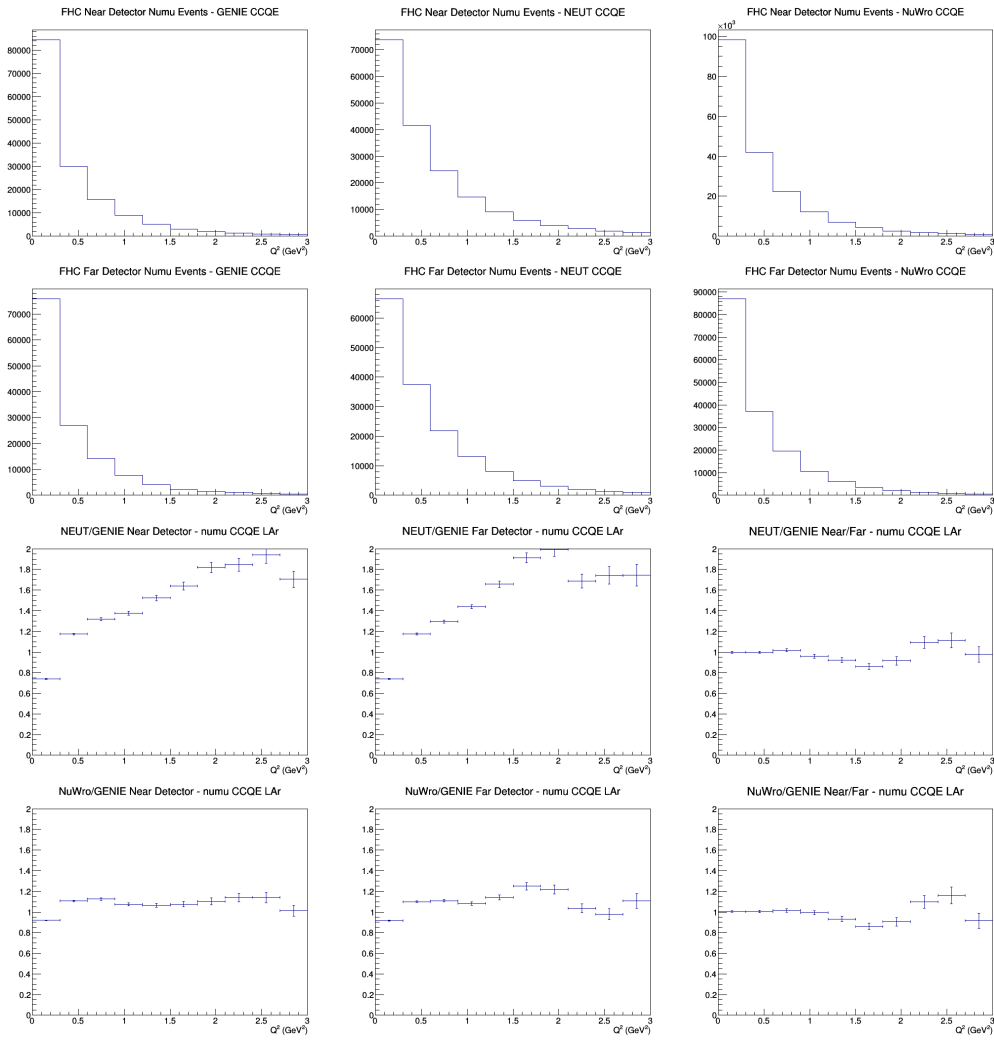
A.1 numu CCQE no efficiencies



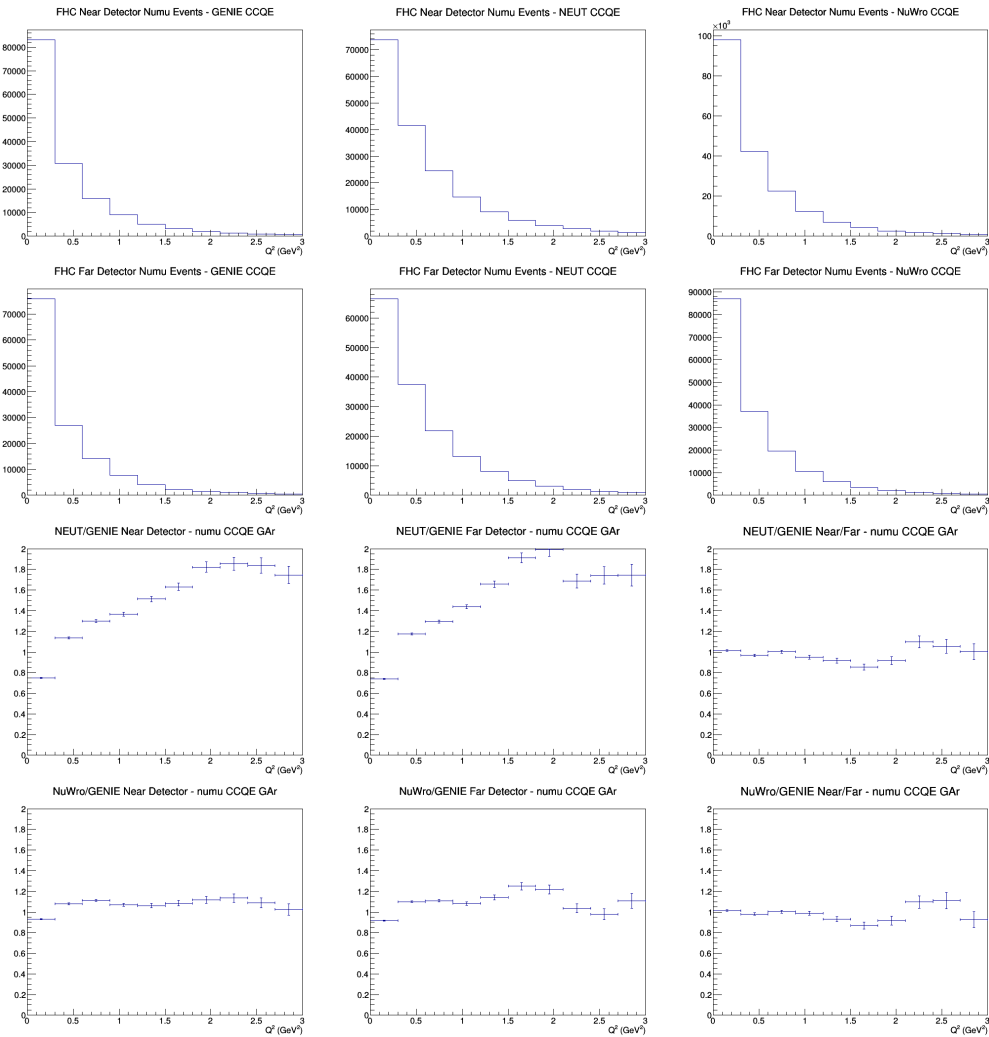
A.2 numu CCQE FGT efficiencies



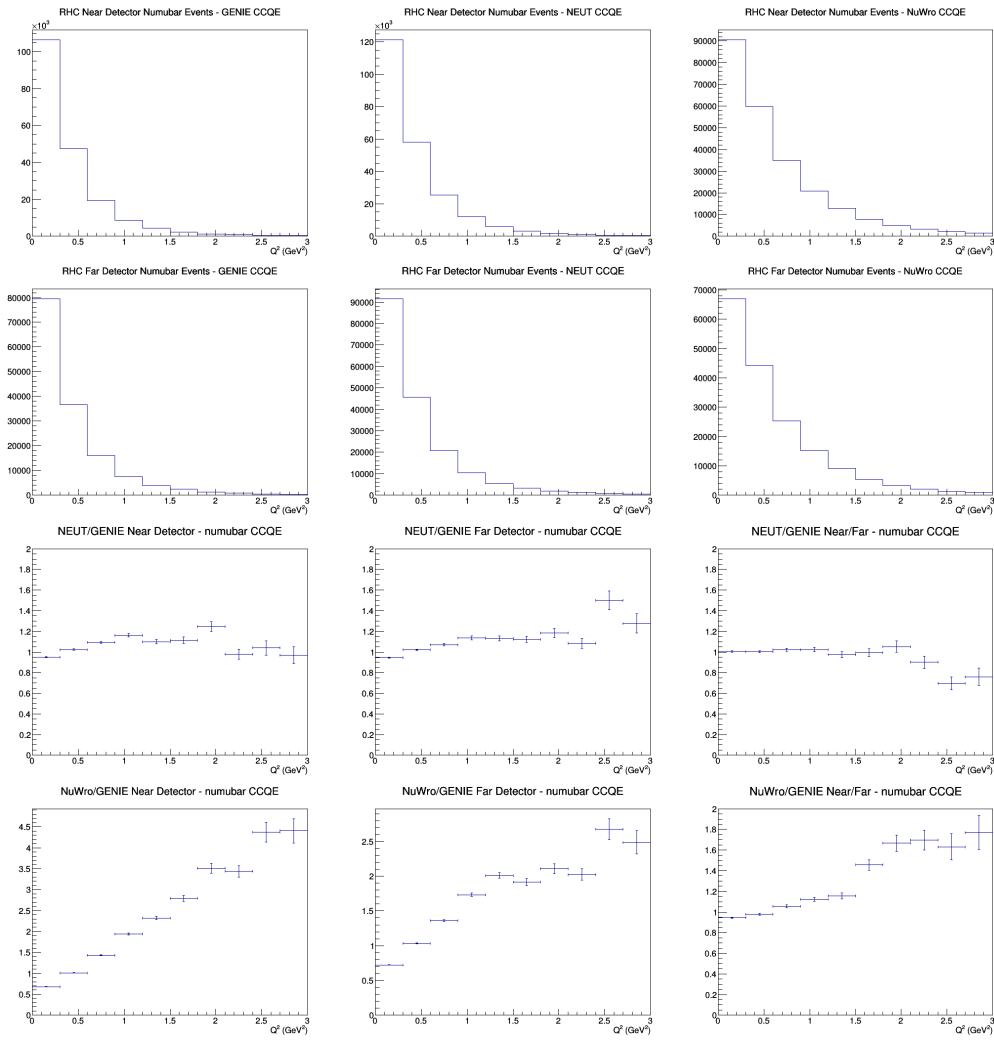
A.3 numu CCQE LAr efficiencies



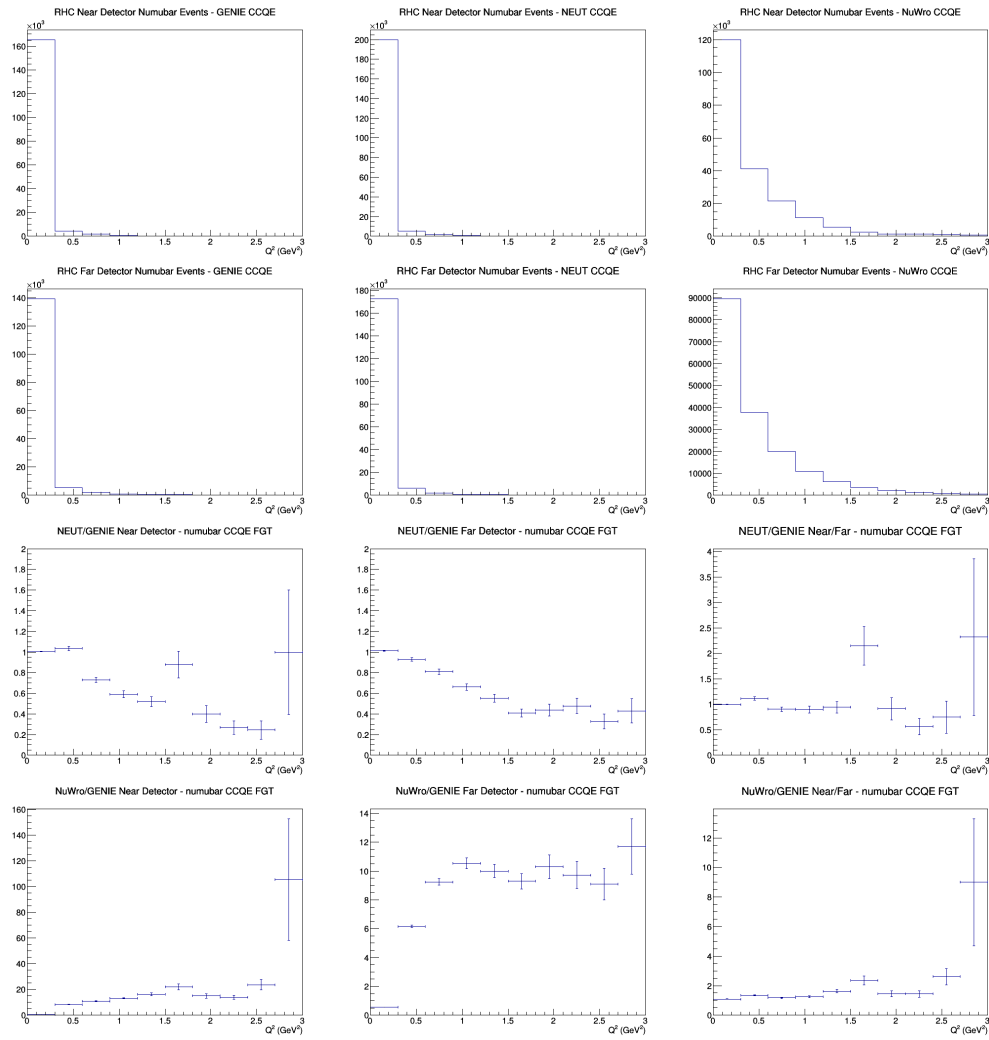
A.4 numu CCQE GAr efficiencies



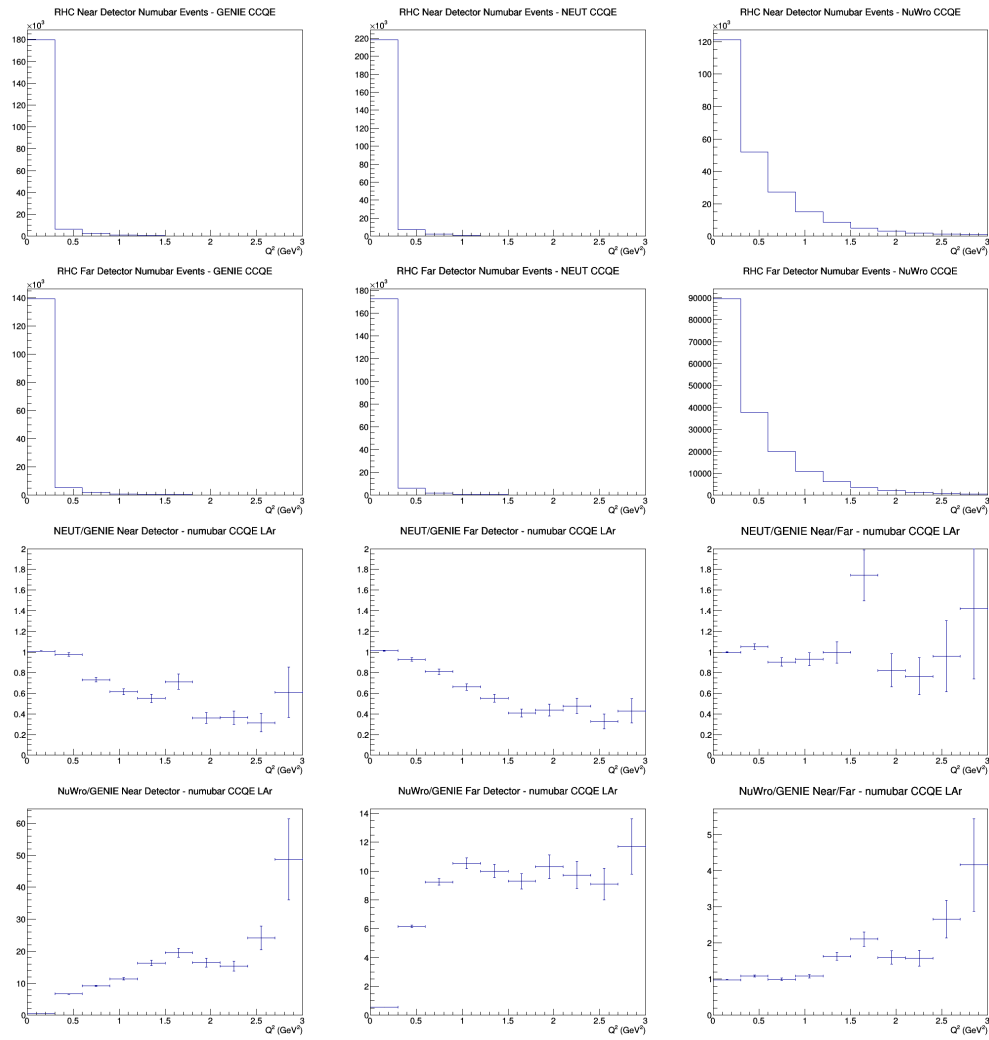
A.5 numubar CCQE no efficiencies



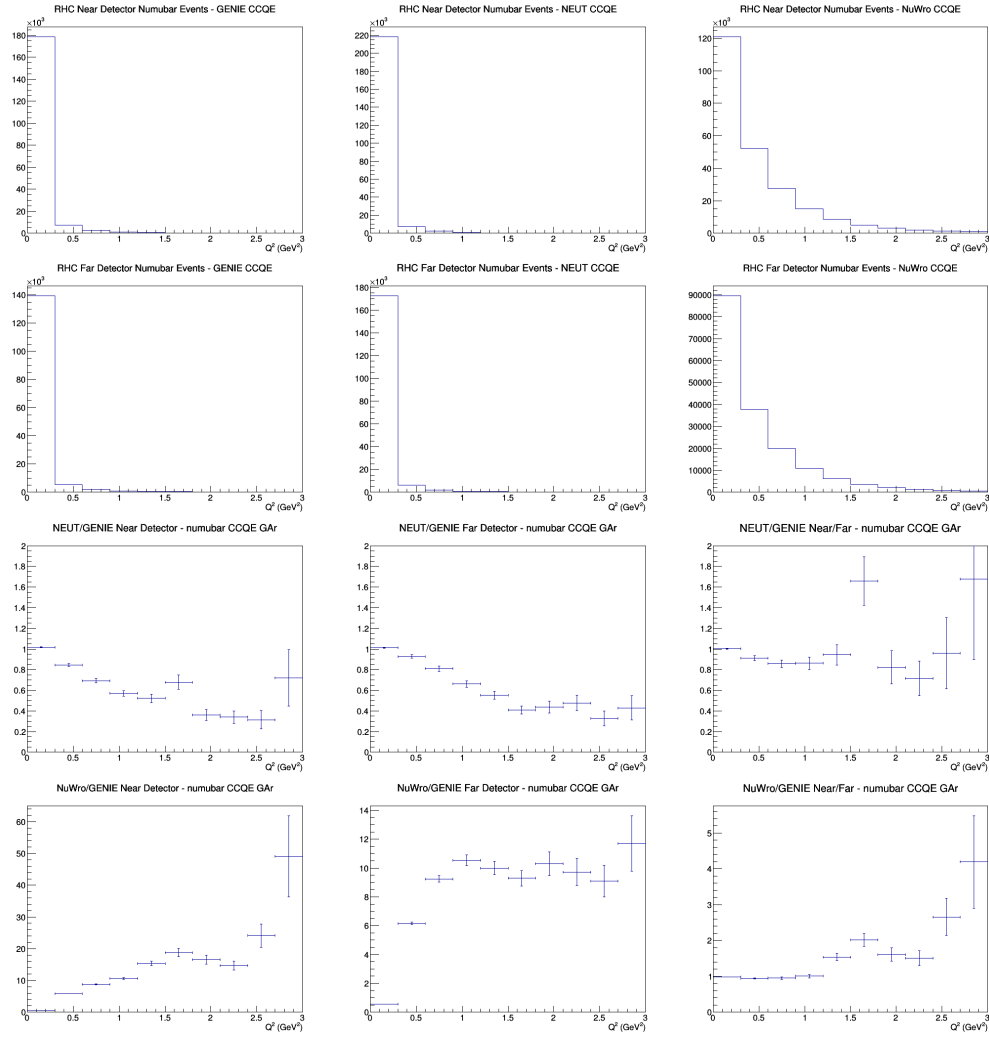
A.6 numubar CCQE FGT efficiencies



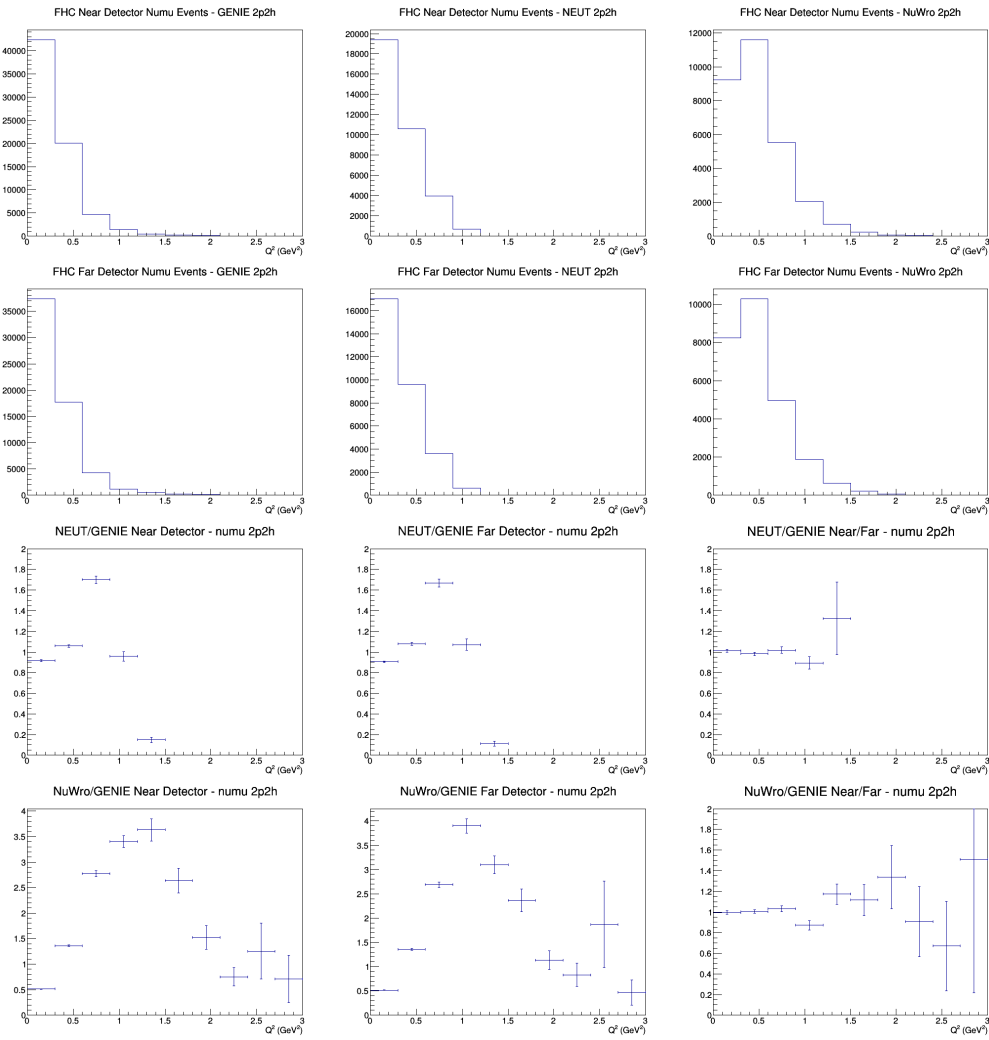
A.7 numubar CCQE LAr efficiencies



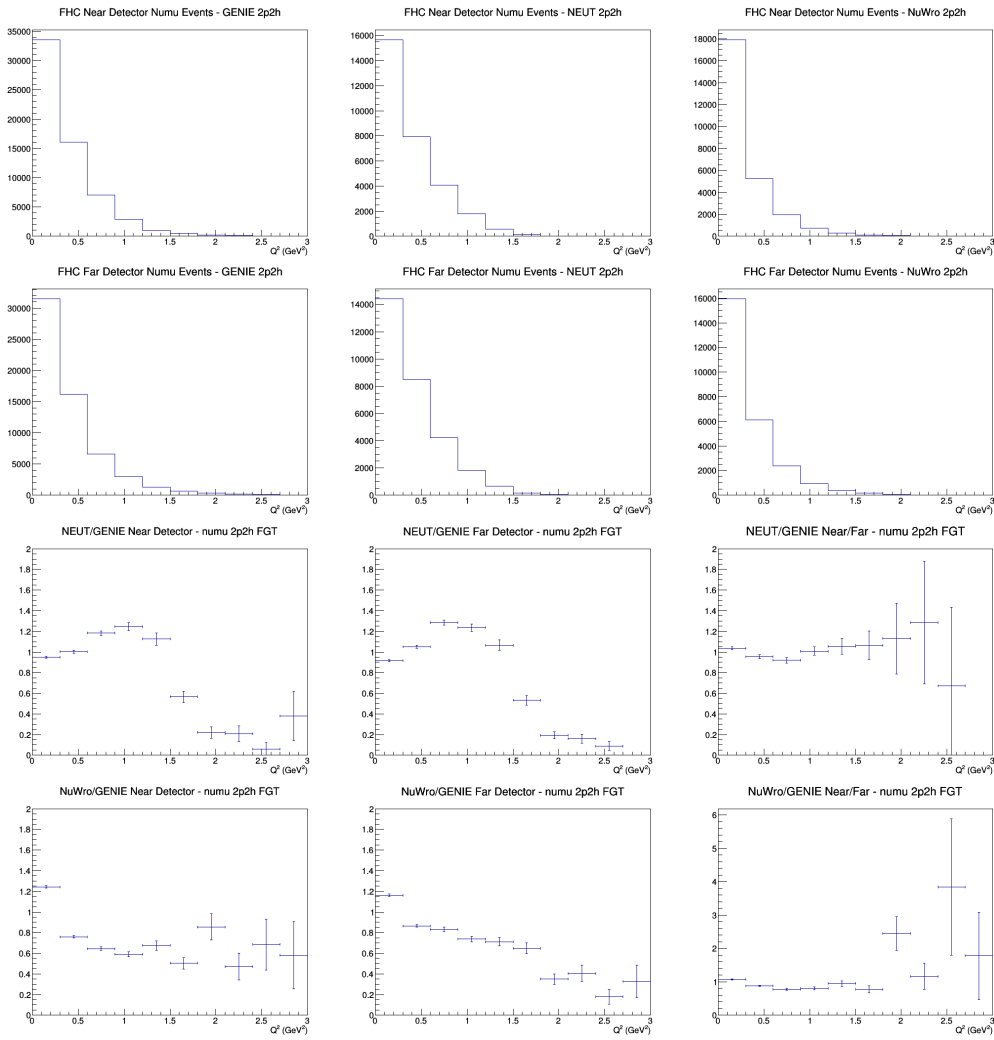
A.8 numubar CCQE GAr efficiencies



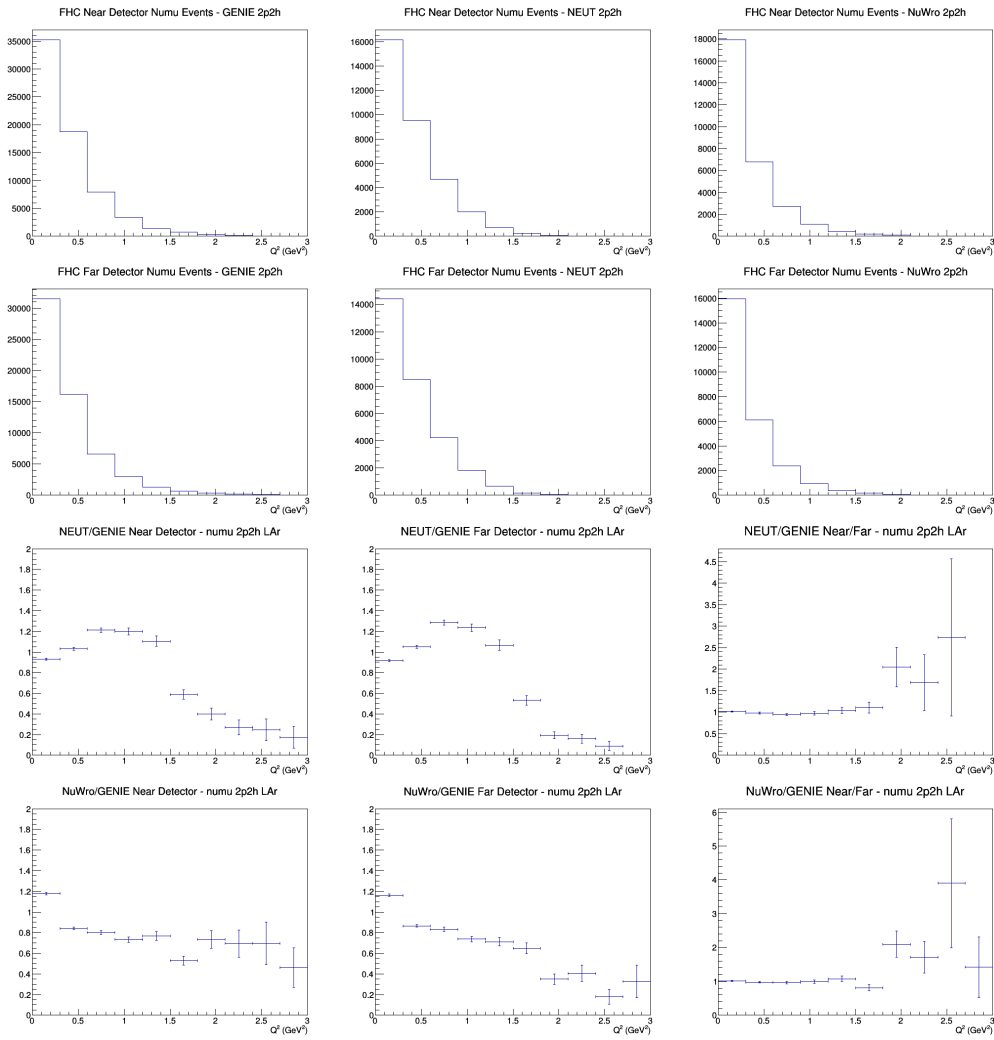
A.9 numu 2p2h no efficiencies



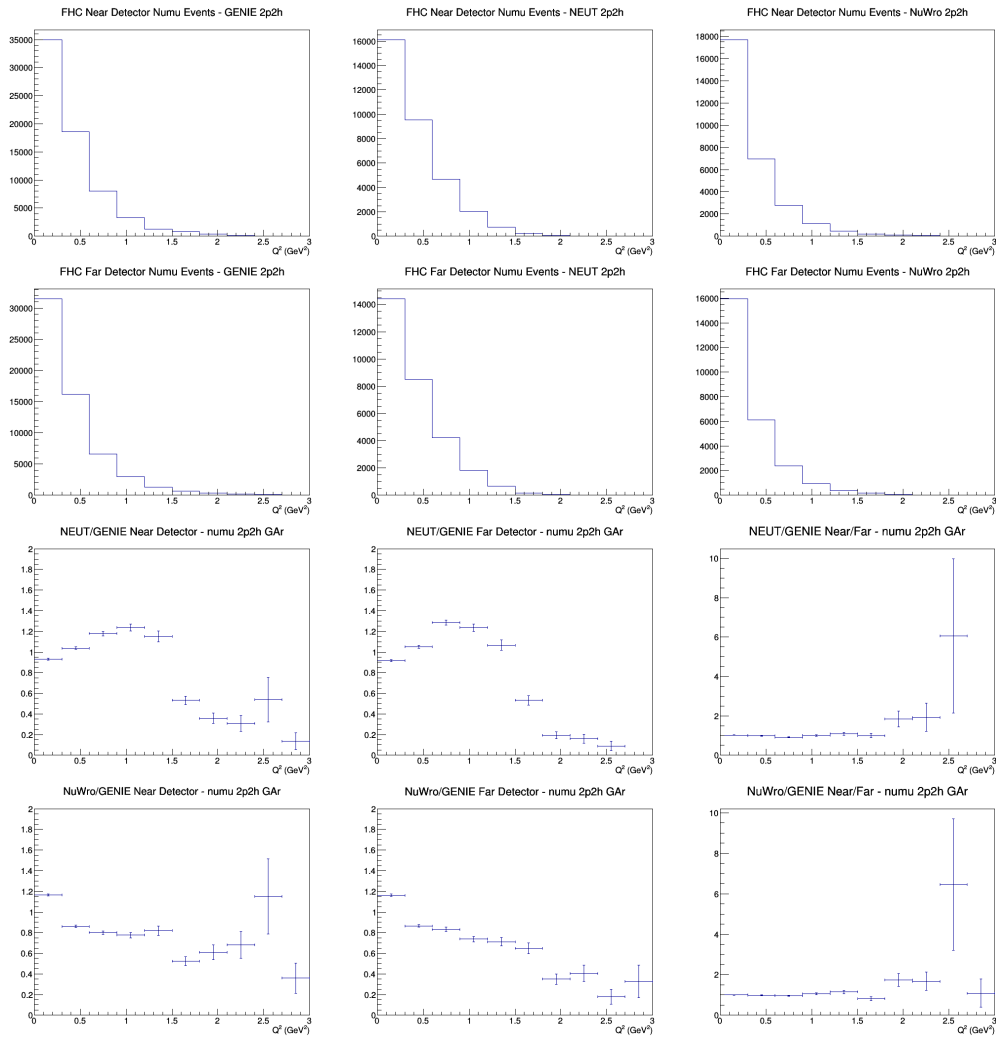
A.10 numu 2p2h FGT efficiencies



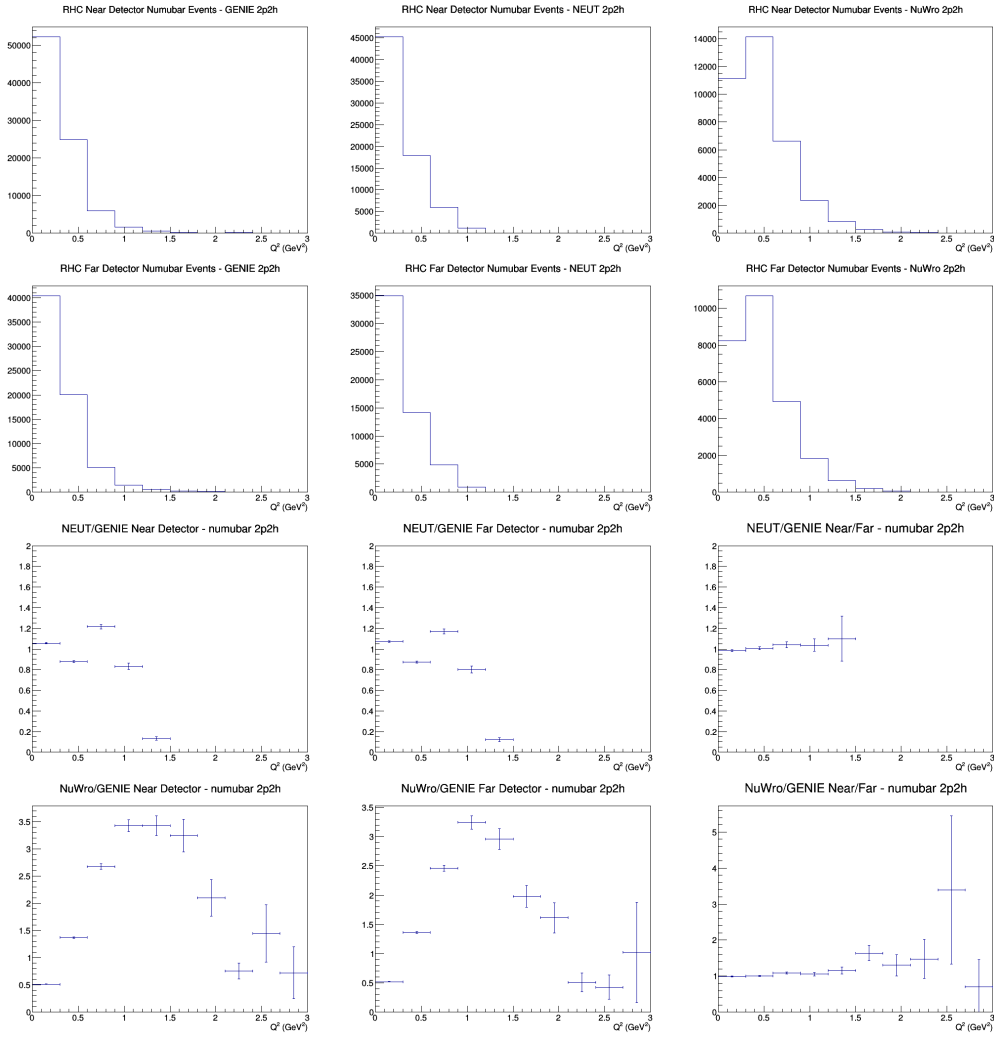
A.11 numu 2p2h LAr efficiencies



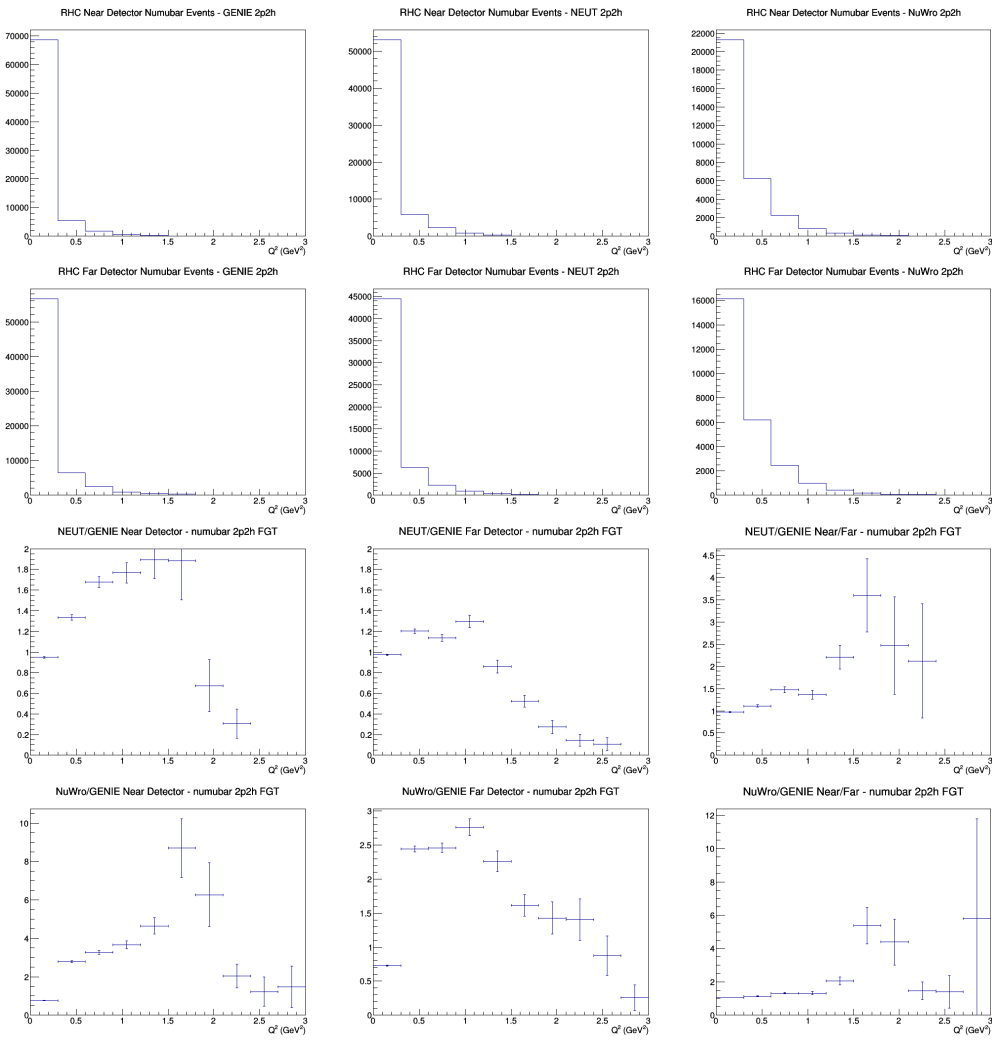
A.12 numu 2p2h GAr efficiencies



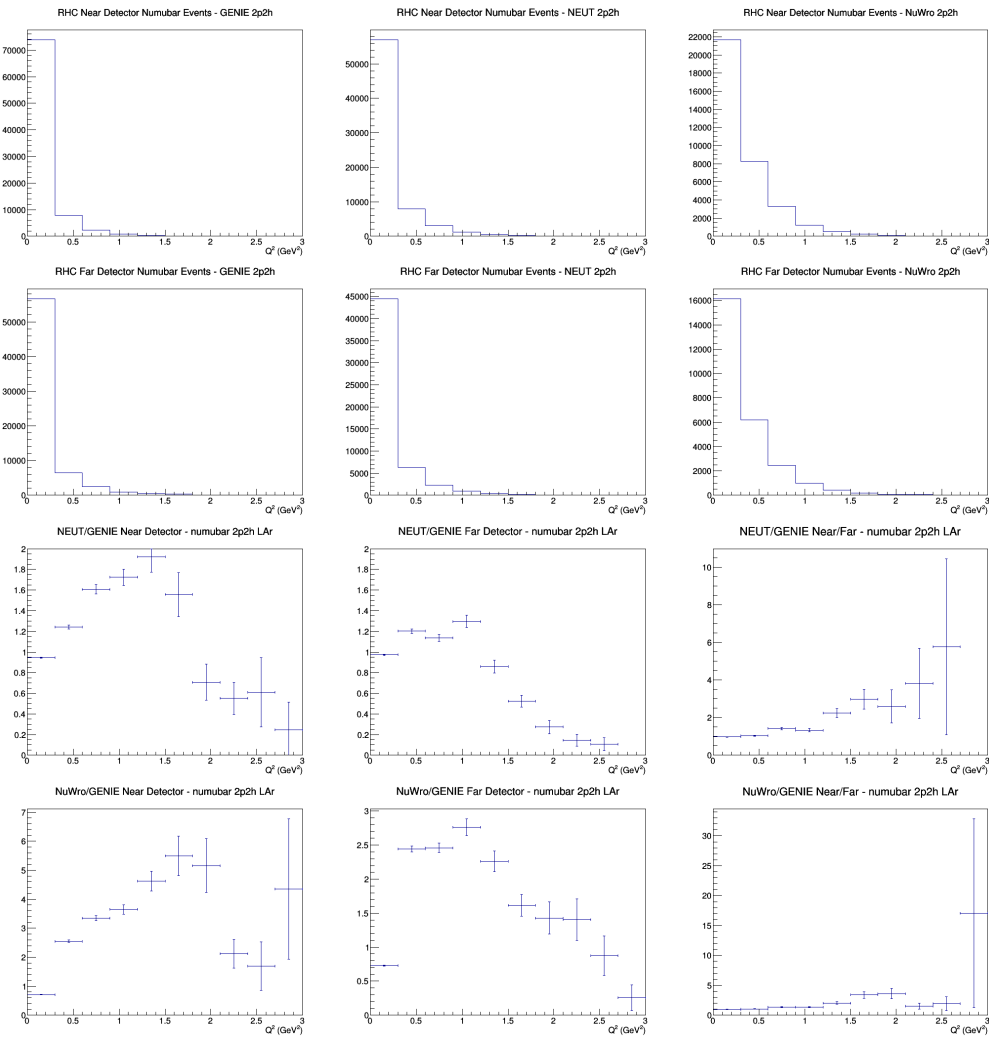
A.13 numubar 2p2h no efficiencies



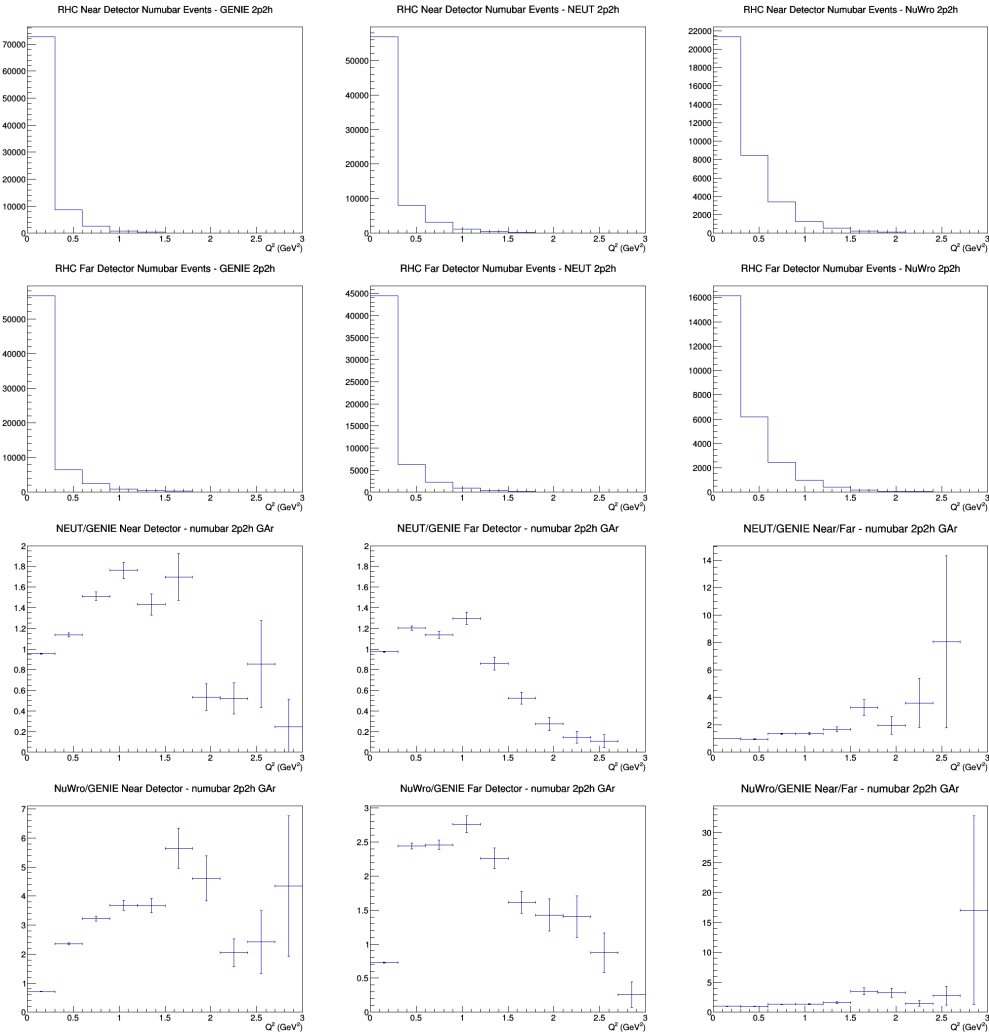
A.14 numubar 2p2h FGT efficiencies



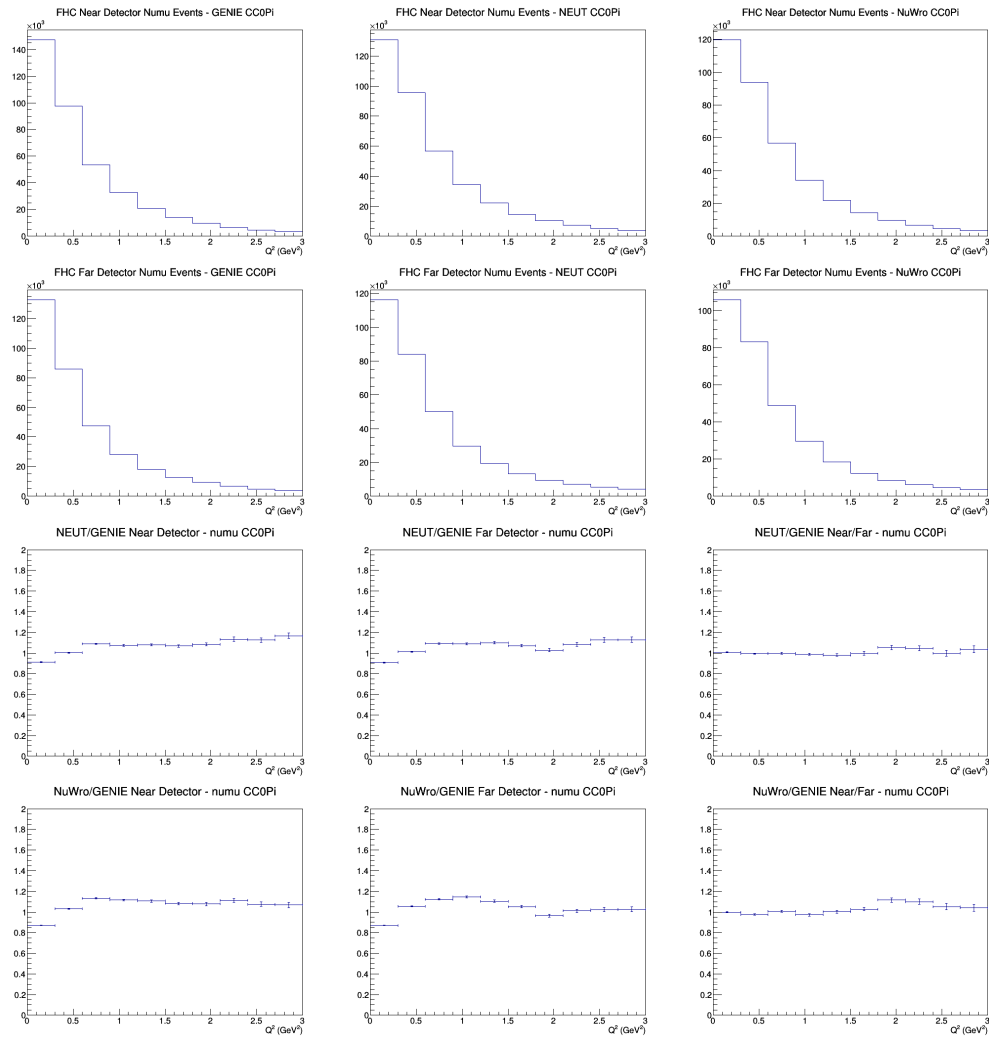
A.15 numubar 2p2h LAr efficiencies



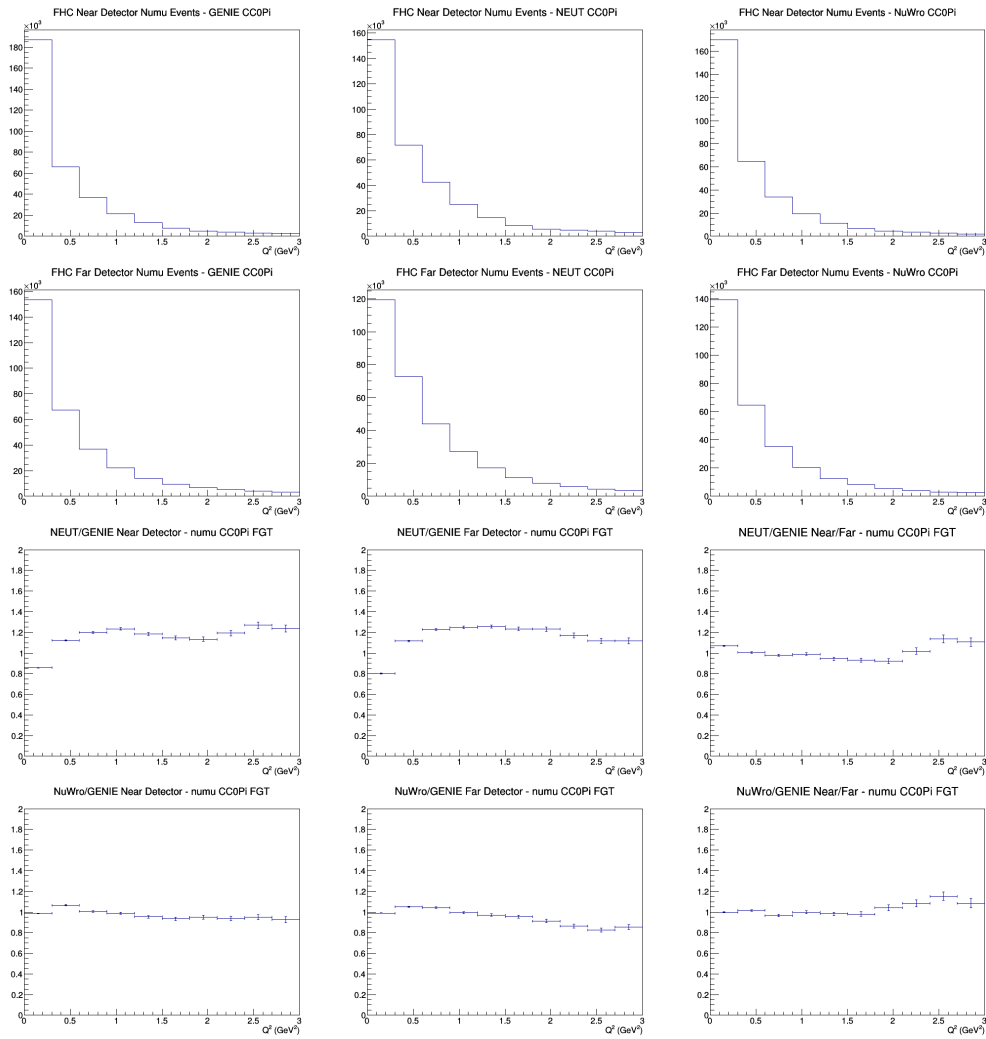
A.16 numubar 2p2h GAr efficiencies



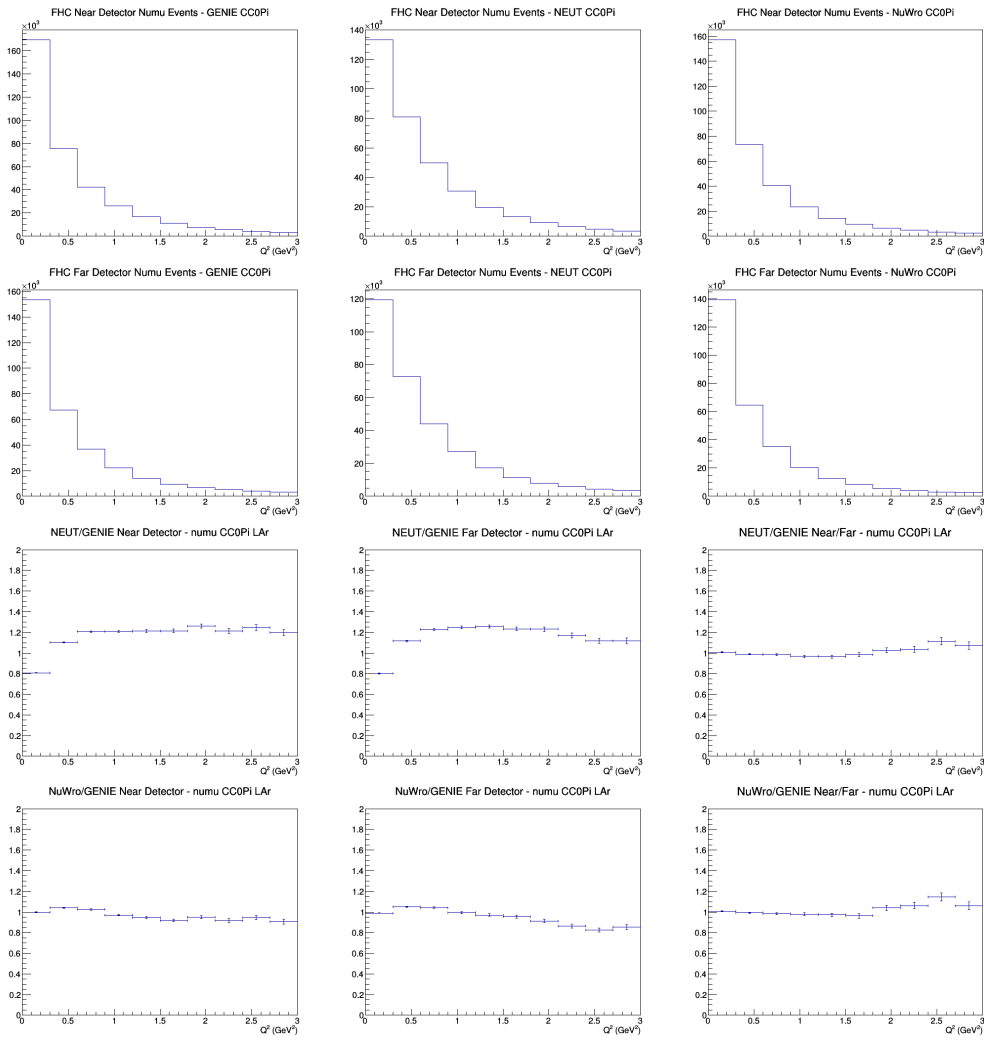
A.17 numu CC0Pi no efficiencies



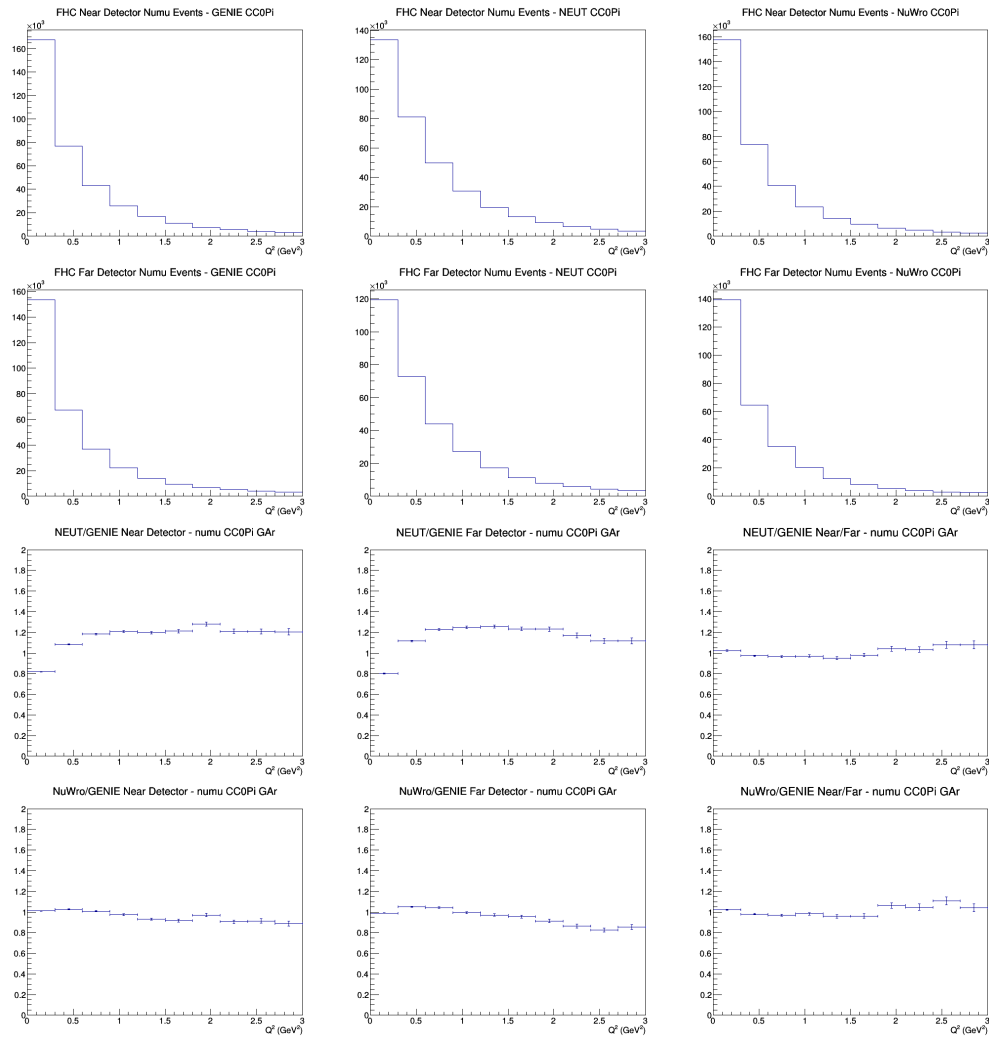
A.18 numu CC0Pi FGT efficiencies



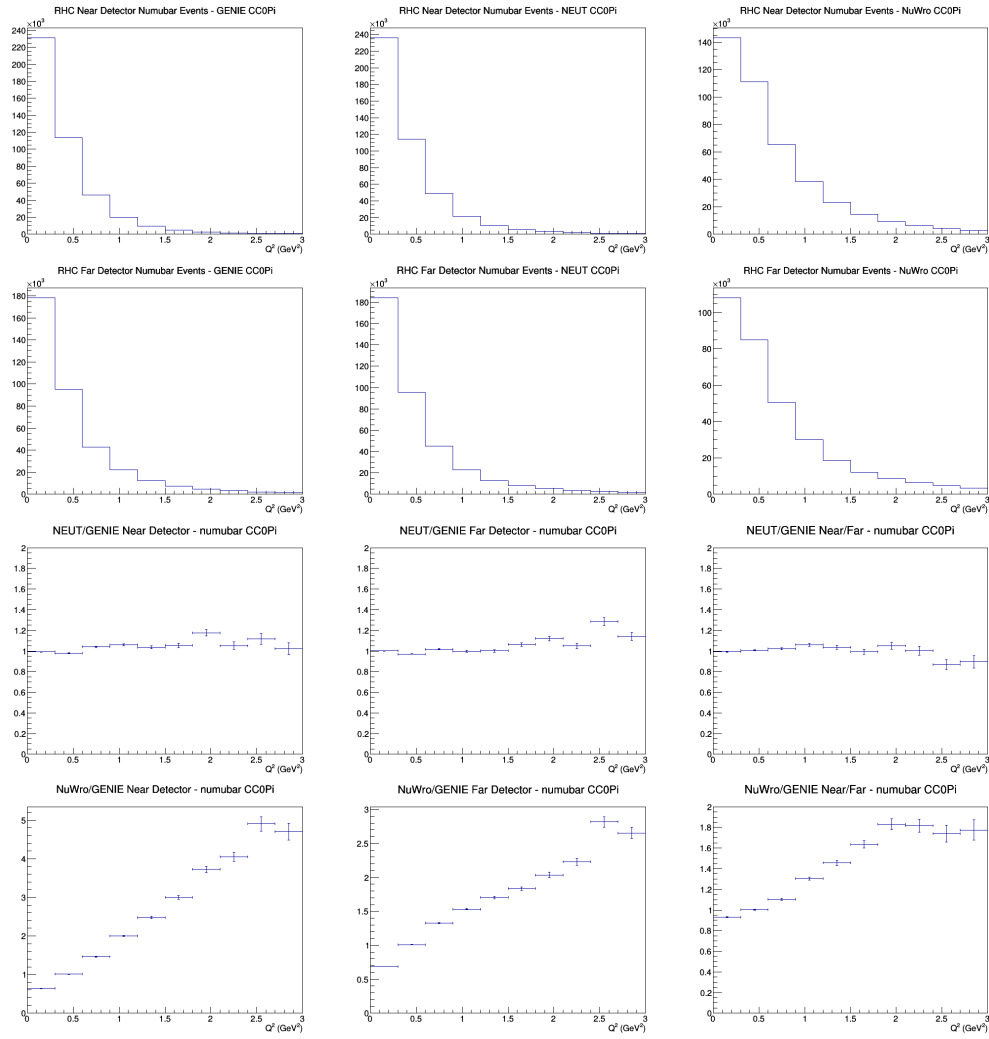
A.19 numu CC0Pi LAr efficiencies



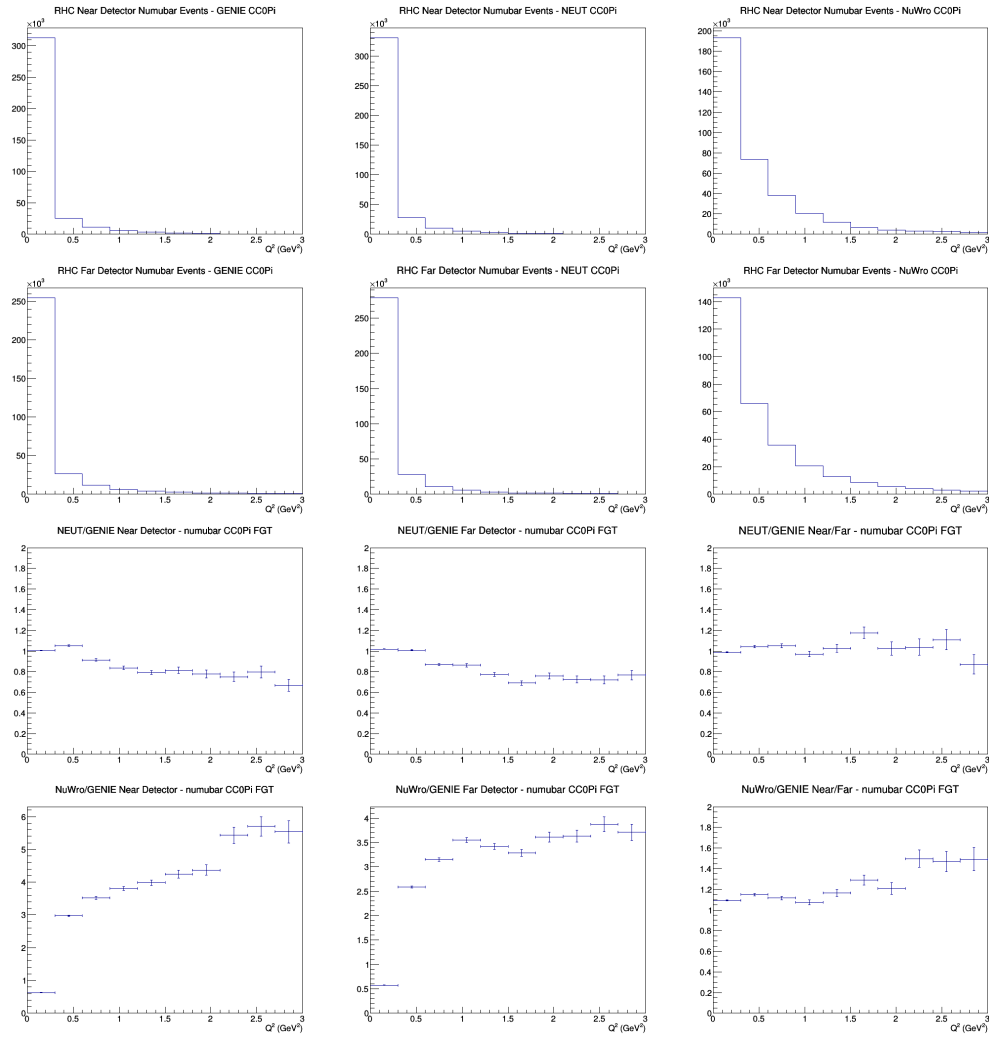
A.20 numu CC0Pi GAr efficiencies



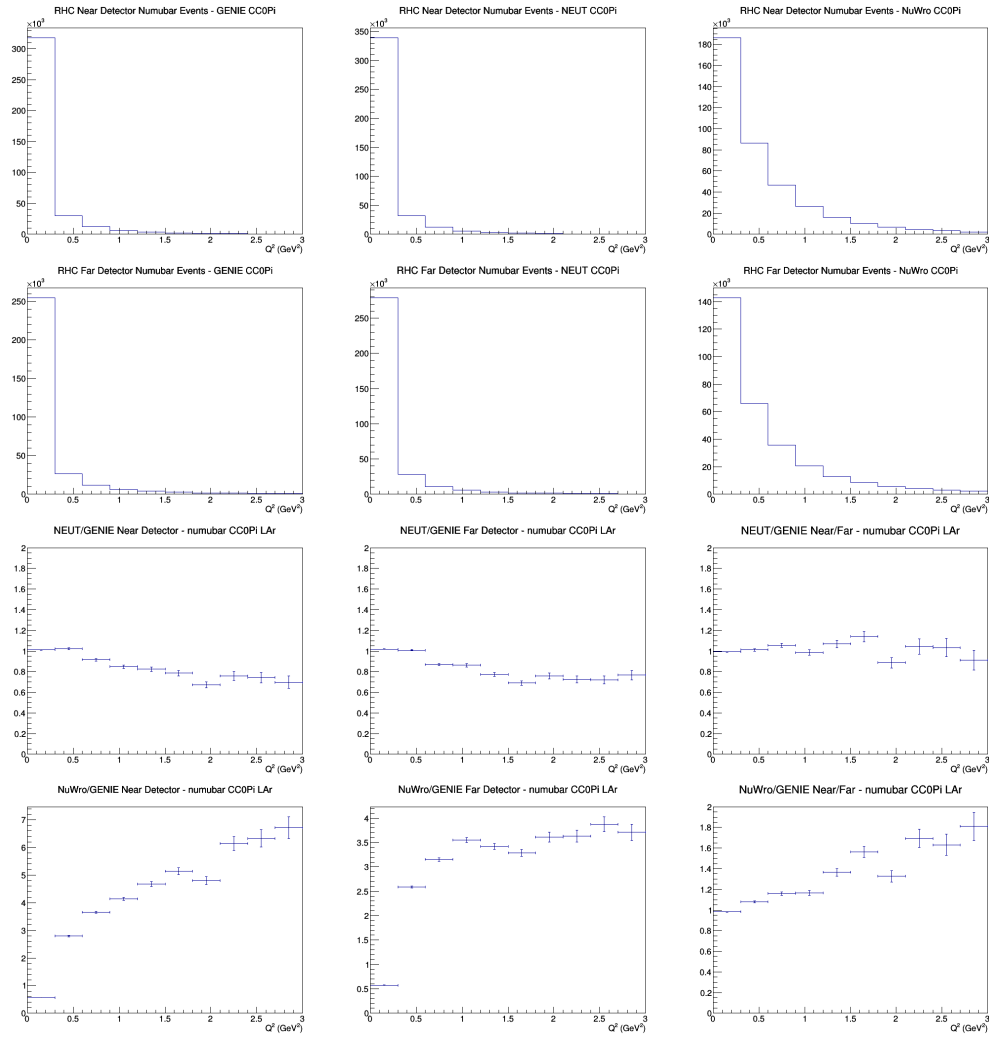
A.21 numubar CC0Pi no efficiencies



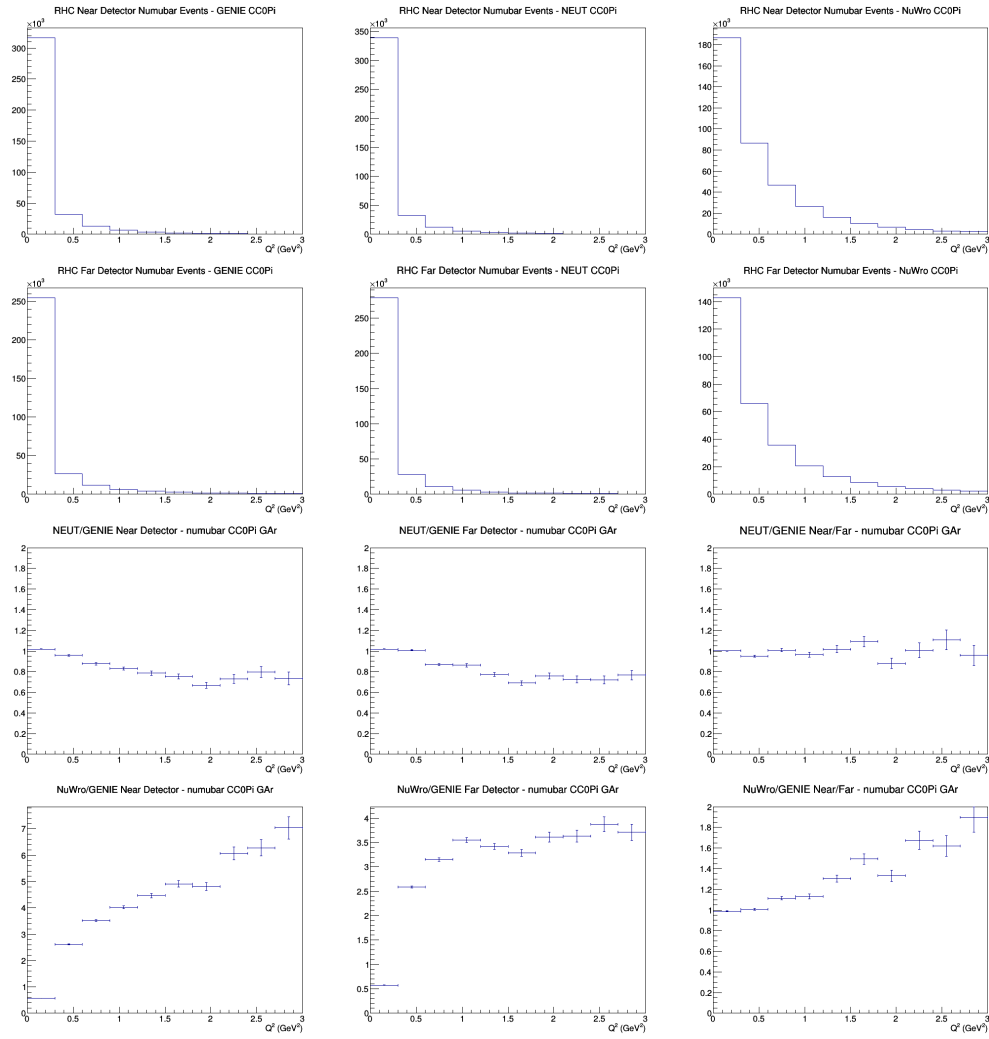
A.22 numubar CC0Pi FGT efficiencies



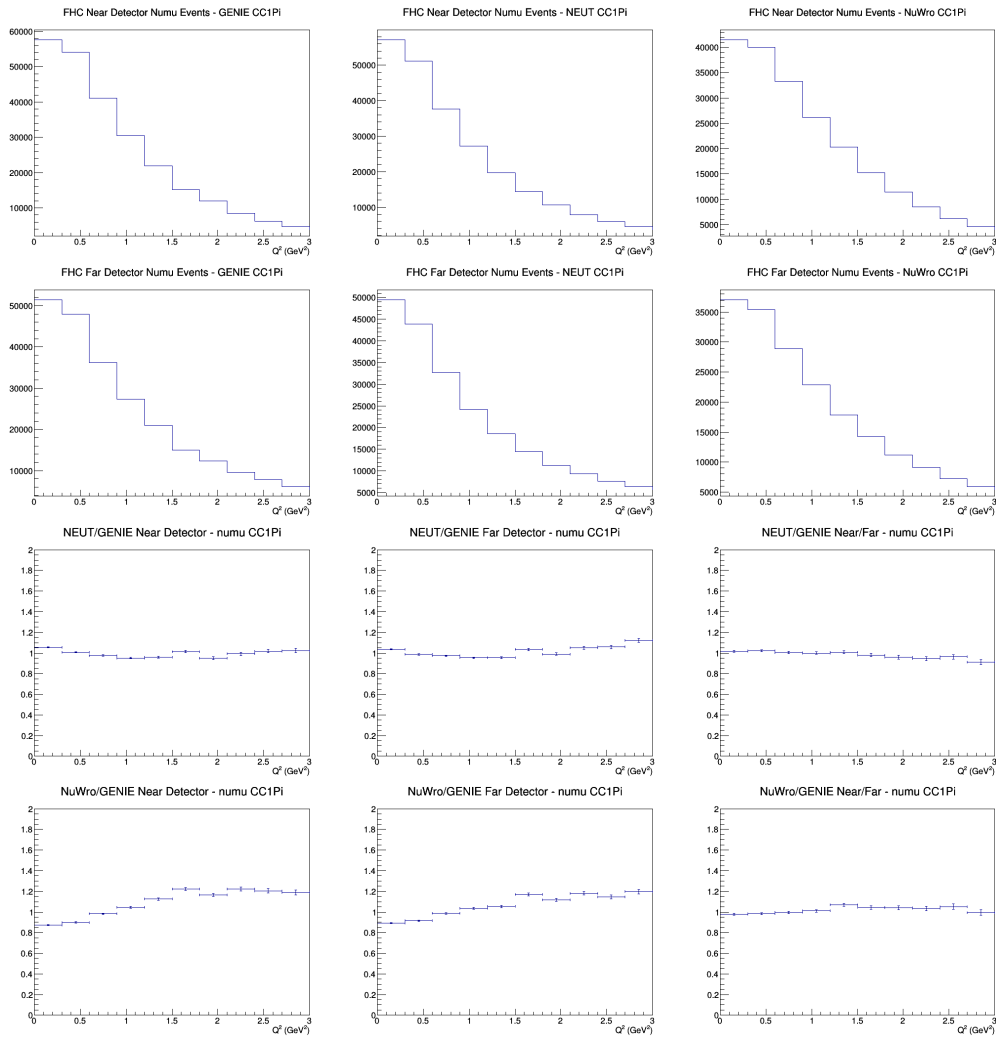
A.23 numubar CC0Pi LAr efficiencies



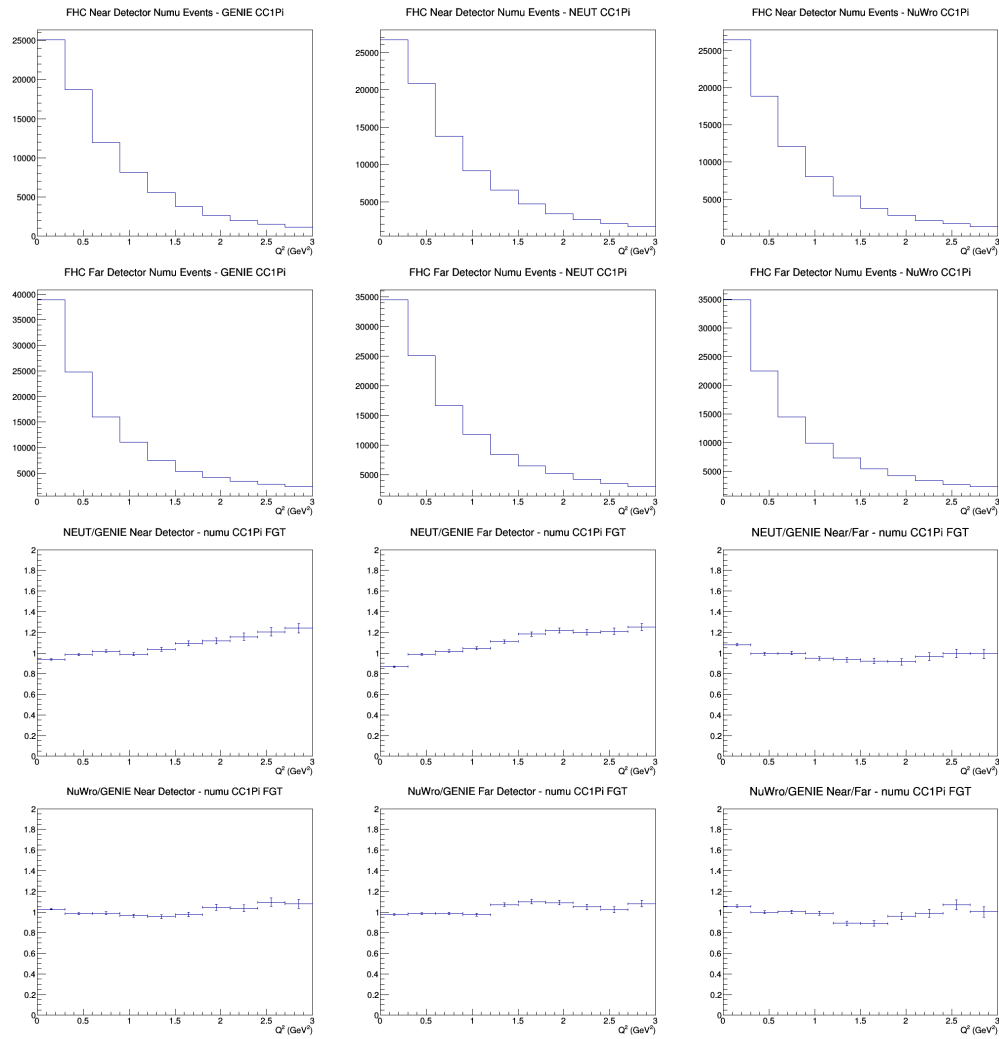
A.24 numubar CC0Pi GAr efficiencies



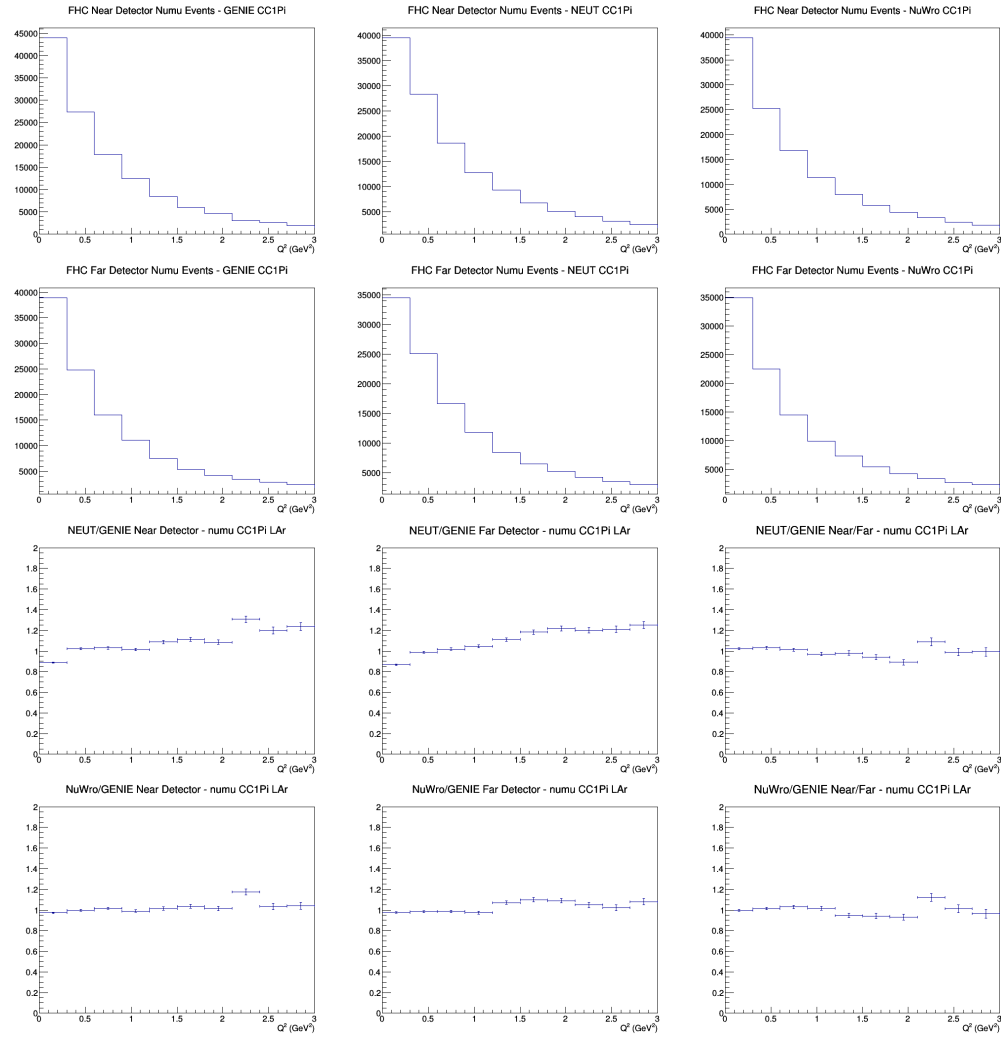
A.25 numu CC1Pi no efficiencies



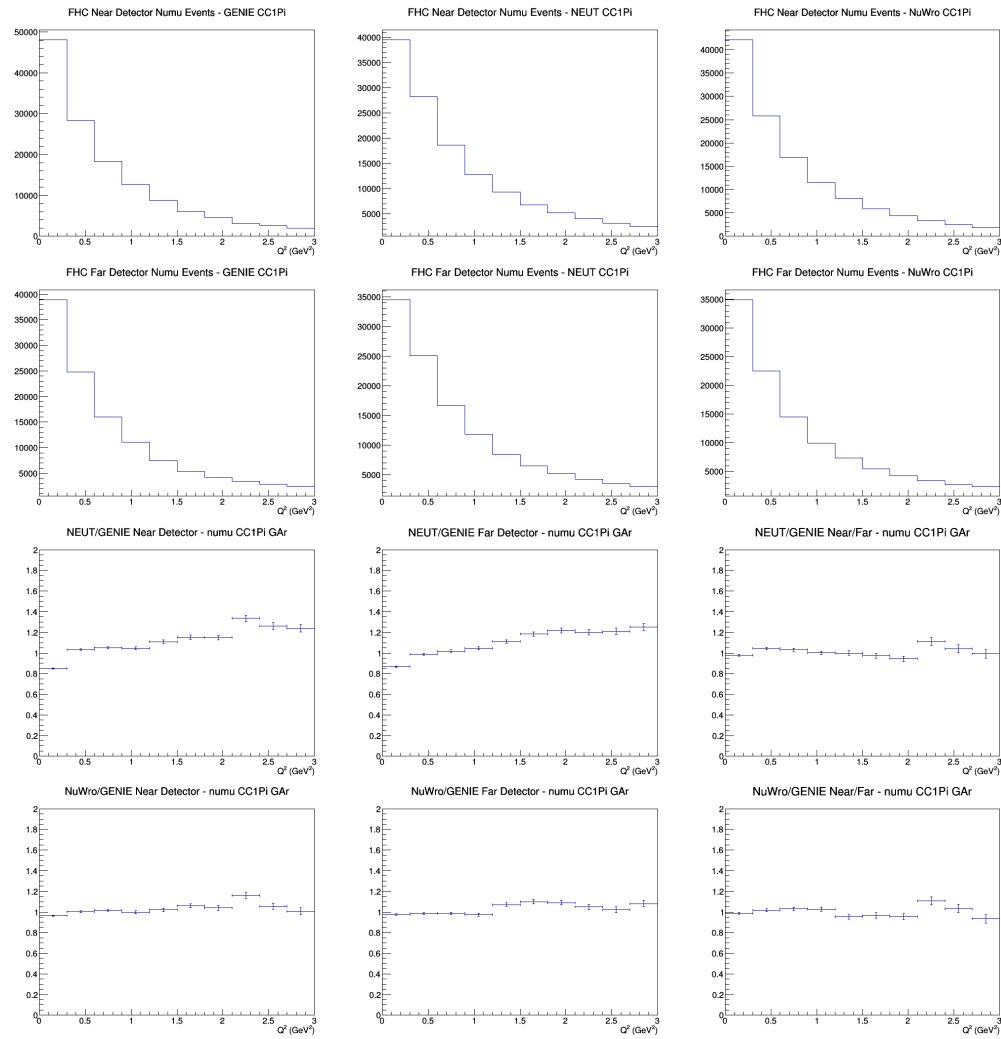
A.26 numu CC1Pi FGT efficiencies



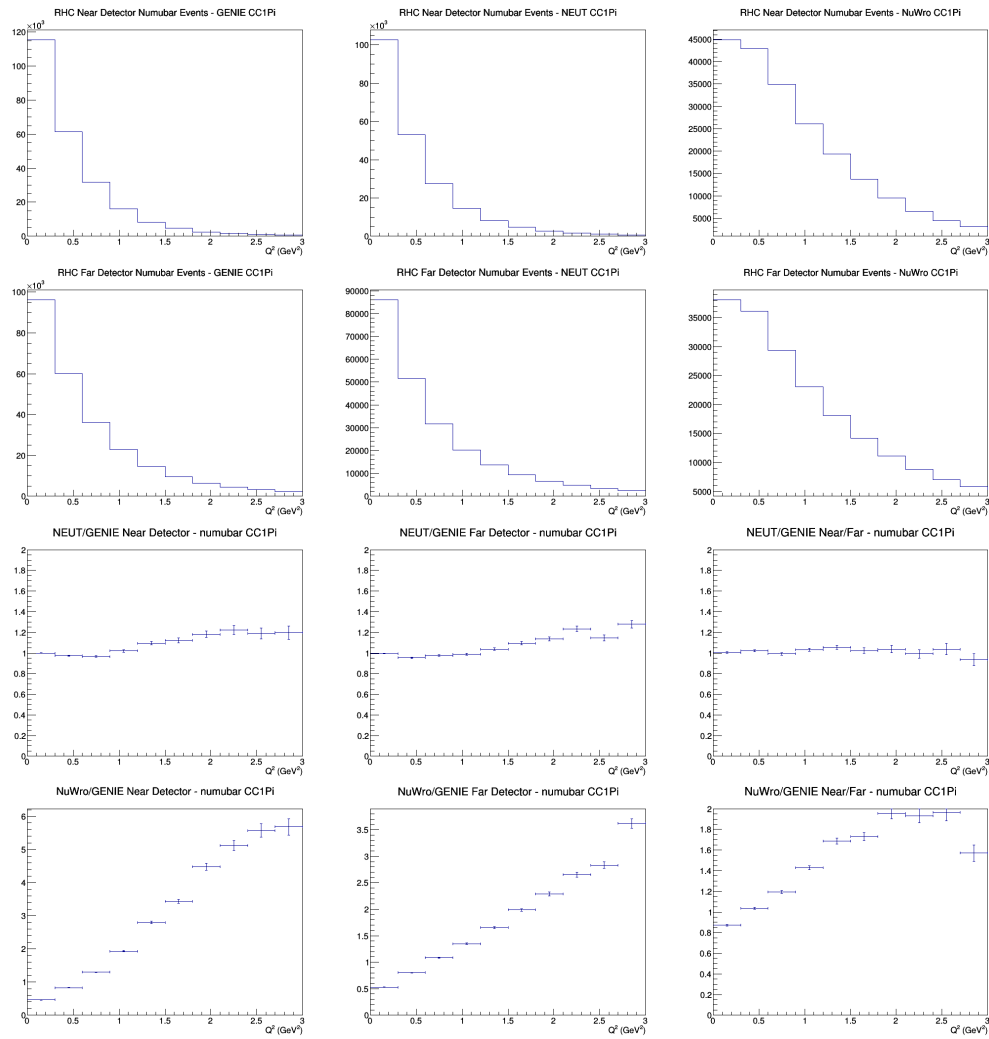
A.27 numu CC1Pi LAr efficiencies



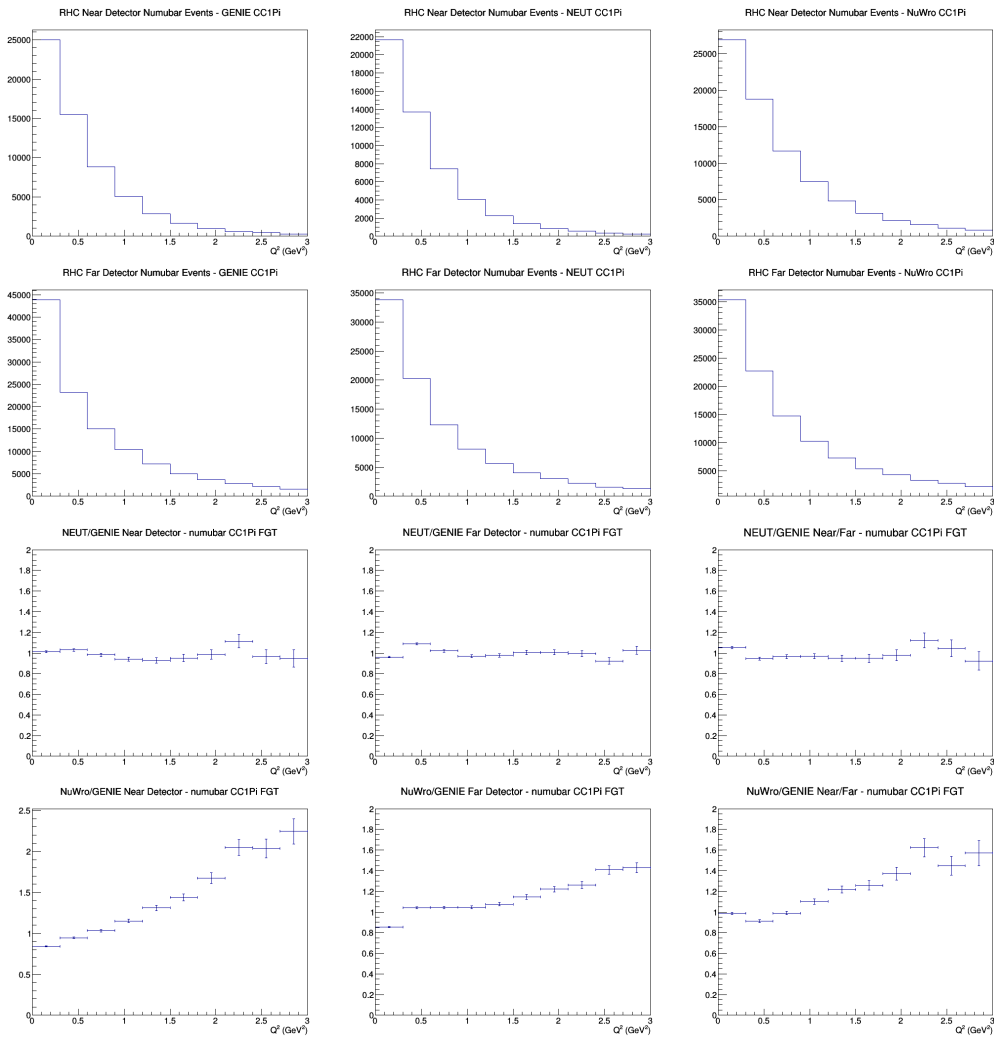
A.28 numu CC1Pi GAr efficiencies



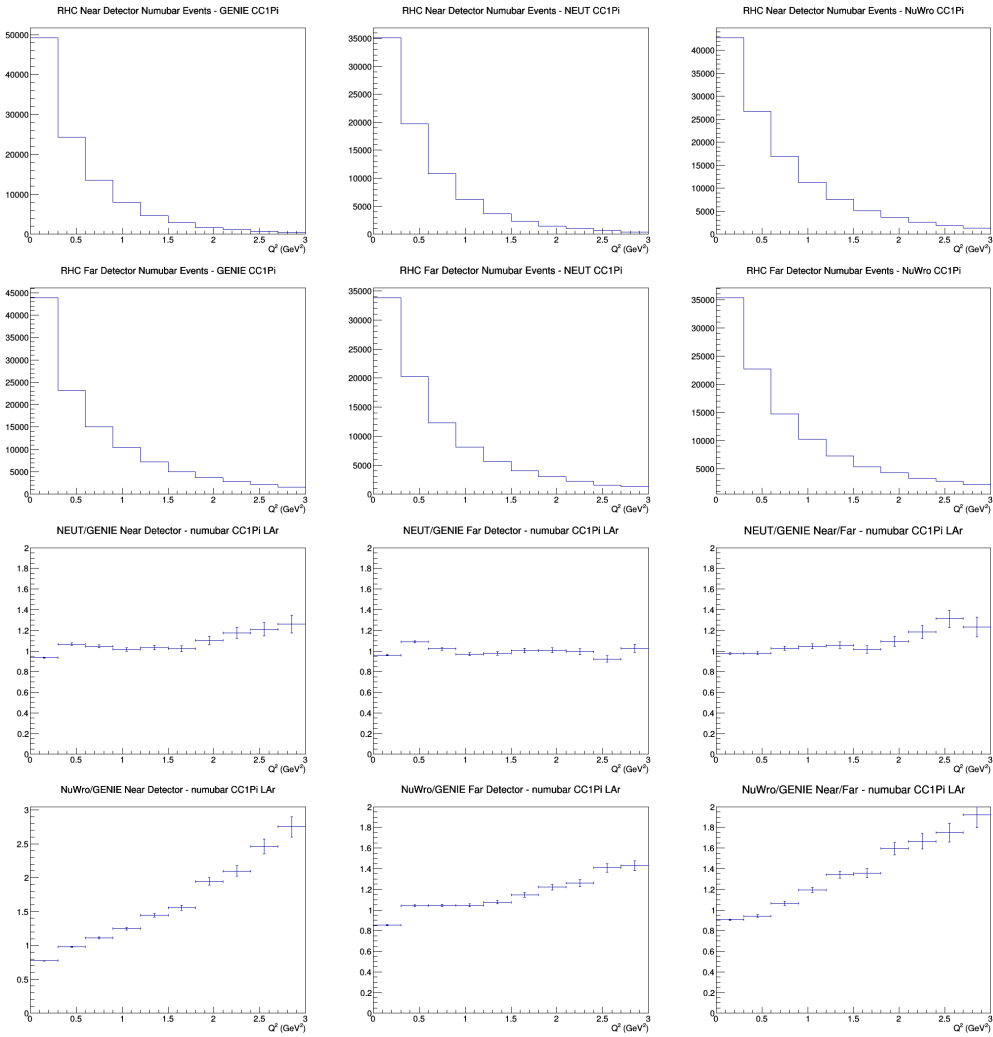
A.29 numubar CC1Pi no efficiencies



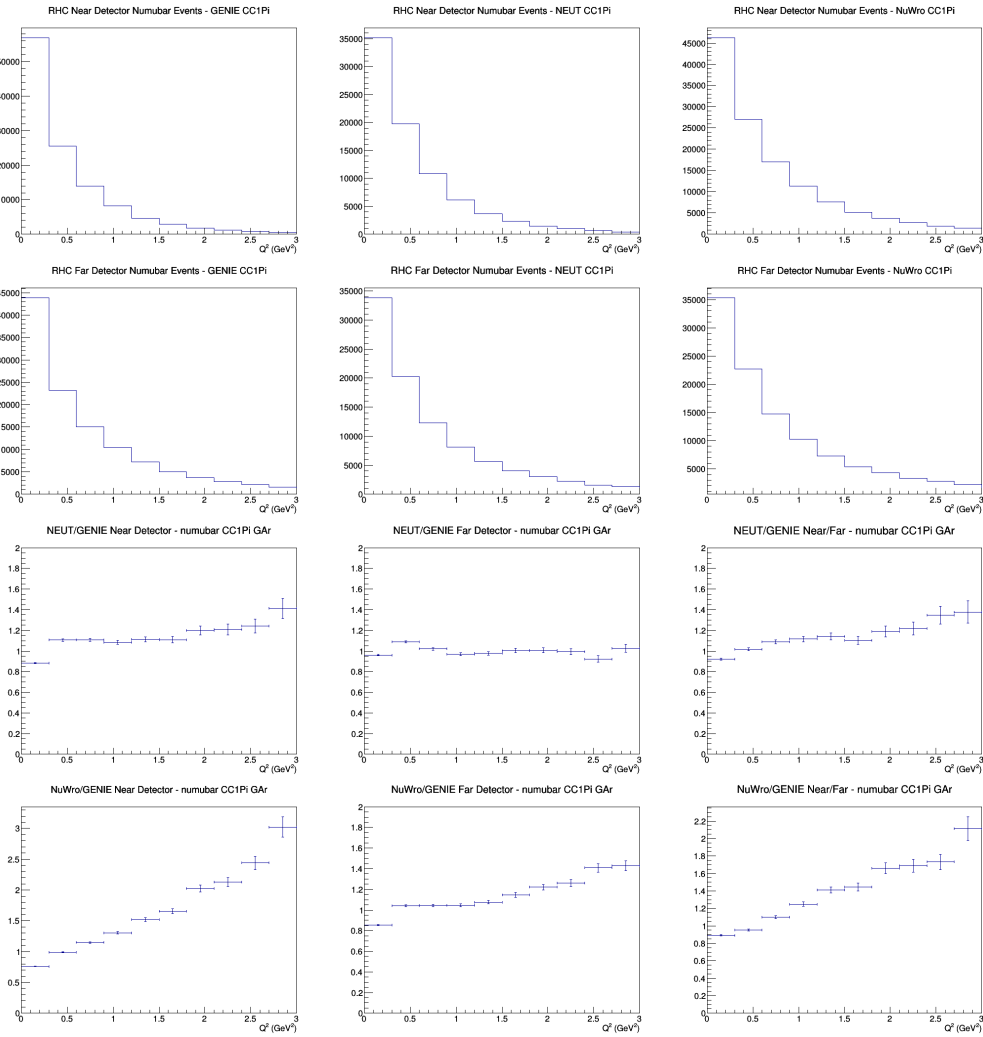
A.30 numubar CC1Pi FGT efficiencies



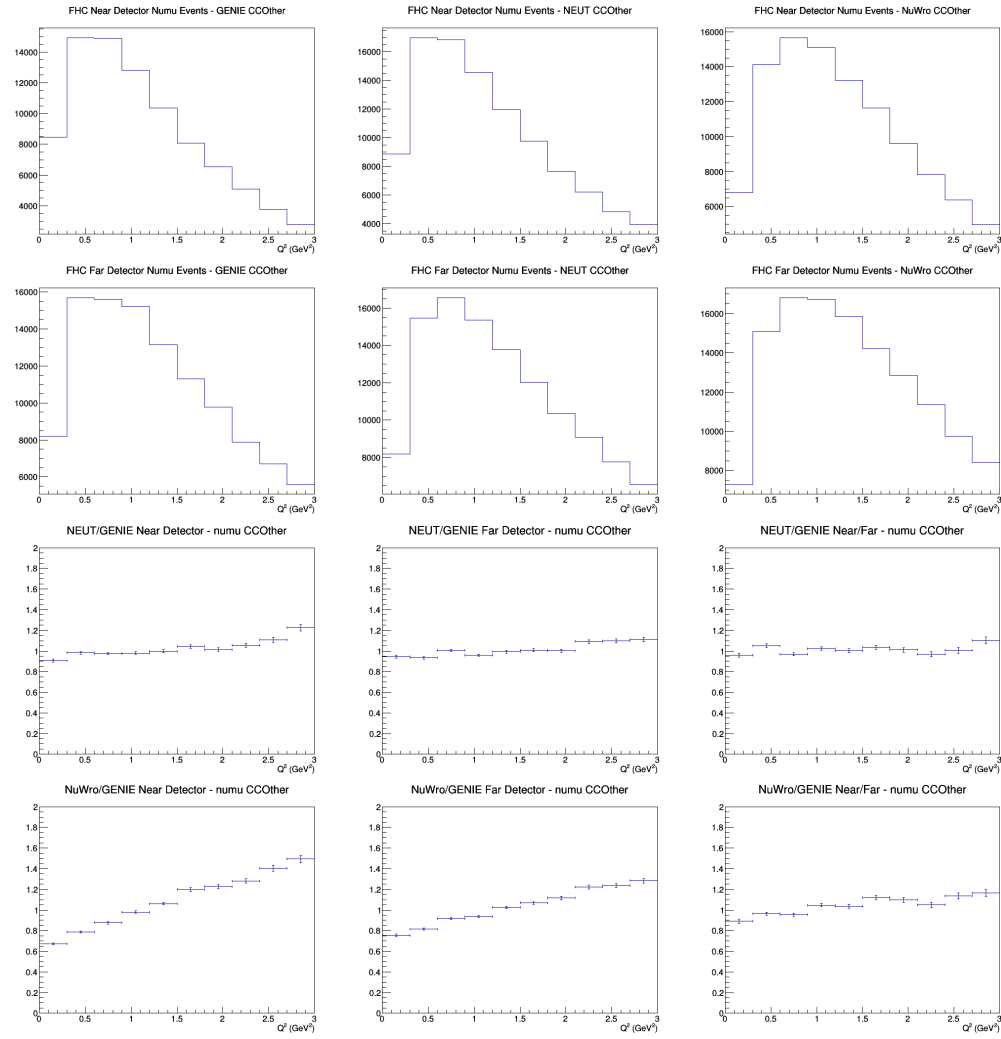
A.31 numubar CC1Pi LAr efficiencies



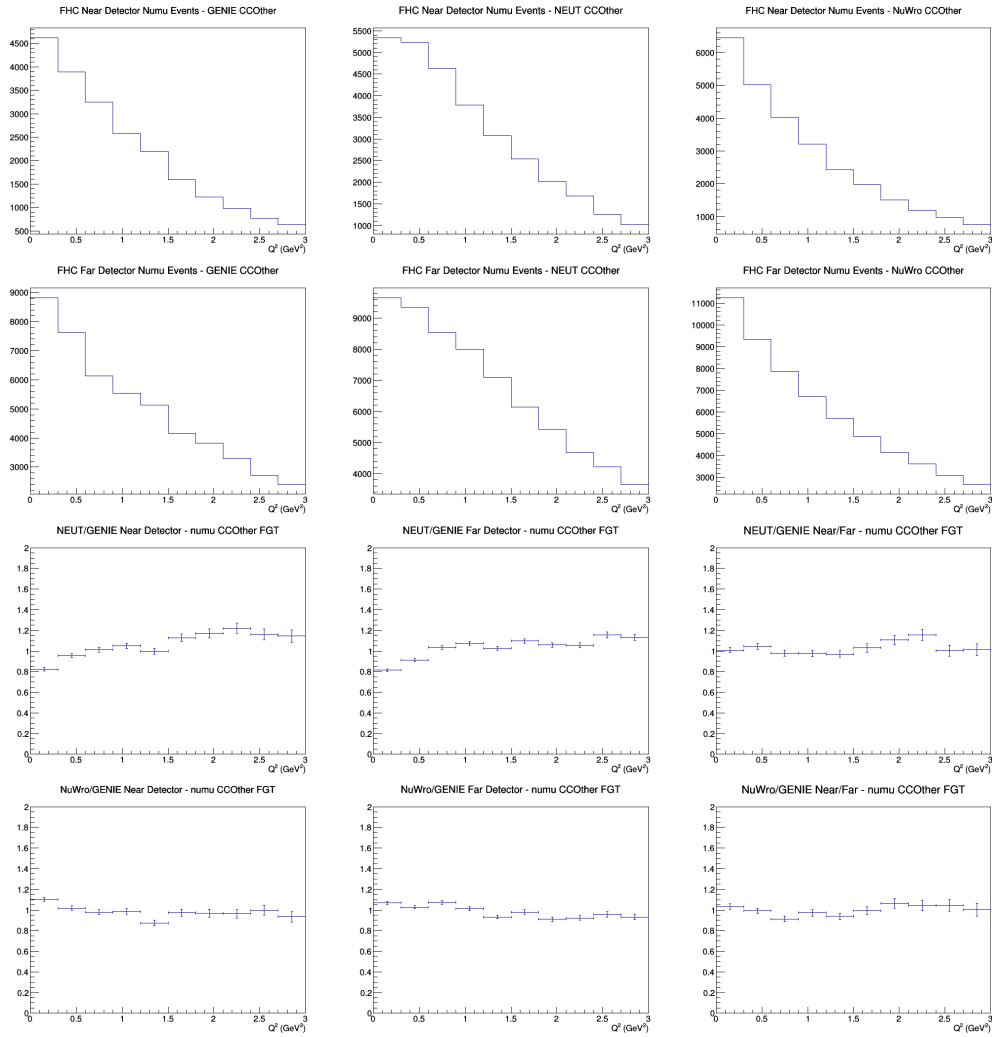
A.32 numubar CC1Pi GAr efficiencies



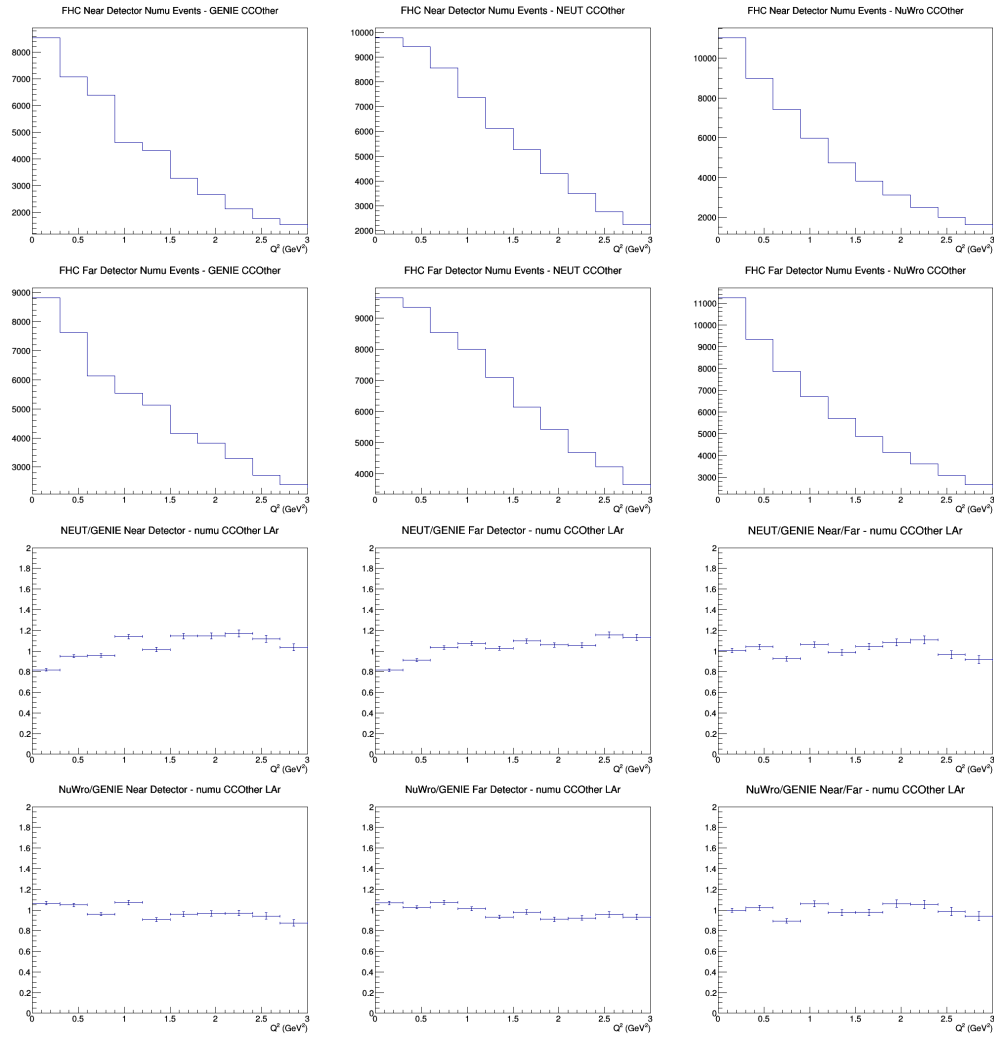
A.33 numu CCOther no efficiencies



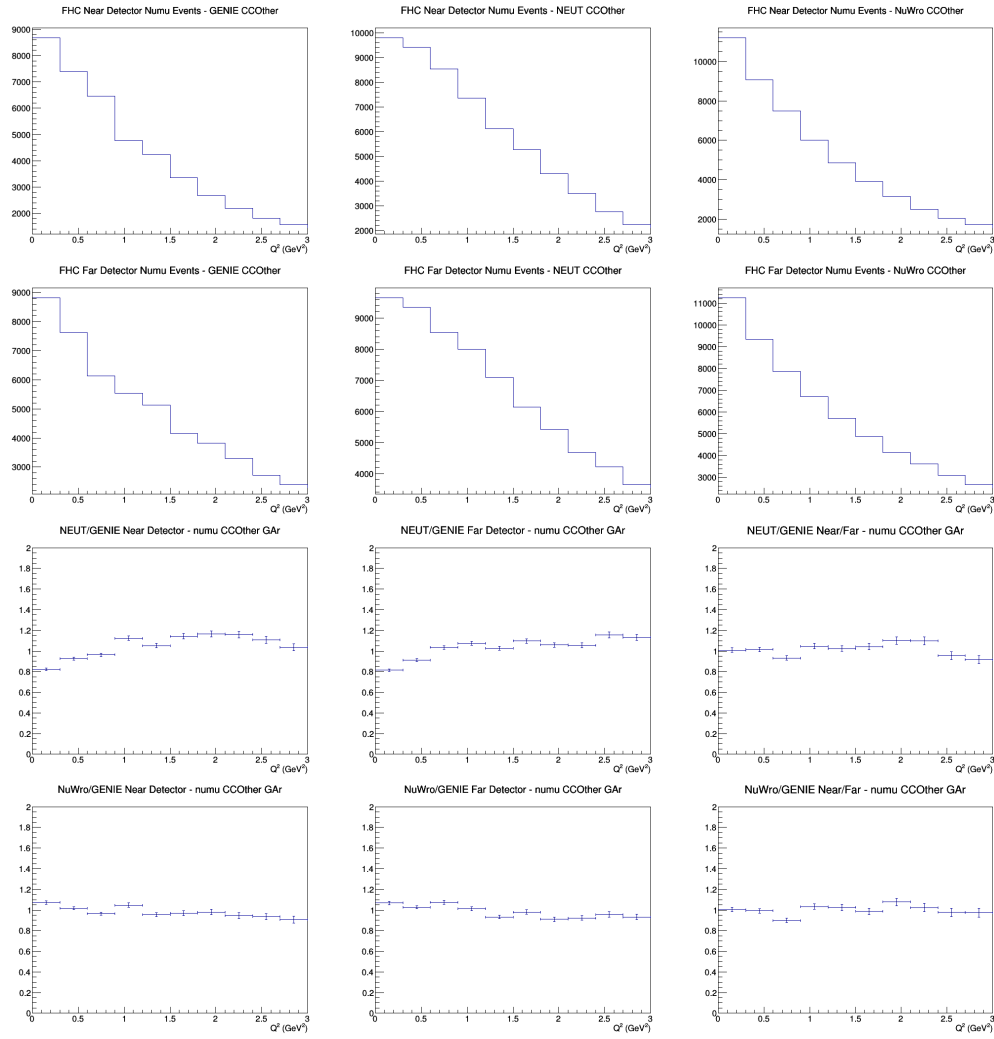
A.34 numu CCOther FGT efficiencies



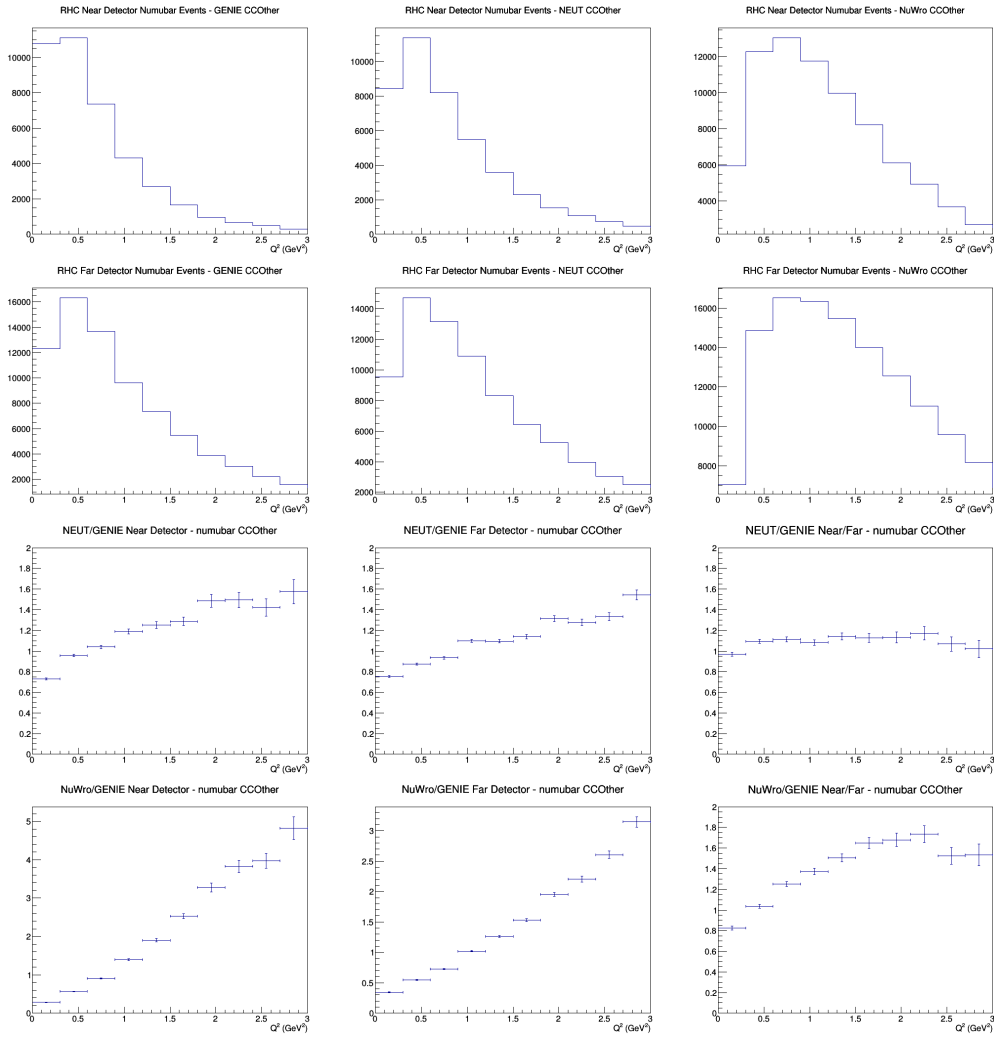
A.35 numu CCOther LAr efficiencies



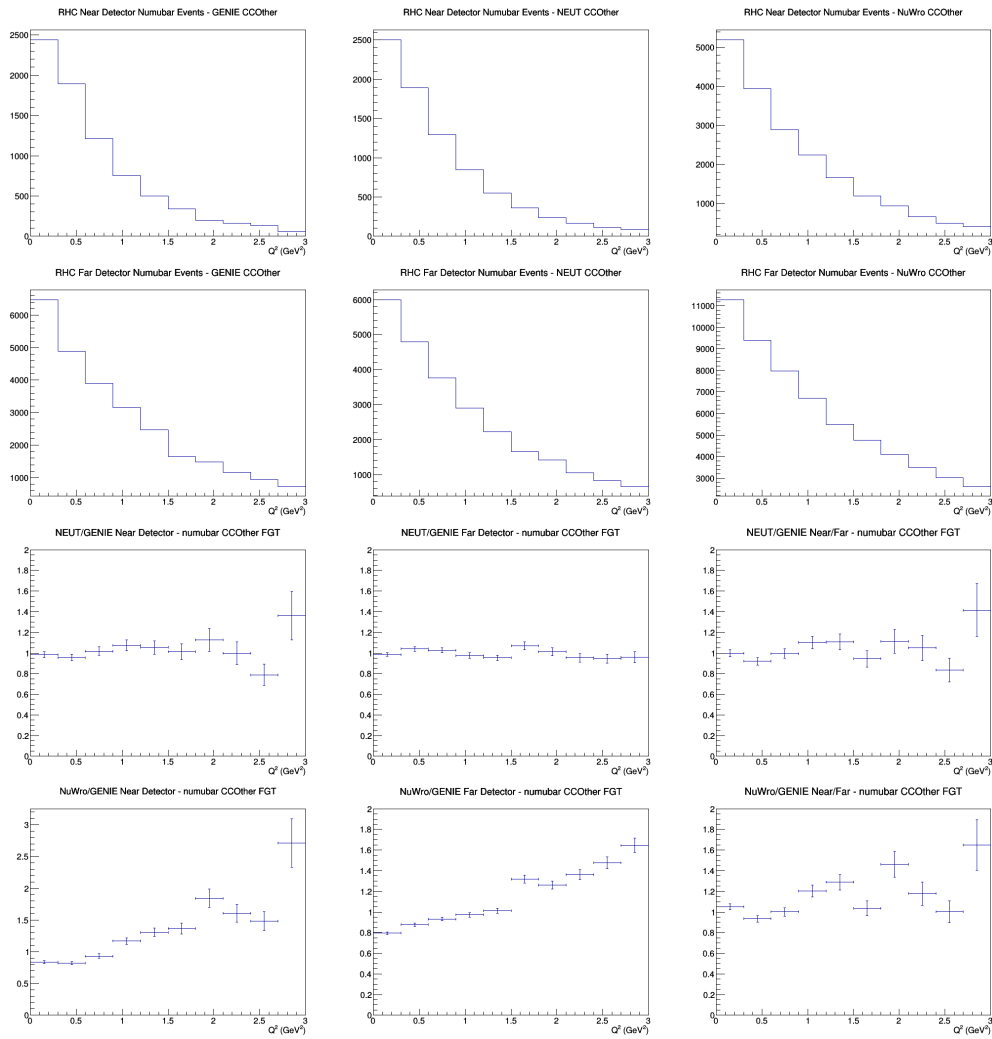
A.36 numu CCOther GAr efficiencies



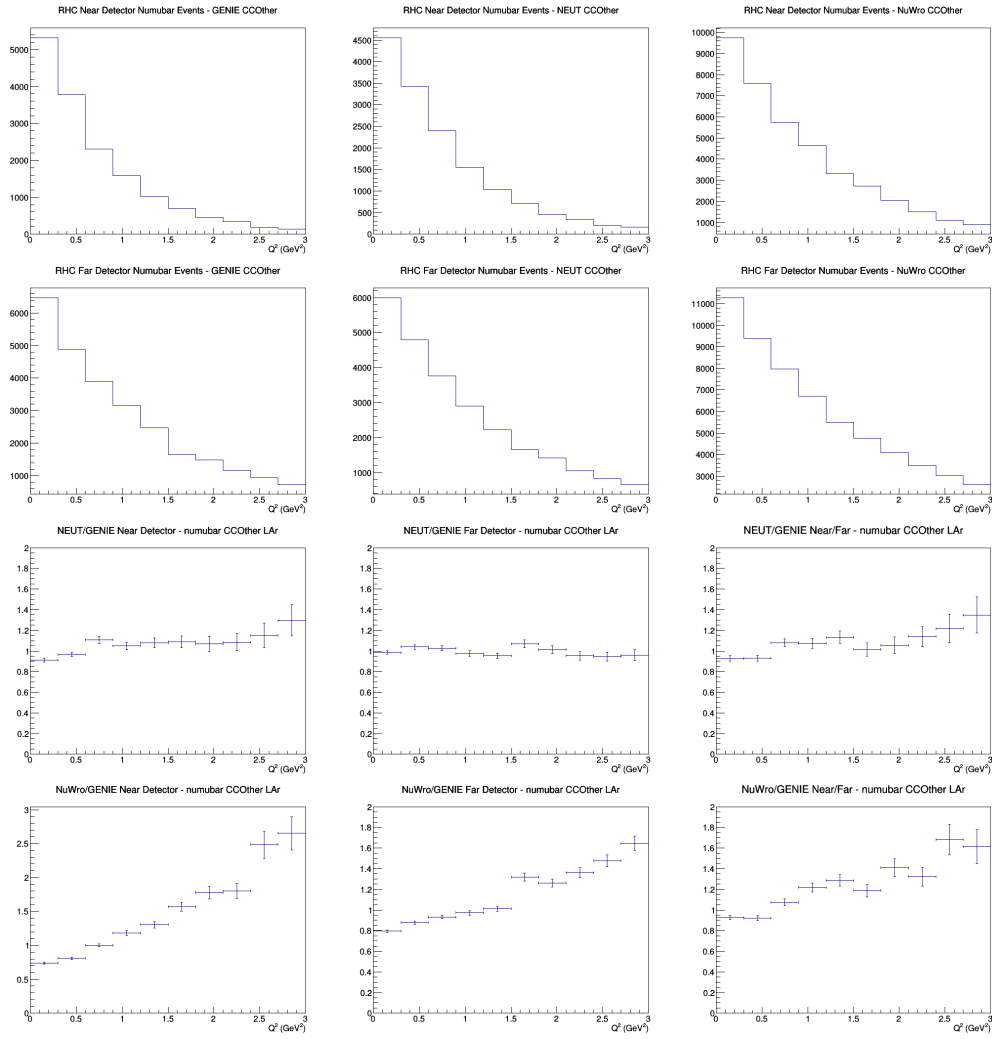
A.37 numubar CCOther no efficiencies



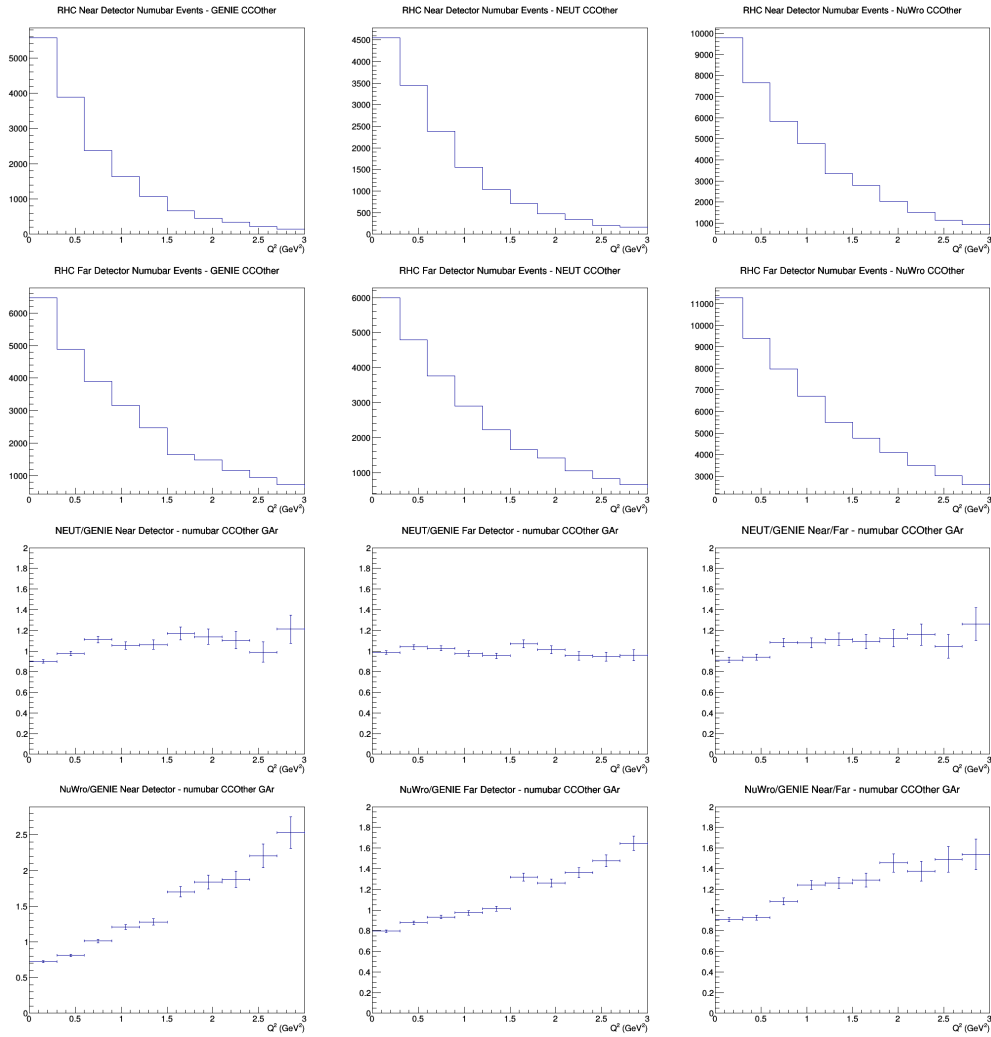
A.38 numubar CCOther FGT efficiencies



A.39 numubar CCOther LAr efficiencies



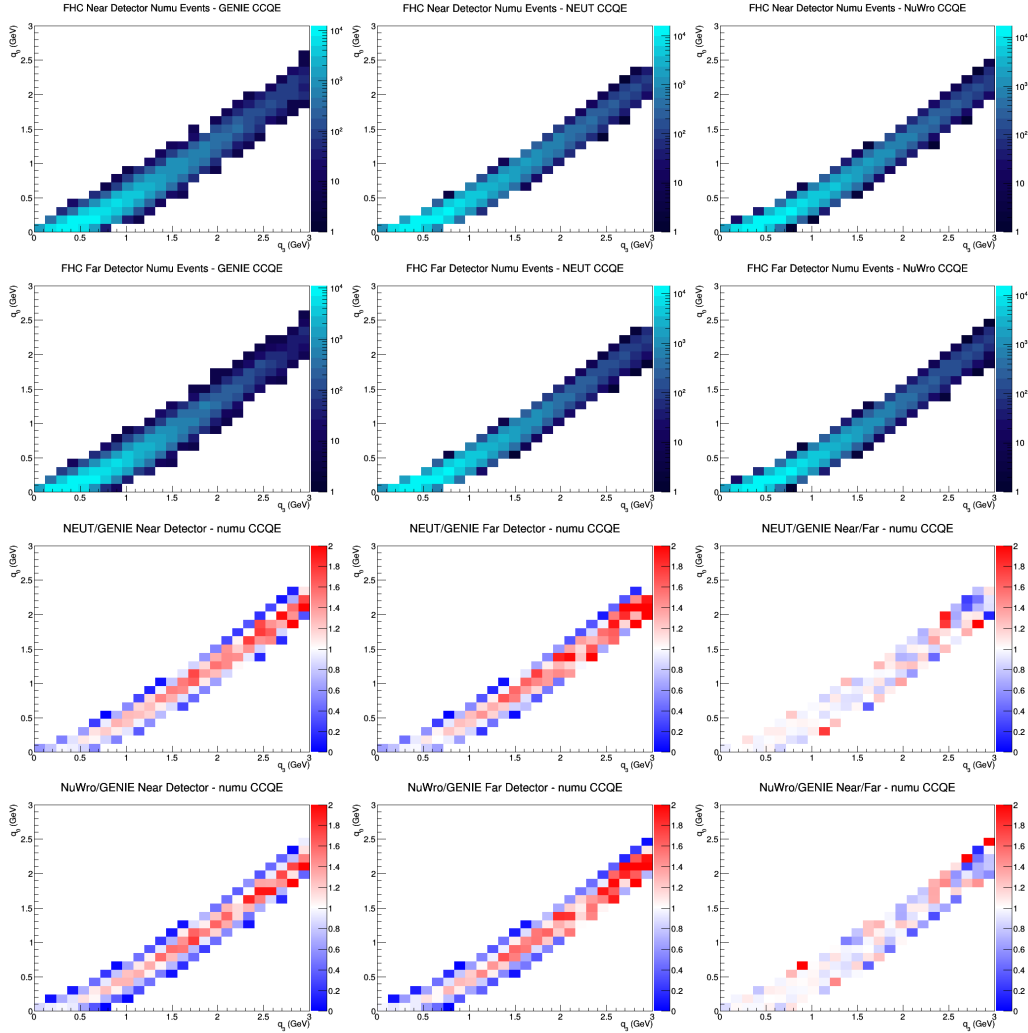
A.40 numubar CCOther GAr efficiencies



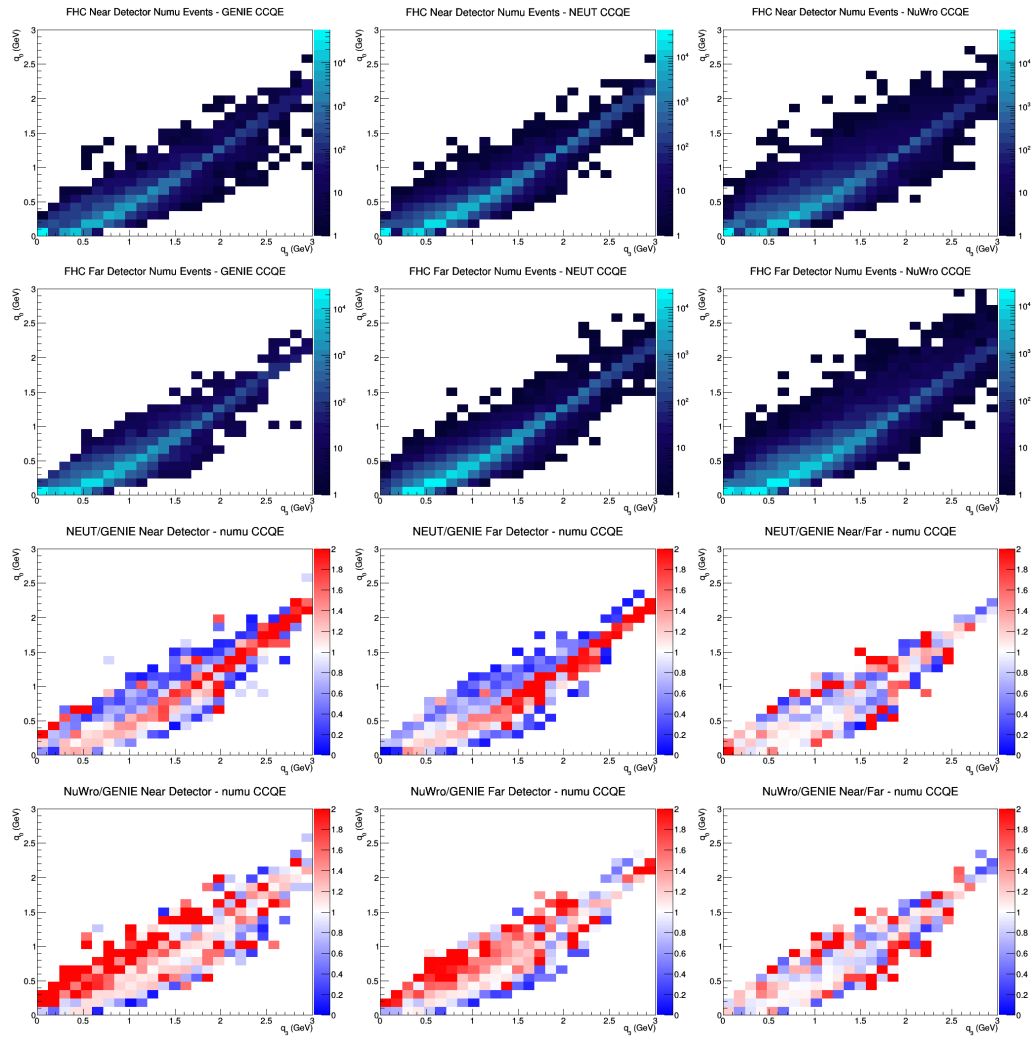
B q_0 vs. q_3 Plots

This appendix includes all the plots not show in Section 3.2. For full description of the files, please make reference to that section. The plots will be put in the same order as before.

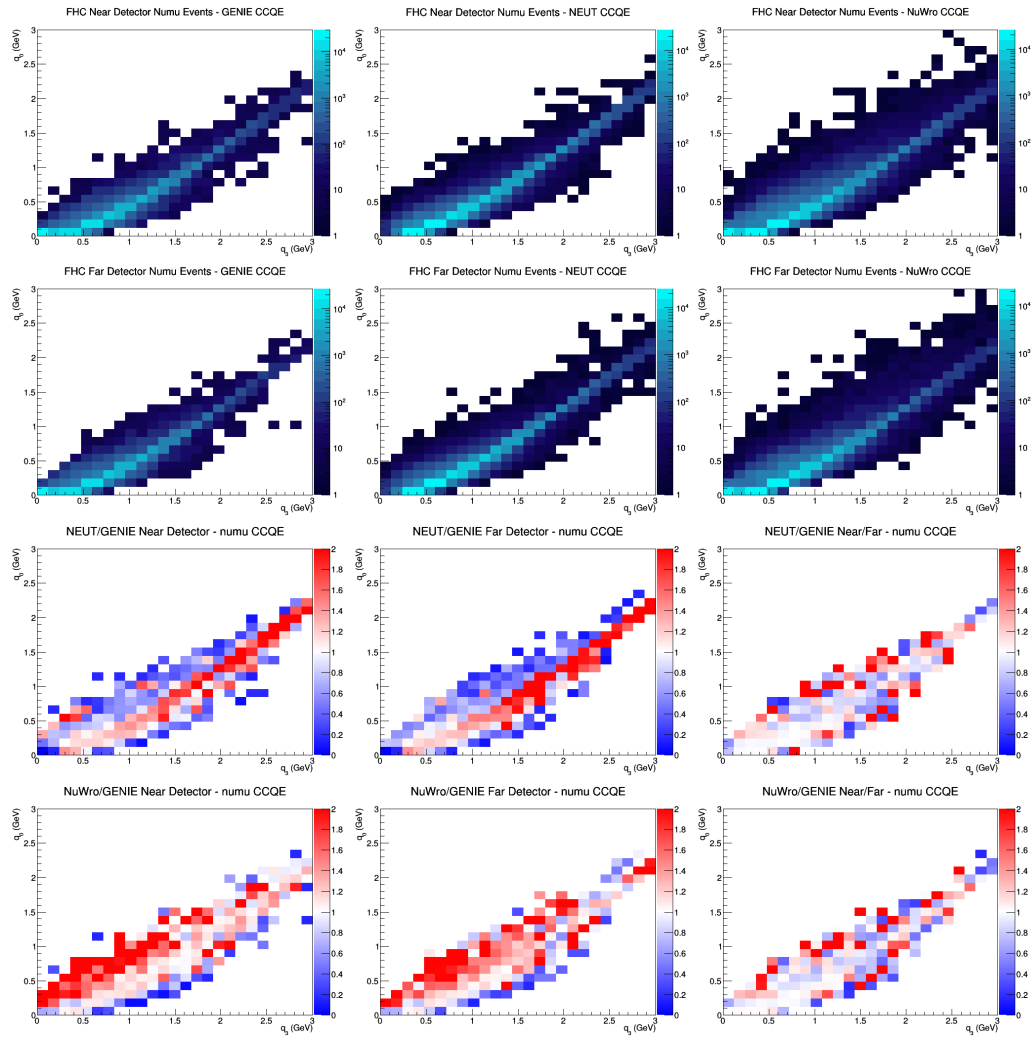
B.1 numu CCQE no efficiencies



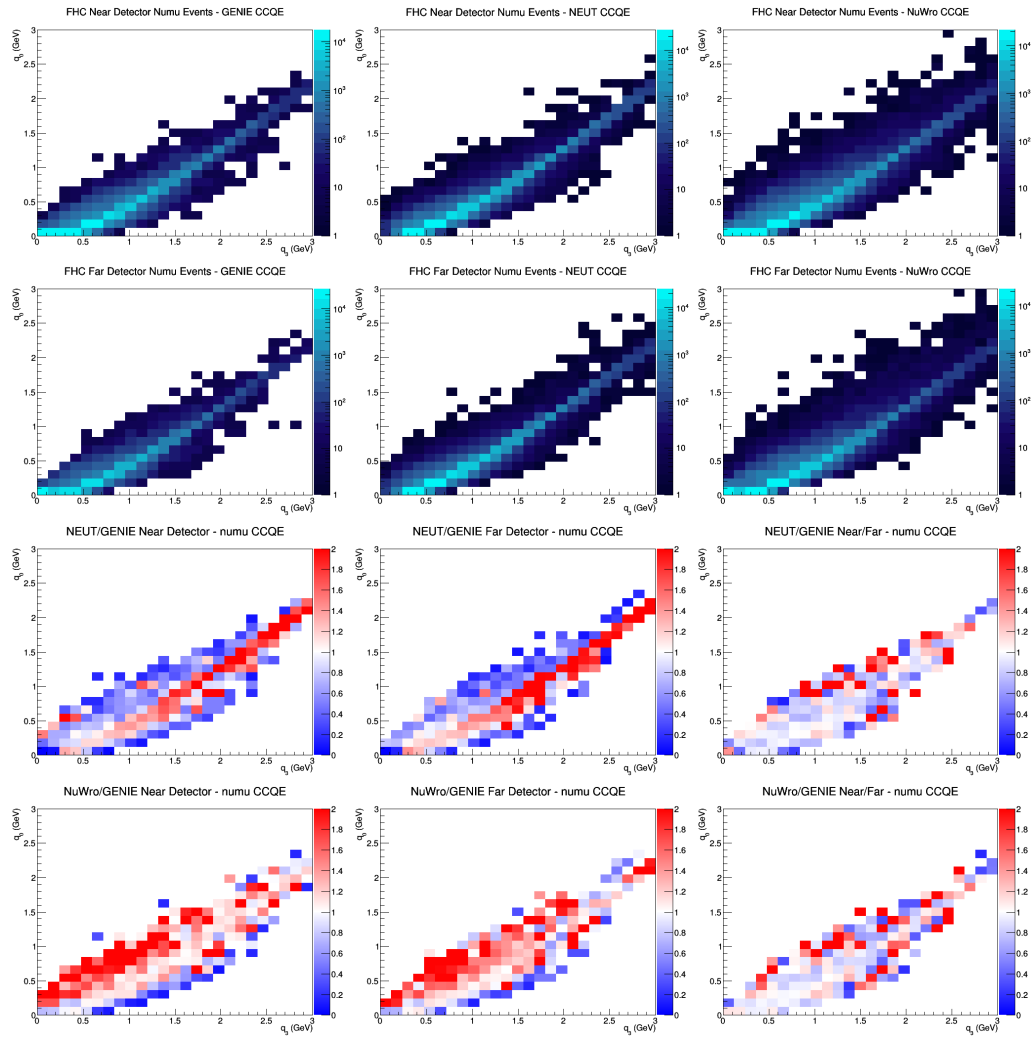
B.2 numu CCQE FGT efficiencies



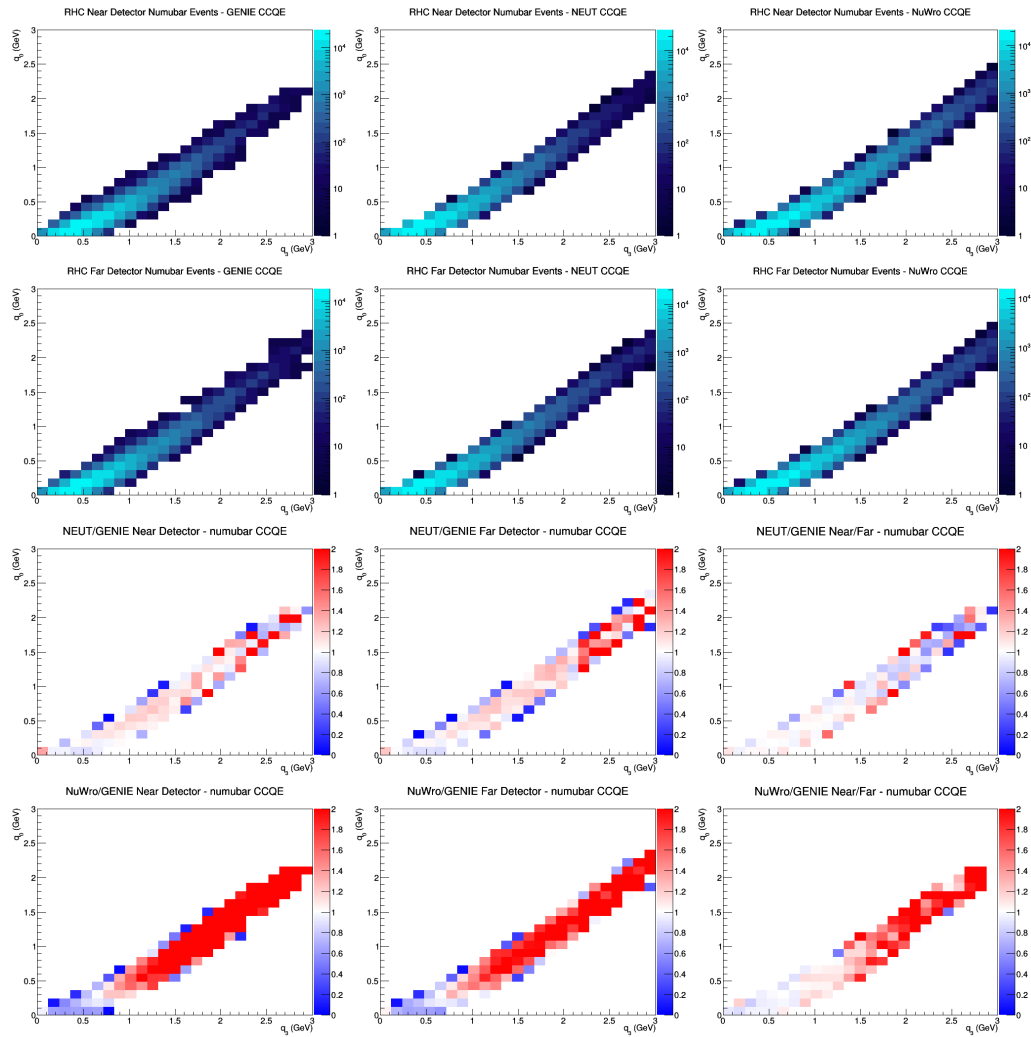
B.3 numu CCQE LAr efficiencies



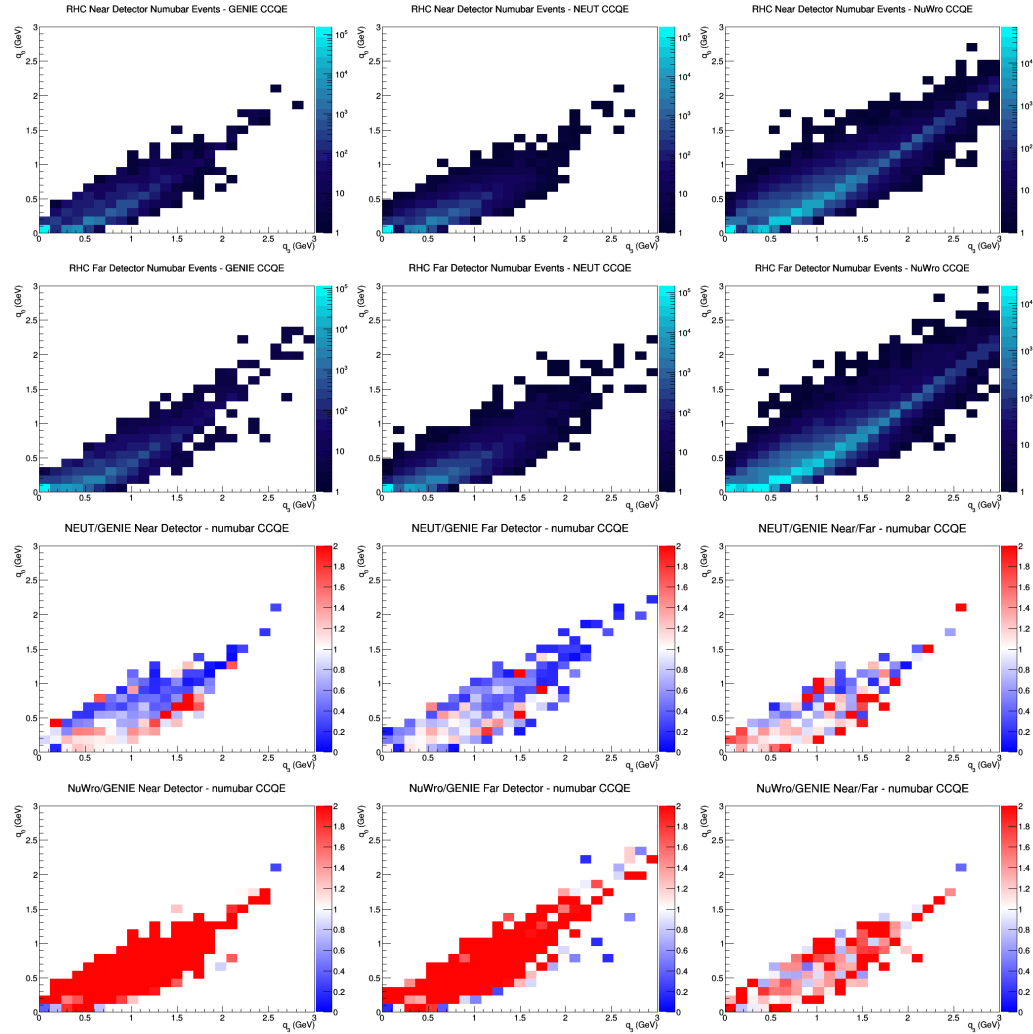
B.4 numu CCQE GAr efficiencies



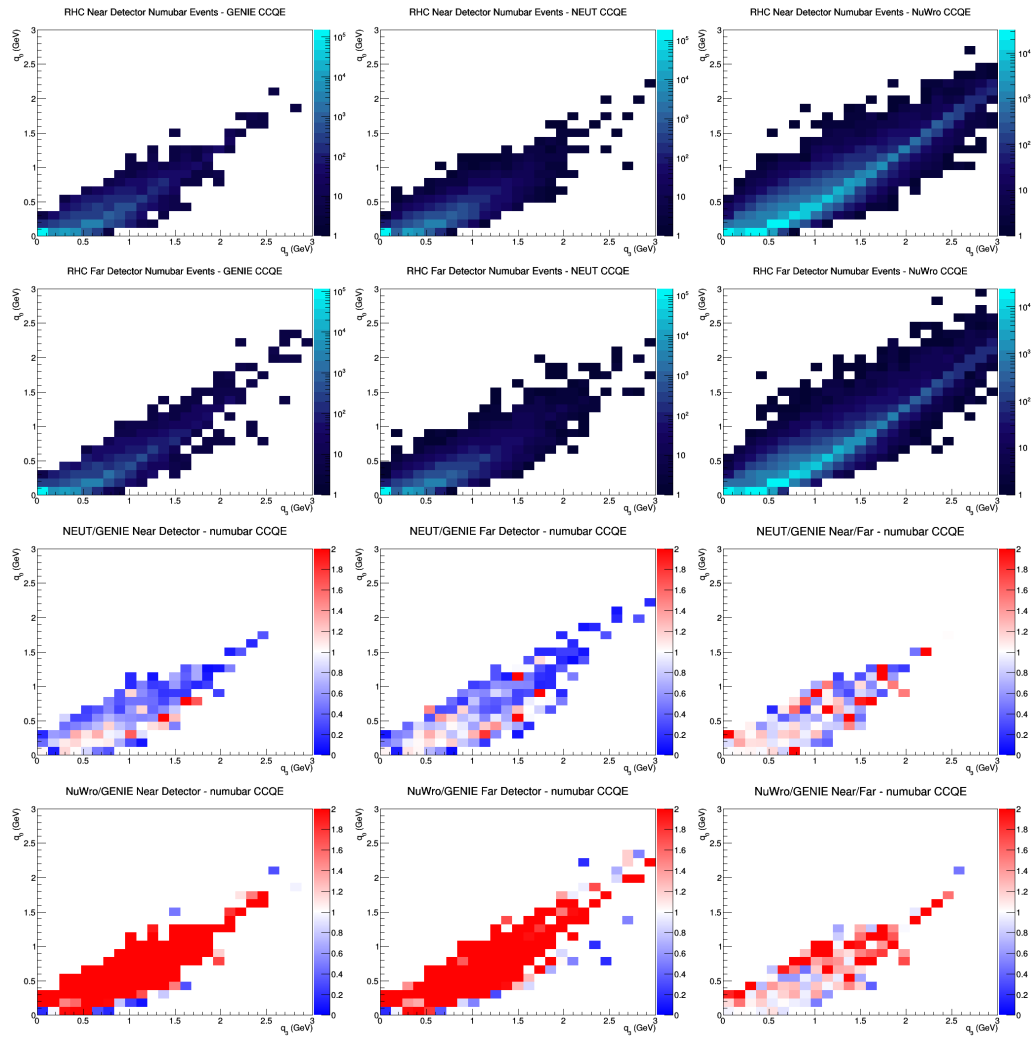
B.5 numubar CCQE no efficiencies



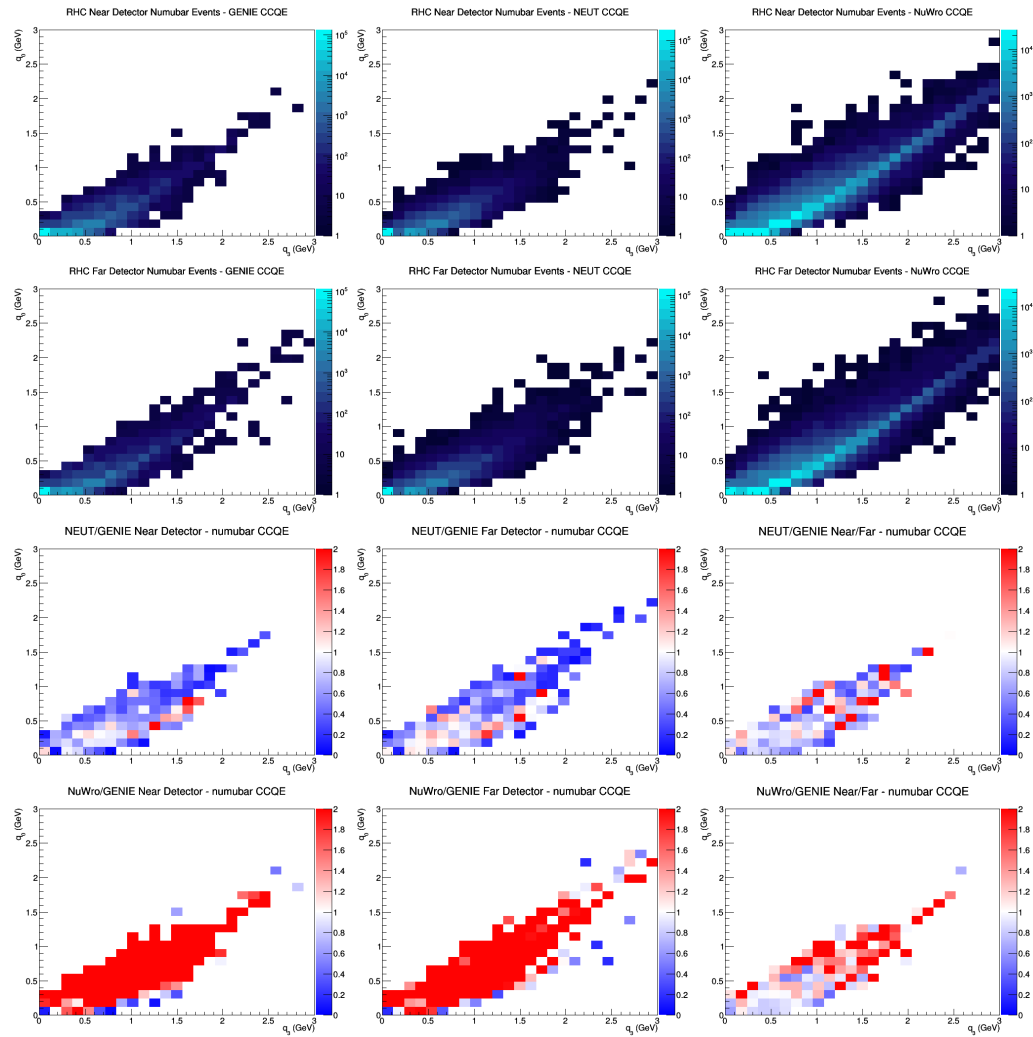
B.6 numubar CCQE FGT efficiencies



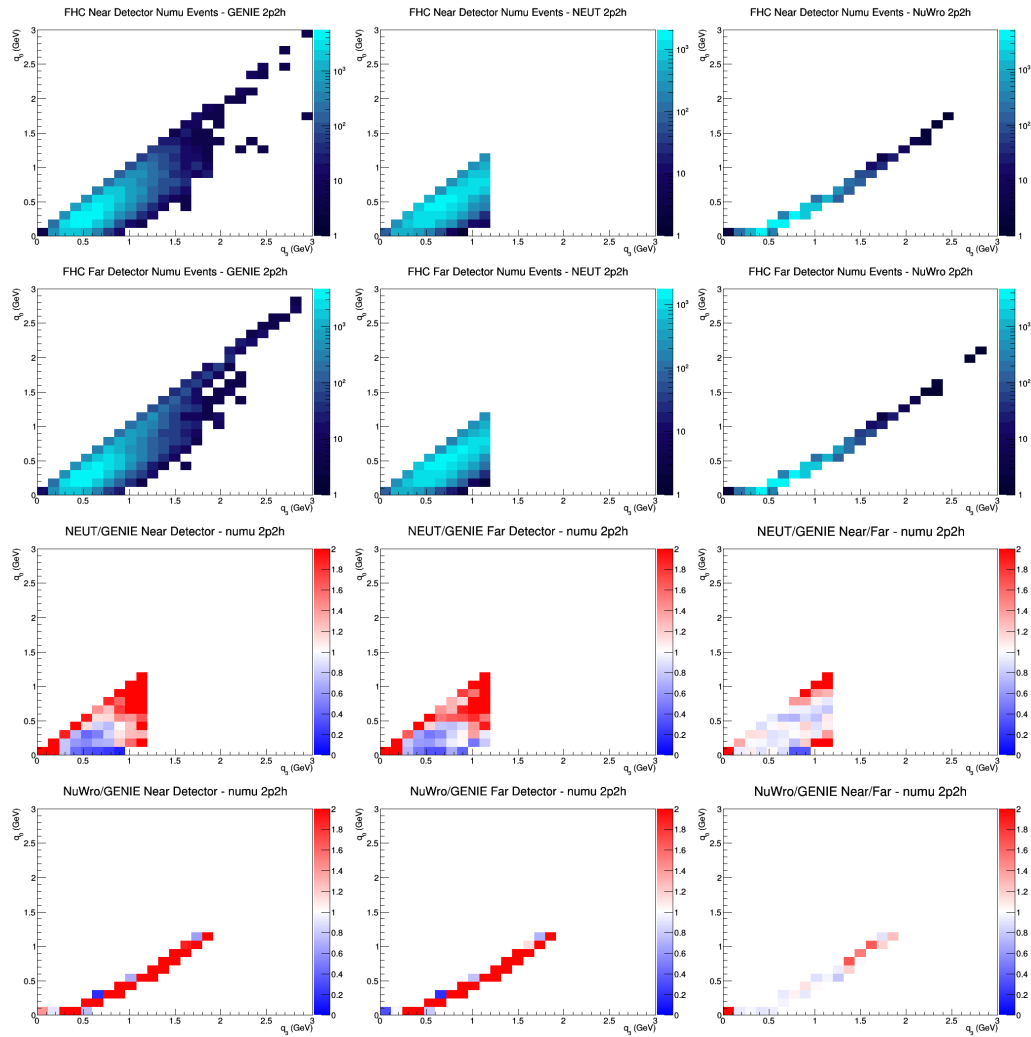
B.7 numubar CCQE LAr efficiencies



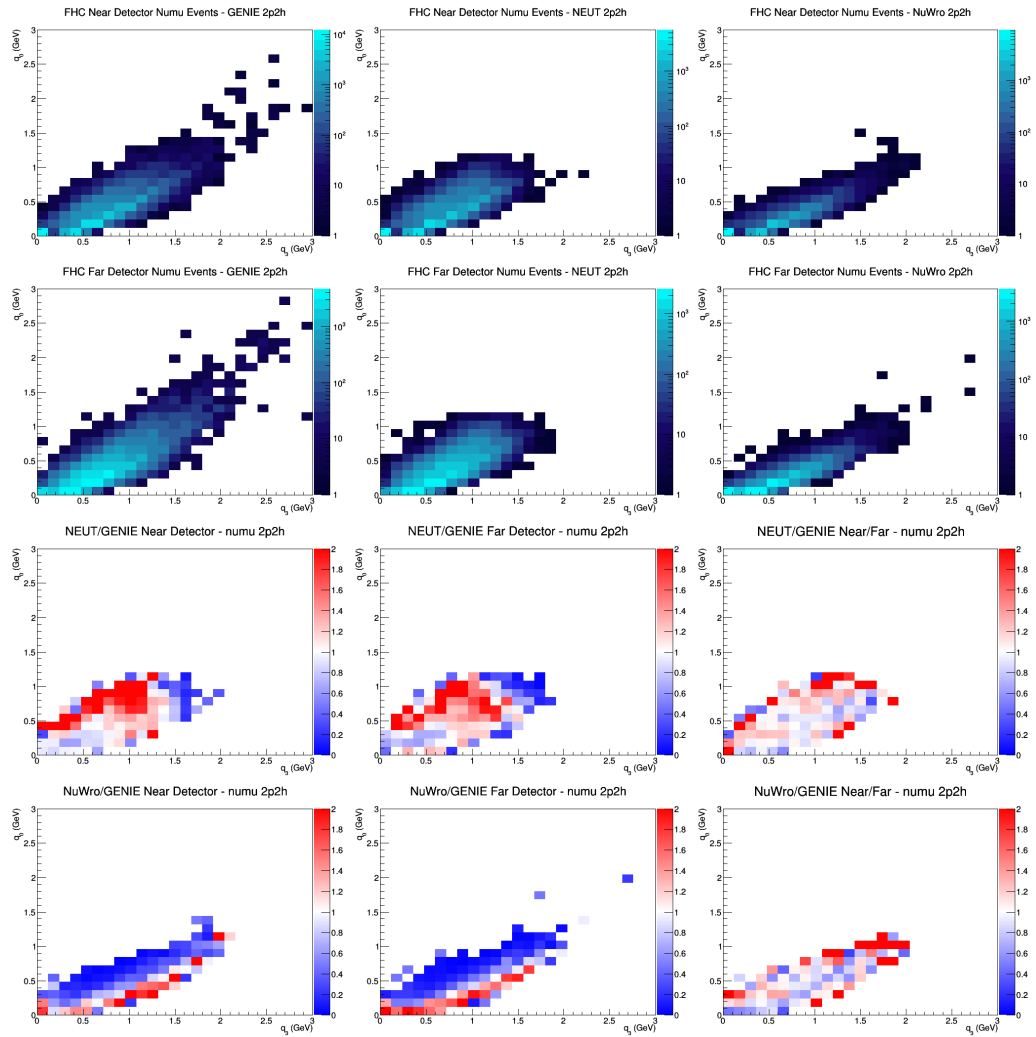
B.8 numubar CCQE GAr efficiencies



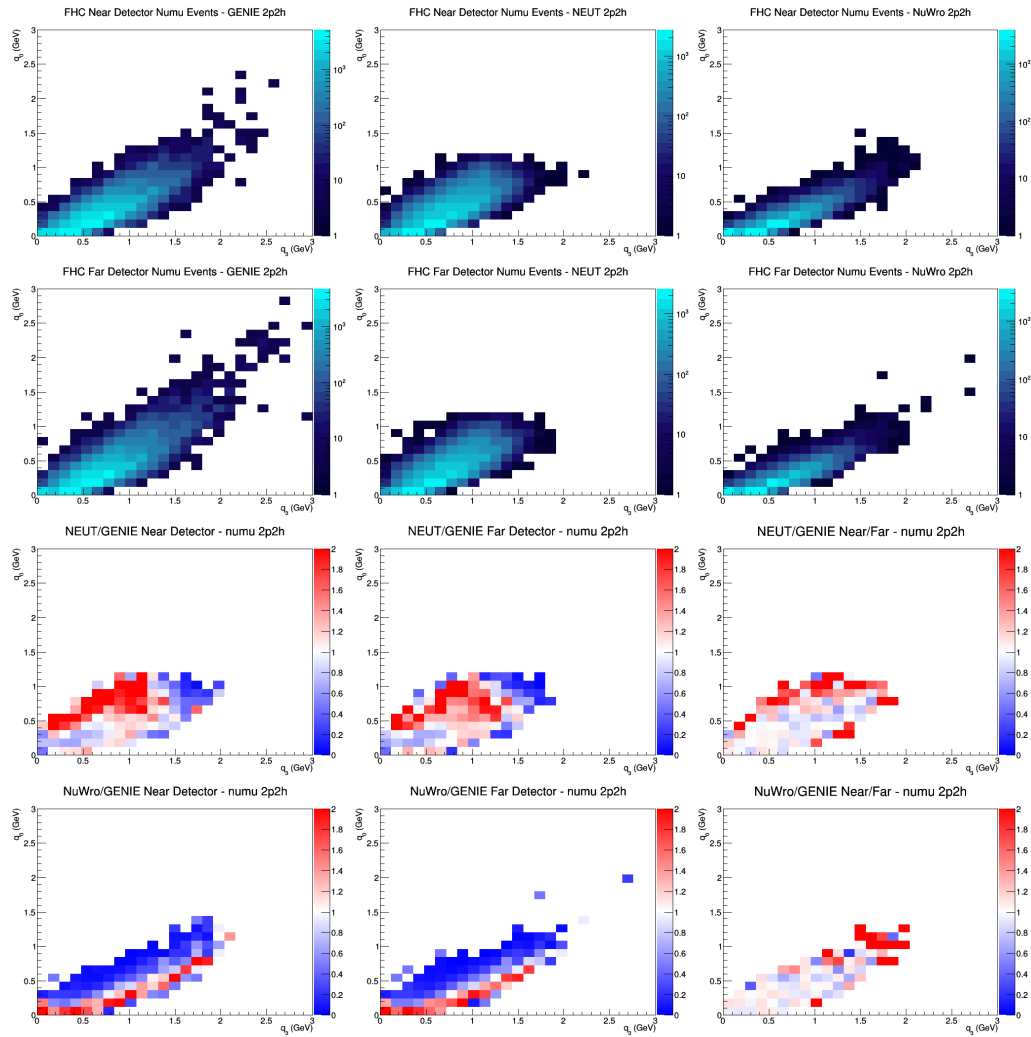
B.9 numu 2p2h no efficiencies



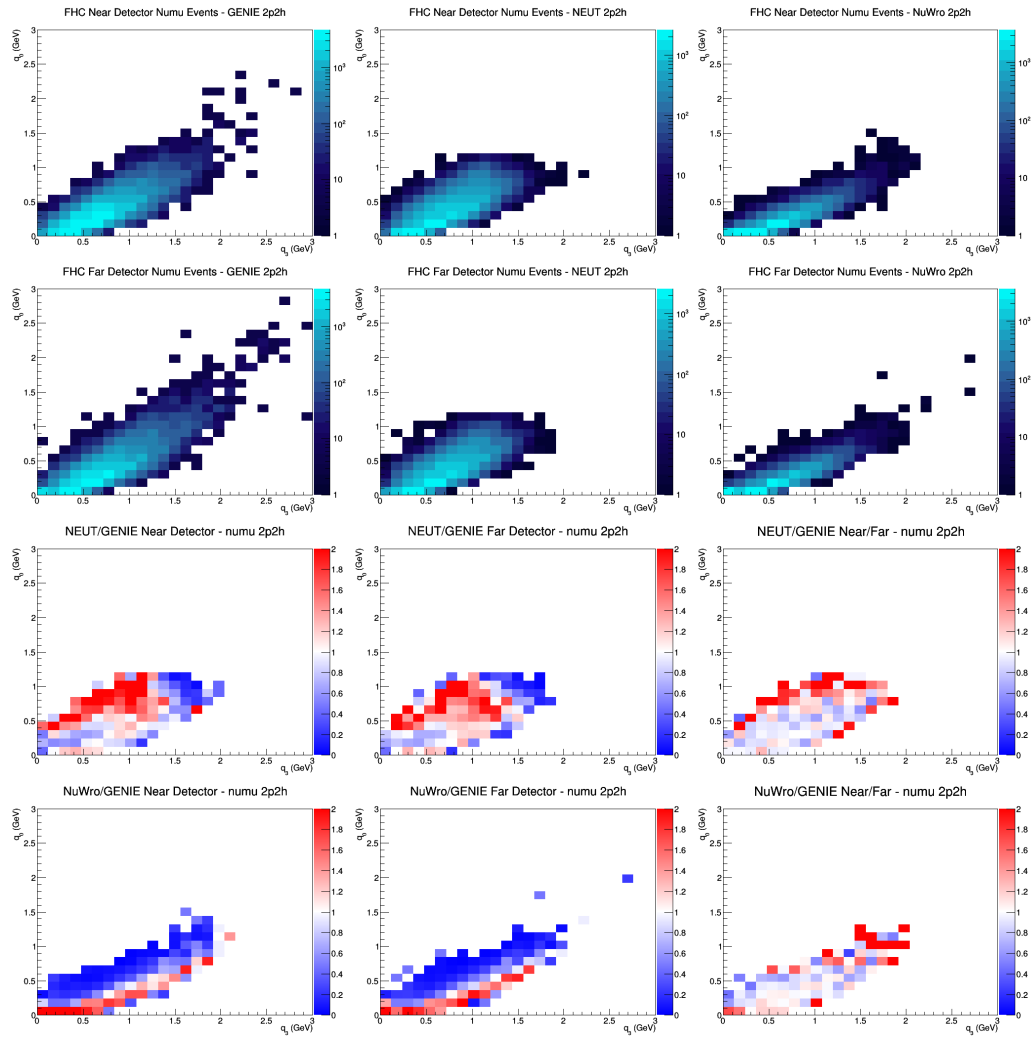
B.10 numu 2p2h FGT efficiencies



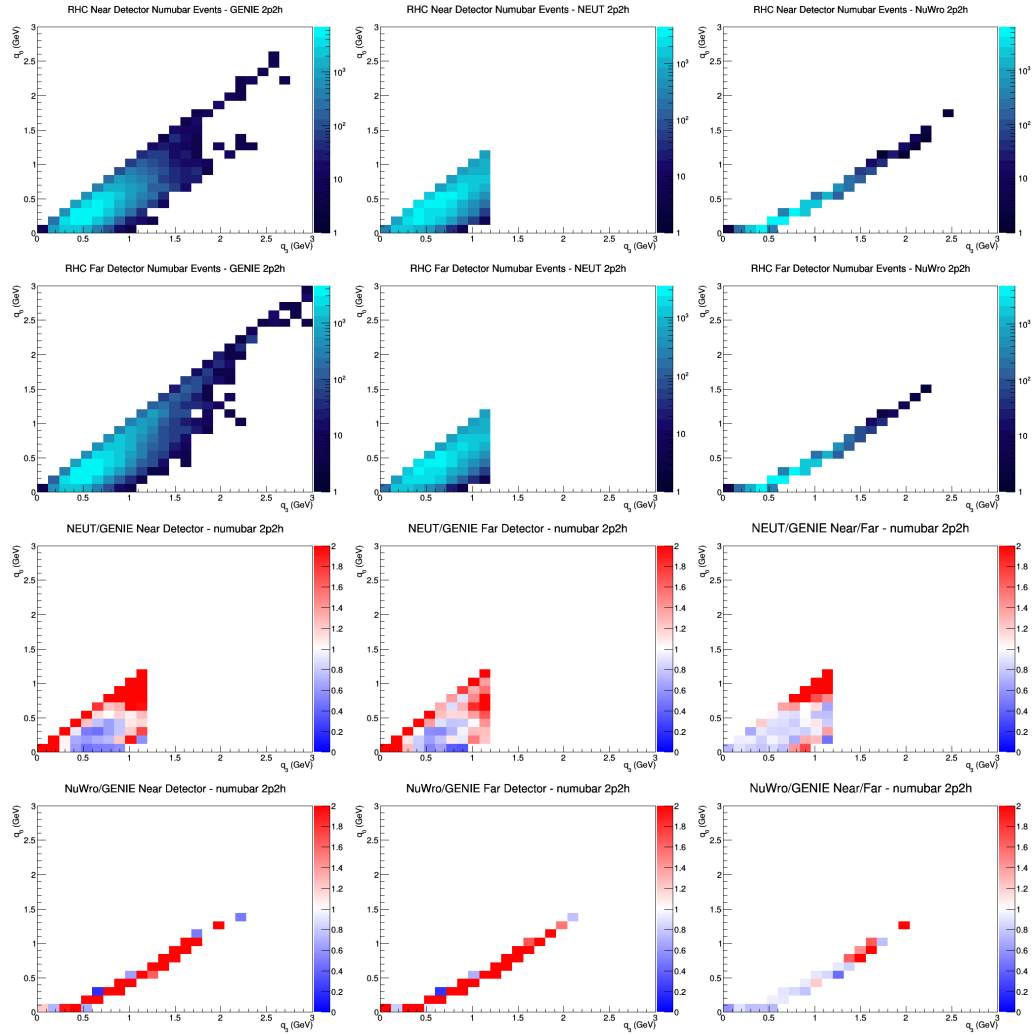
B.11 numu 2p2h LAr efficiencies



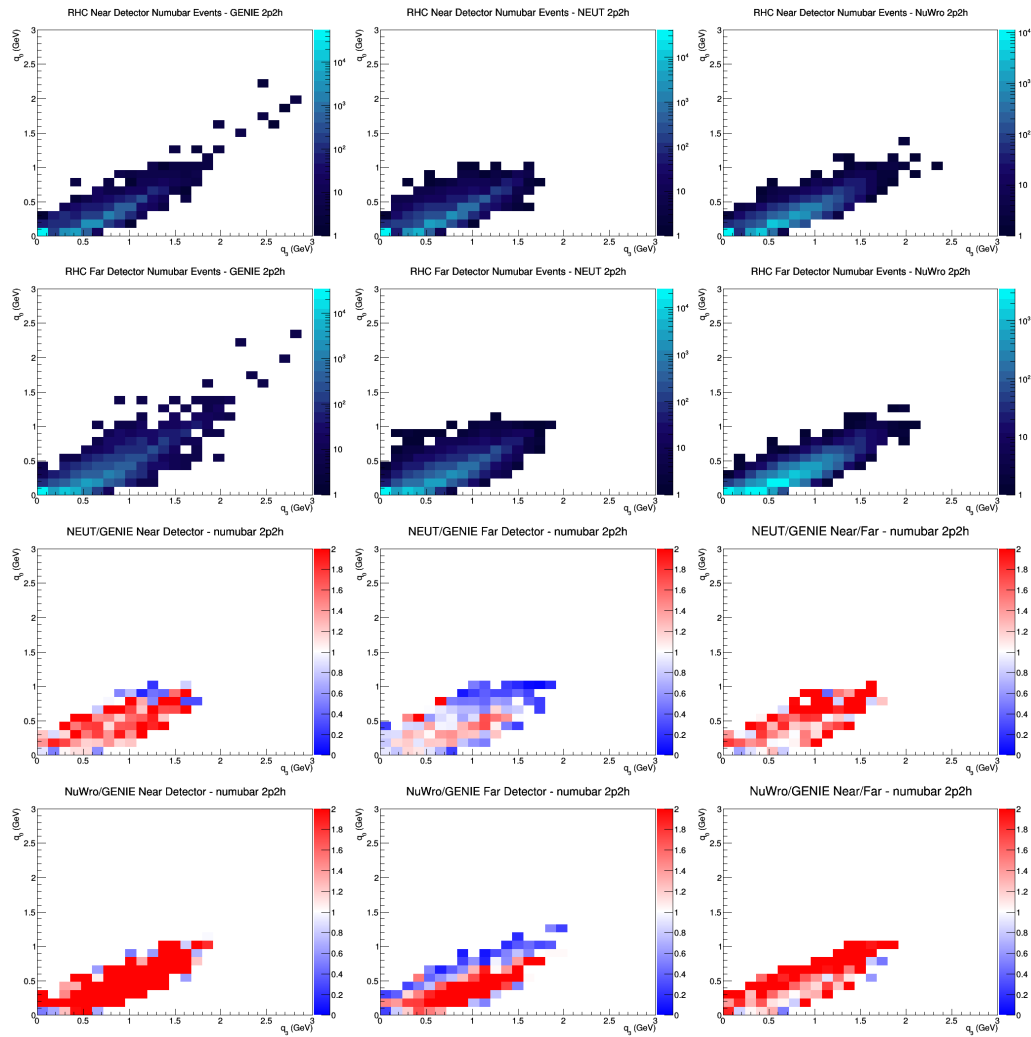
B.12 numu 2p2h GAr efficiencies



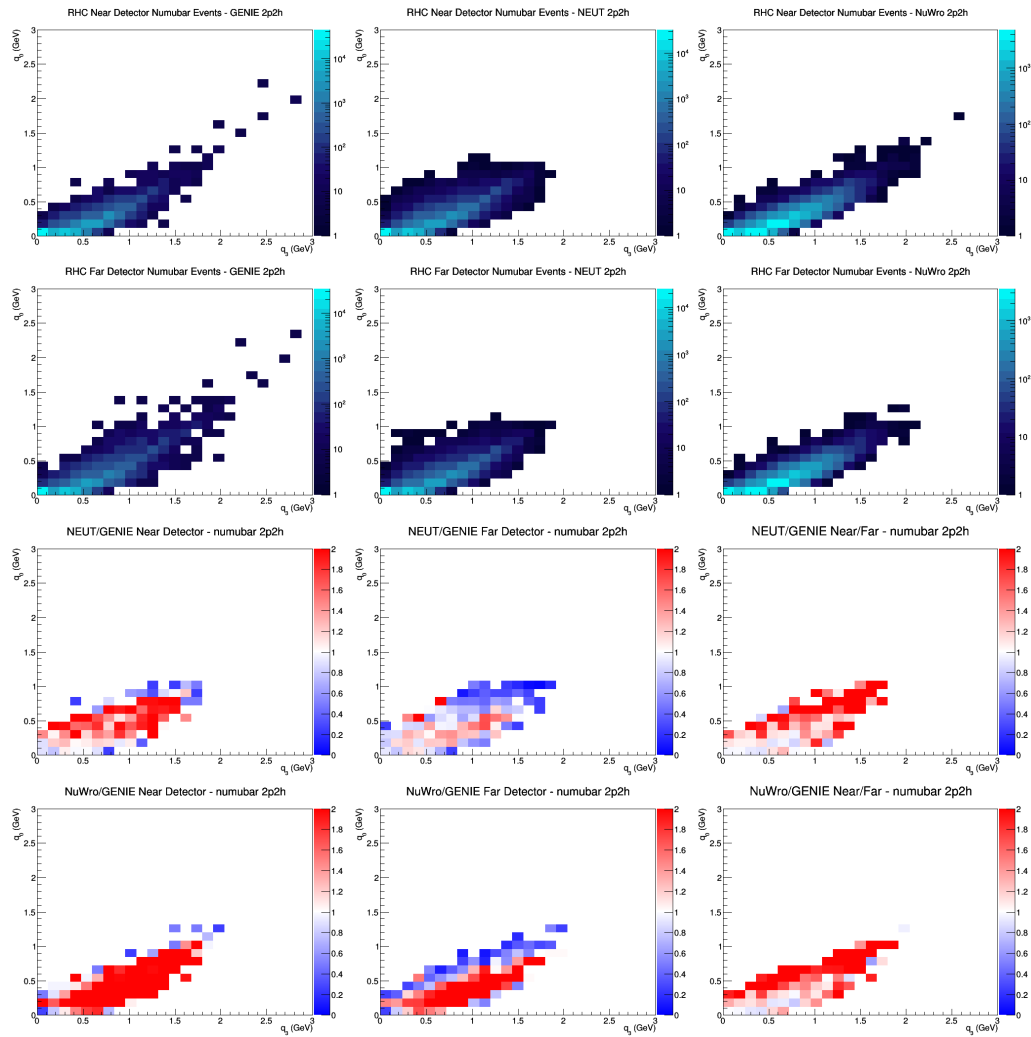
B.13 numubar 2p2h no efficiencies



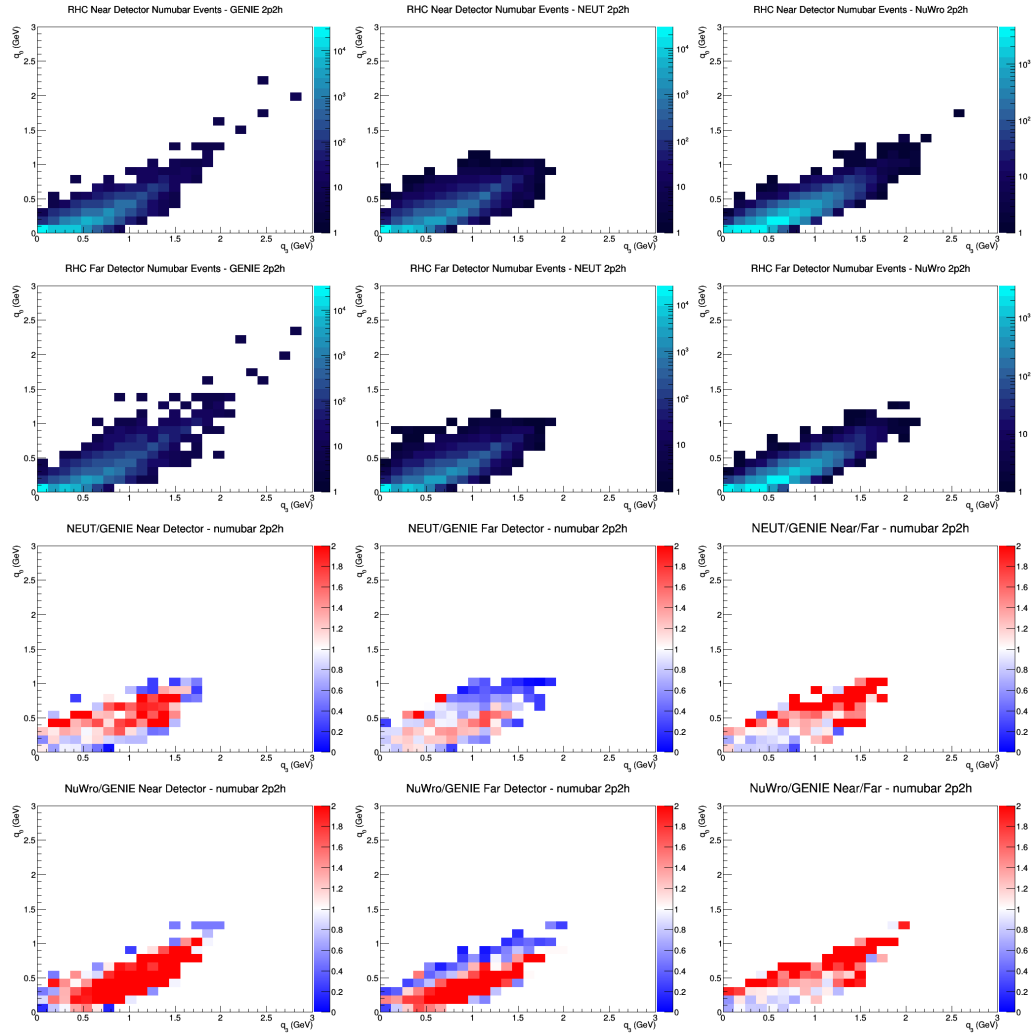
B.14 numubar 2p2h FGT efficiencies



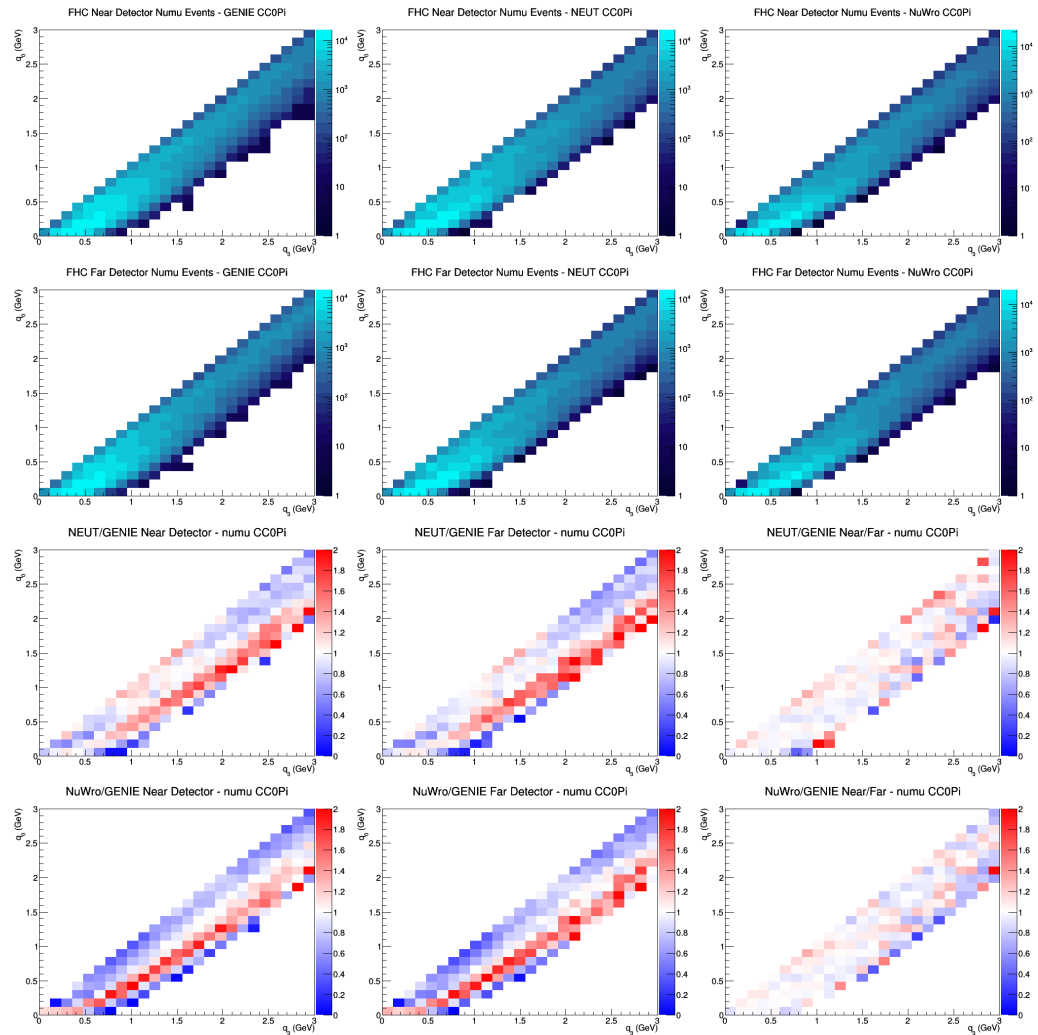
B.15 numubar 2p2h LAr efficiencies



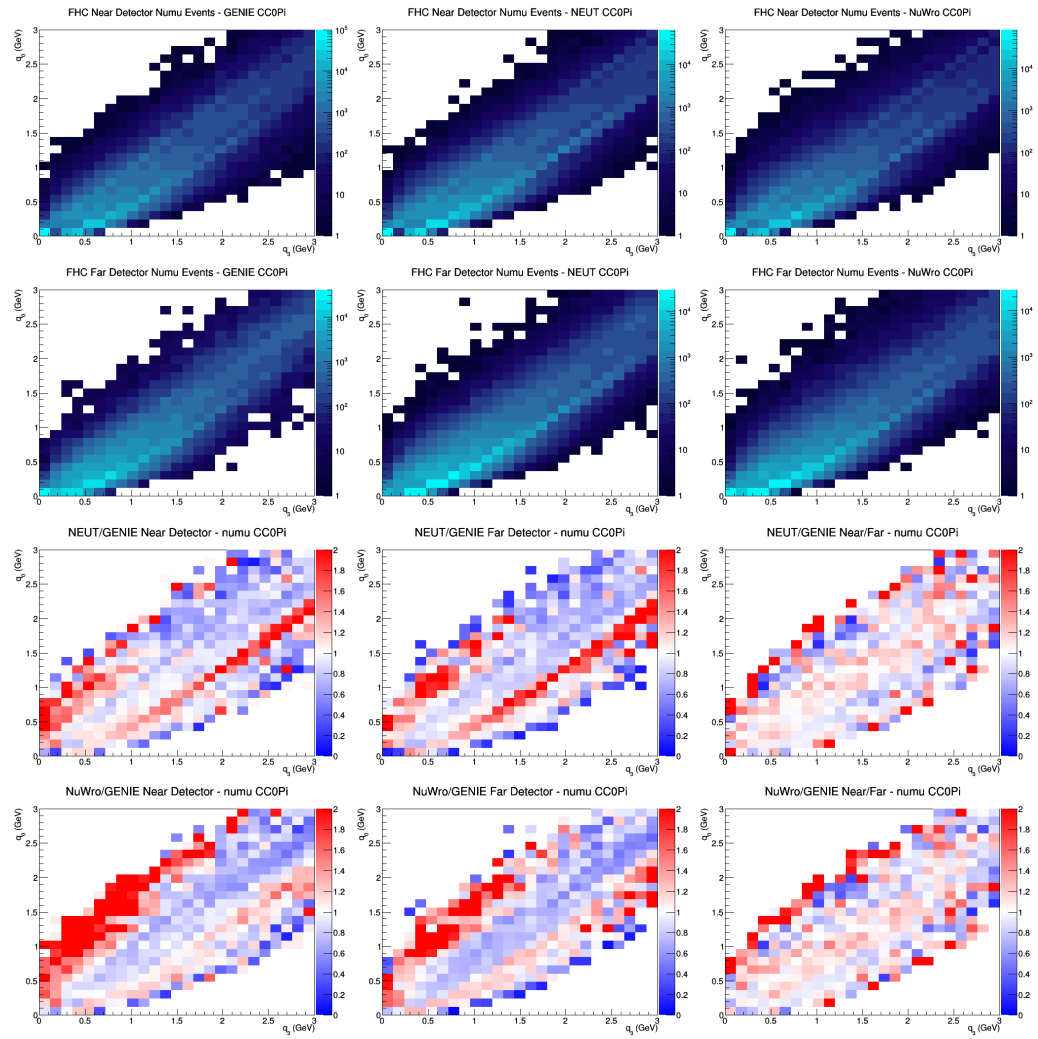
B.16 numubar 2p2h GAr efficiencies



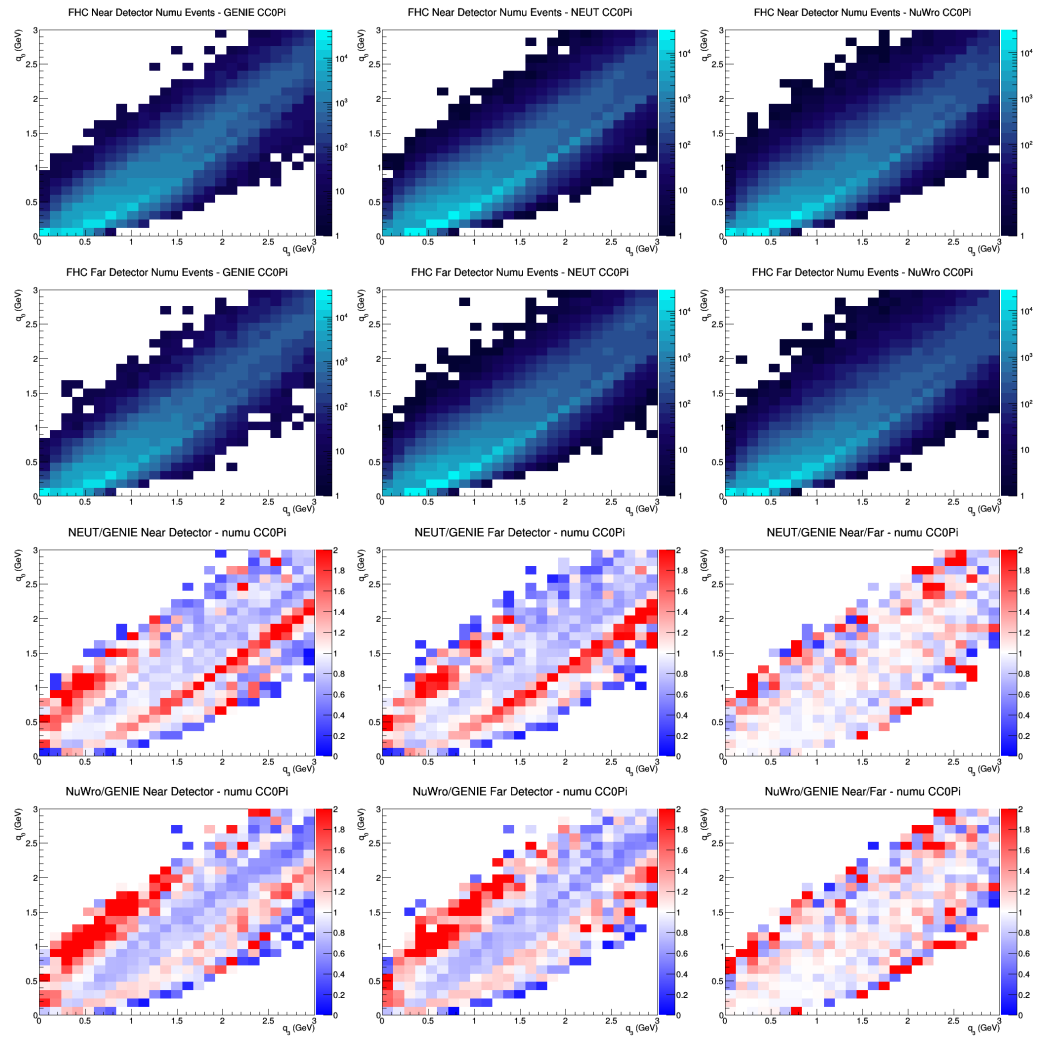
B.17 numu CC0Pi no efficiencies



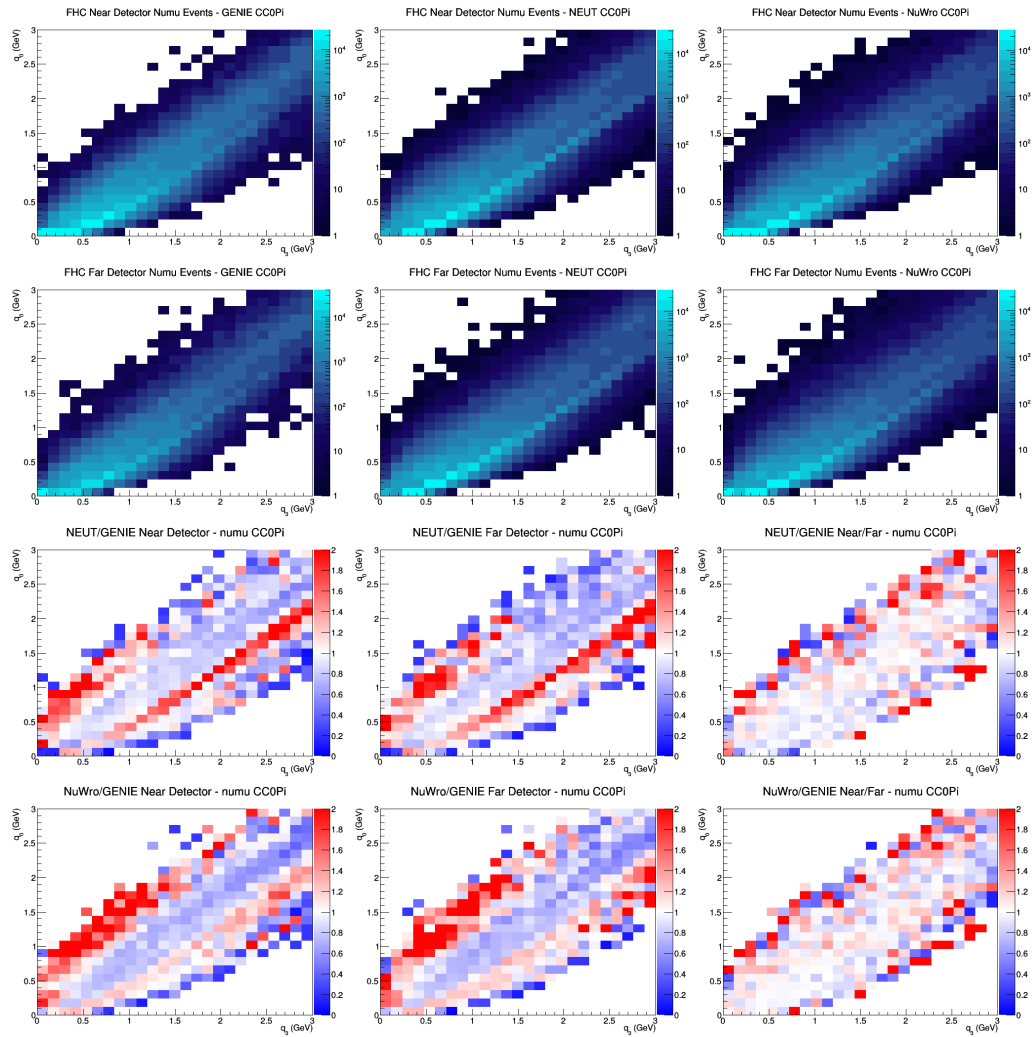
B.18 numu CC0Pi FGT efficiencies



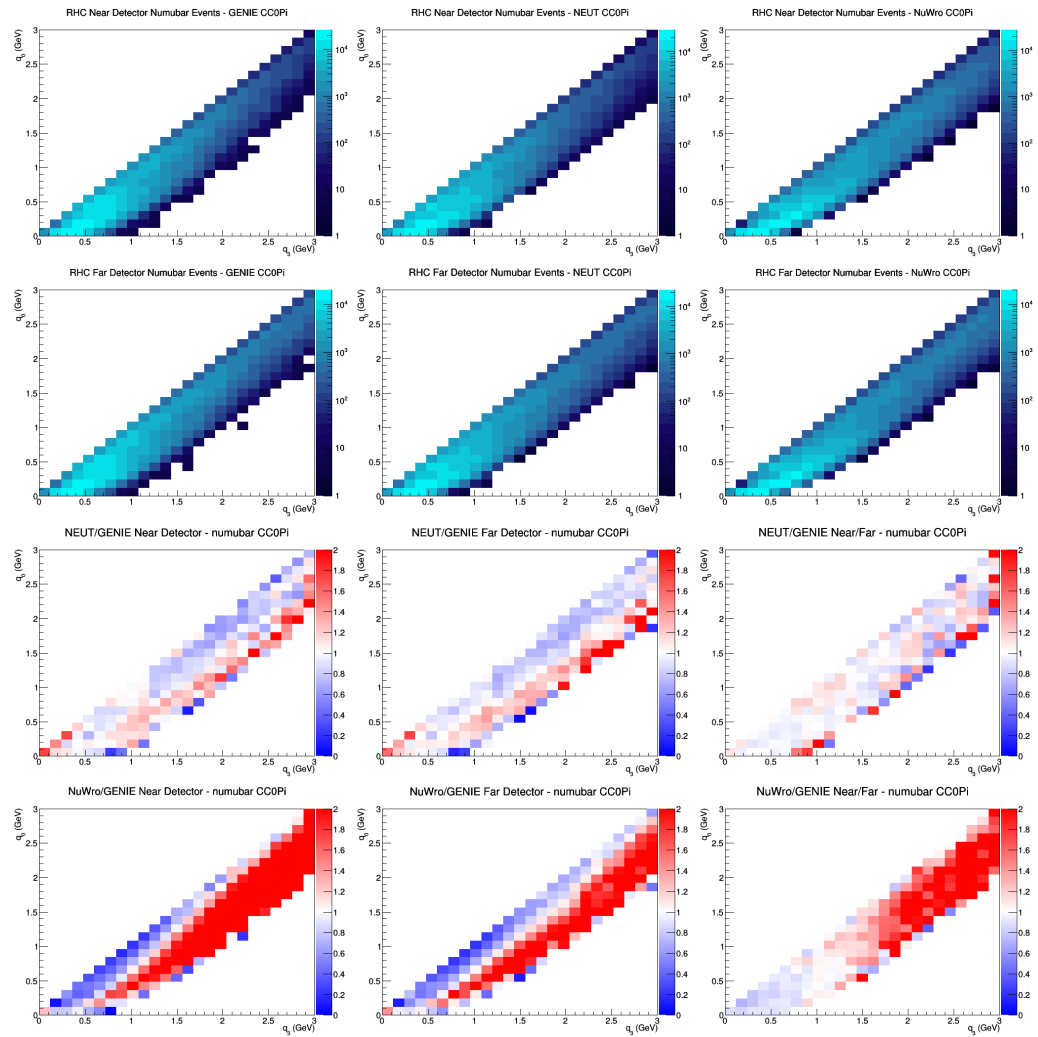
B.19 numu CC0Pi LAr efficiencies



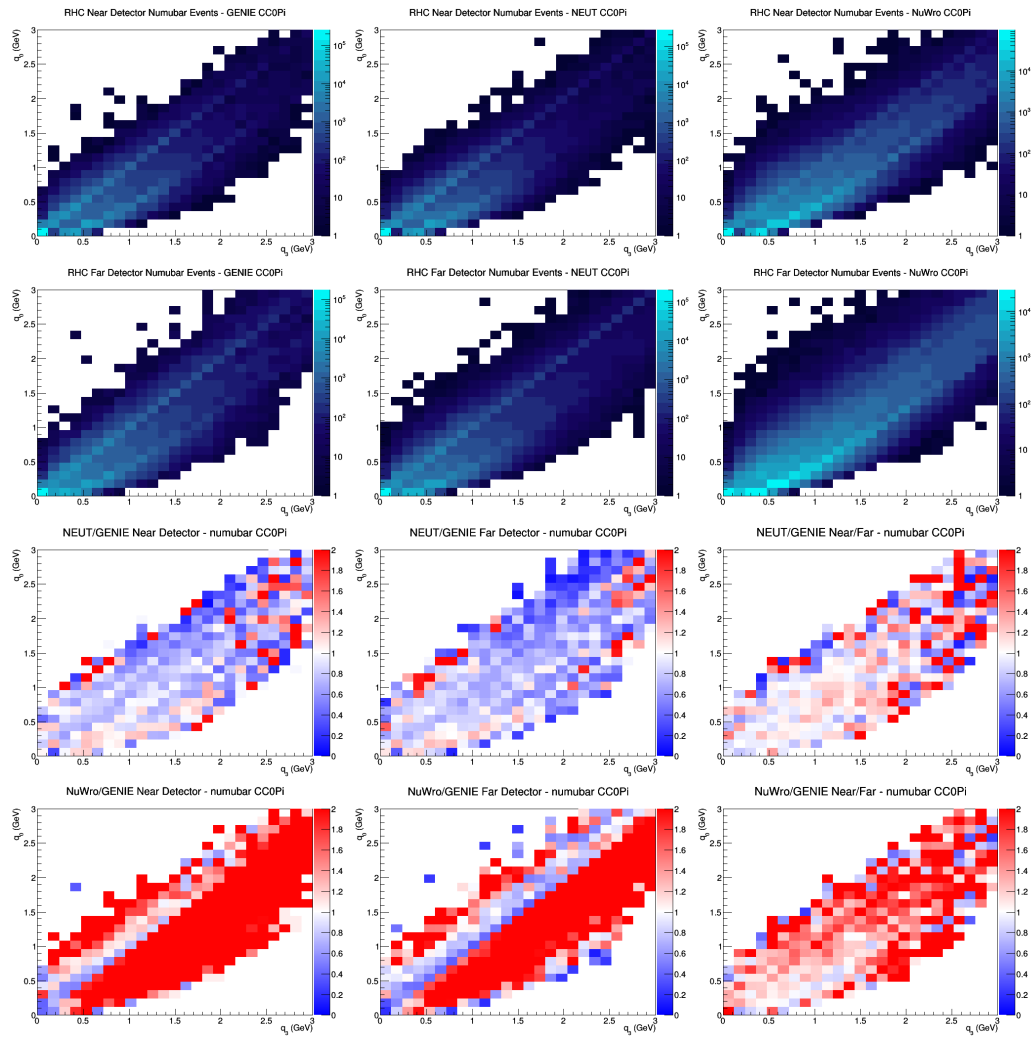
B.20 numu CC0Pi GAr efficiencies



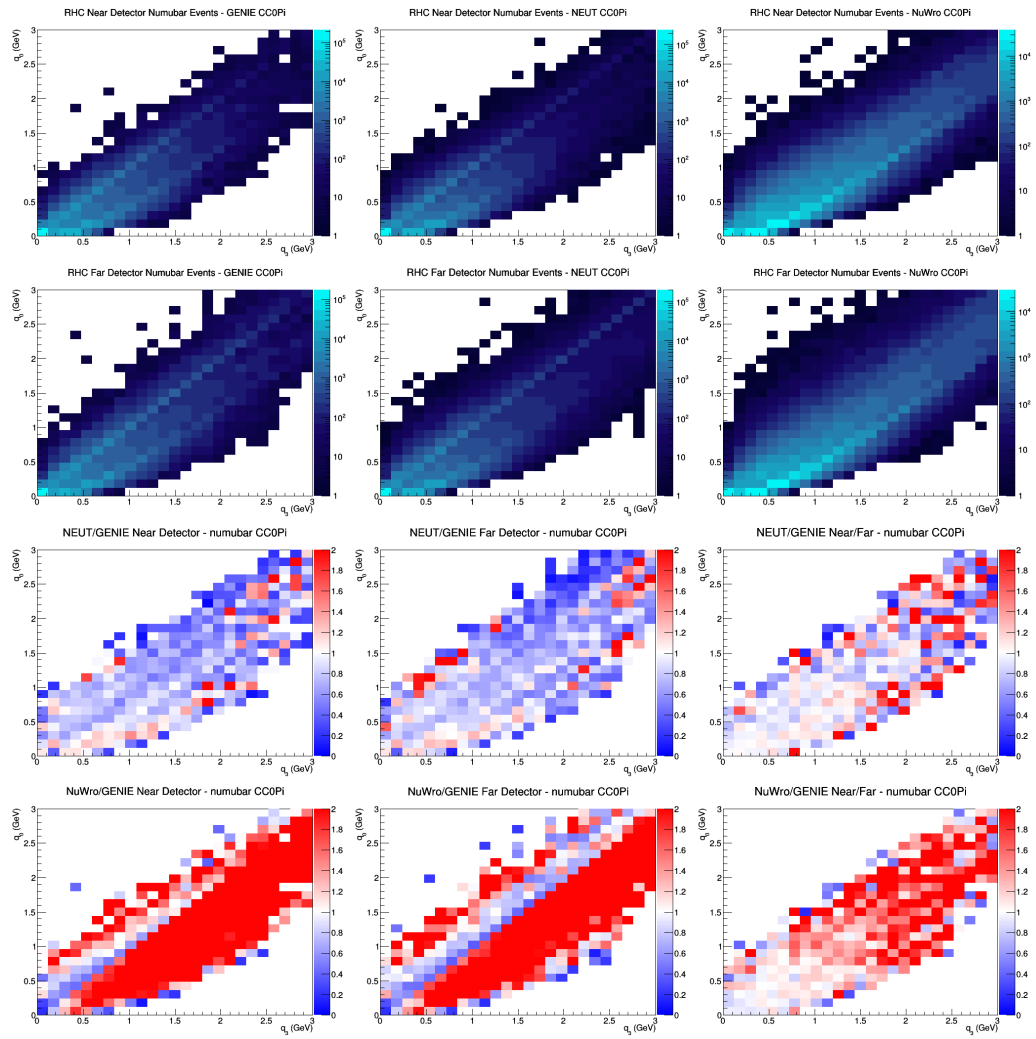
B.21 numubar CC0Pi no efficiencies



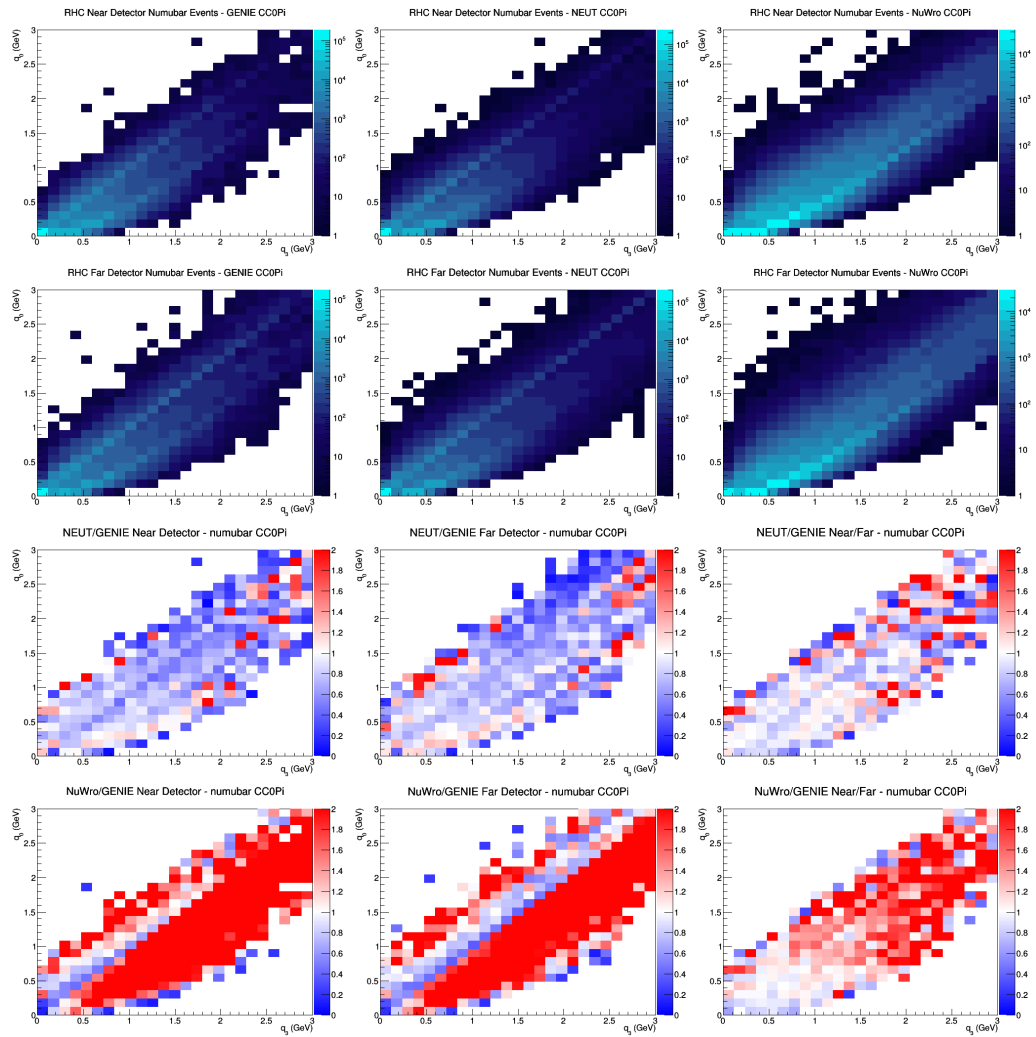
B.22 numubar CC0Pi FGT efficiencies



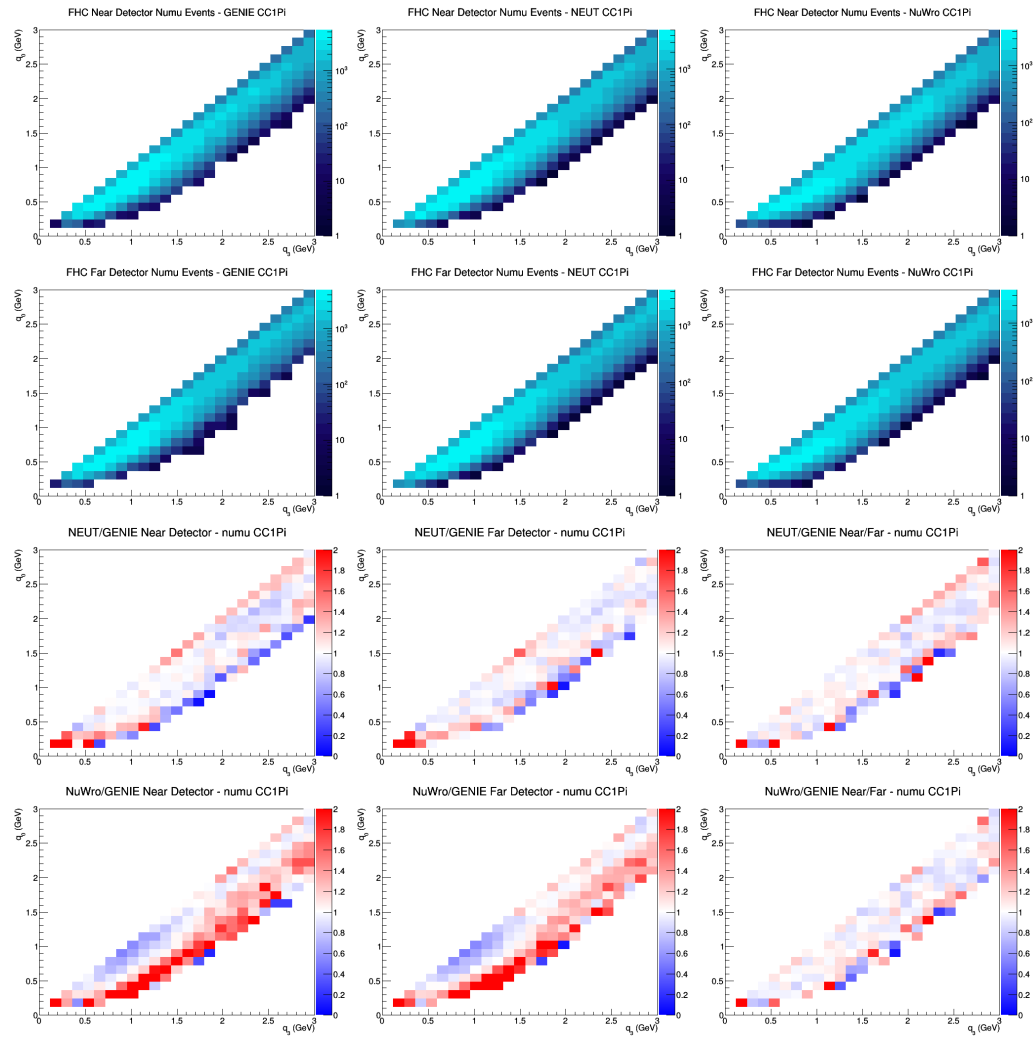
B.23 numubar CC0Pi LAr efficiencies



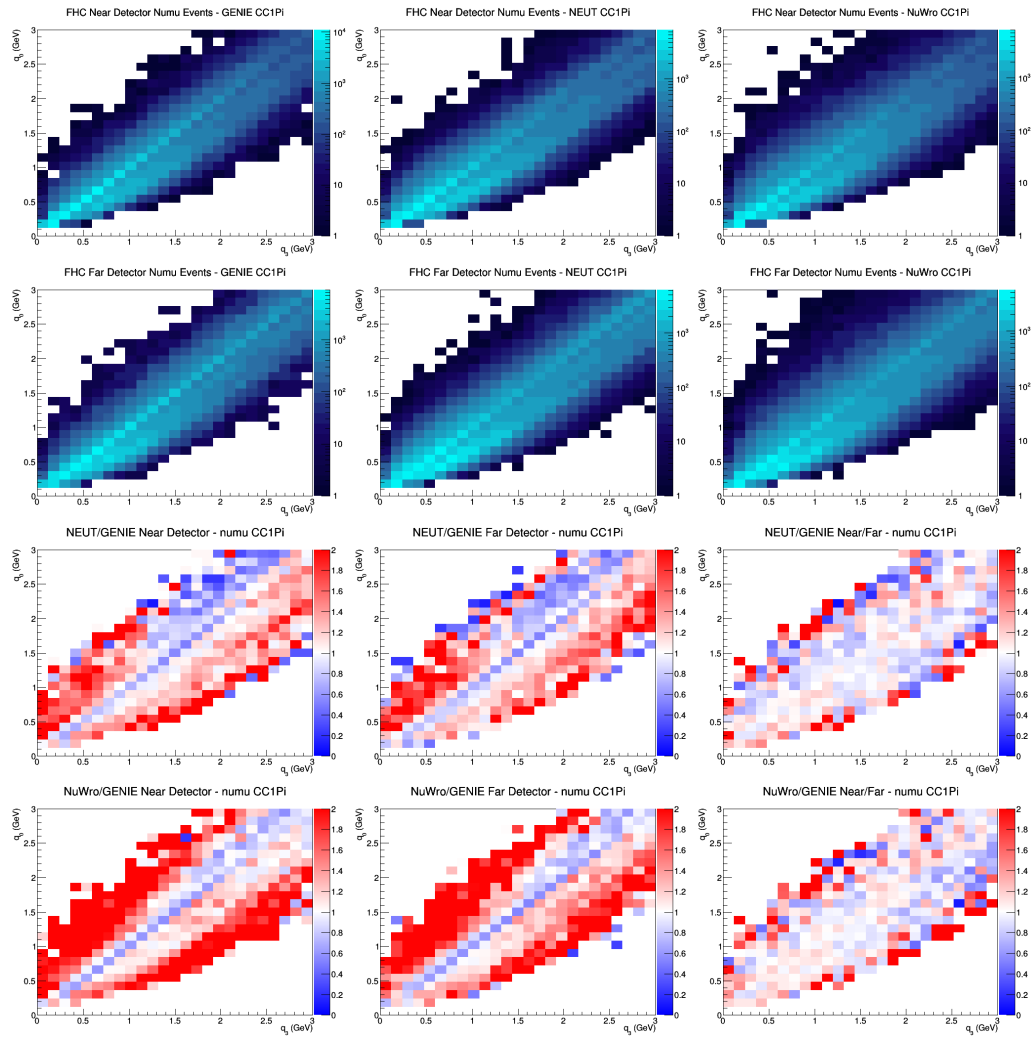
B.24 numubar CC0Pi GAr efficiencies



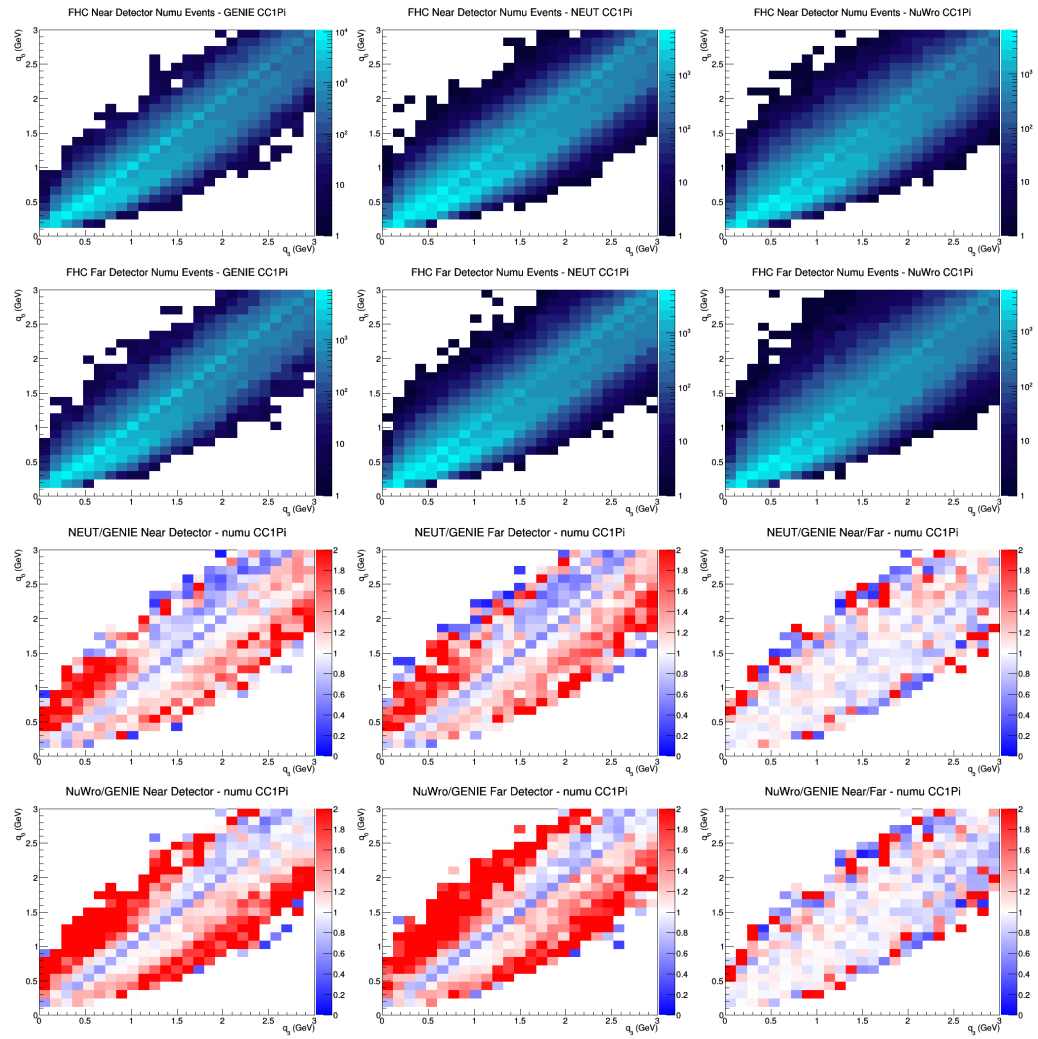
B.25 numu CC1Pi no efficiencies



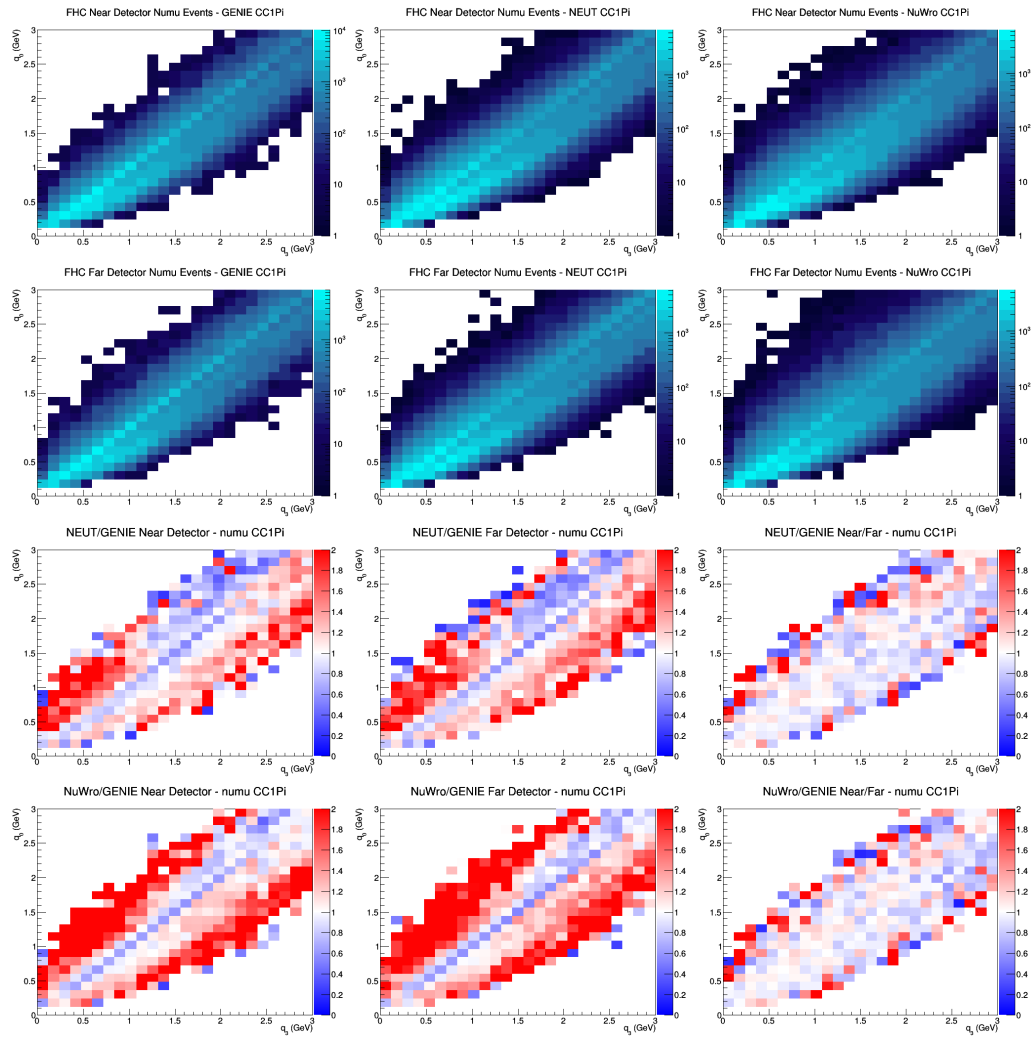
B.26 numu CC1Pi FGT efficiencies



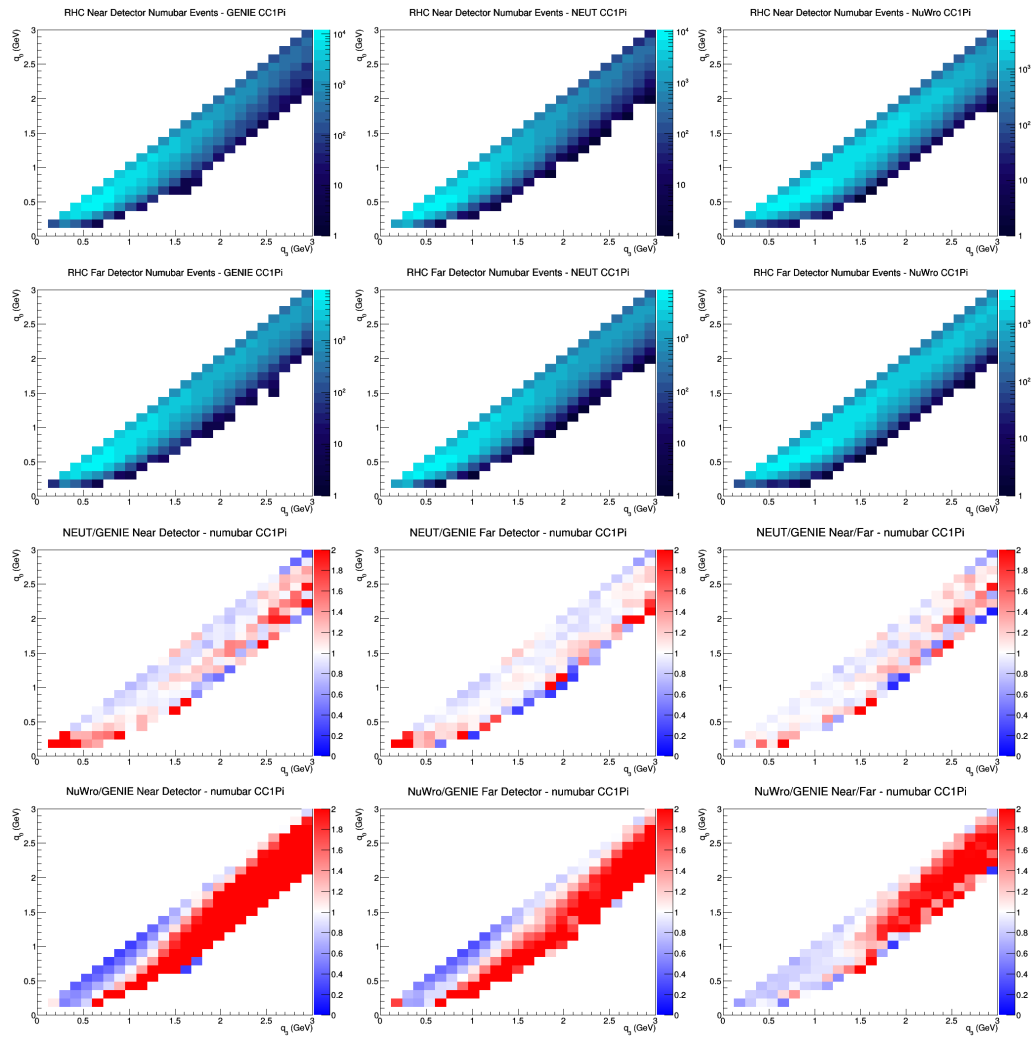
B.27 numu CC1Pi LAr efficiencies



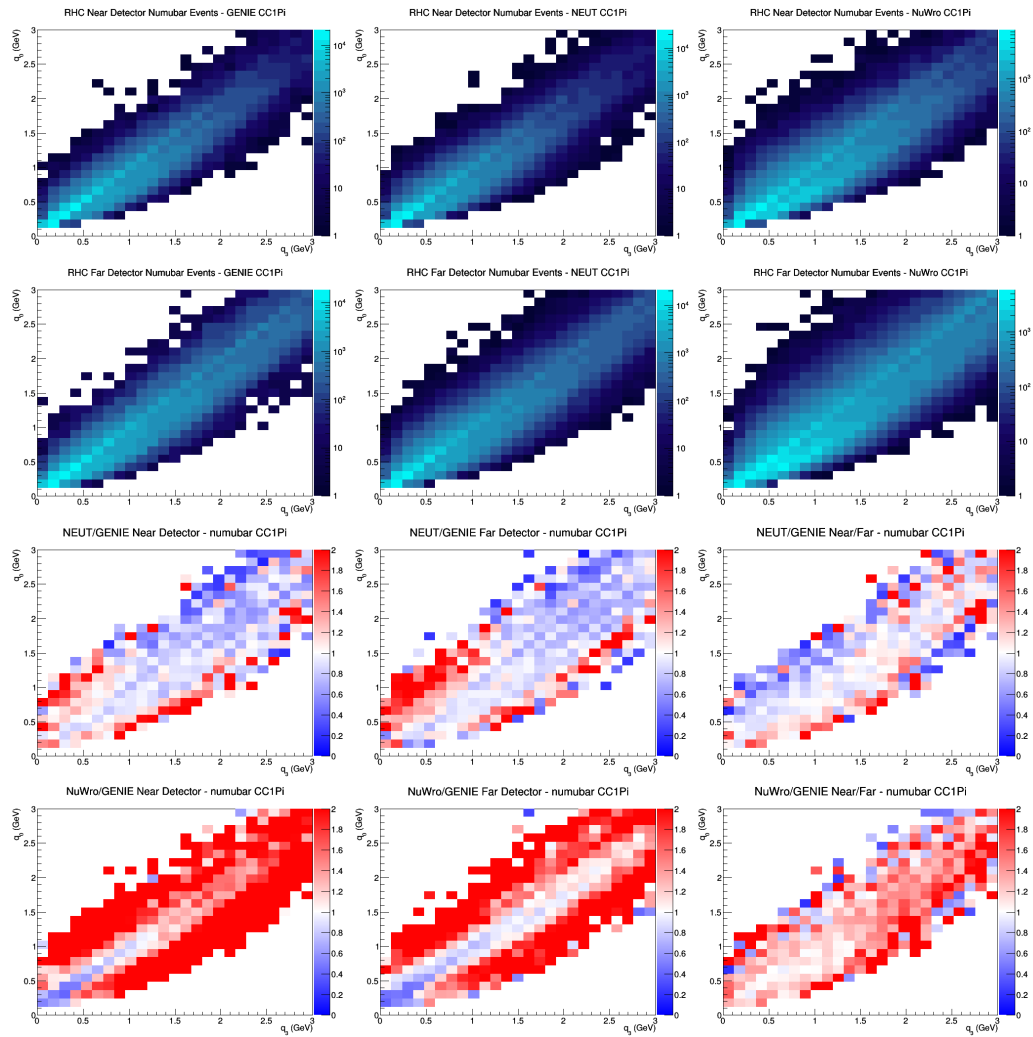
B.28 numu CC1Pi GAr efficiencies



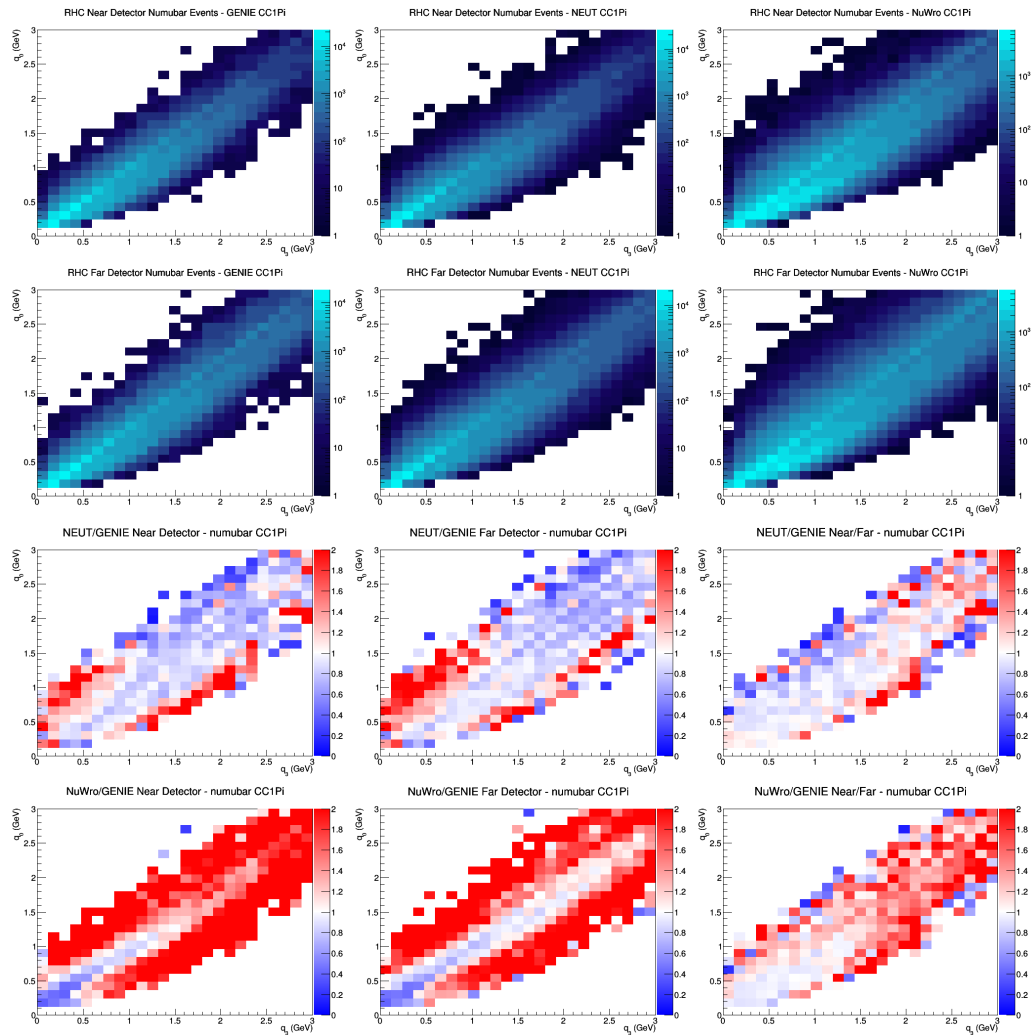
B.29 numubar CC1Pi no efficiencies



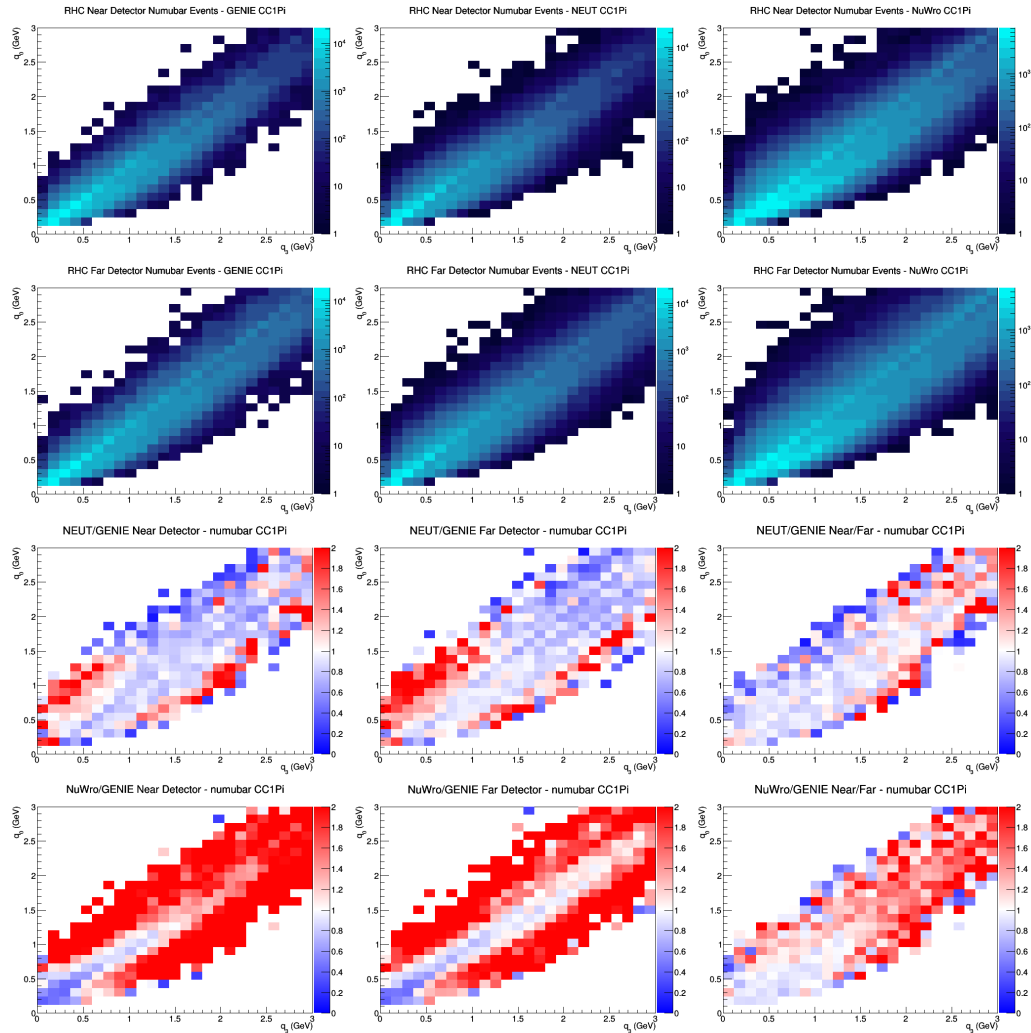
B.30 numubar CC1Pi FGT efficiencies



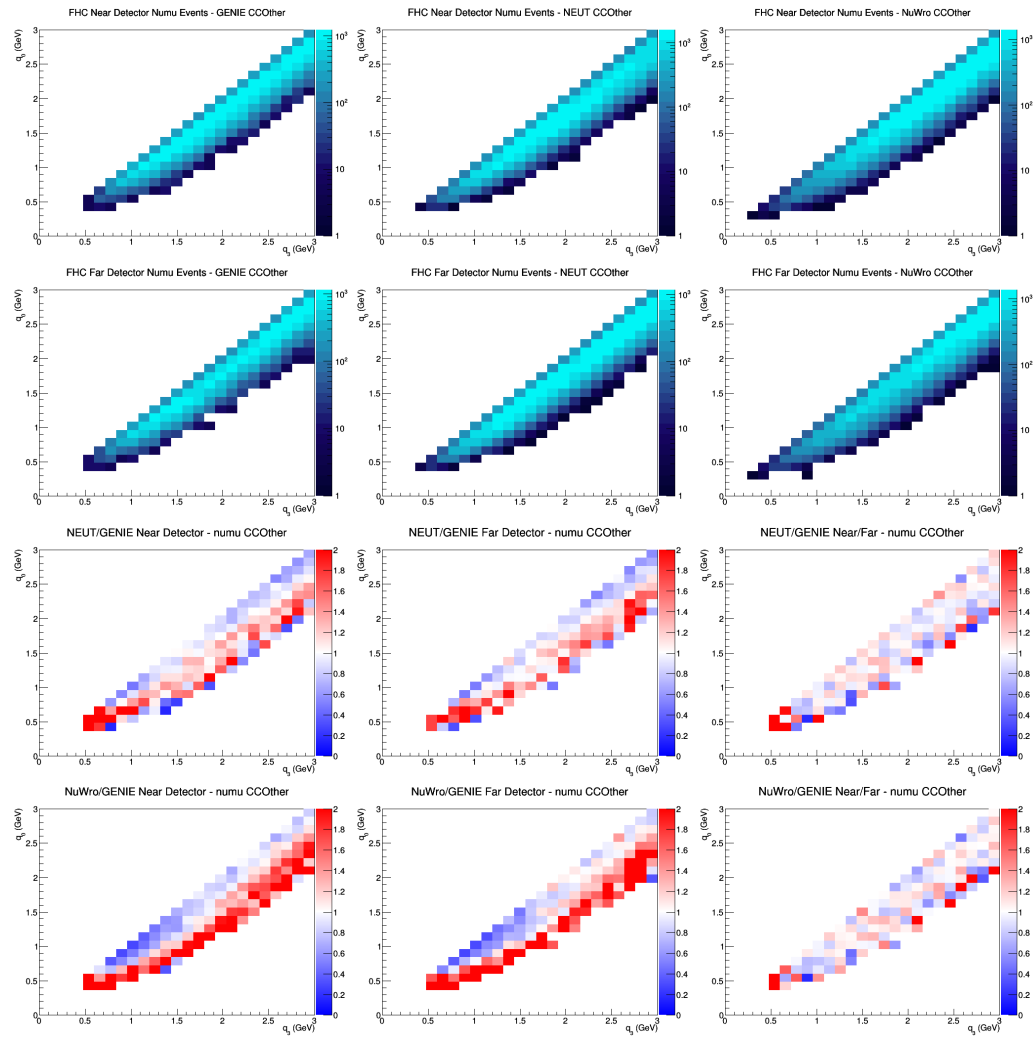
B.31 numubar CC1Pi LAr efficiencies



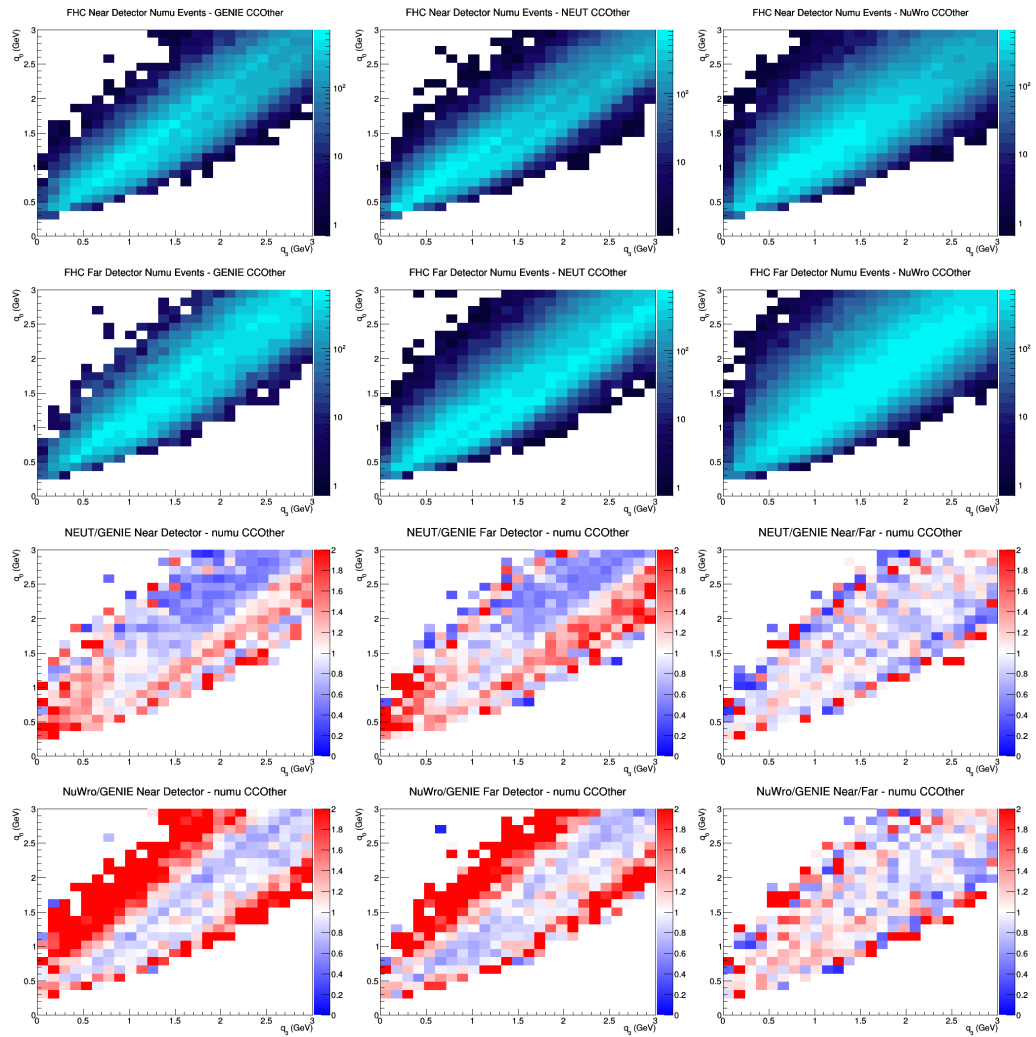
B.32 numubar CC1Pi GAr efficiencies



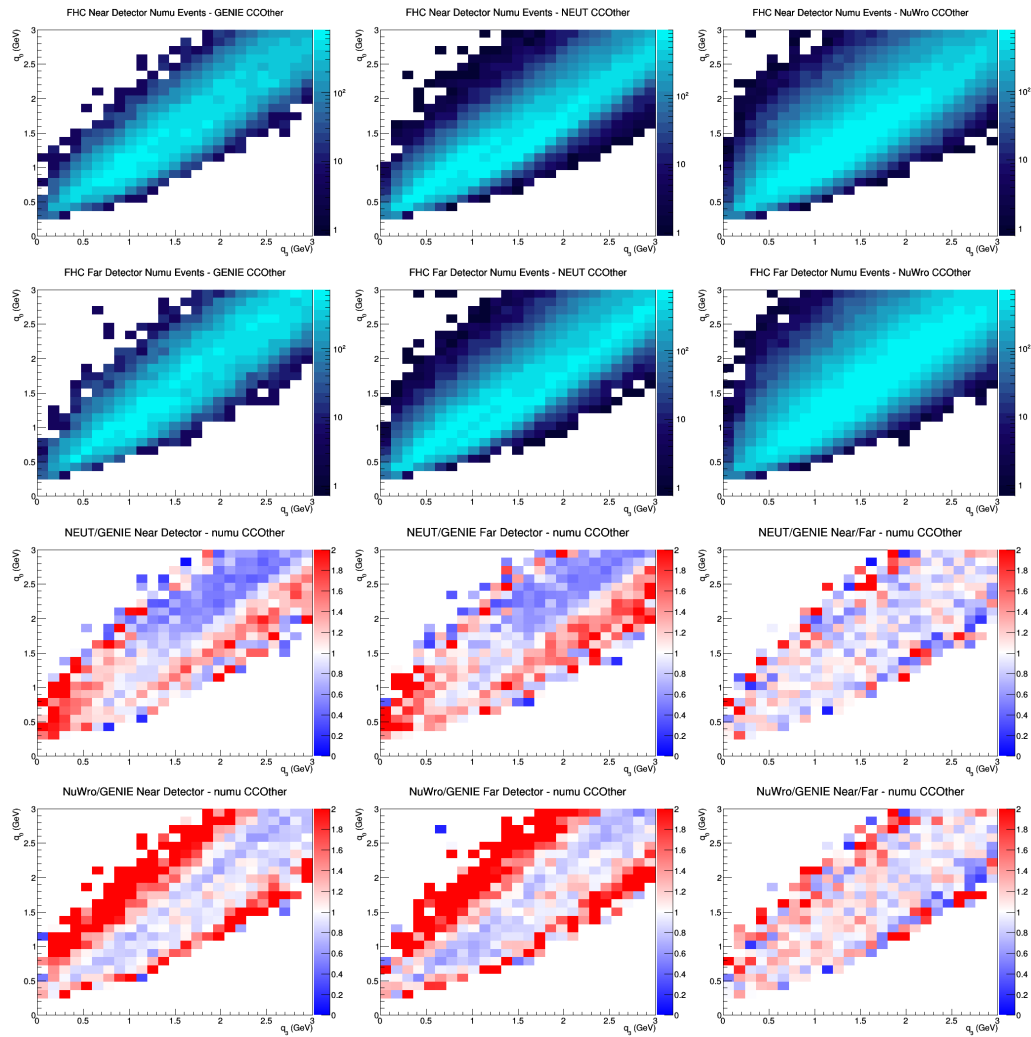
B.33 numu CCOther no efficiencies



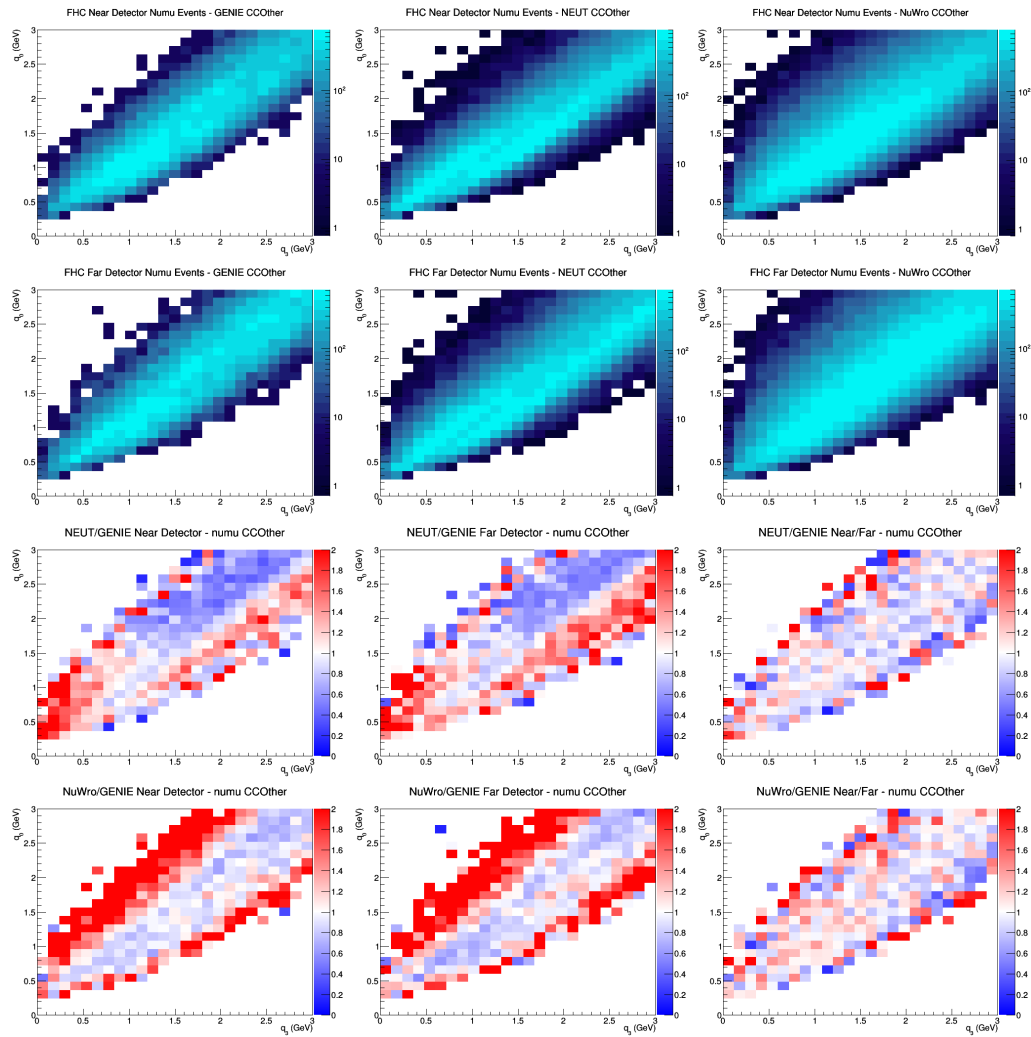
B.34 numu CCOther FGT efficiencies



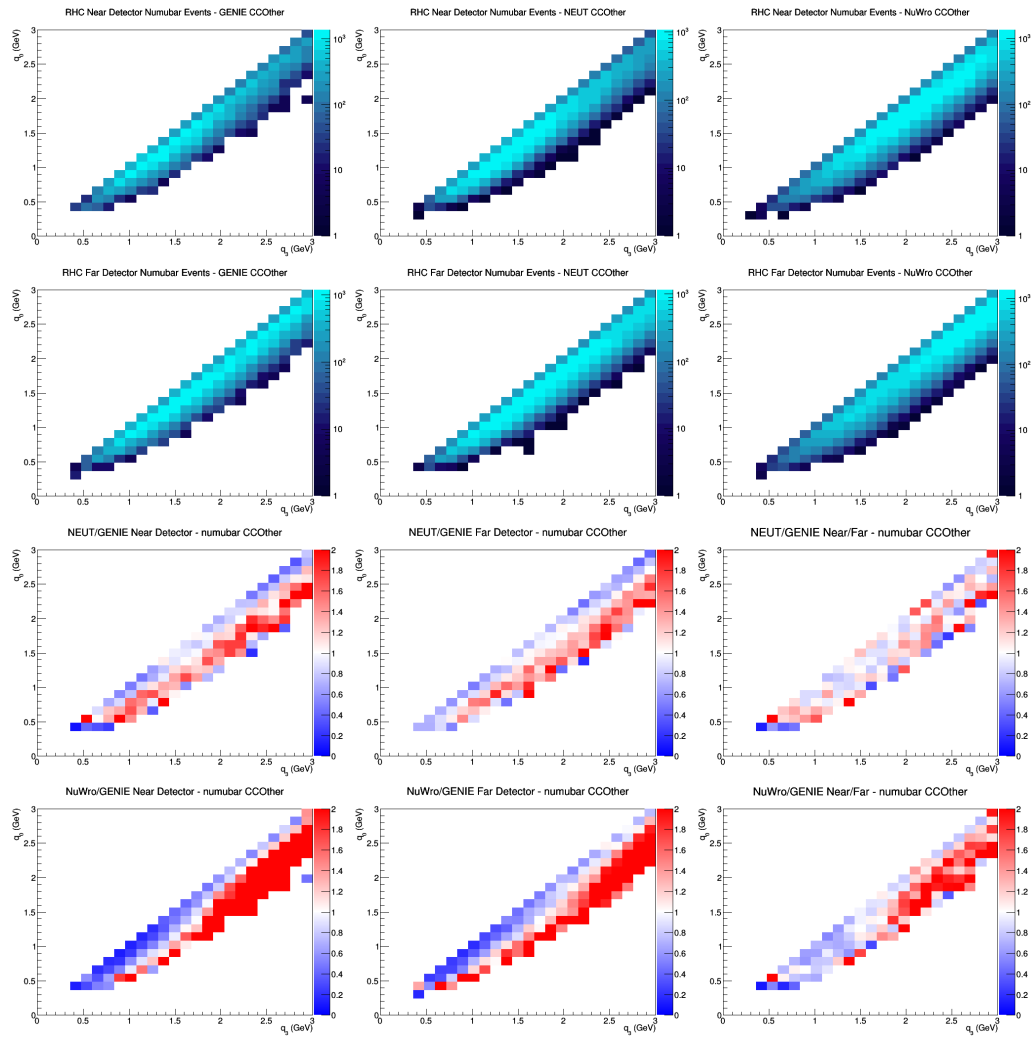
B.35 numu CCOther LAr efficiencies



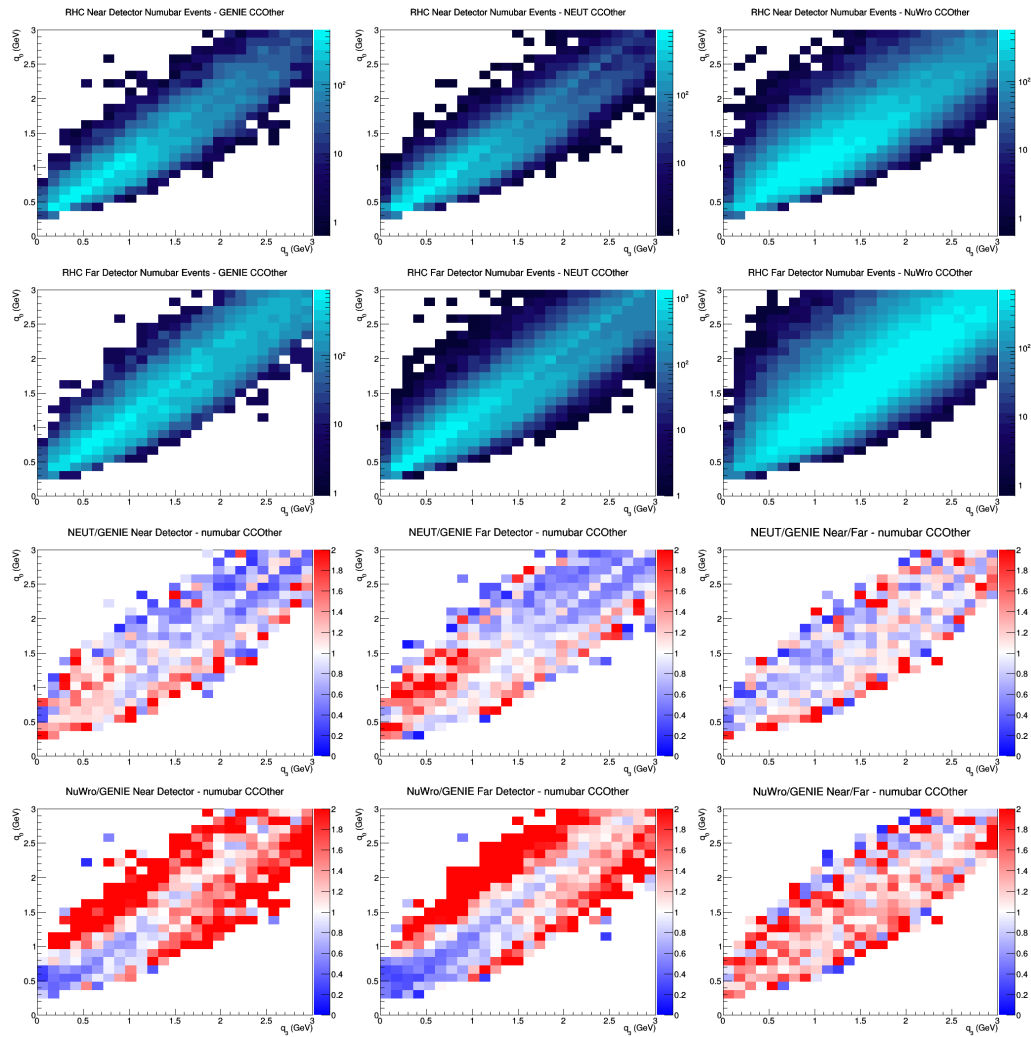
B.36 numu CCOther GAr efficiencies



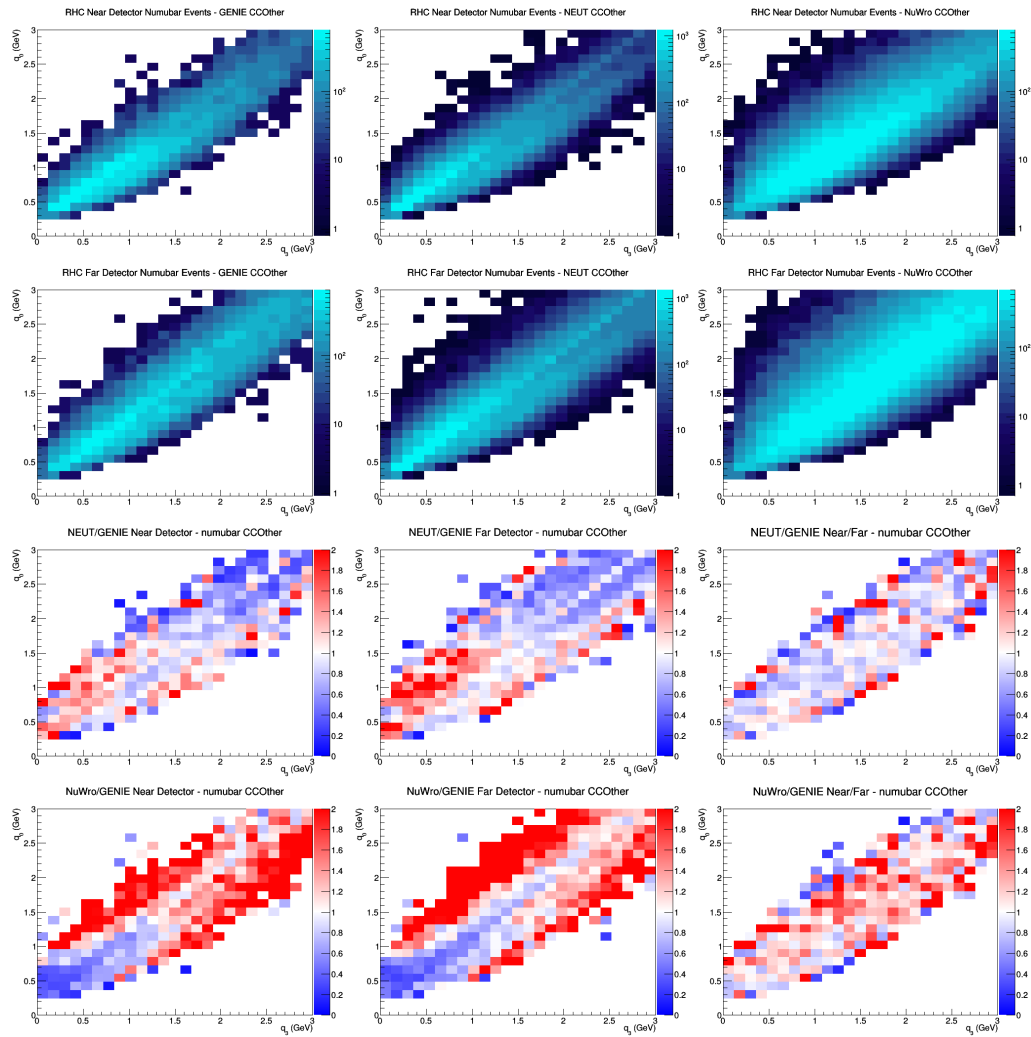
B.37 numubar CCOther no efficiencies



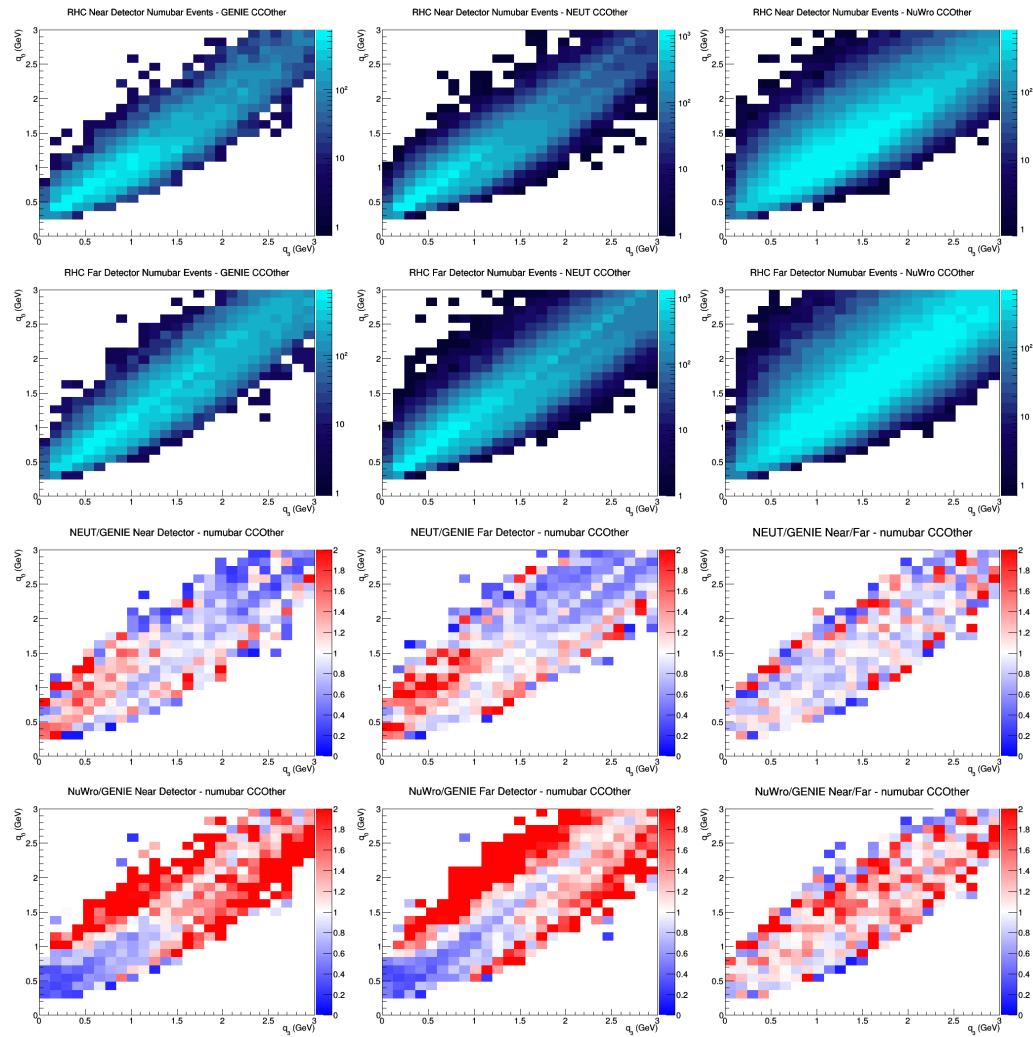
B.38 numubar CCOther FGT efficiencies



B.39 numubar CCOther LAr efficiencies



B.40 numubar CCOther GAr efficiencies

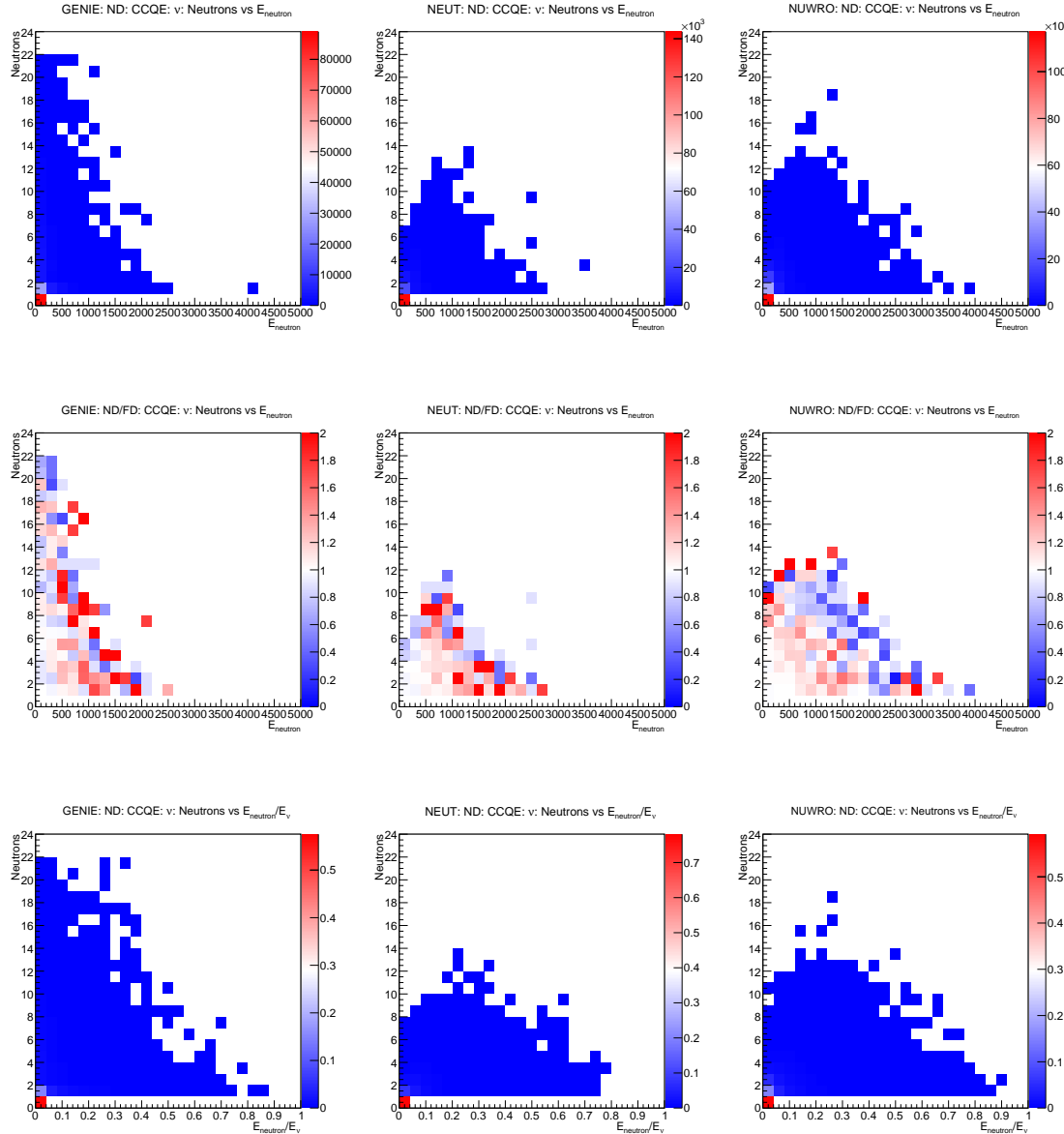


C Neutron Multiplicities & Energy

This appendix includes all the plots not shown in Section ???. For full description of the files, please make reference to that section. The plots will be put in the same order as before.

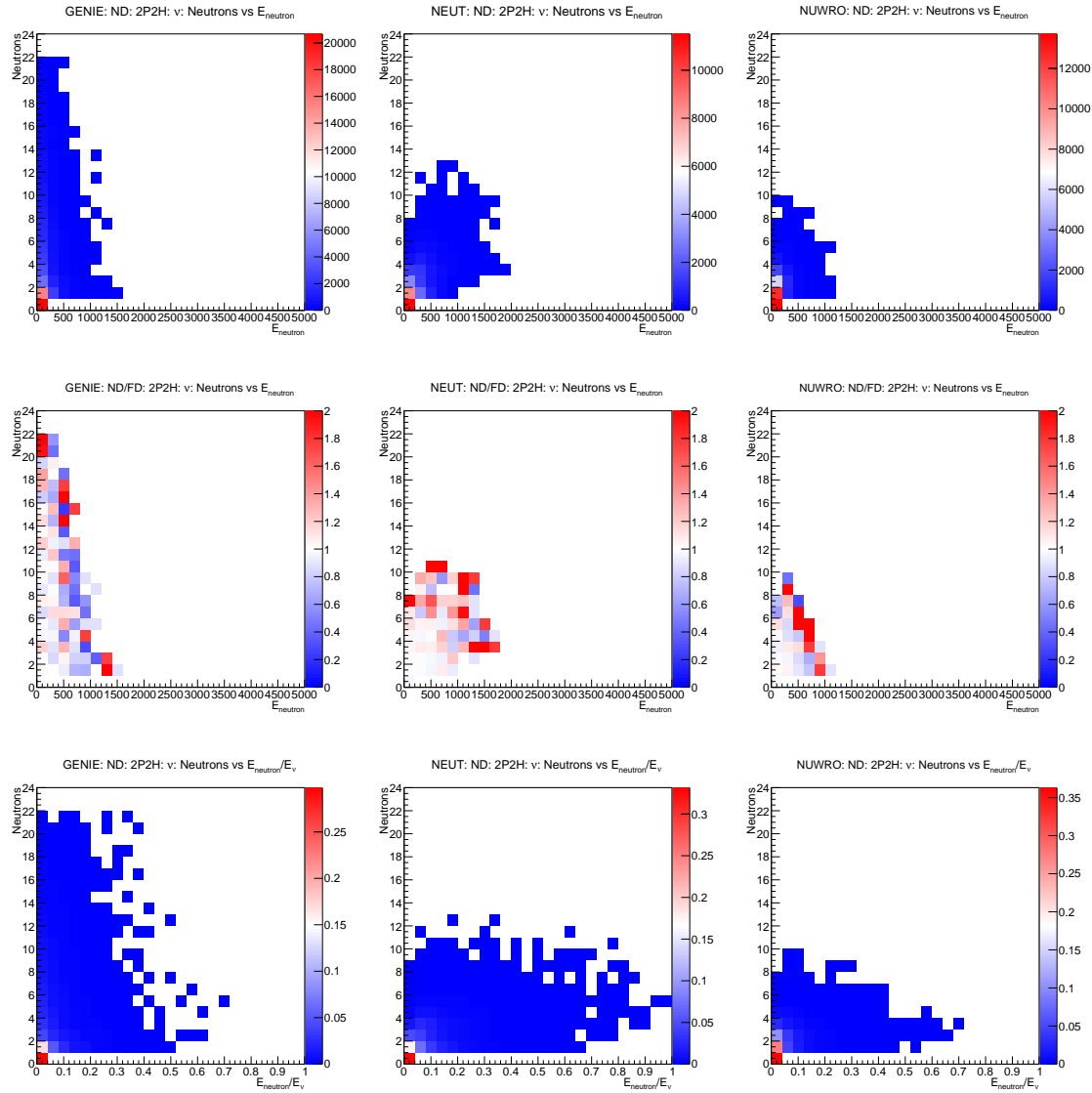
C.1 ν Plots

C.1.1 CCQE

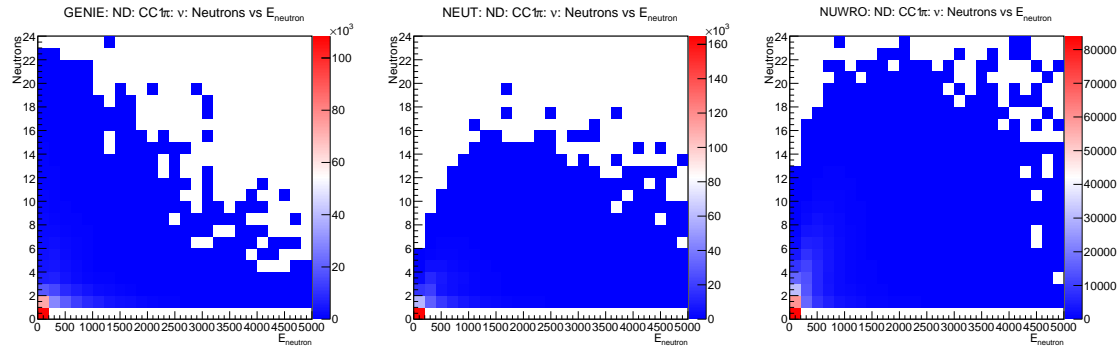


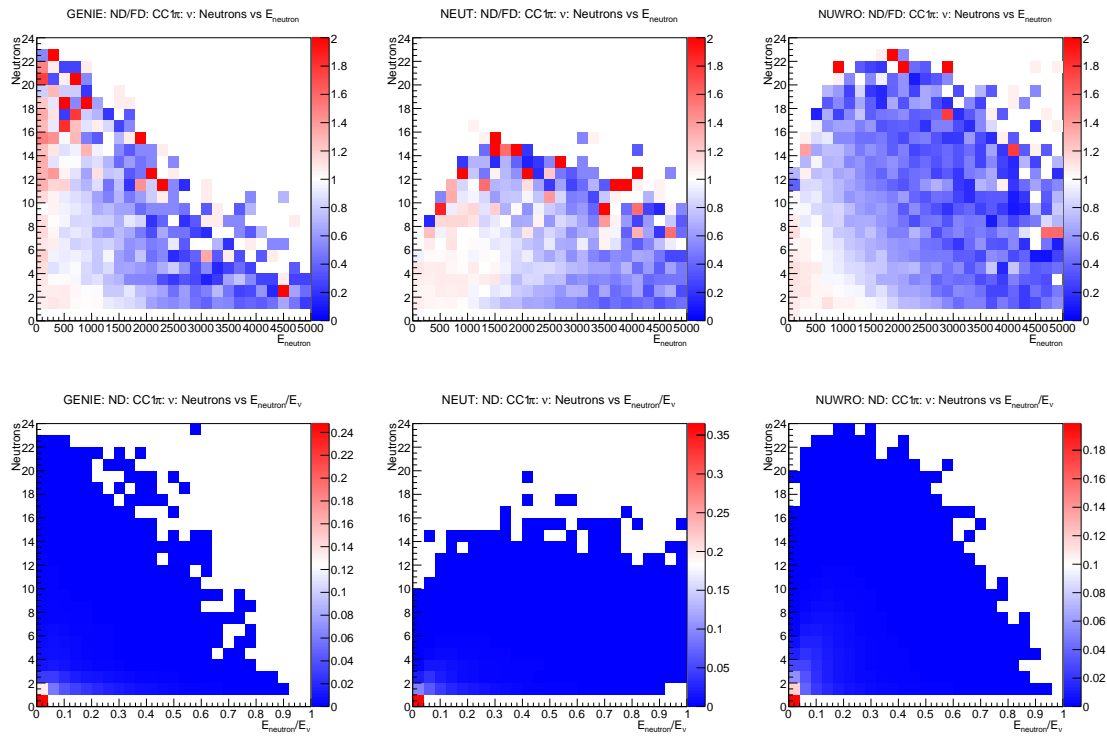
C.1.2 2P2H

These are the same as shown in Section ??.

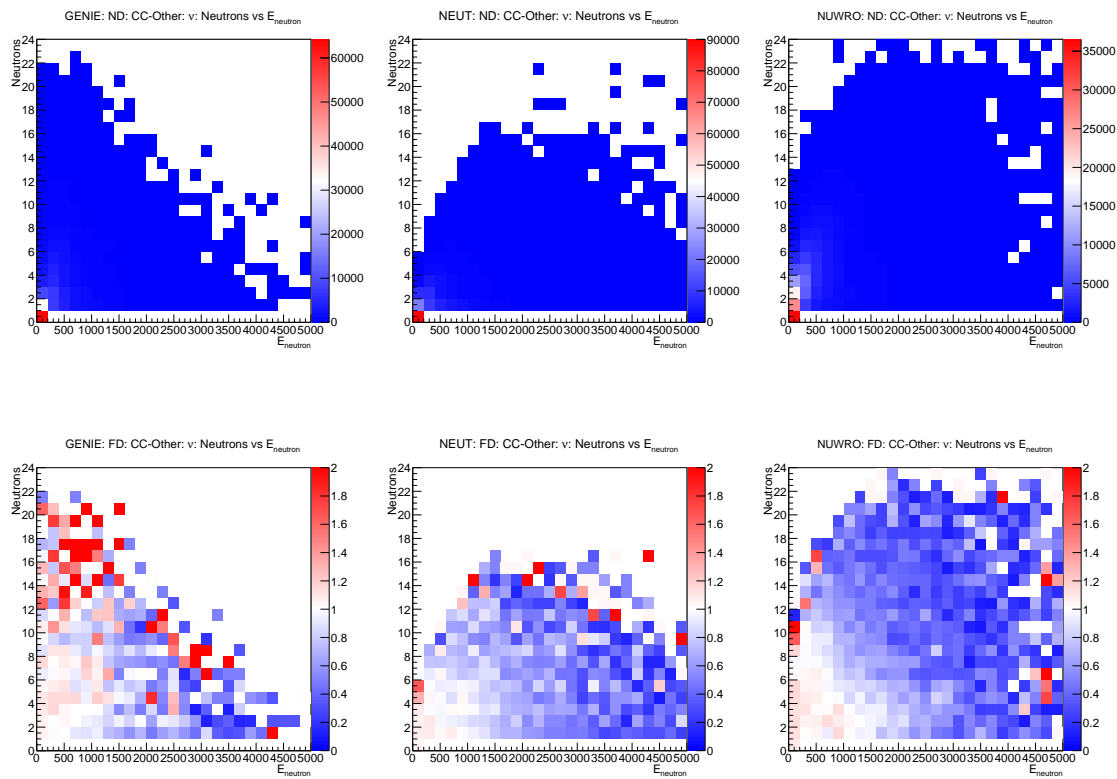


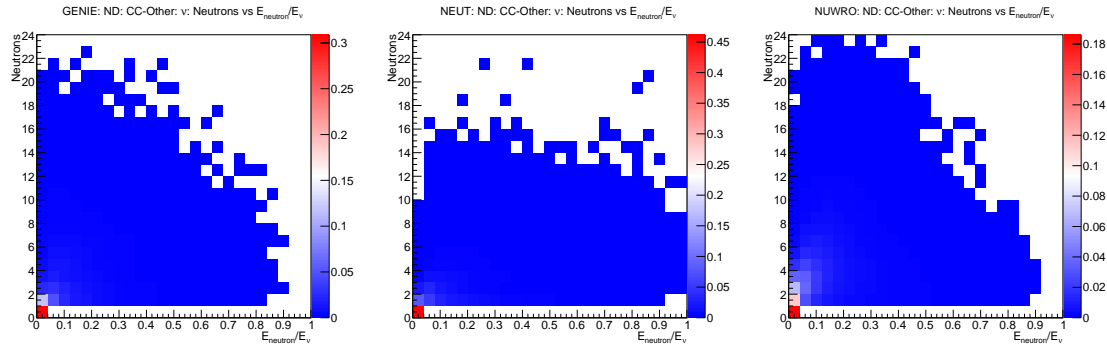
C.1.3 CC1 π





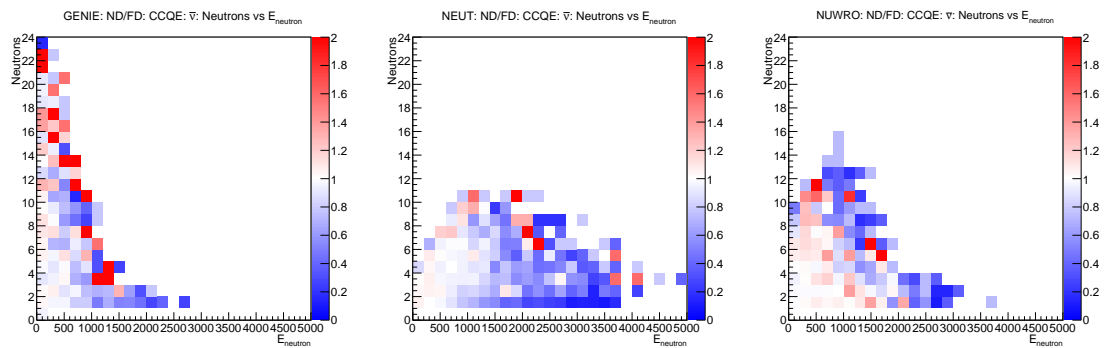
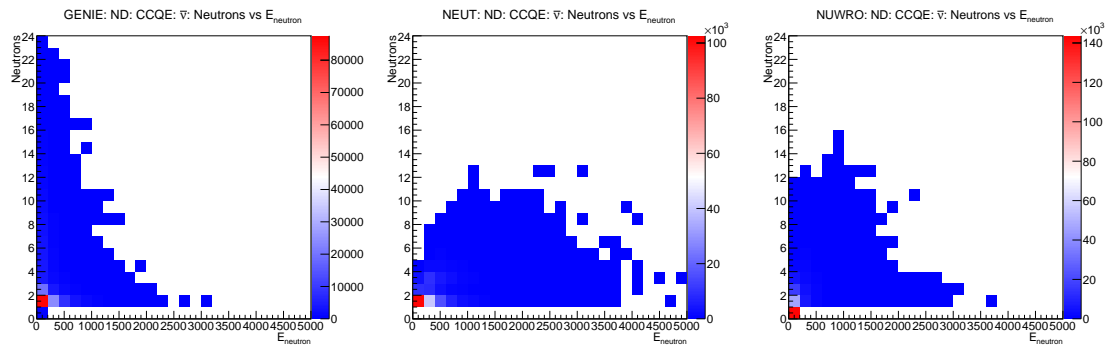
C.1.4 CC-Other

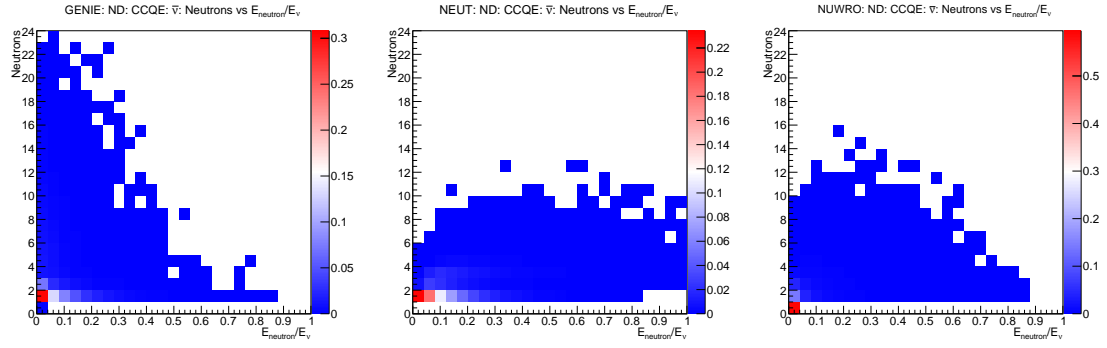




C.2 $\bar{\nu}$ Plots

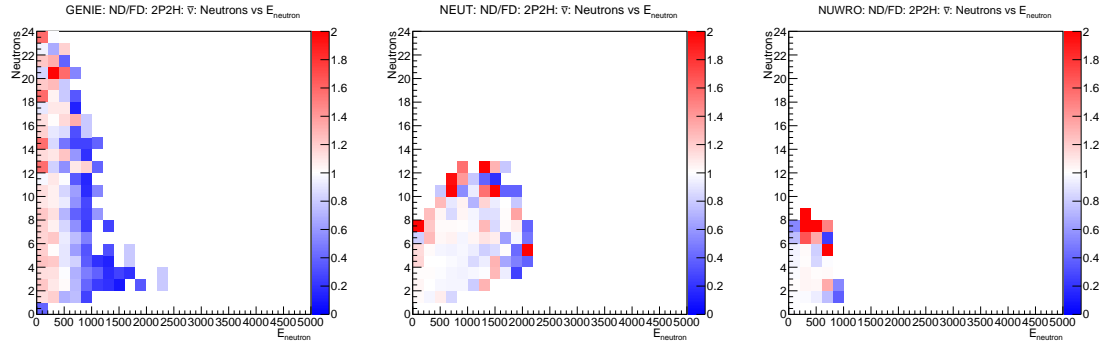
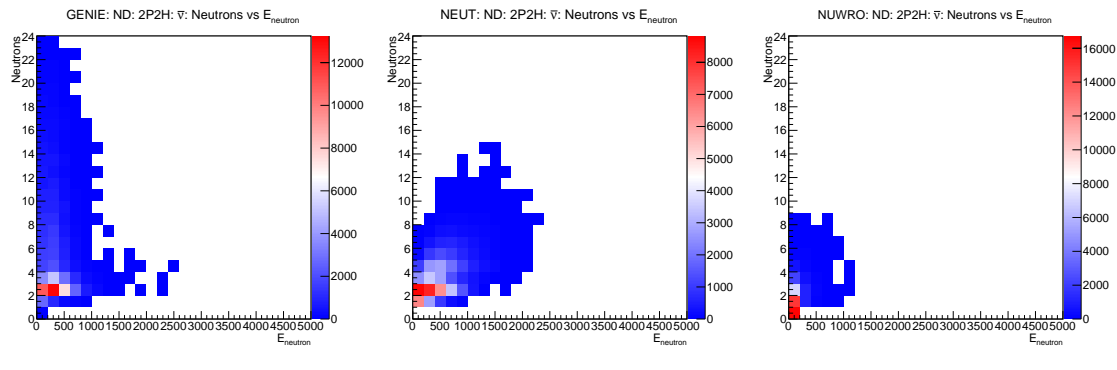
C.2.1 CCQE

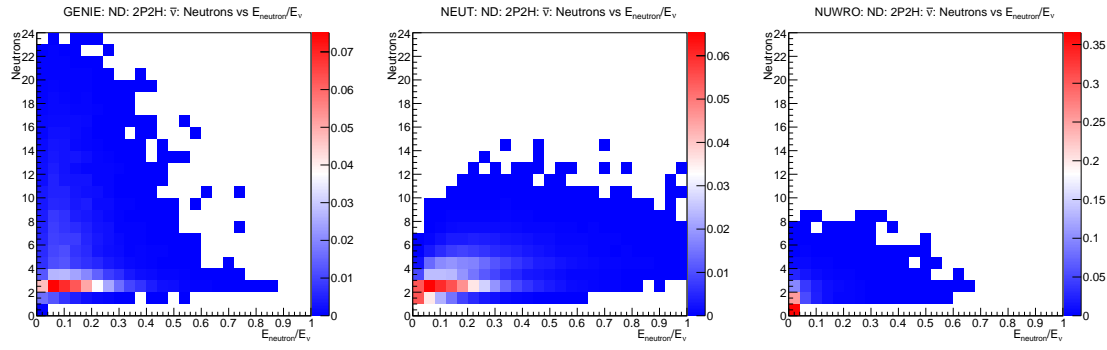




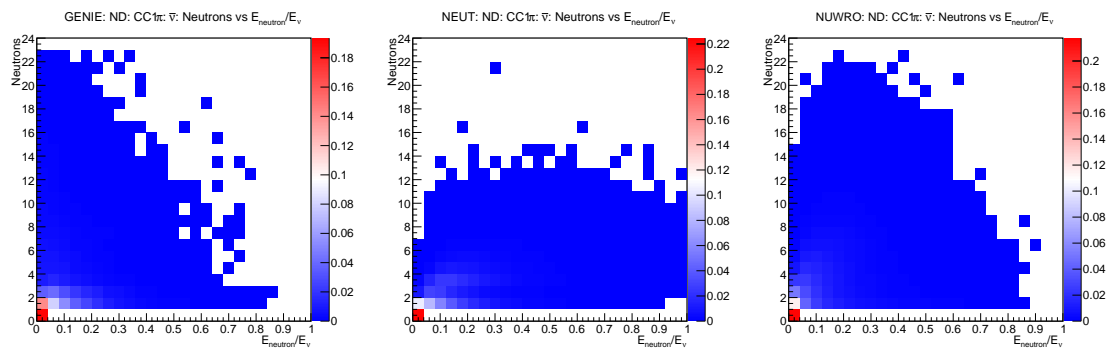
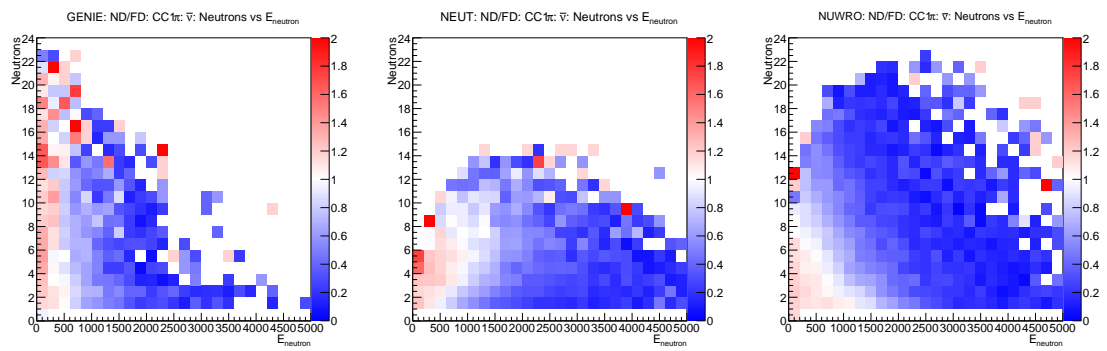
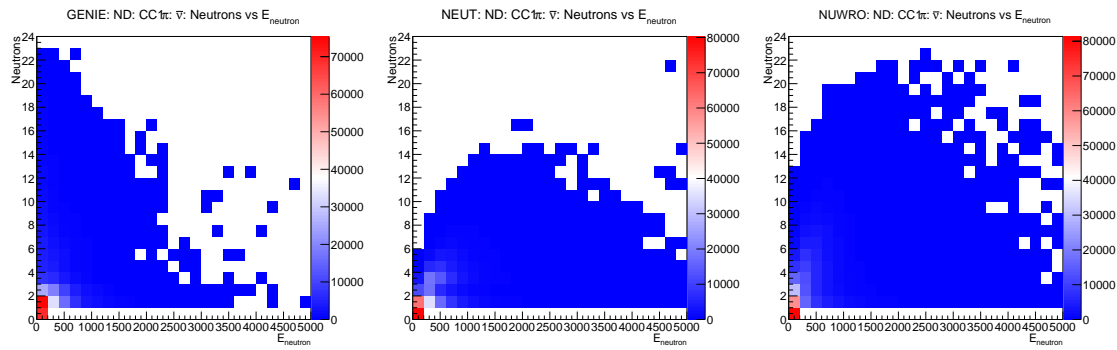
C.2.2 2P2H

These are the same as shown in Section ??.

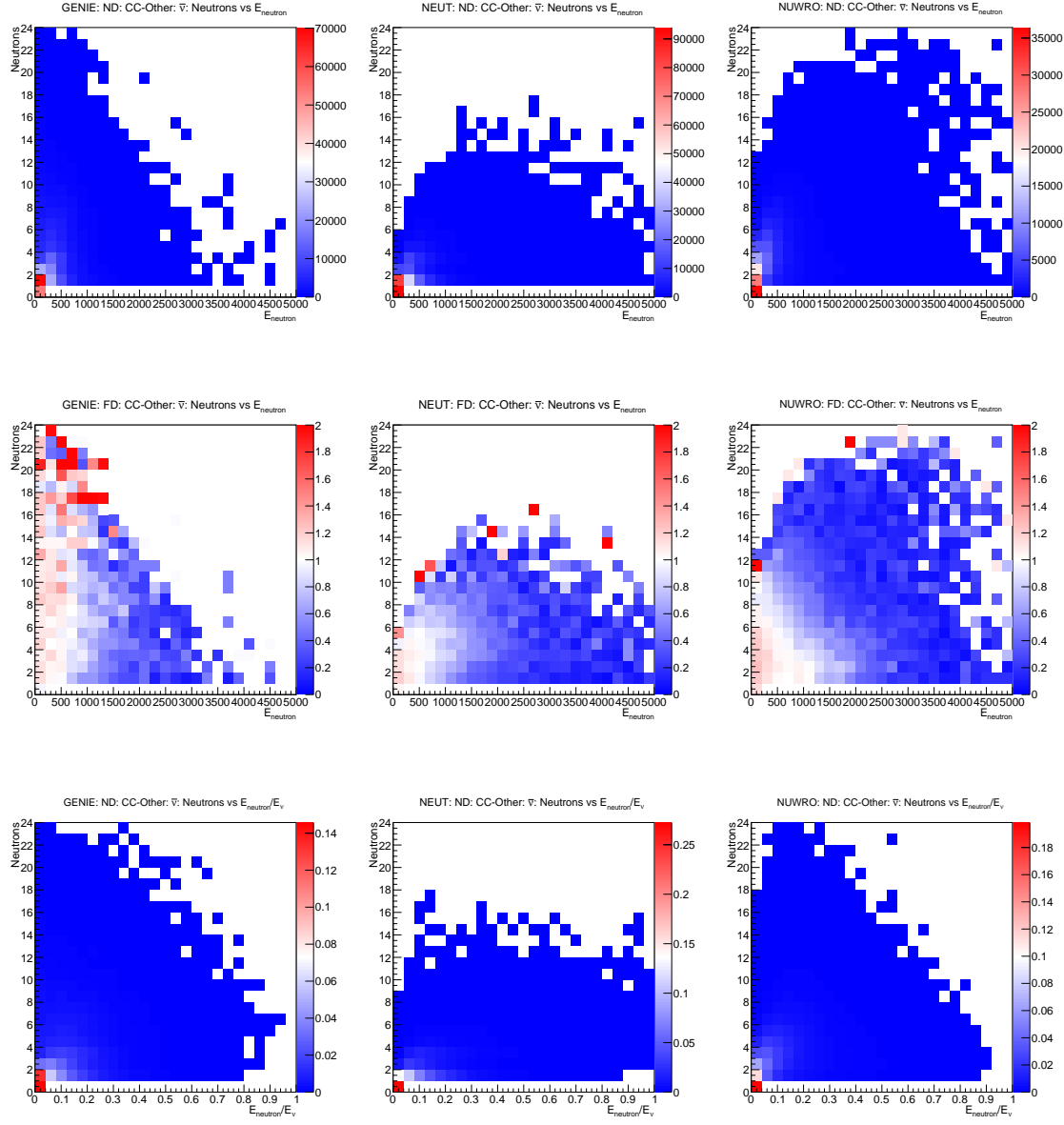




C.2.3 CC1 π



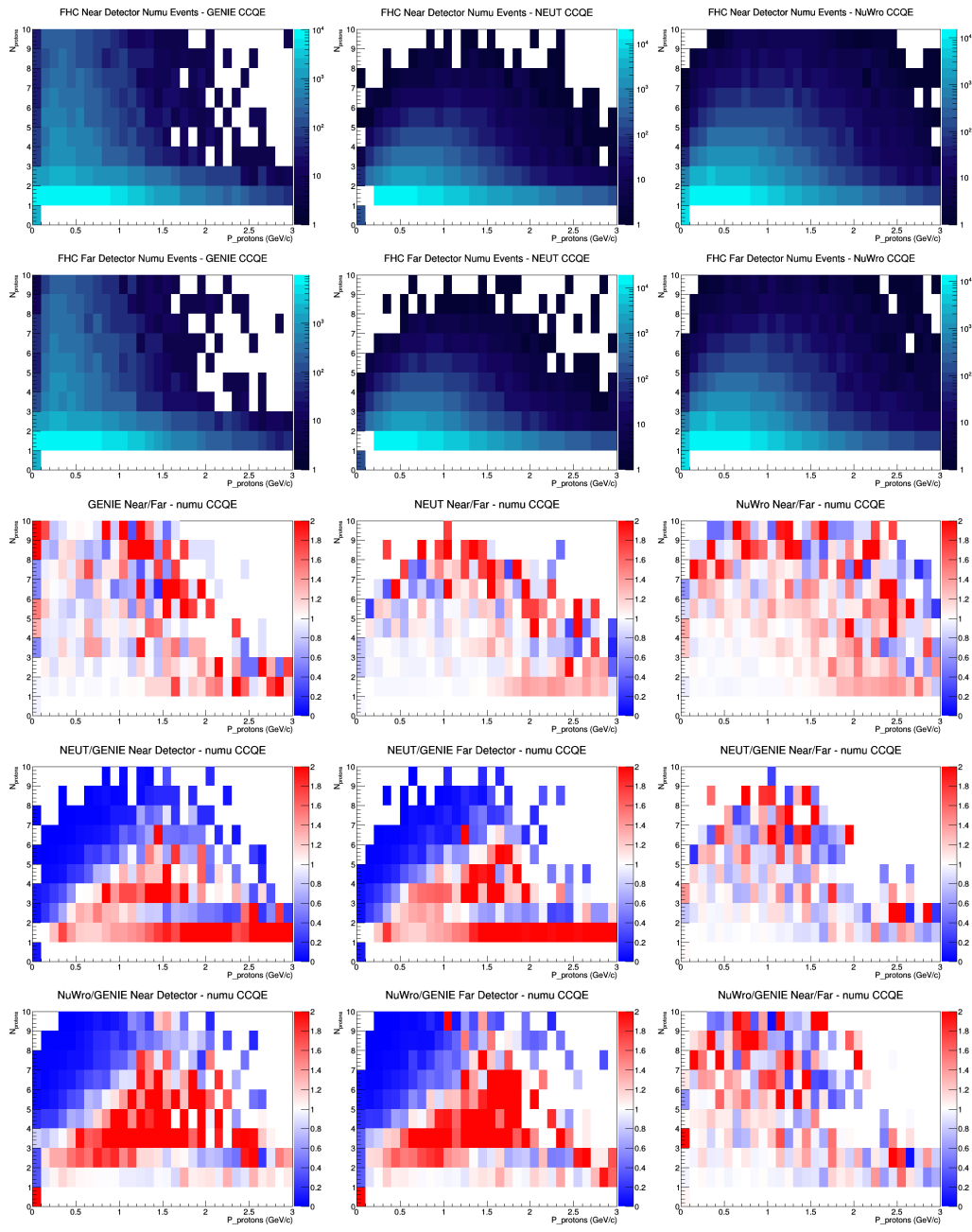
C.2.4 CC-Other



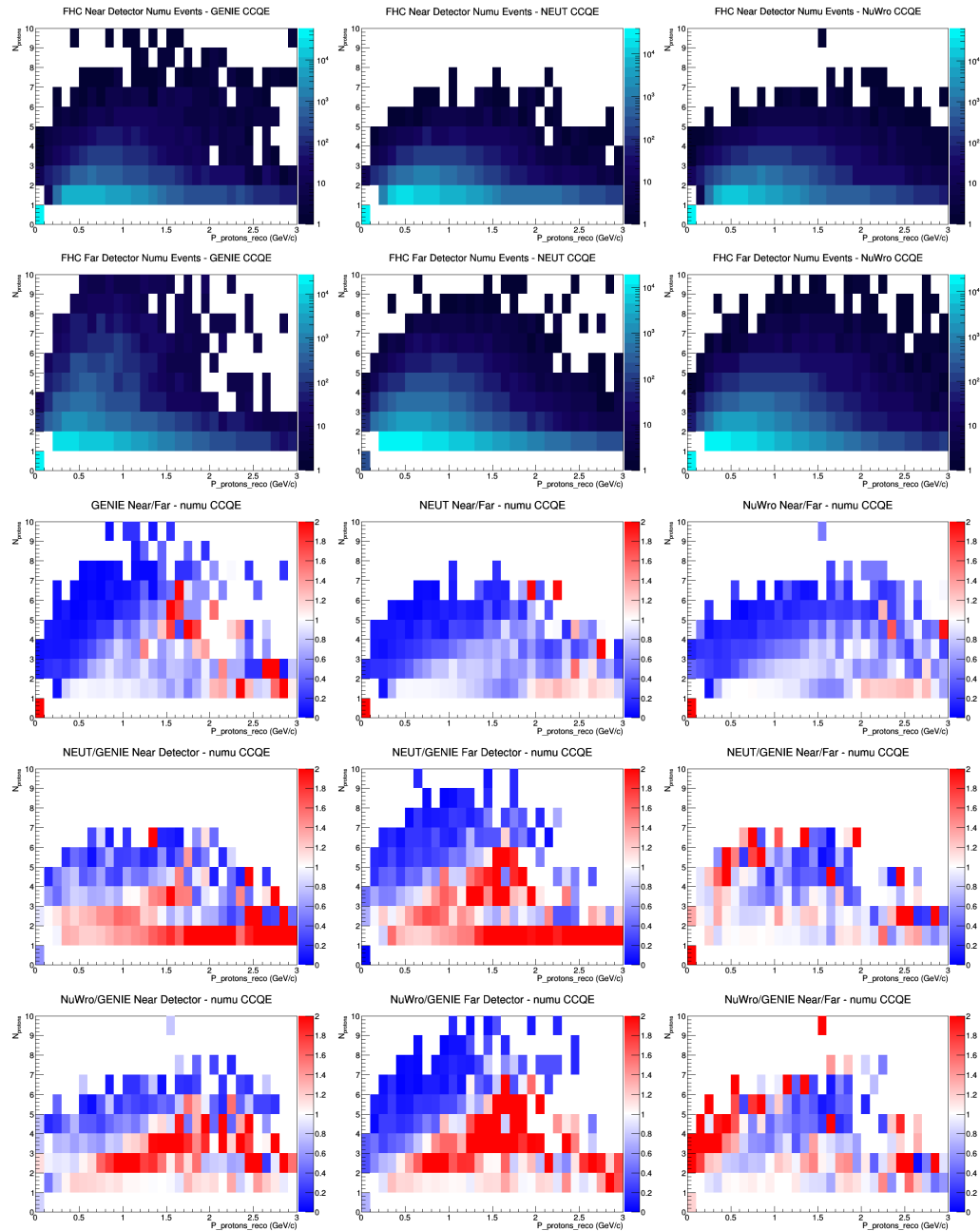
D Proton Multiplicity vs Total Proton Momentum Plots

This appendix includes all the plots not shown in Section 4.2. For full description of the files, please make reference to that section. The plots will be put in the same order as before.

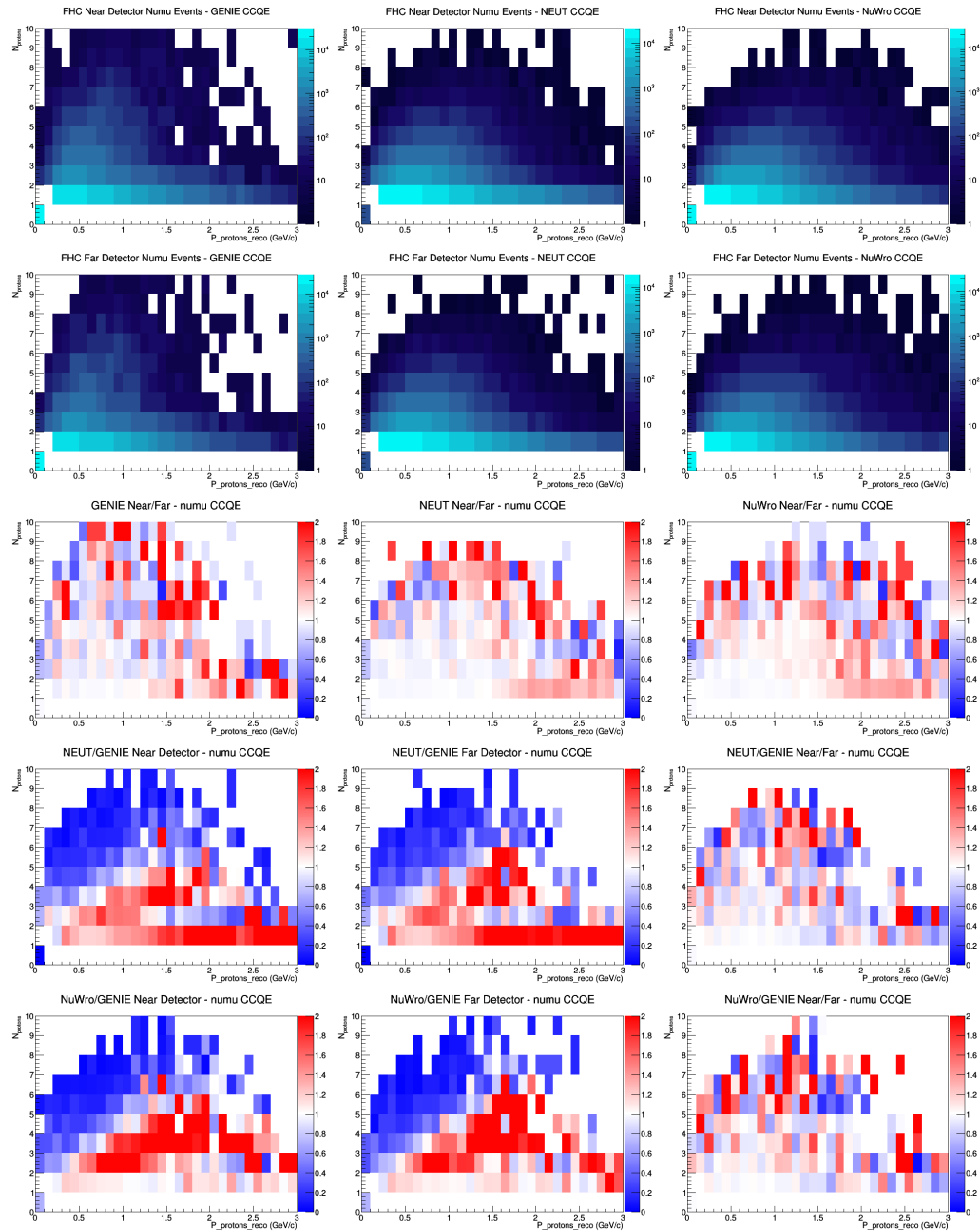
D.1 numu CCQE no efficiencies



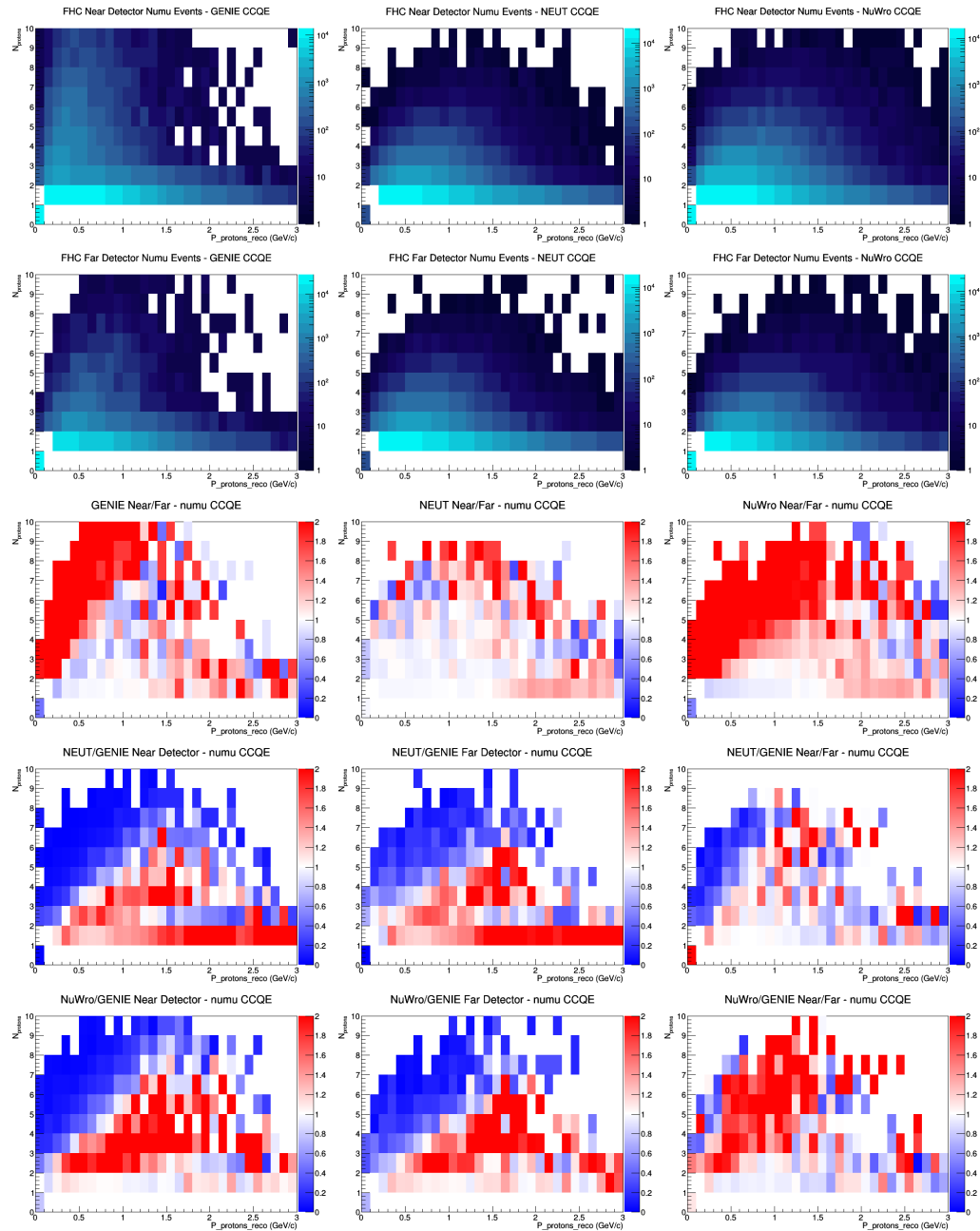
D.2 numu CCQE FGT efficiencies



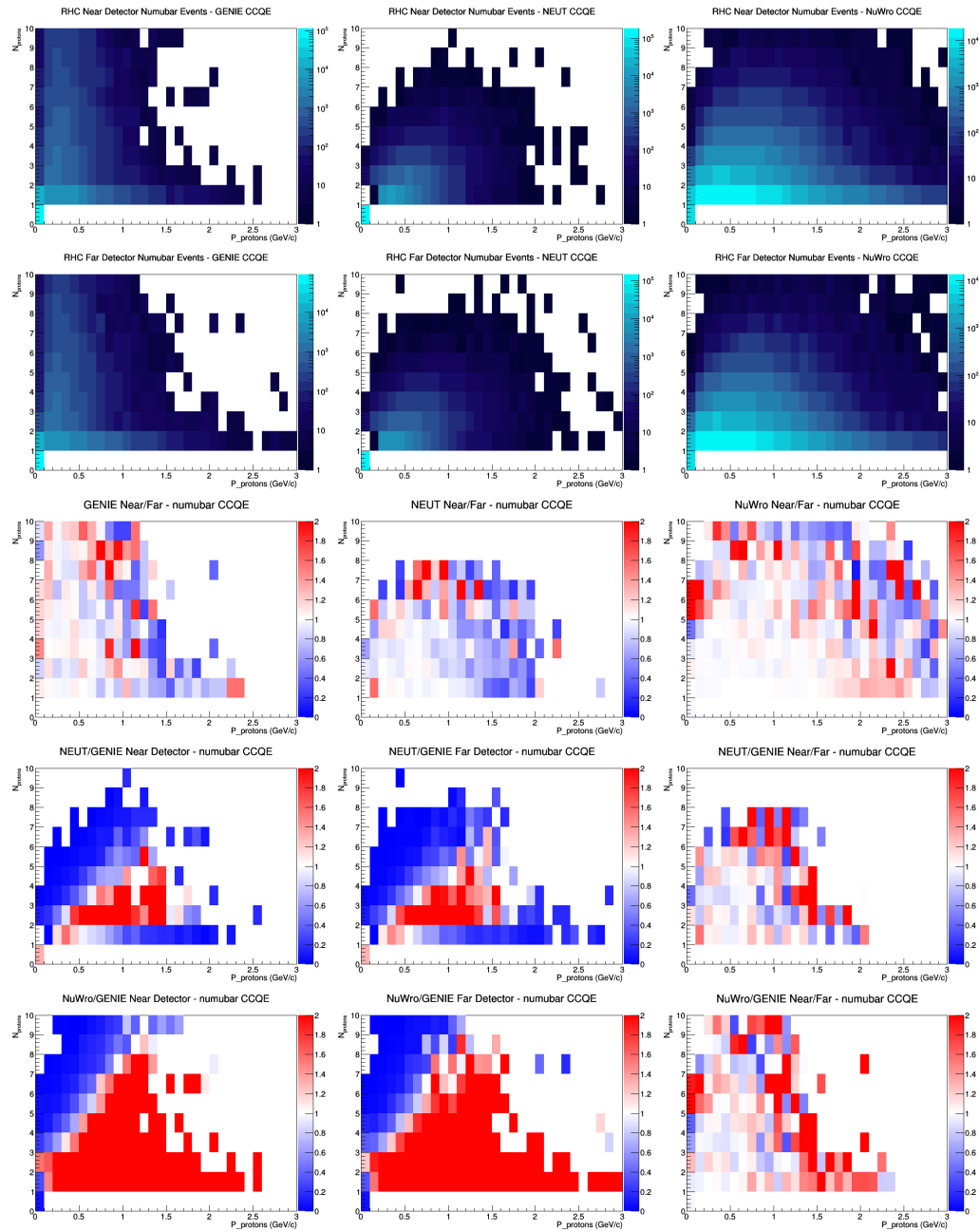
D.3 numu CCQE LAr efficiencies



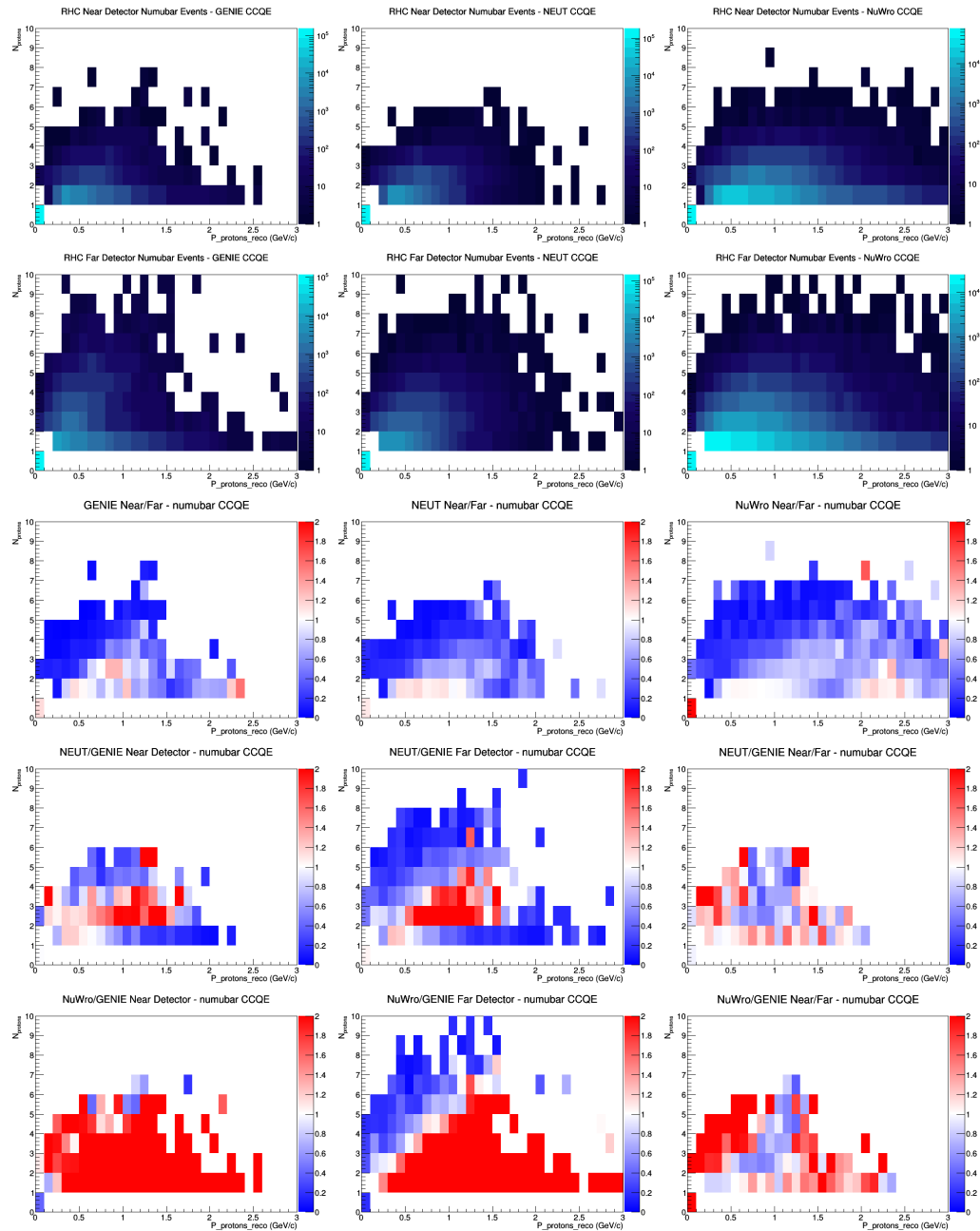
D.4 numu CCQE GAr efficiencies



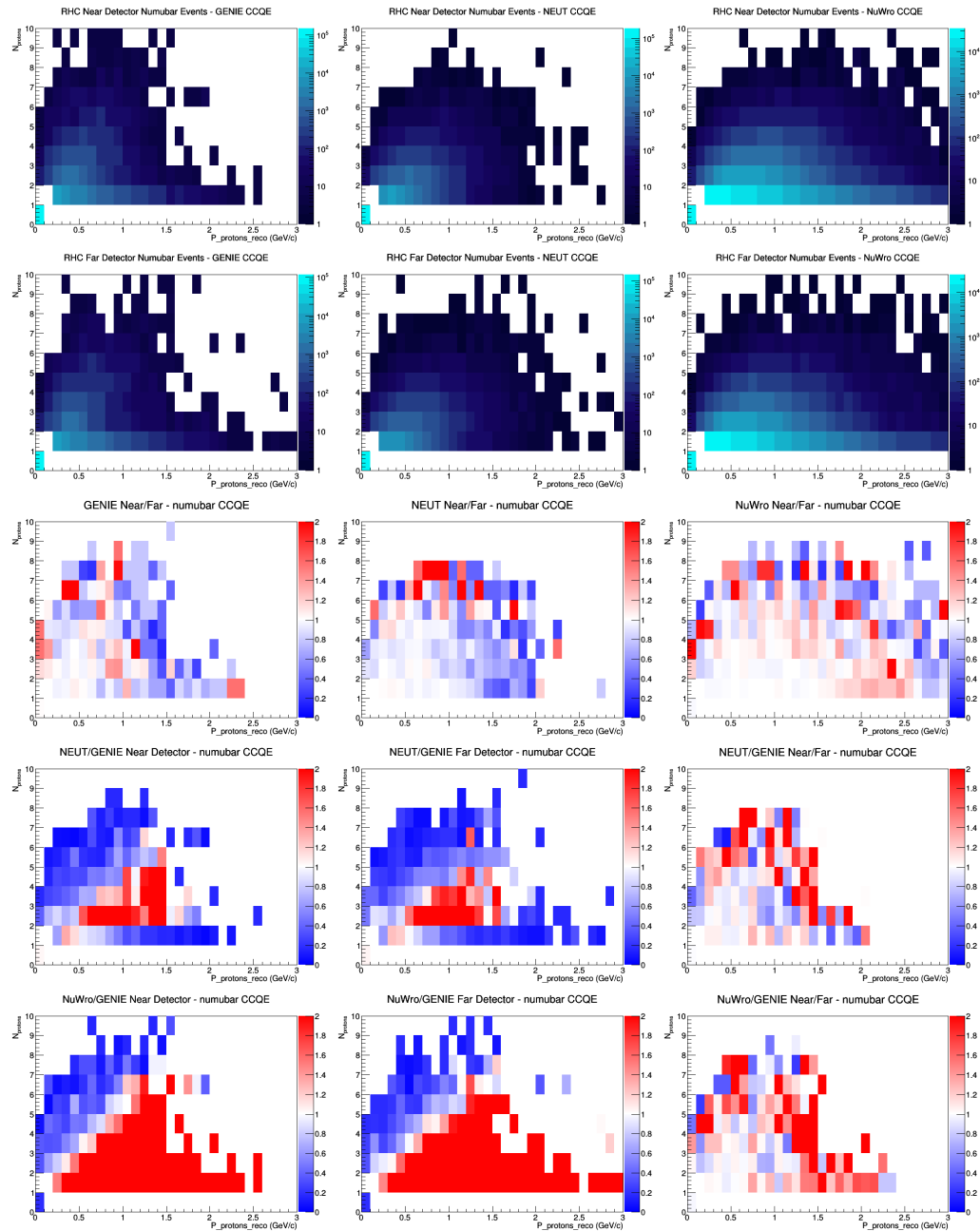
D.5 numubar CCQE no efficiencies



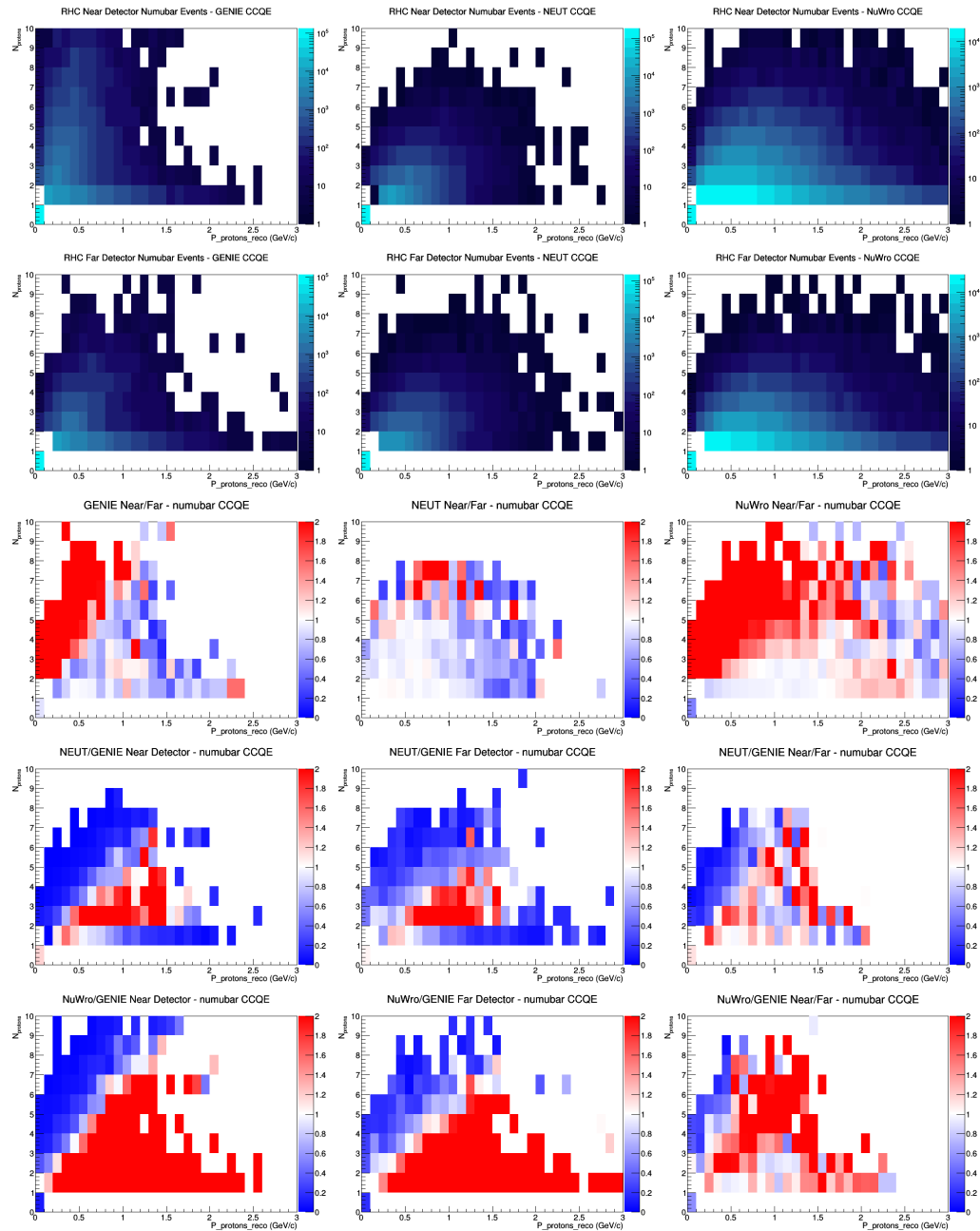
D.6 numubar CCQE FGT efficiencies



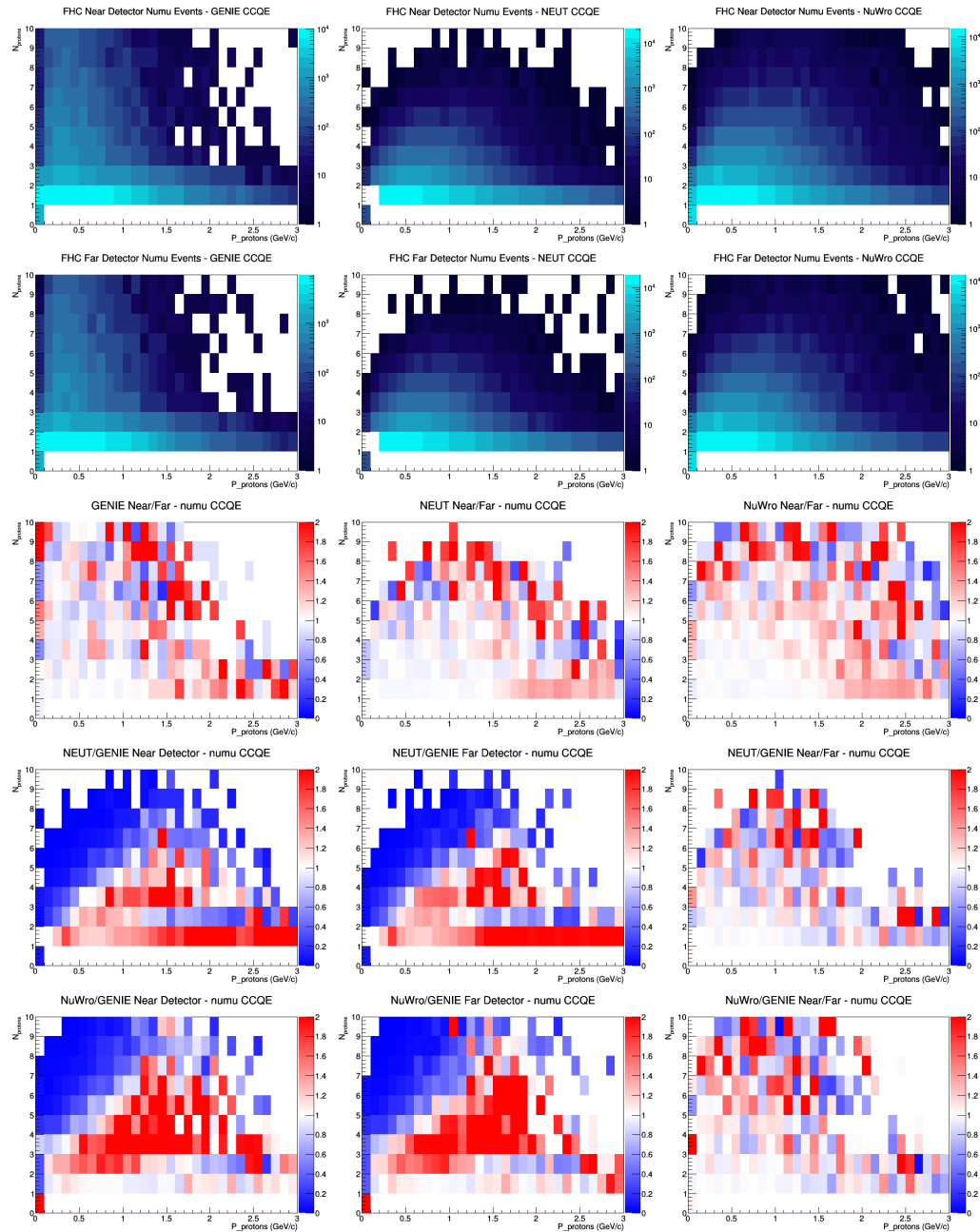
D.7 numubar CCQE LAr efficiencies



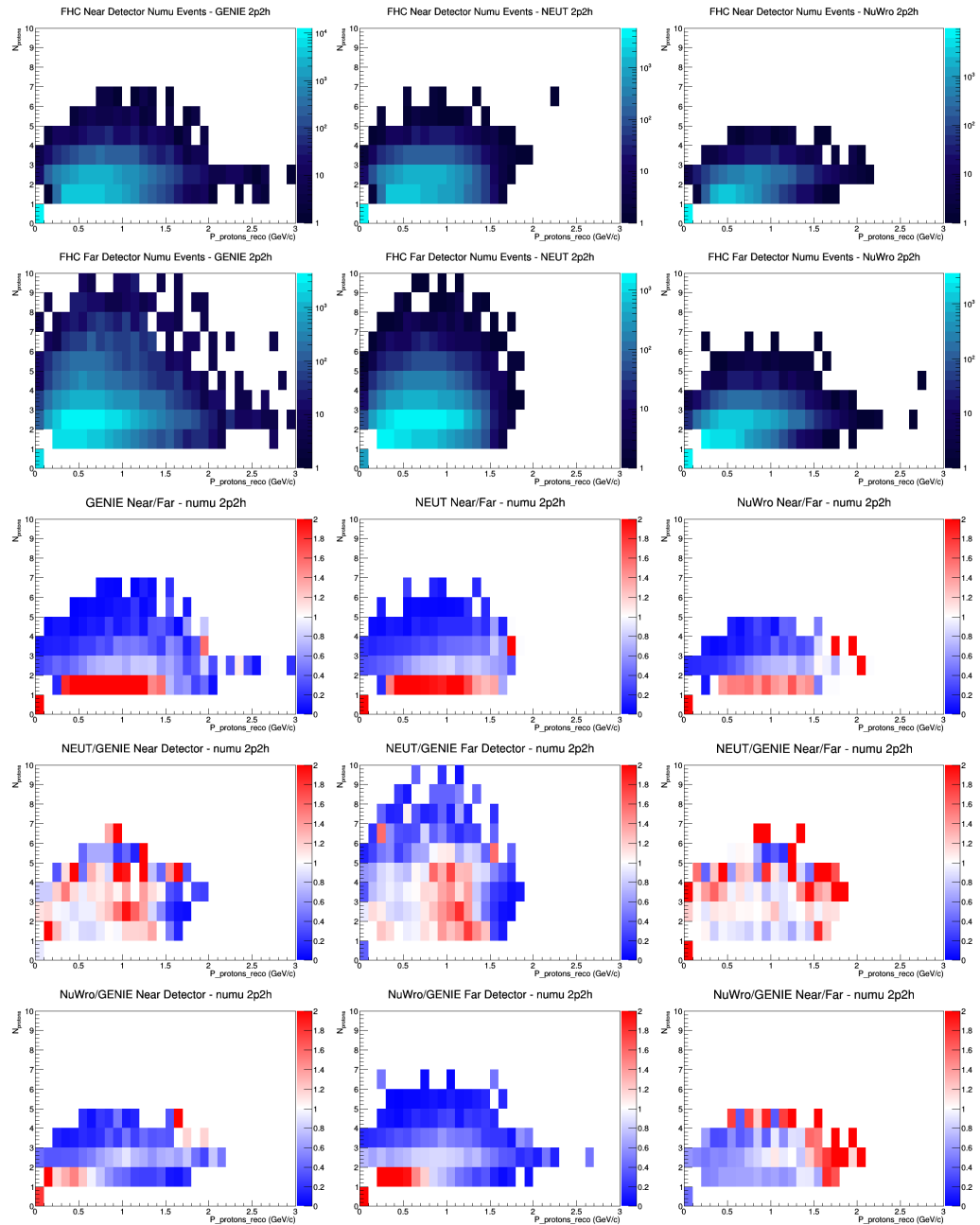
D.8 numubar CCQE GAr efficiencies



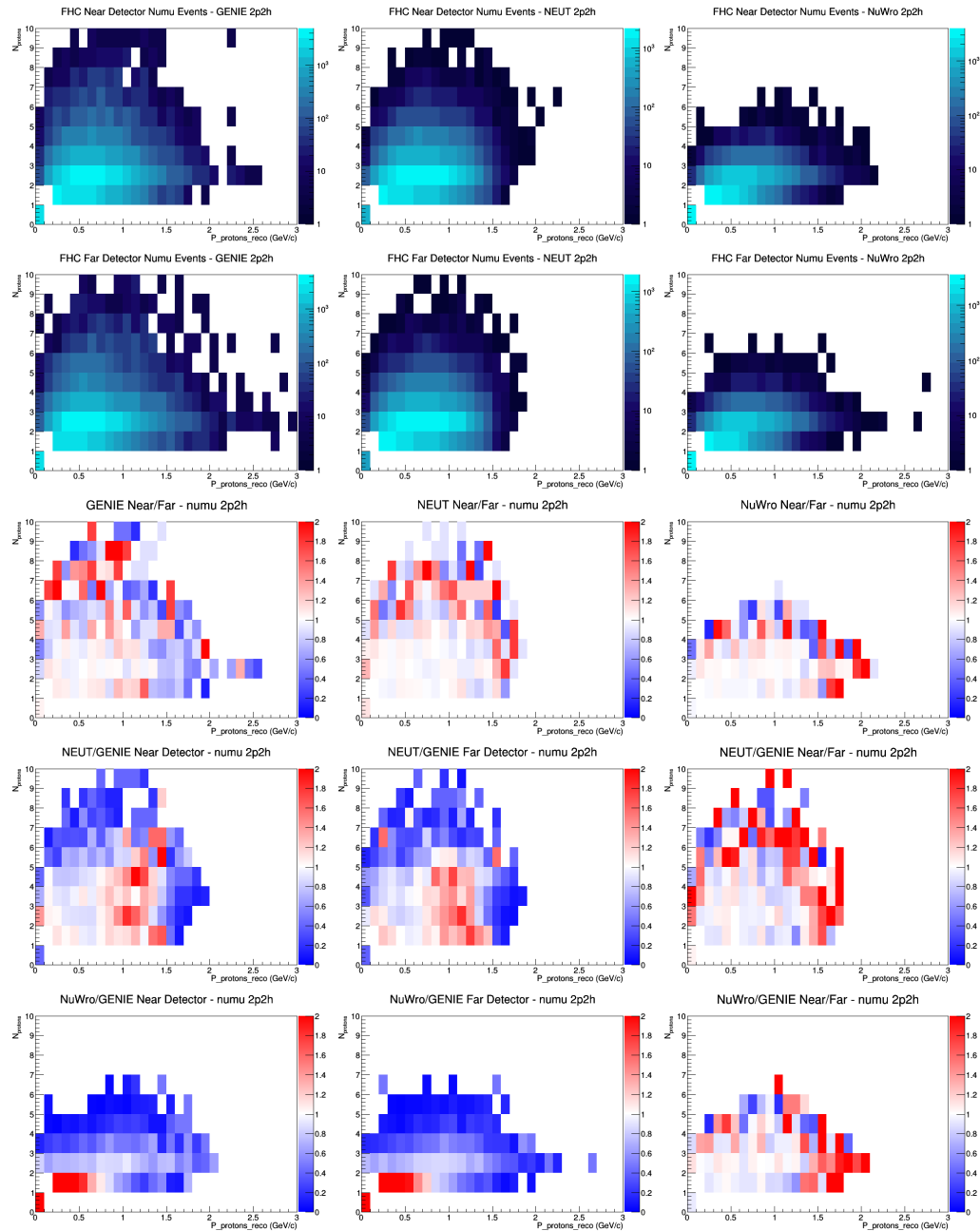
D.9 numu 2p2h no efficiencies



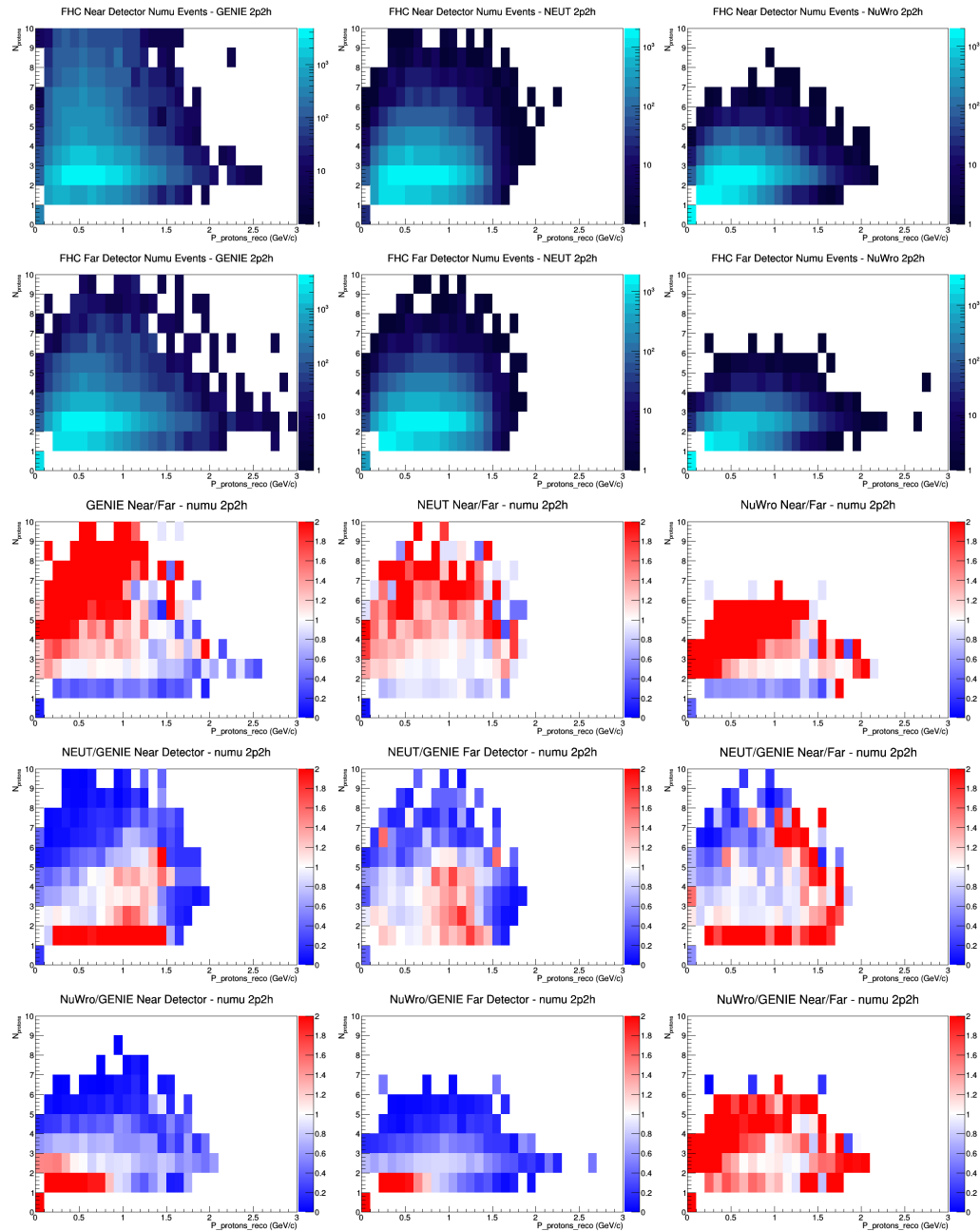
D.10 numu 2p2h FGT efficiencies



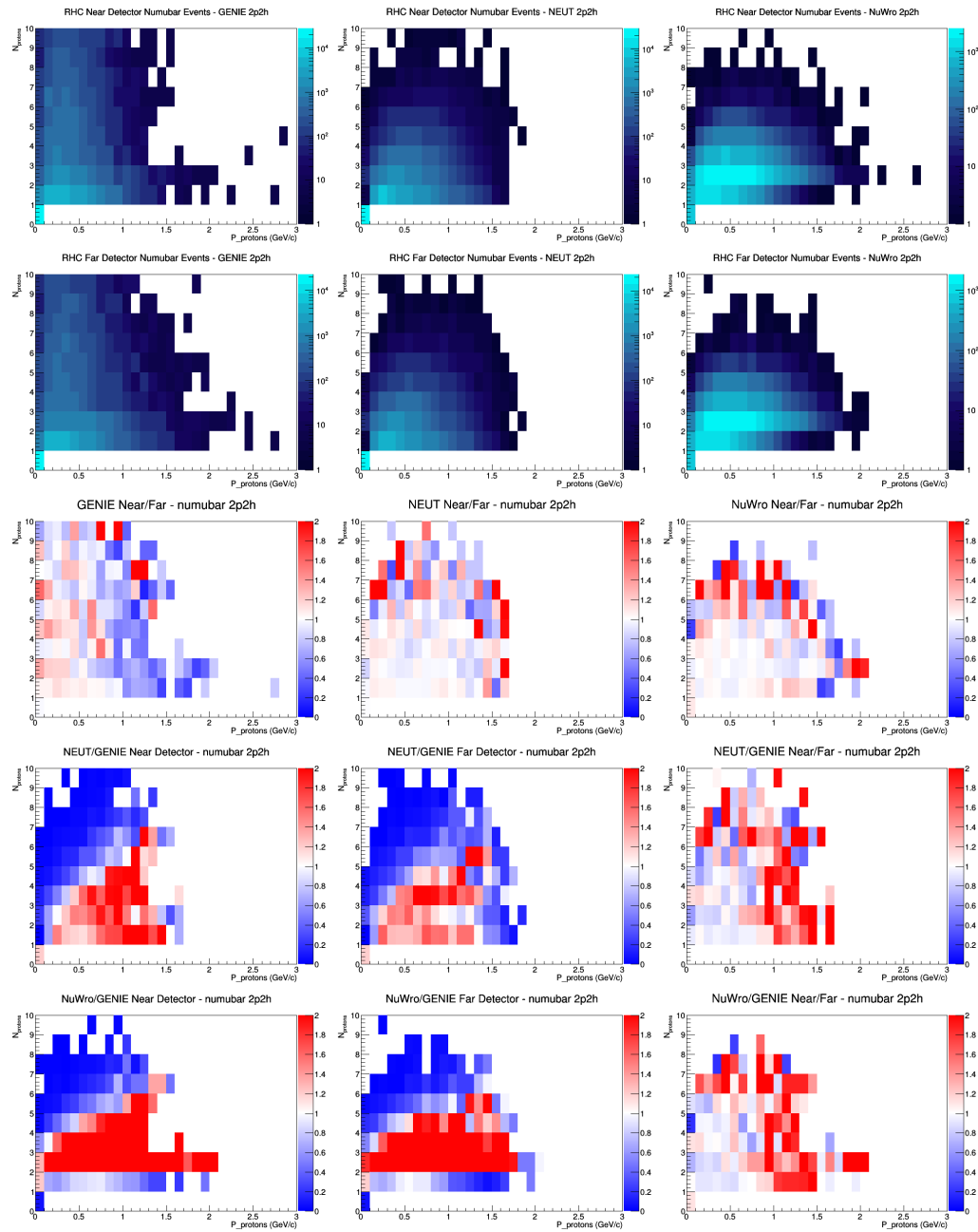
D.11 numu 2p2h LAr efficiencies



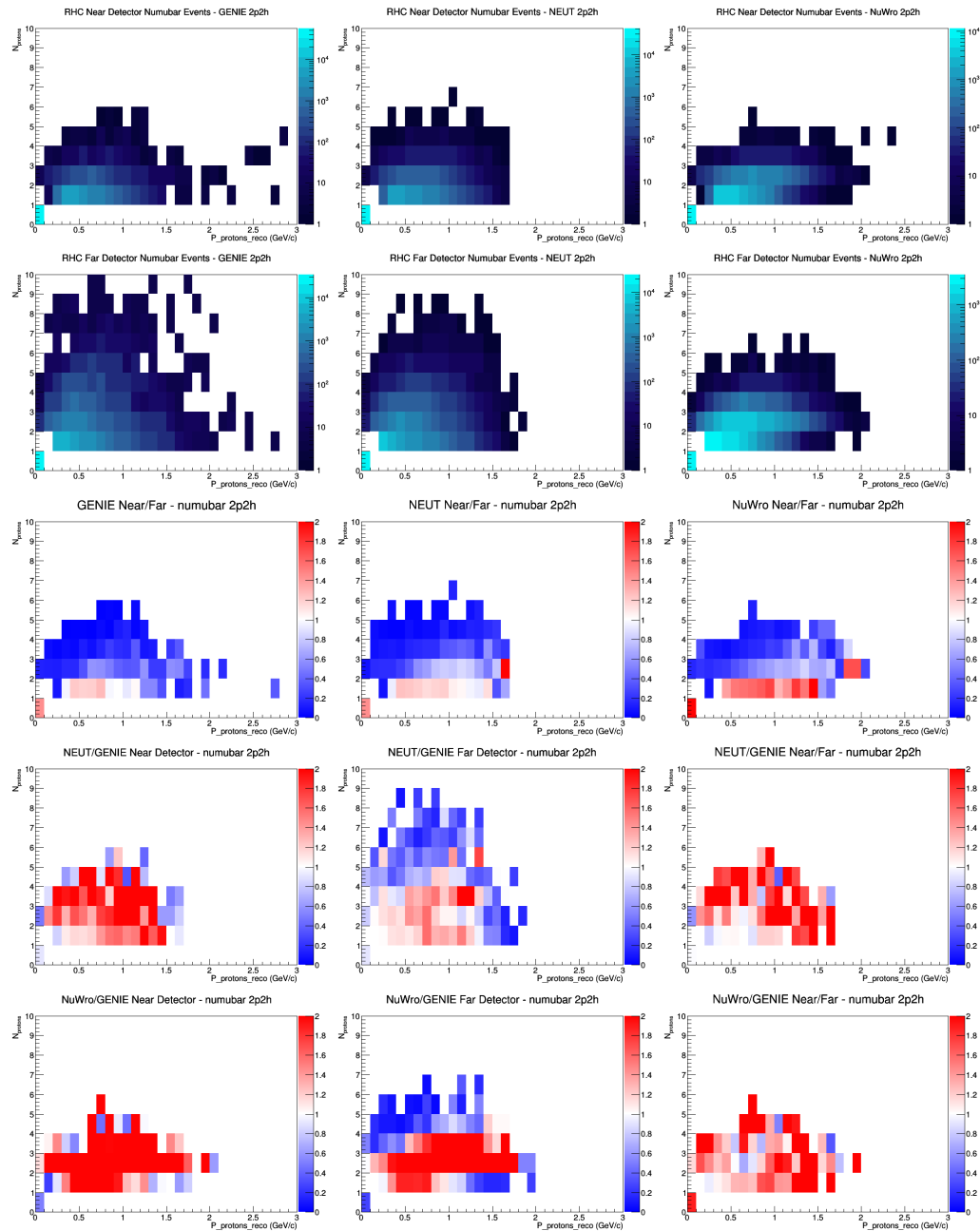
D.12 numu 2p2h GAr efficiencies



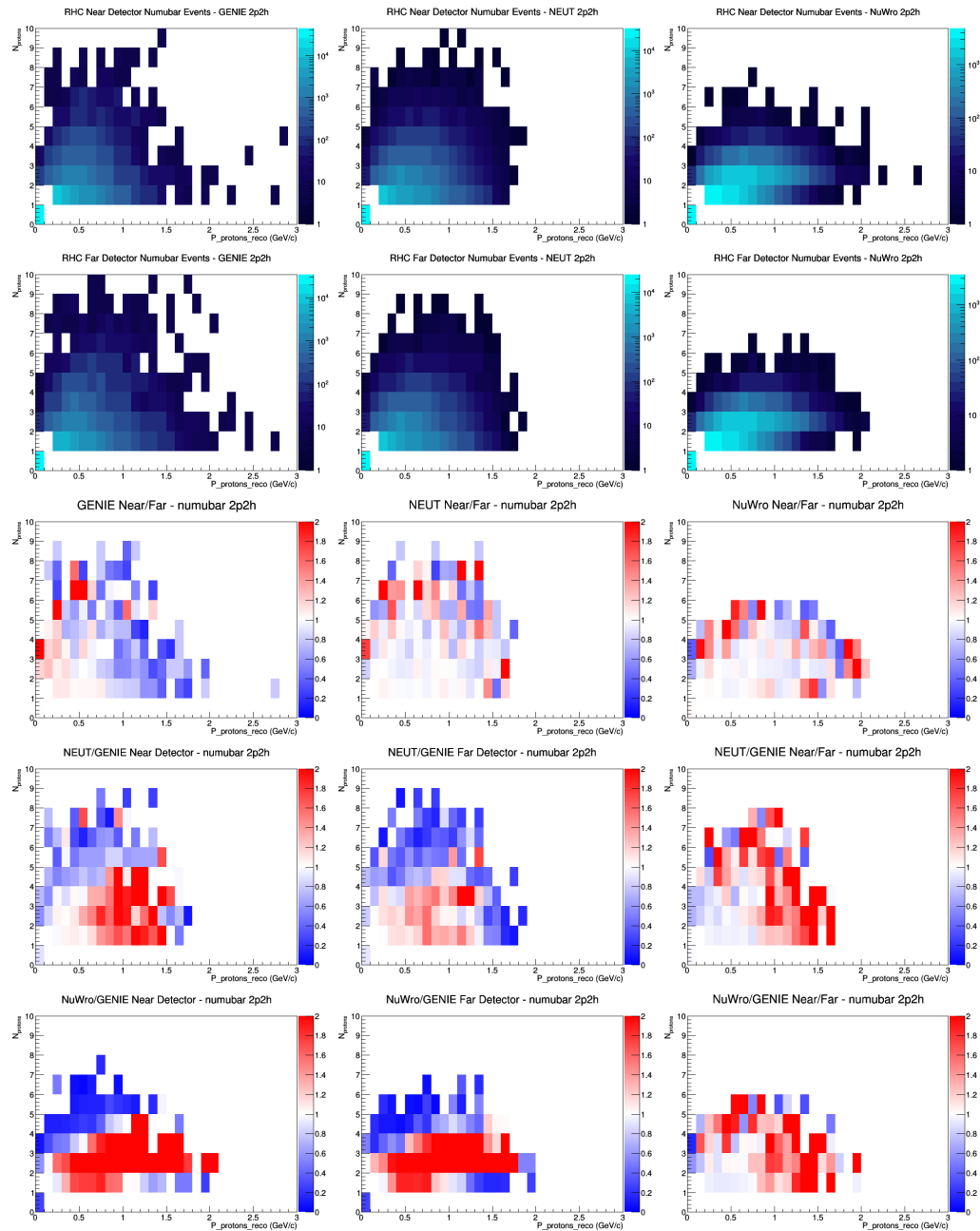
D.13 numubar 2p2h no efficiencies



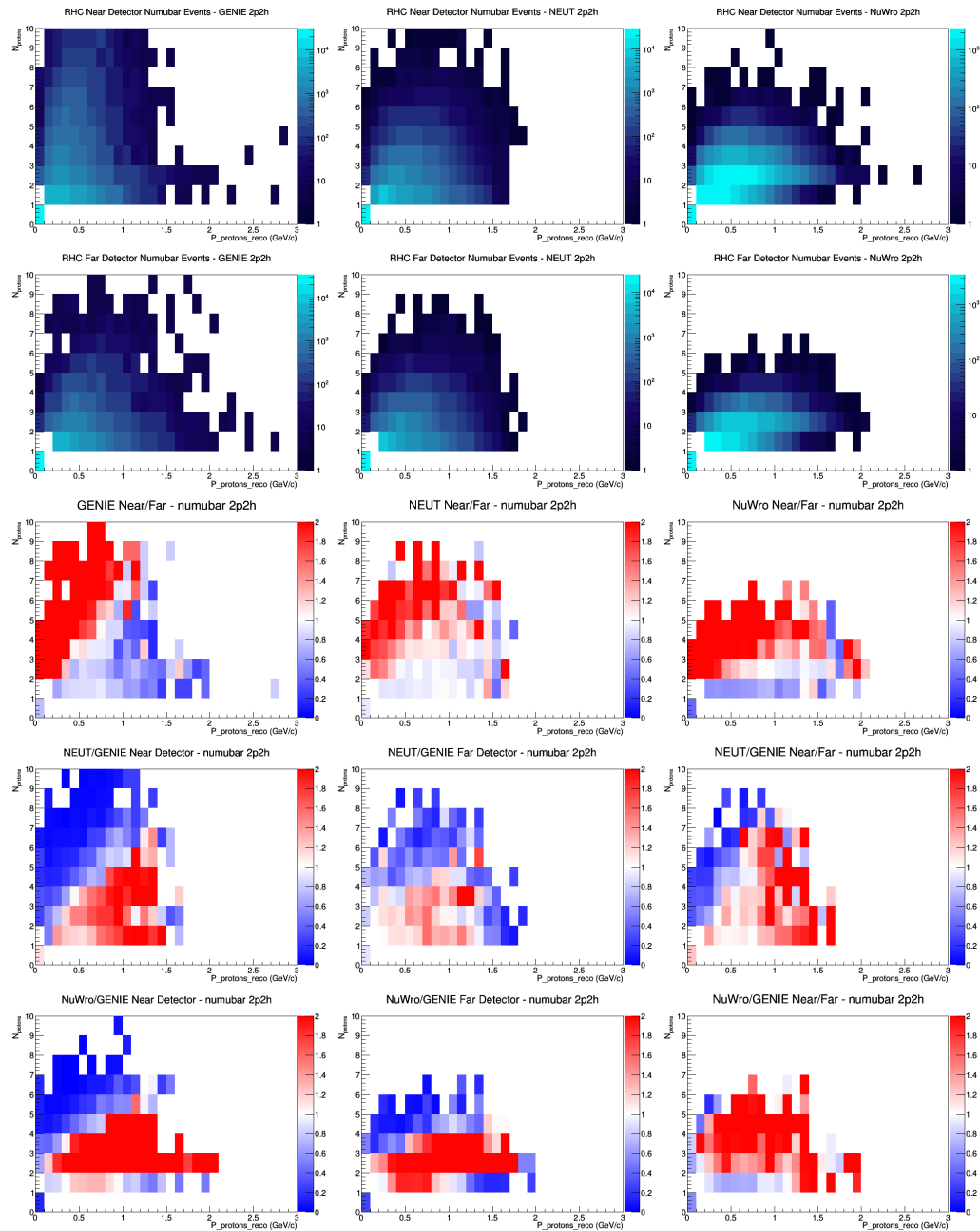
D.14 numubar 2p2h FGT efficiencies



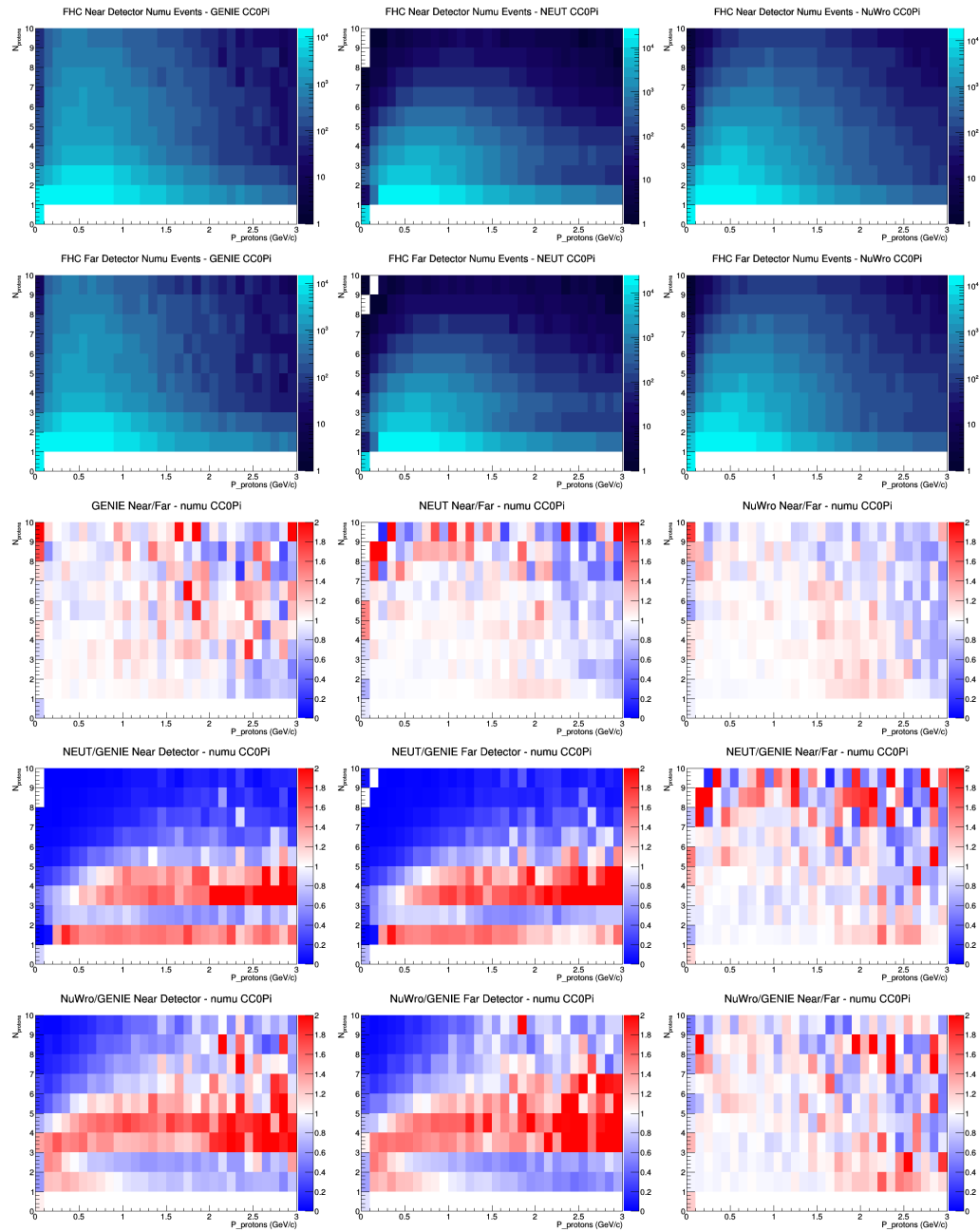
D.15 numubar 2p2h LAr efficiencies



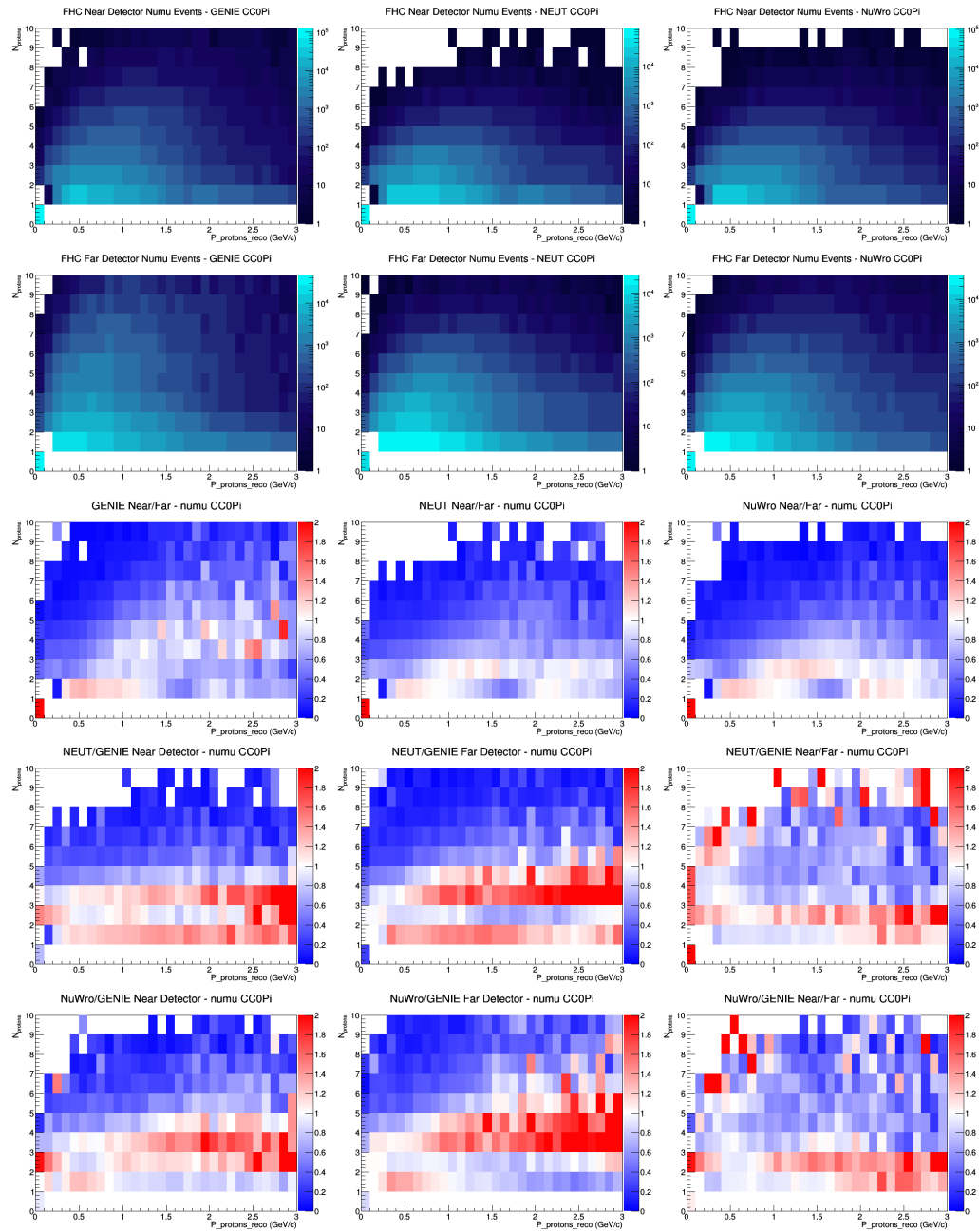
D.16 numubar 2p2h GAr efficiencies



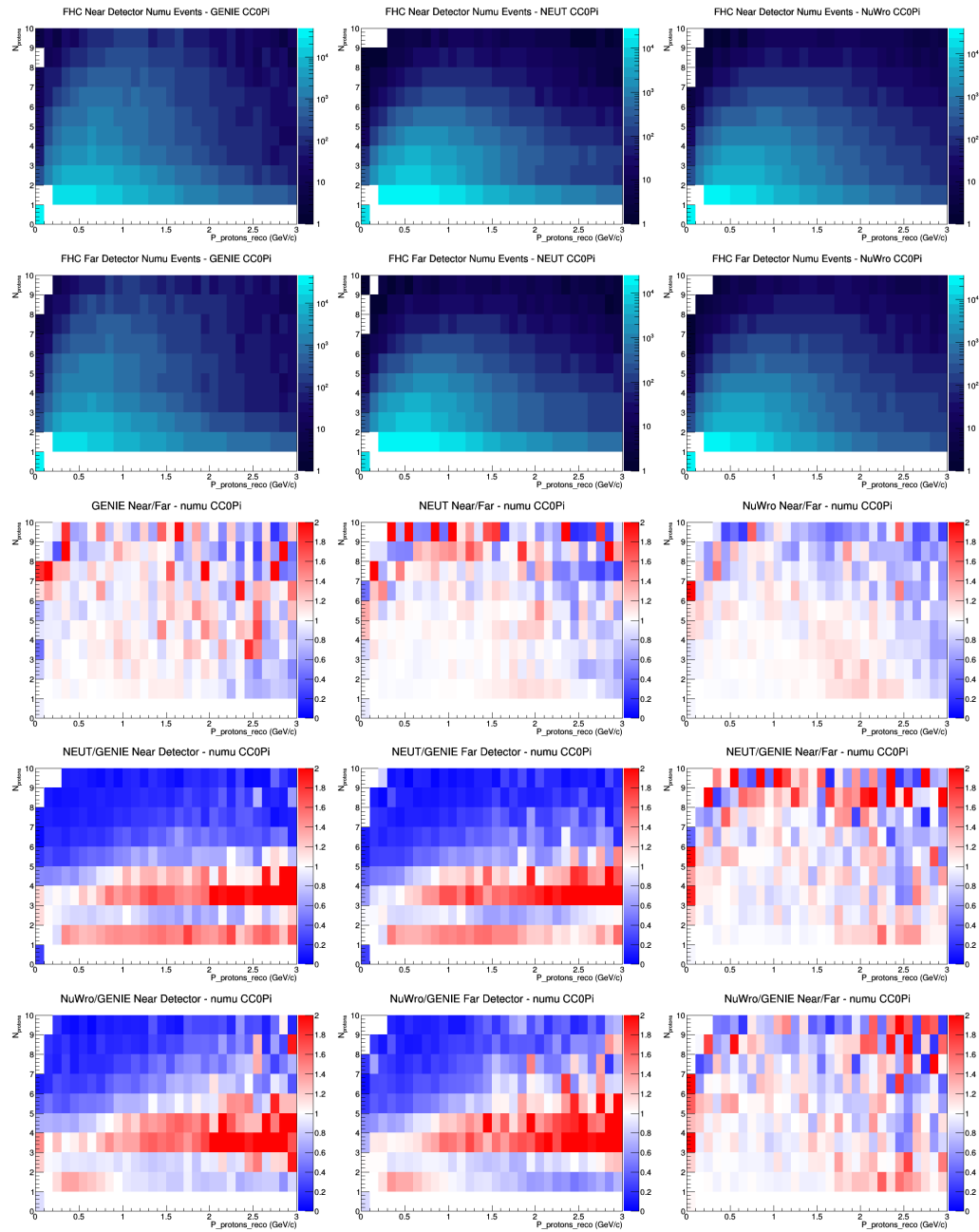
D.17 numu CC0Pi no efficiencies



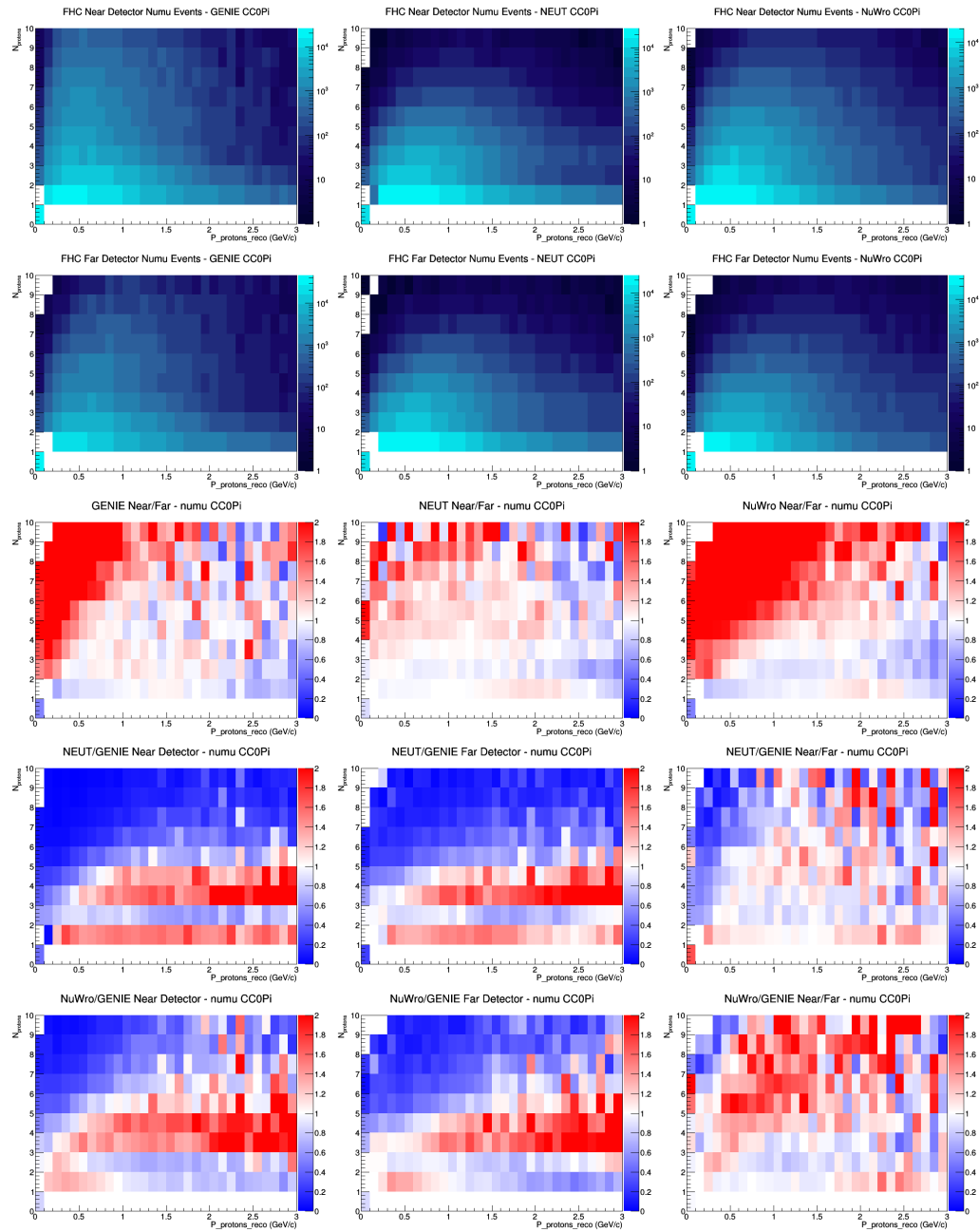
D.18 numu CC0Pi FGT efficiencies



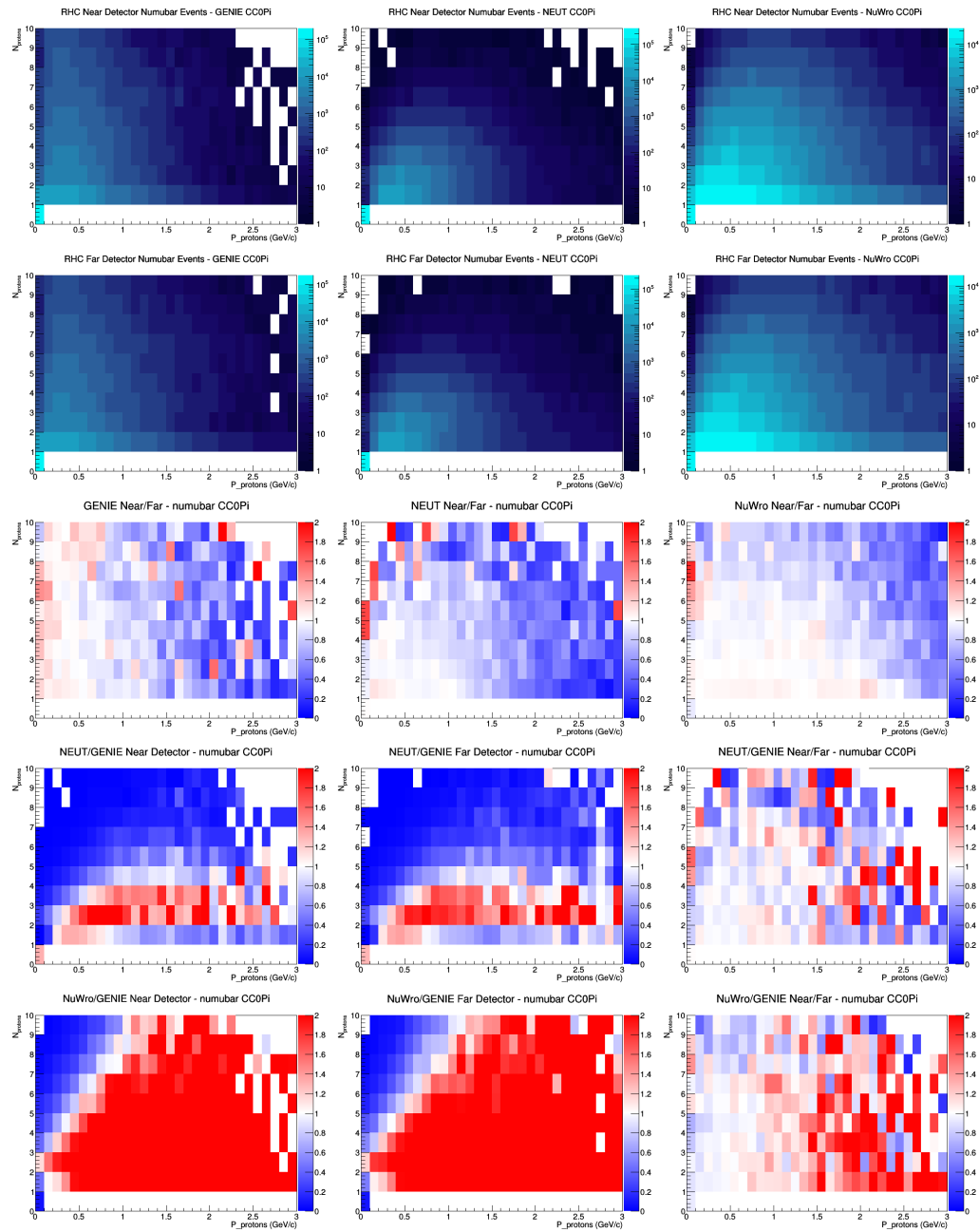
D.19 numu CC0Pi LAr efficiencies



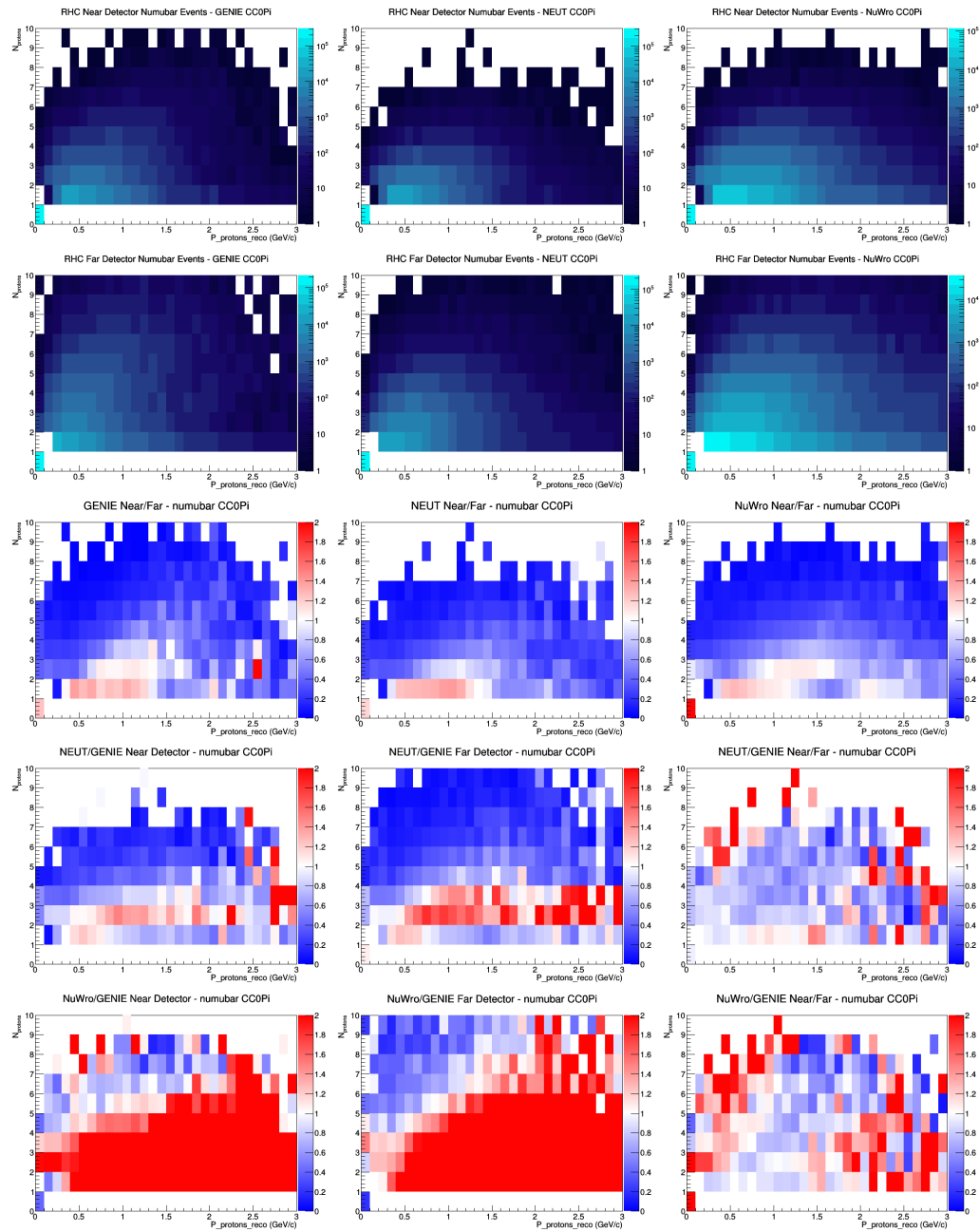
D.20 numu CC0Pi GAr efficiencies



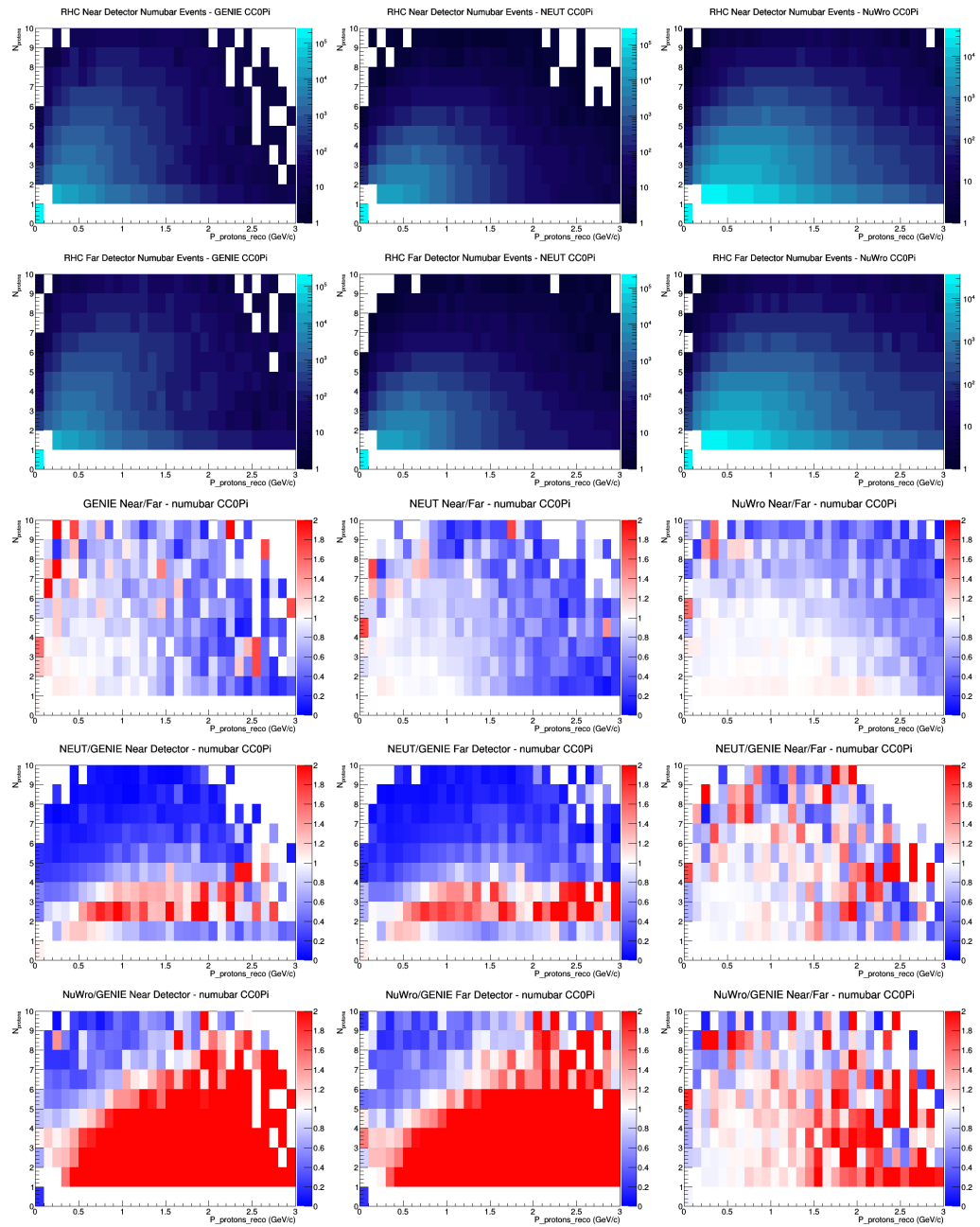
D.21 numubar CC0Pi no efficiencies



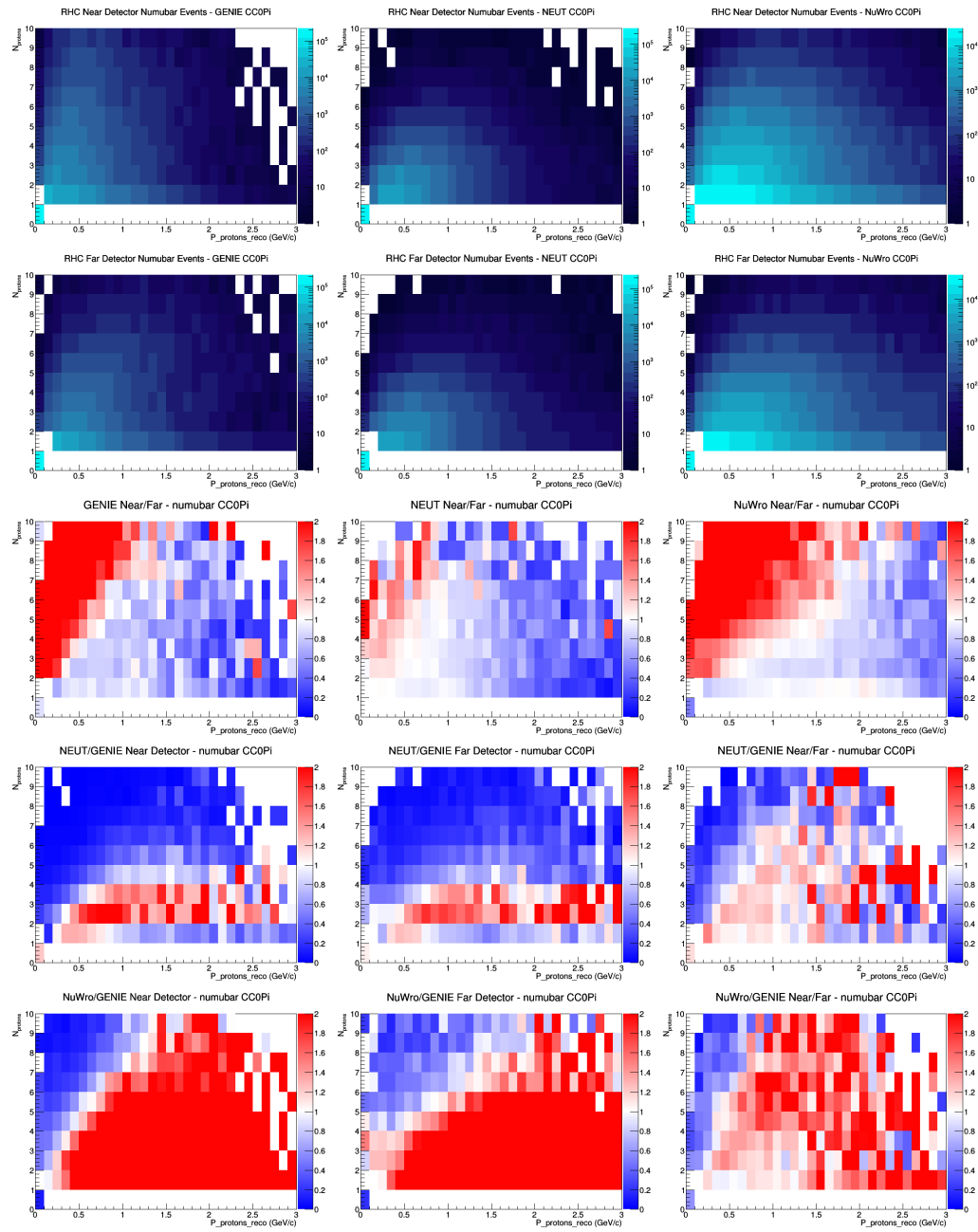
D.22 numubar CC0Pi FGT efficiencies



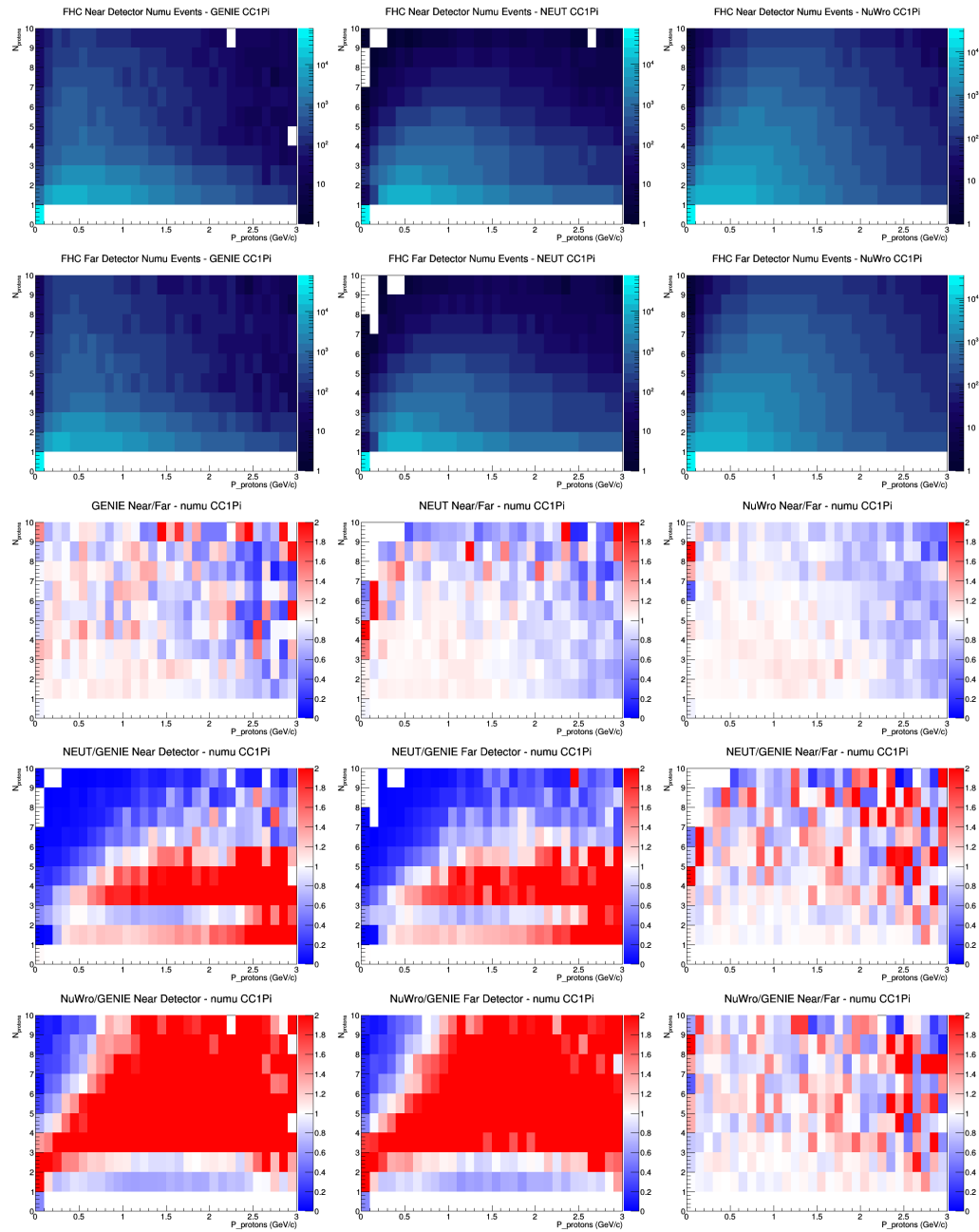
D.23 numubar CC0Pi LAr efficiencies



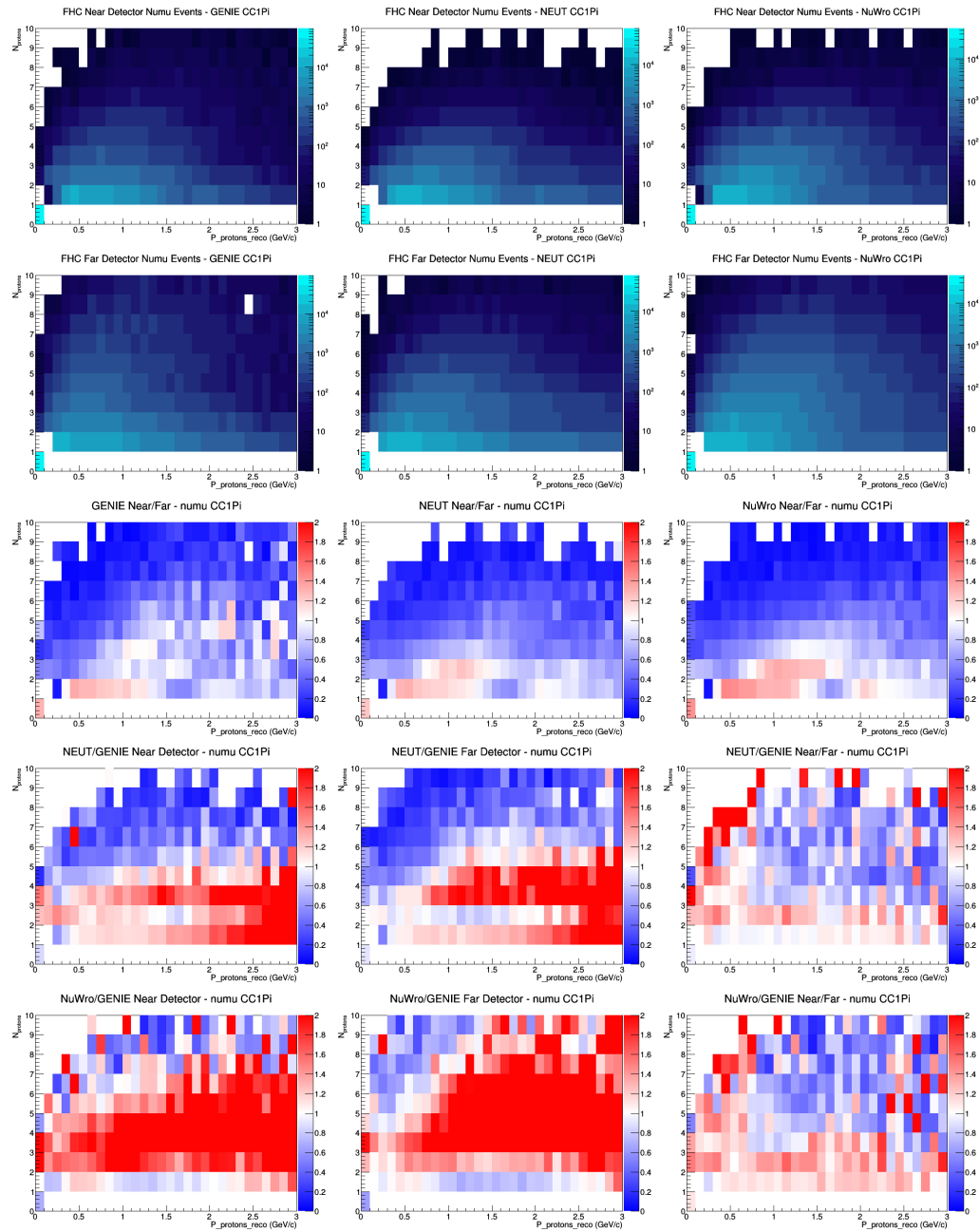
D.24 numubar CC0Pi GAr efficiencies



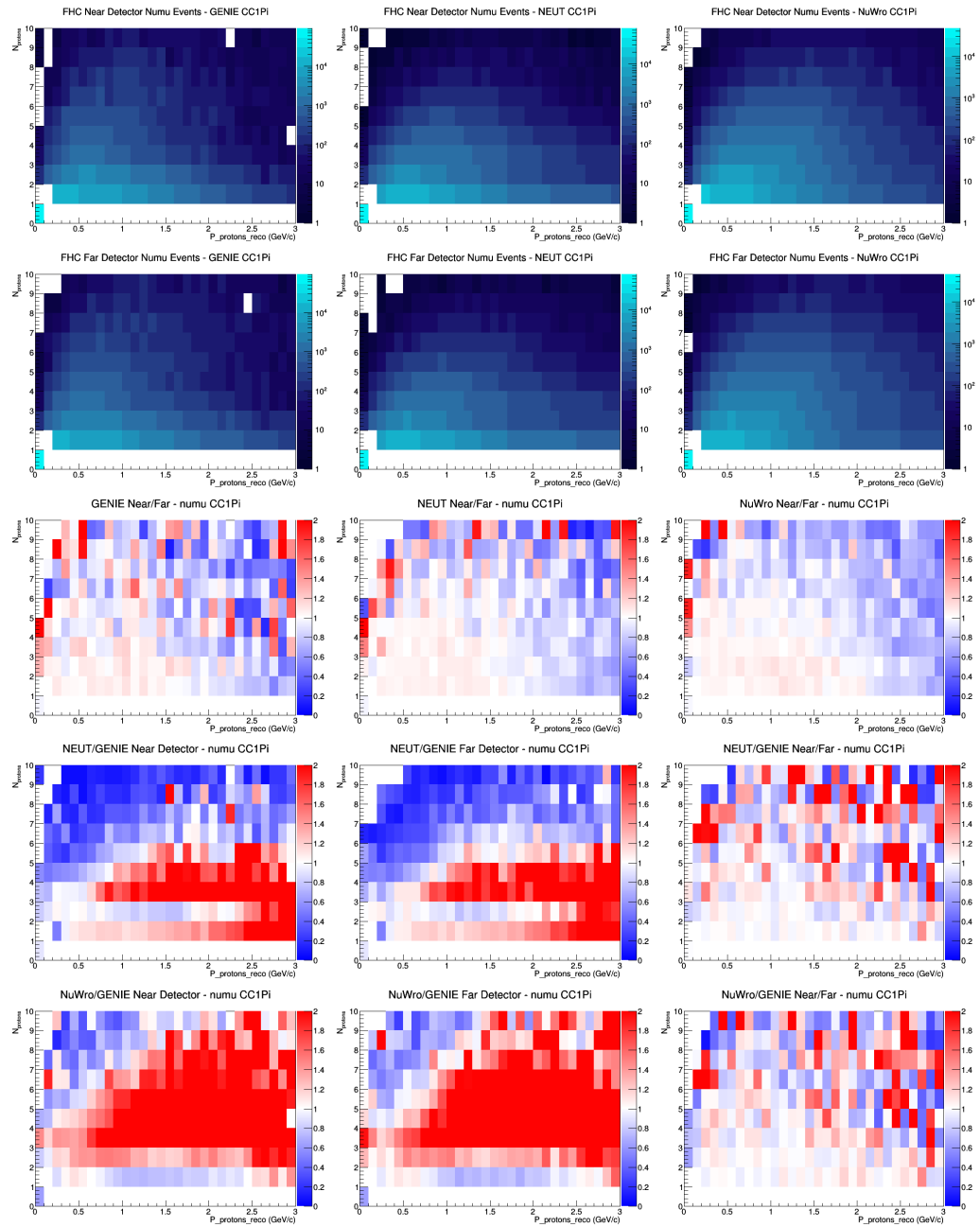
D.25 numu CC1Pi no efficiencies



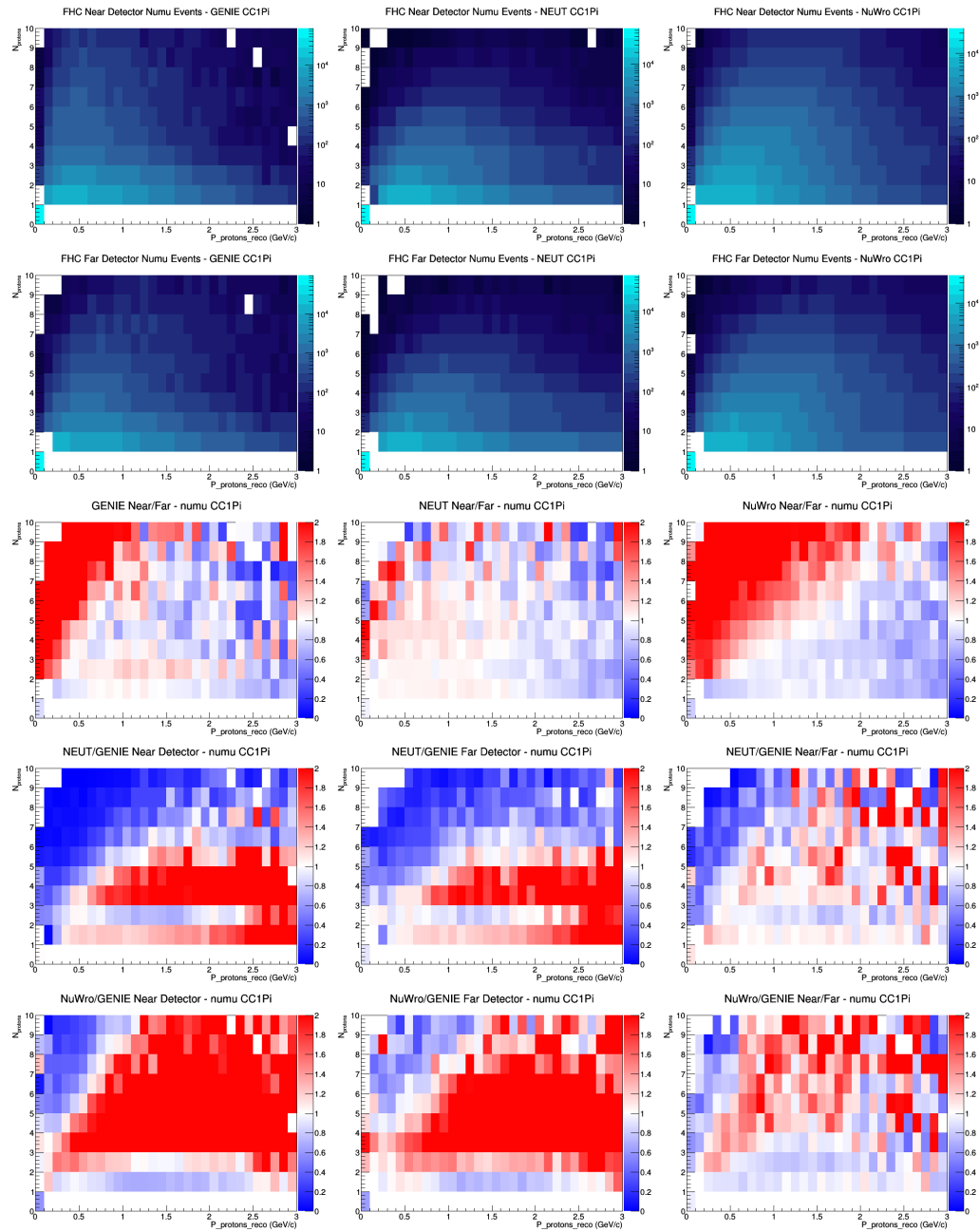
D.26 numu CC1Pi FGT efficiencies



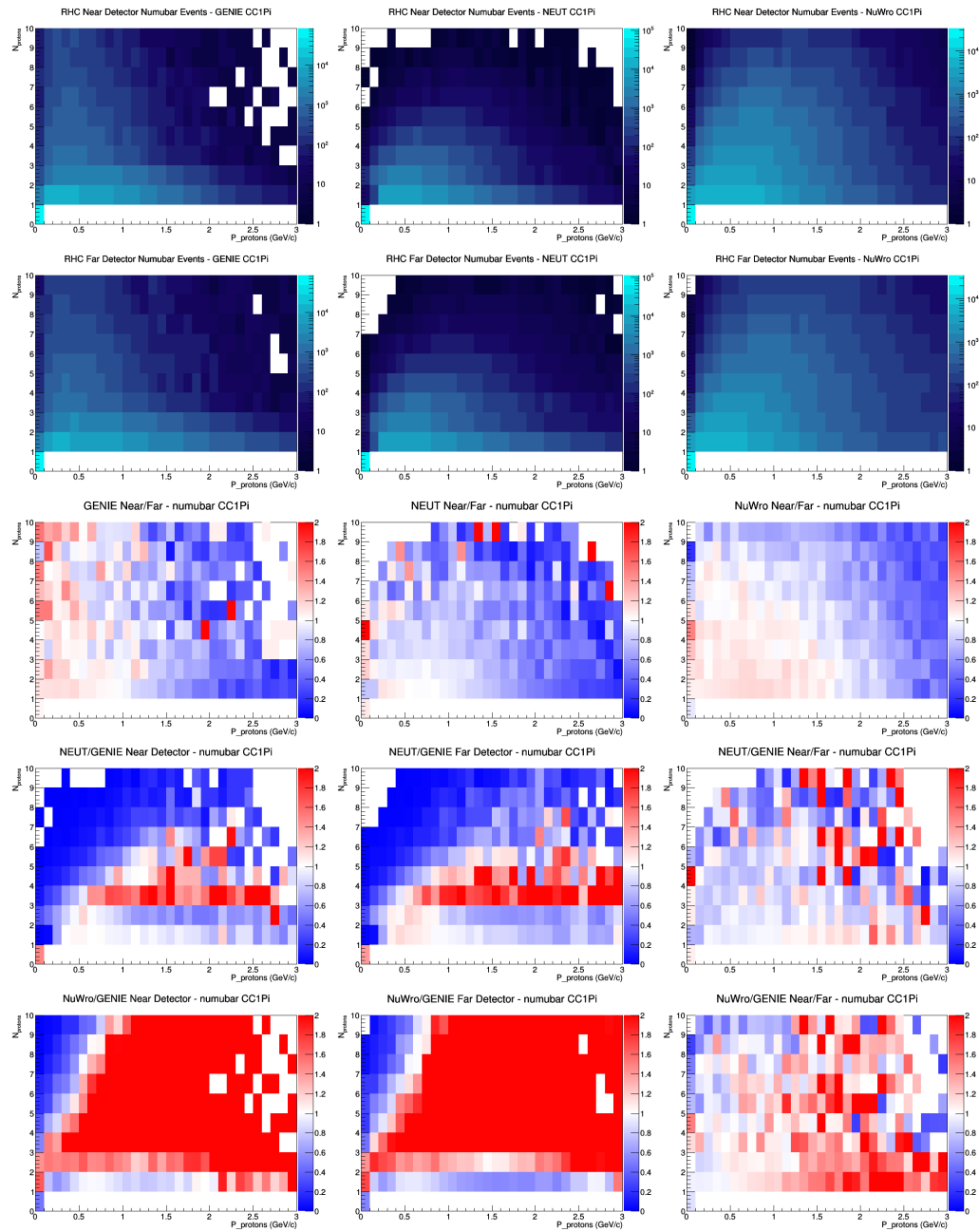
D.27 numu CC1Pi LAr efficiencies



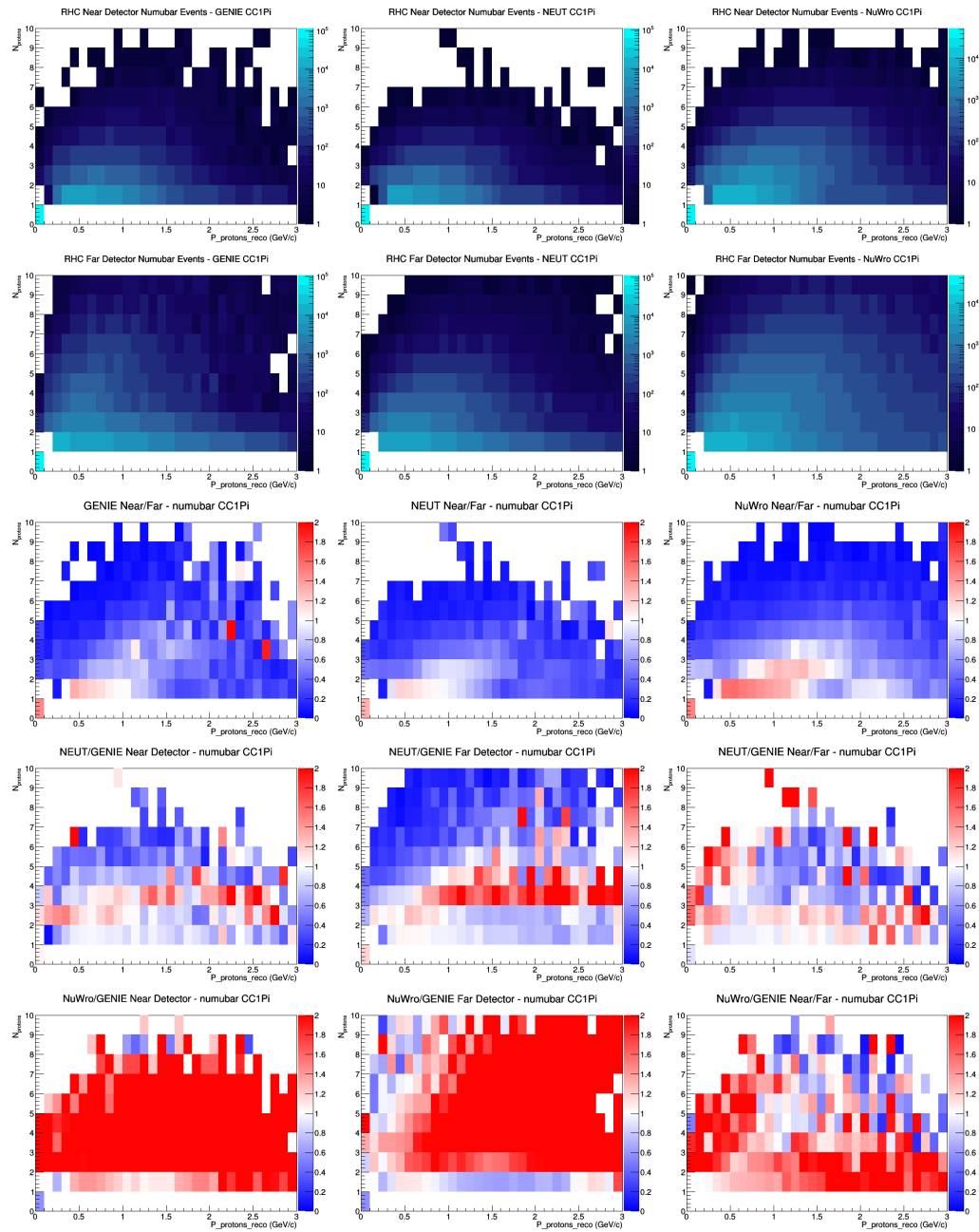
D.28 numu CC1Pi GAr efficiencies



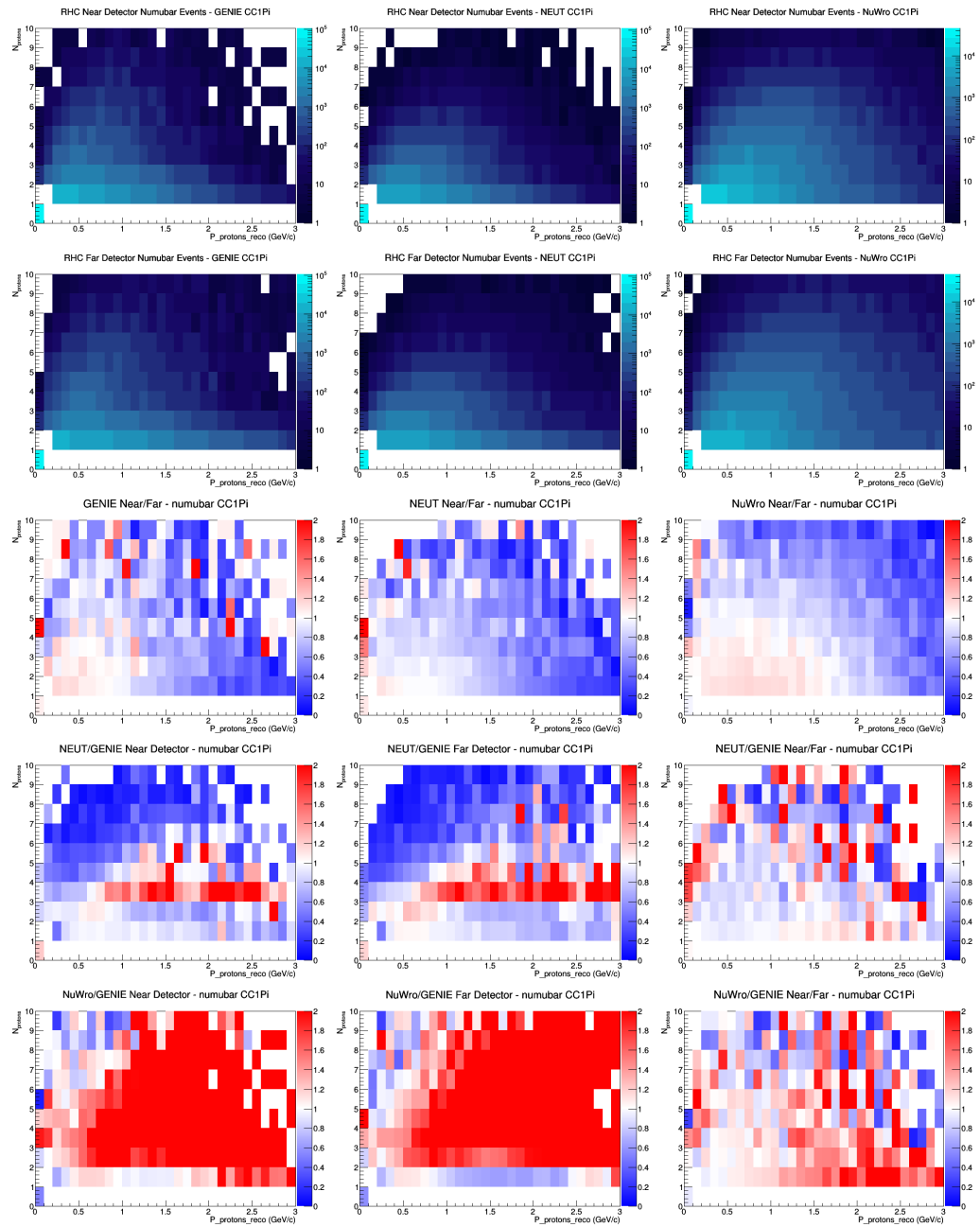
D.29 numubar CC1Pi no efficiencies



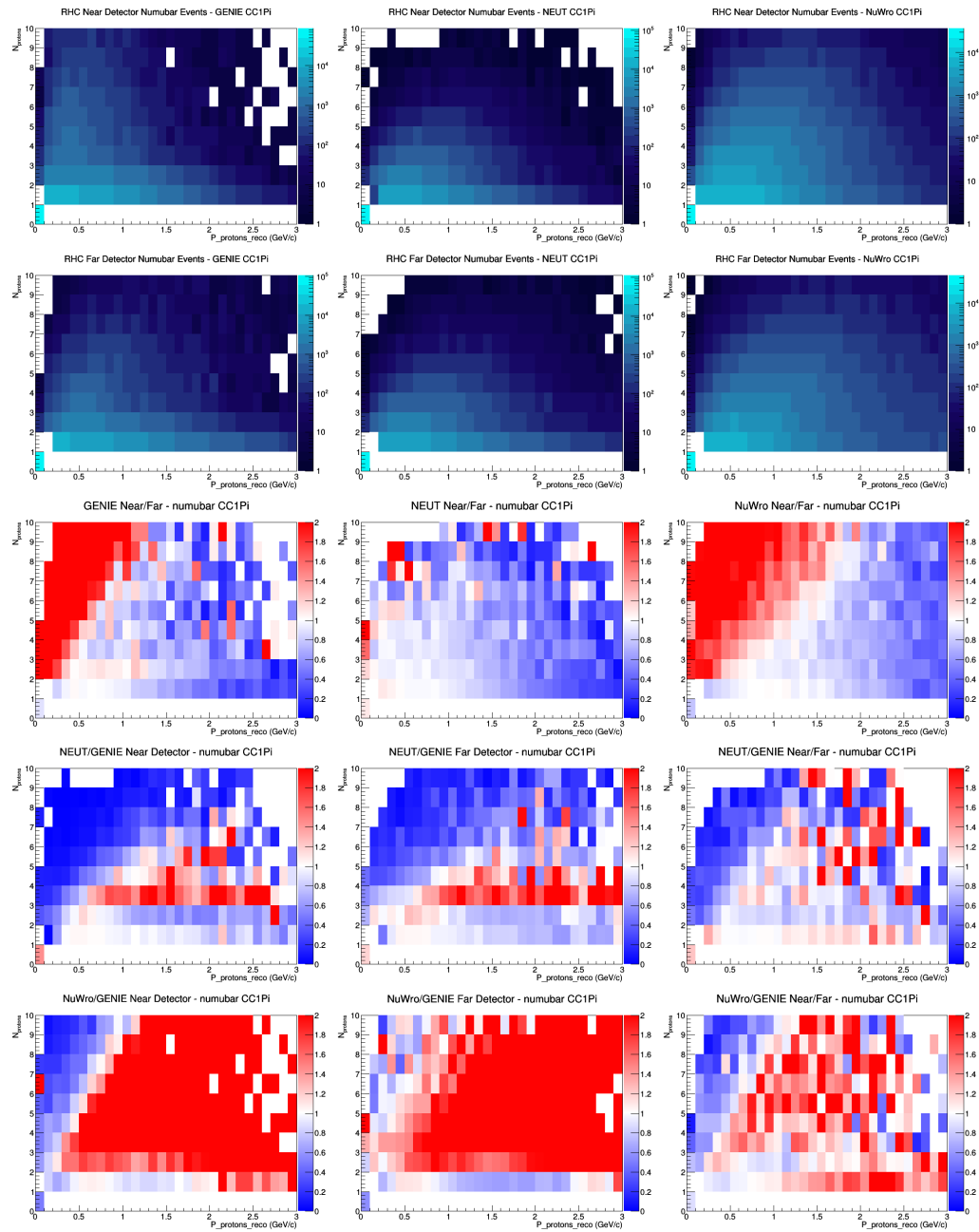
D.30 numubar CC1Pi FGT efficiencies



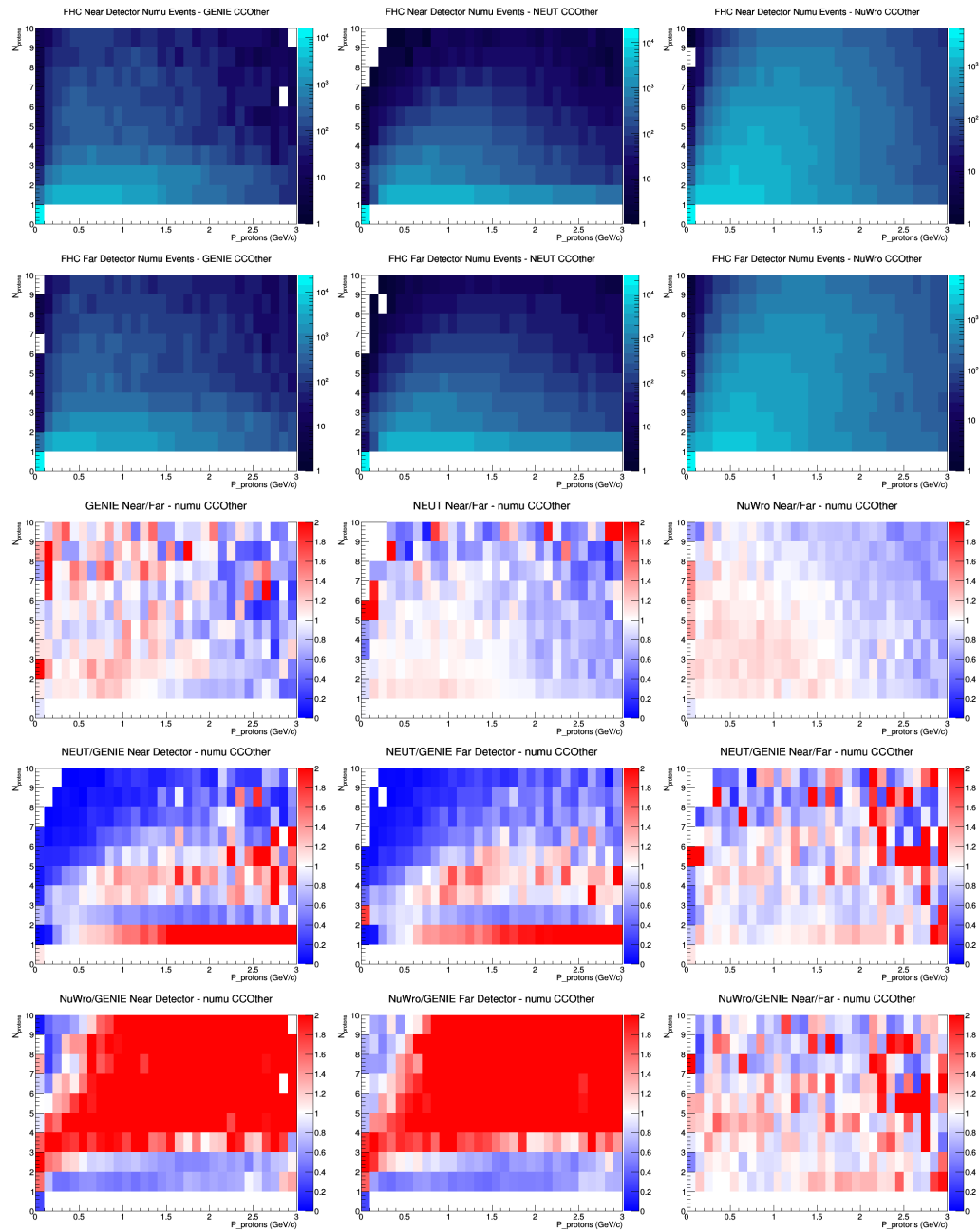
D.31 numubar CC1Pi LAr efficiencies



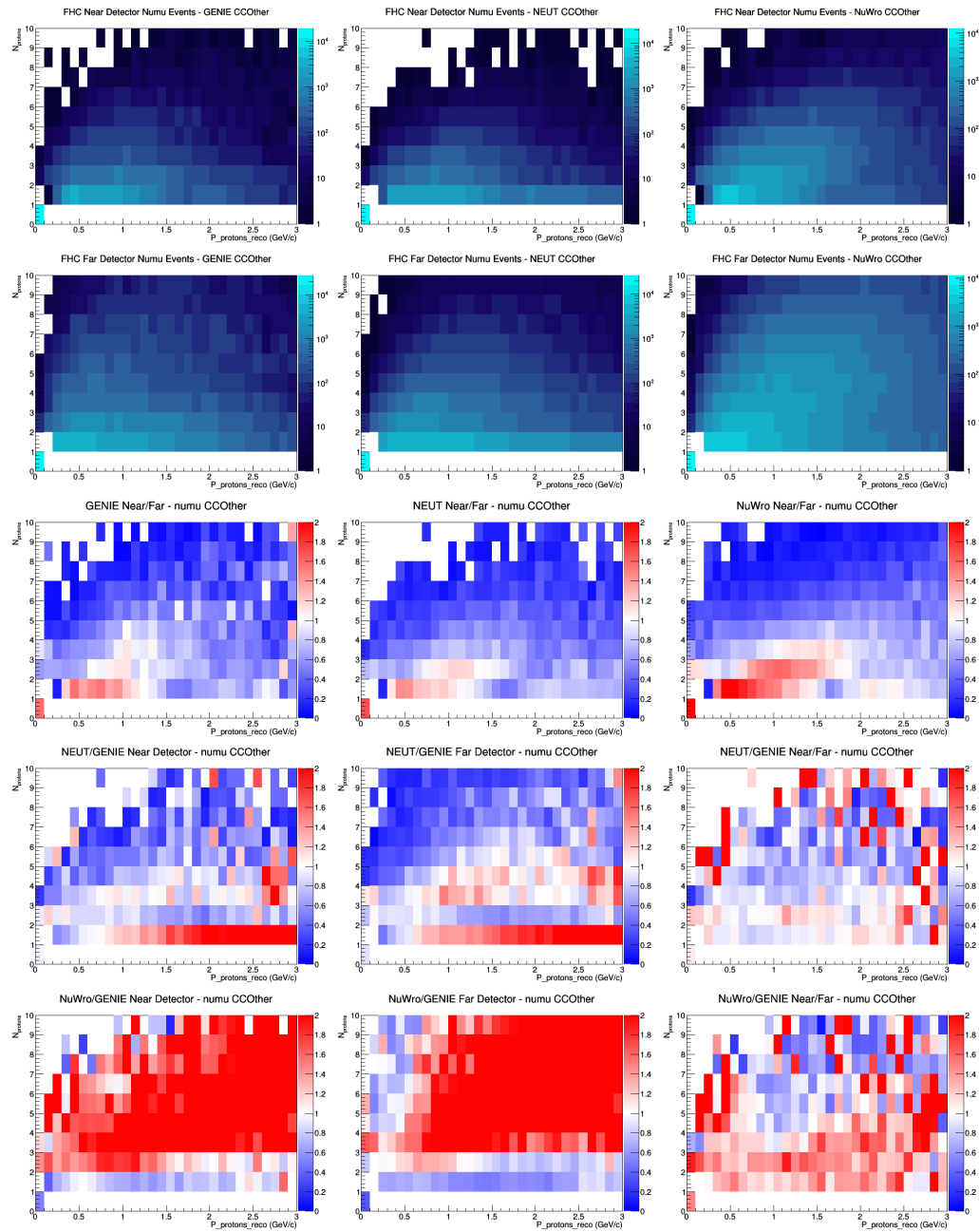
D.32 numubar CC1Pi GAr efficiencies



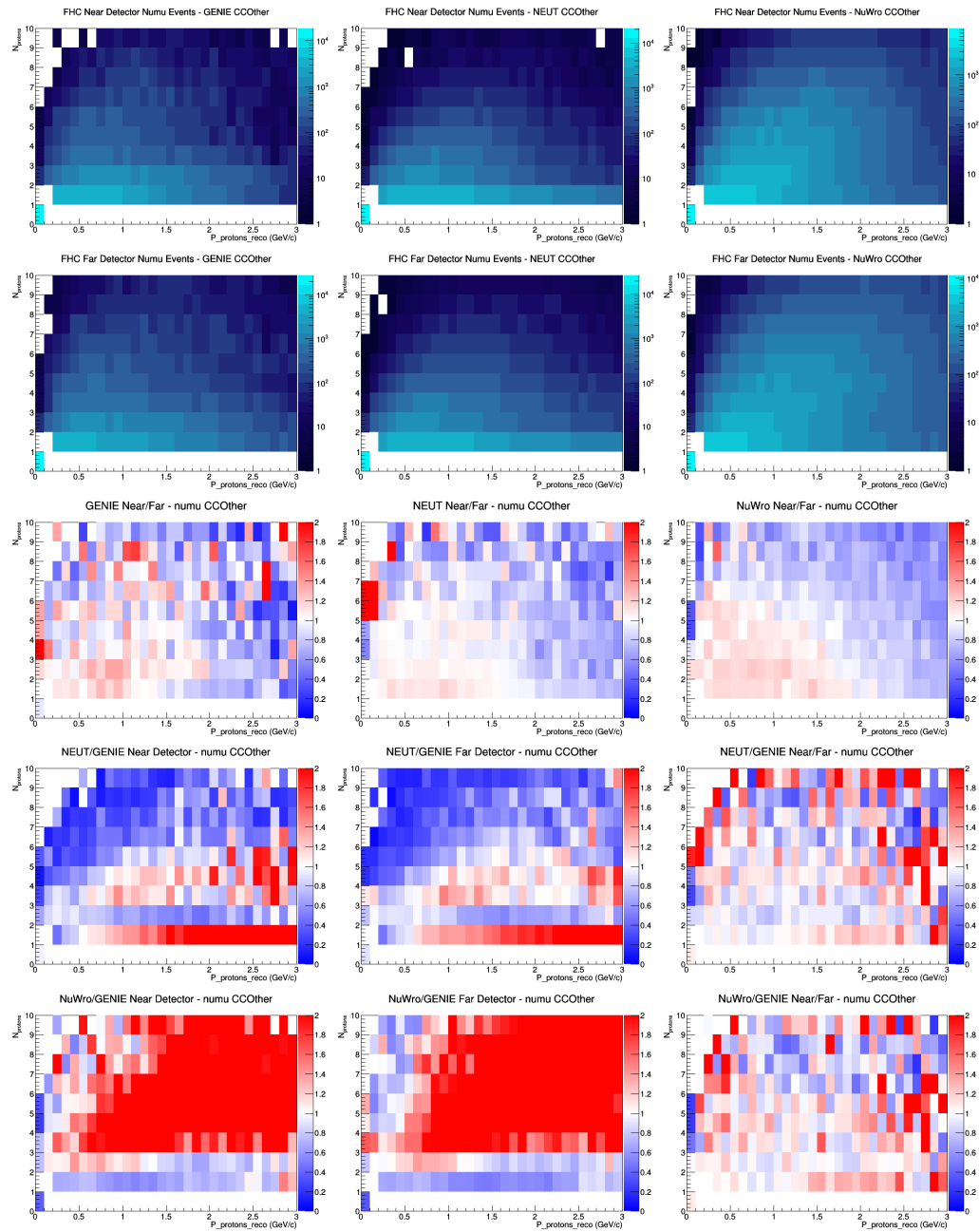
D.33 numu CCOther FGT efficiencies



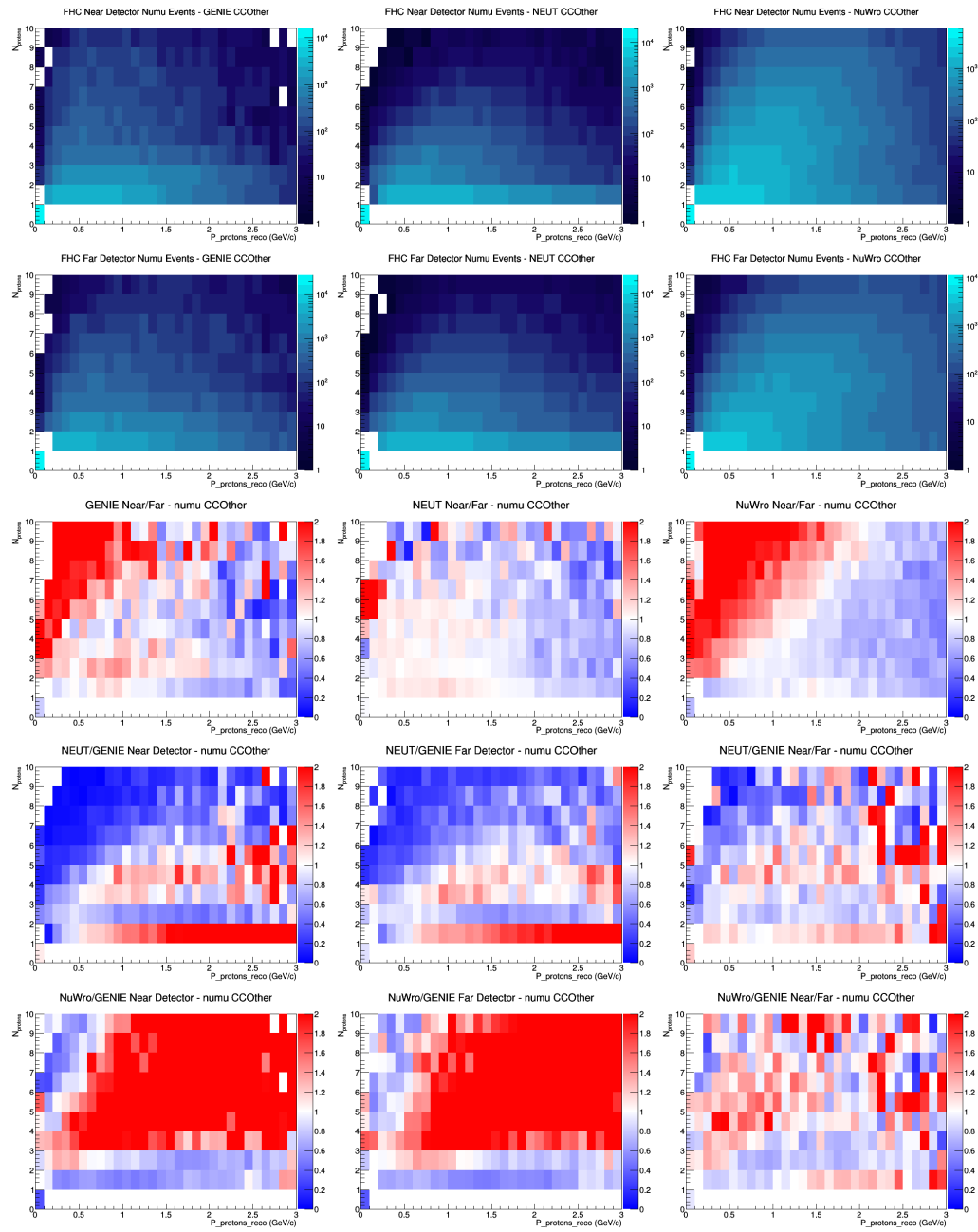
D.34 numu CCOther FGT efficiencies



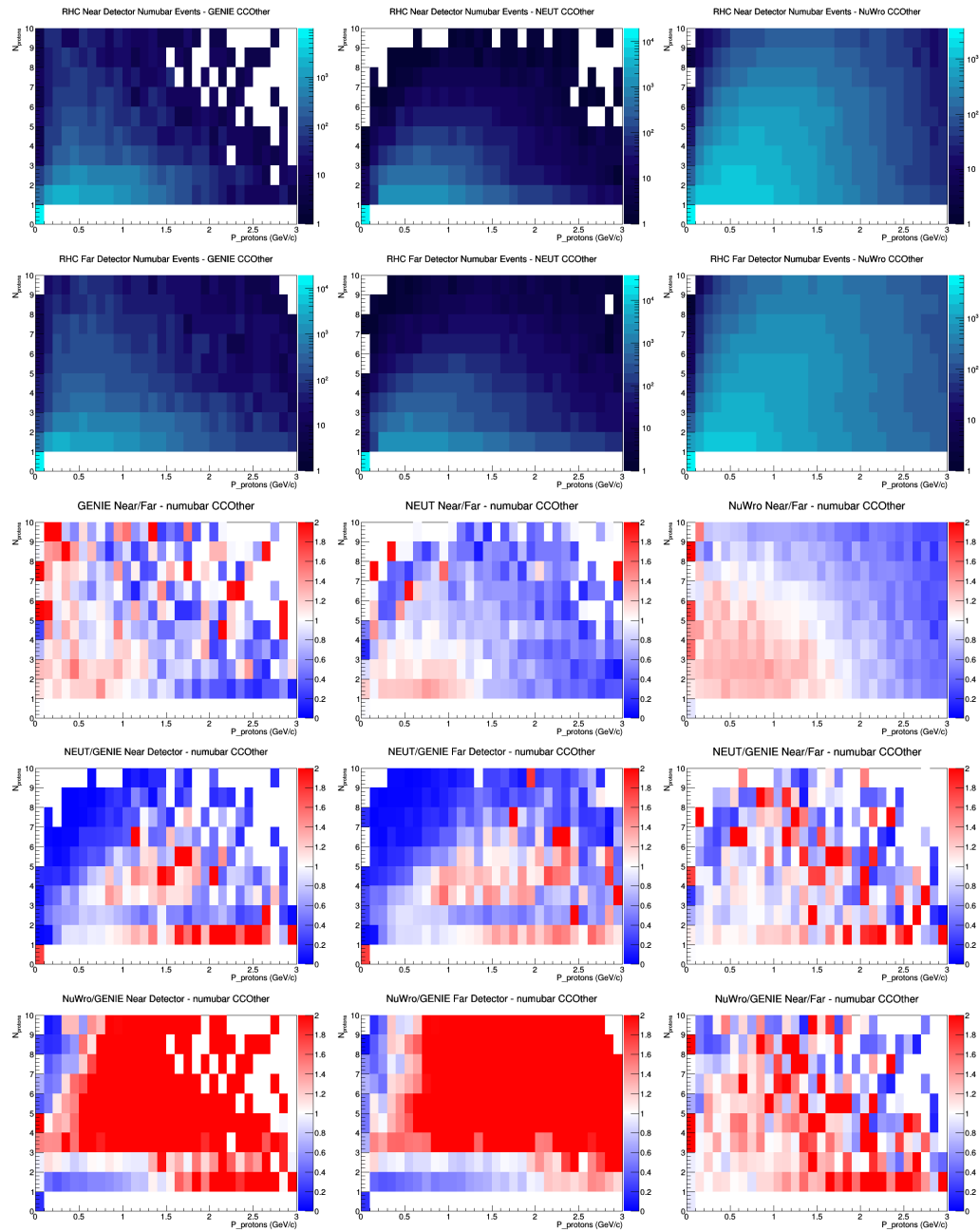
D.35 numu CCOther LAr efficiencies



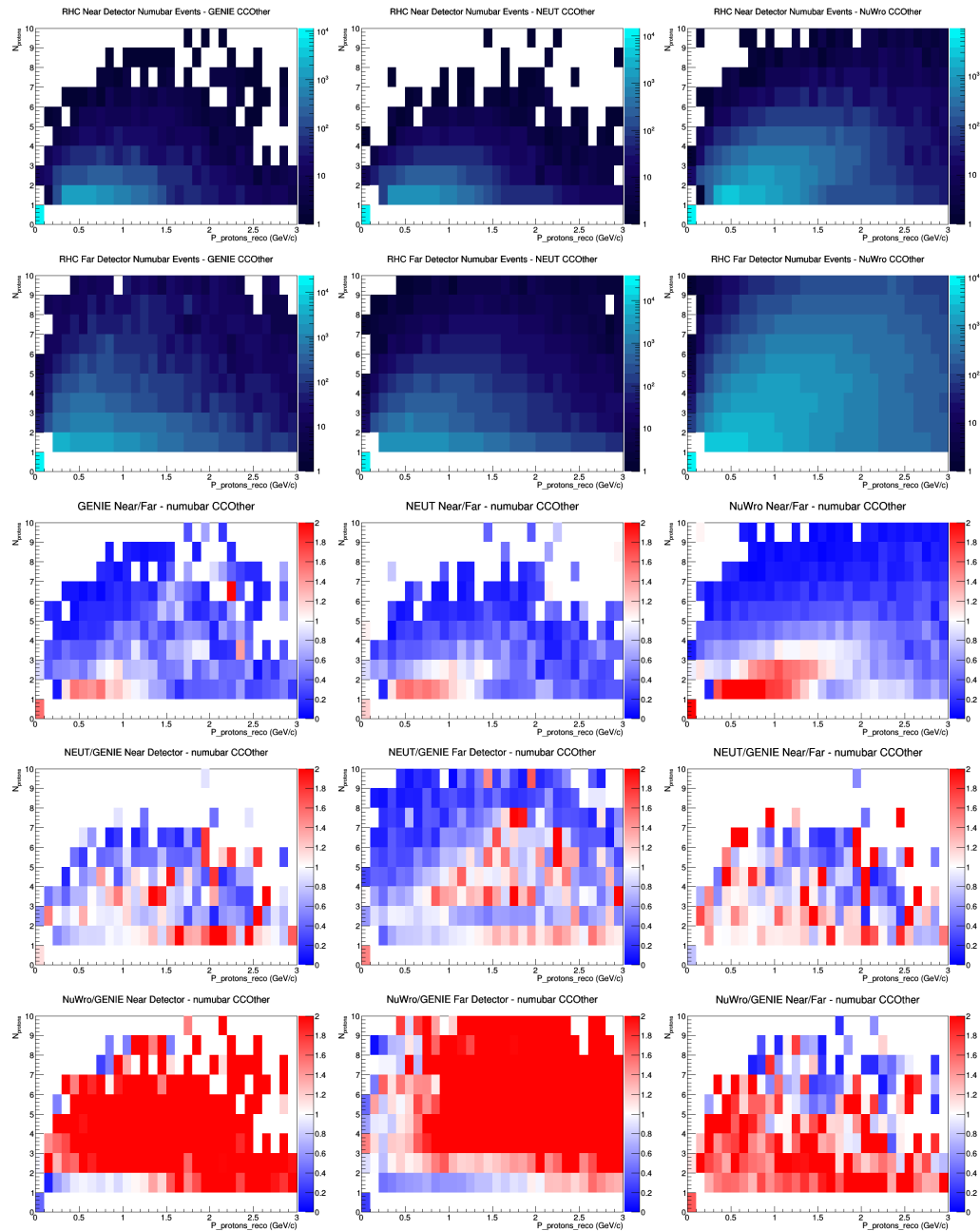
D.36 numu CCOther GAr efficiencies



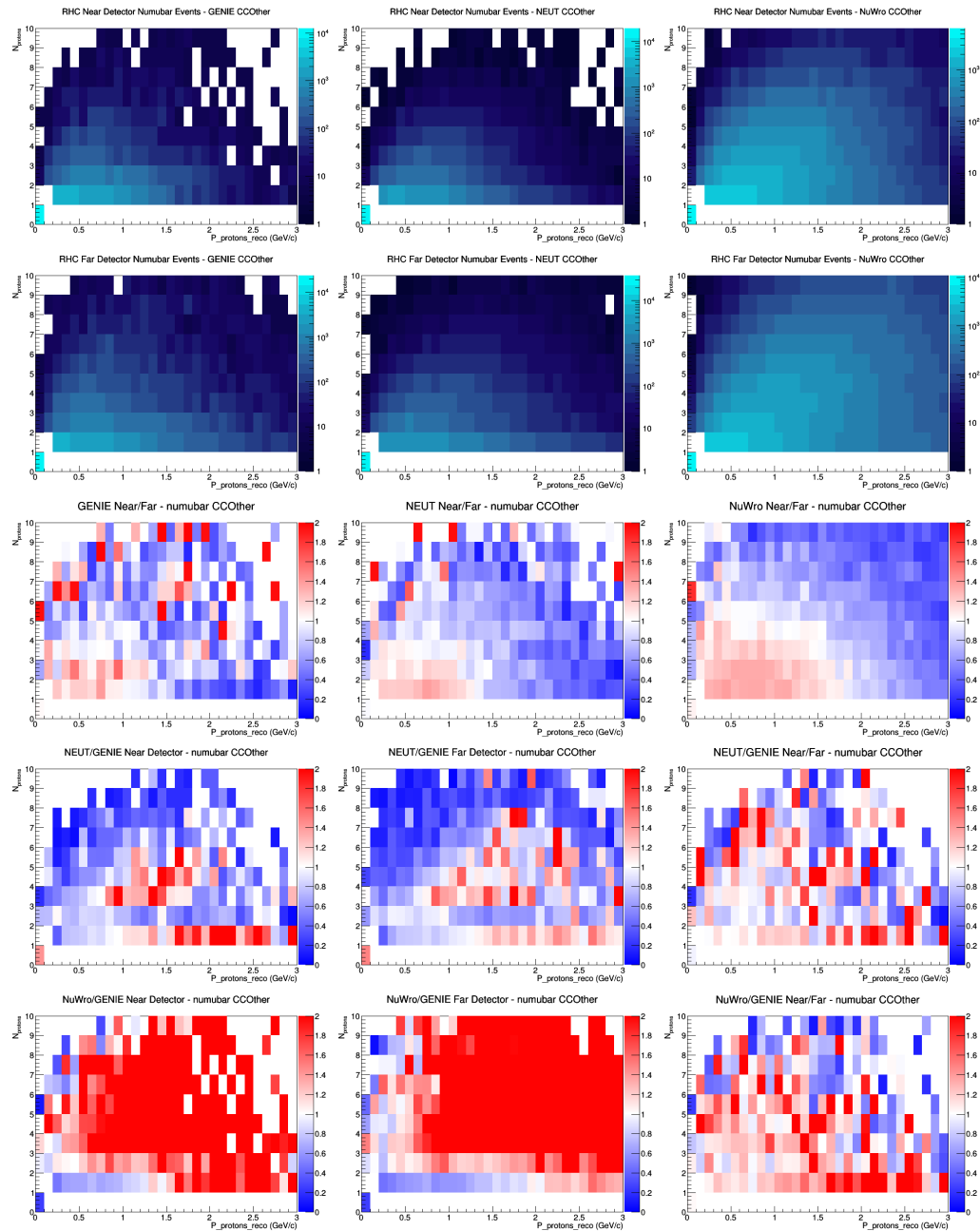
D.37 numubar CCOther no efficiencies



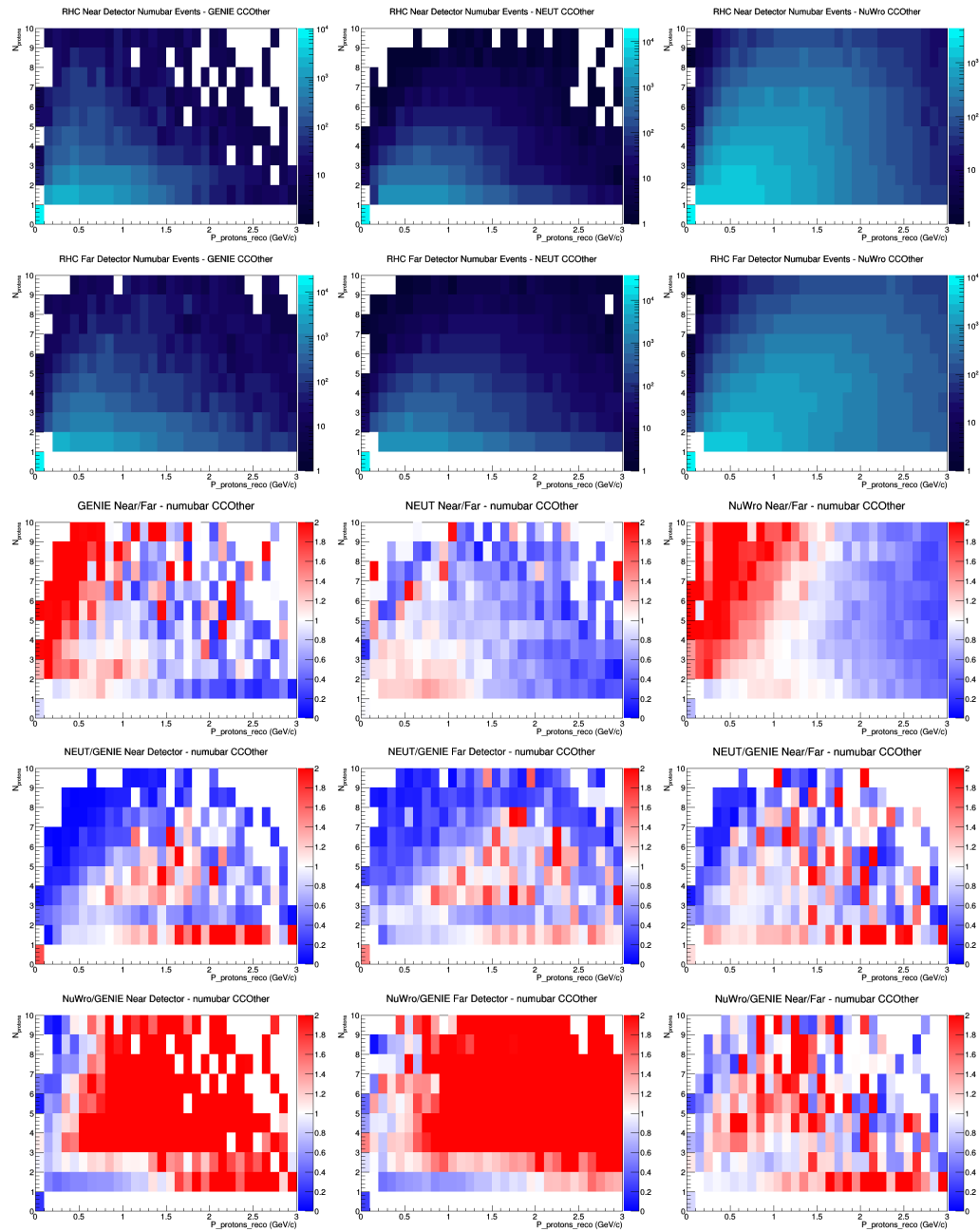
D.38 numubar CCOther FGT efficiencies



D.39 numubar CCOther LAr efficiencies



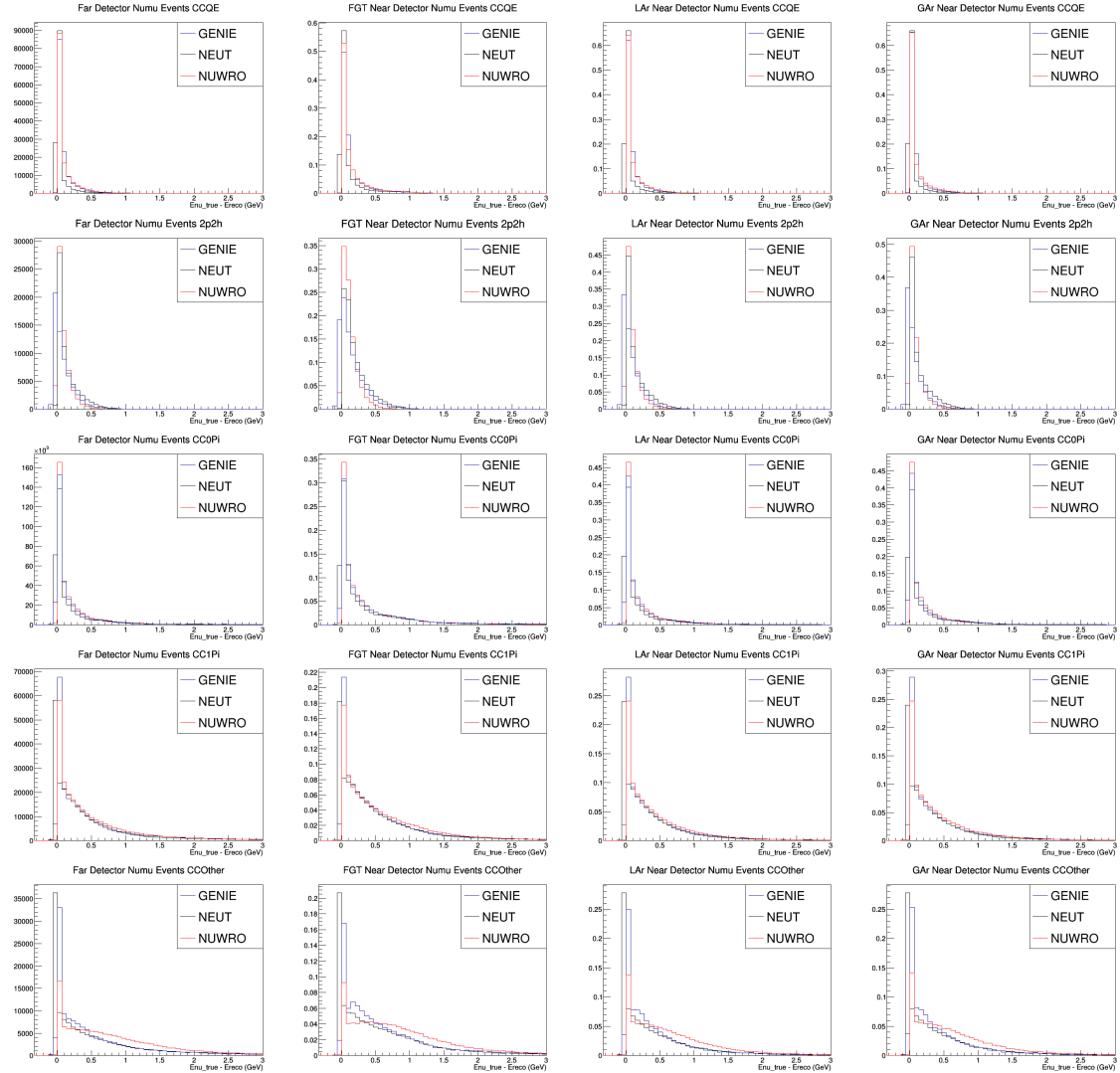
D.40 numubar CCOther GAr efficiencies



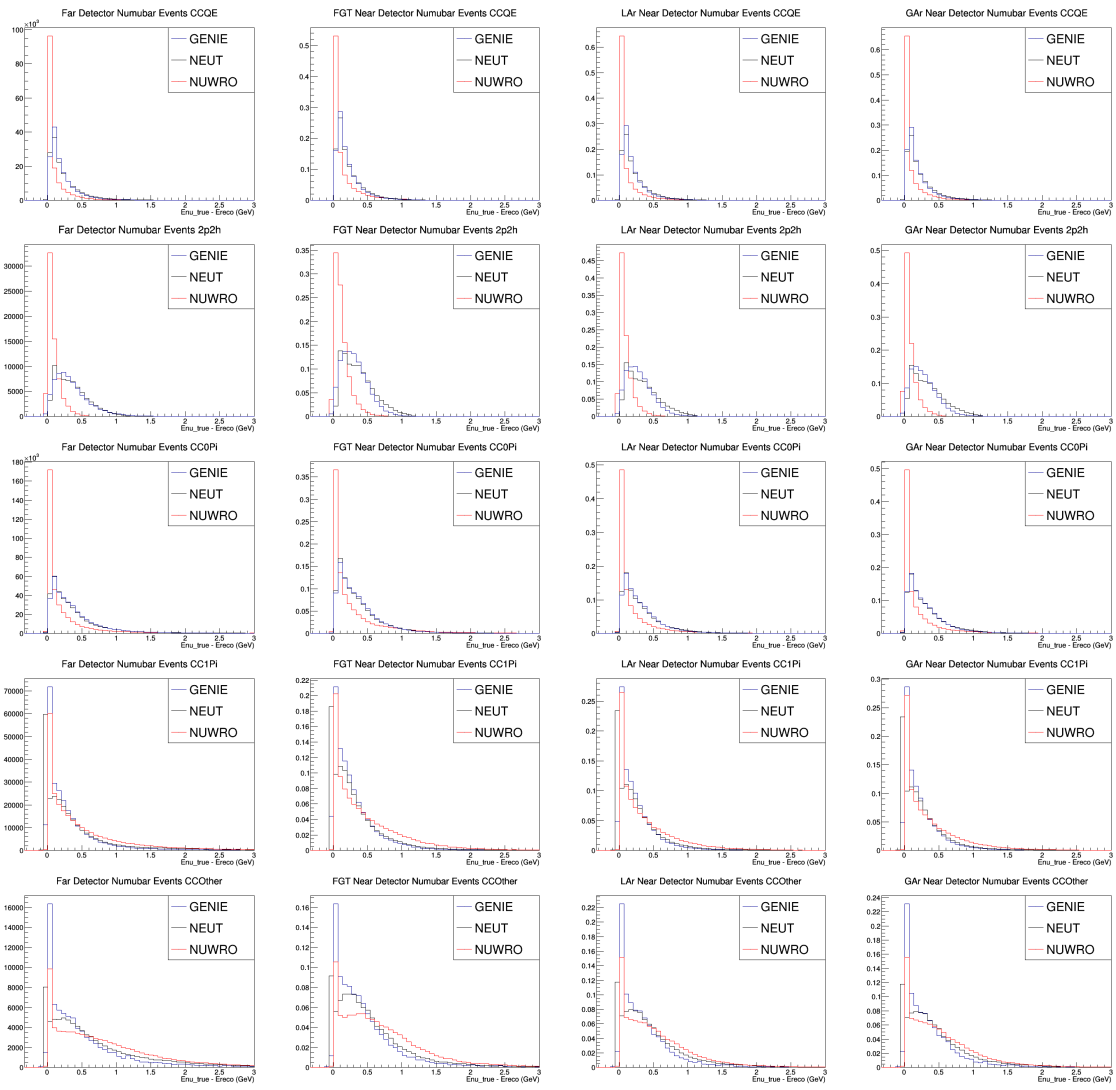
E Etrue - Ereco Plots

This appendix includes all the plots not show in Section 4.3. For full description of the files, please make reference to that section. The plots will be put in the same order as before.

E.1 numu



E.2 numubar



References

- [1] The DUNE Collaboration *Long-Baseline Neutrino Facility (LBNF) and Deep Underground Neutrino Experiment (DUNE) Conceptual Design Report Volume 1: The LBNF and DUNE Projects* arXiv:1601.05471v1
- [2] Maury Goodman *The Deep Underground Neutrino Experiment* Advances in High Energy Physics, vol. 2015, Article ID 256351, 9 pages, 2015. doi:10.1155/2015/256351
- [3] Andreopoulos, C. et al. *The GENIE Neutrino Monte Carlo Generator.* Nucl.Instrum.Meth. A614 (2010) 87-104 arXiv:0905.2517 [hep-ph] FERMILAB-PUB-09-418-CD
- [4] Hayato, Yoshinari *A neutrino interaction simulation program library NEUT.* Acta Phys.Polon. B40 (2009) 2477-2489
- [5] T. Golan, J.T. Sobczyk, J. Zmuda *NuWro: the Wroclaw Monte Carlo Generator of Neutrino Interactions.* Nuclear Physics B - Proceedings Supplements 229 (2012) 499
- [6] P. Stowell, C. Wret, C. Wilkinson, L. Pickering, S. Cartwright, Y. Hayato, K. Mahn, K.S. McFarland, J. Sobczyk, R. Terri, L. Thompson, M.O. Wascko, Y. Uchida *NUISANCE: a neutrino cross-section generator tuning and comparison framework* arXiv:1612:07393v2
- [7] Andreopoulos, et al. *VALOR DUNE Joint Oscillation and Systematics Constraint Fit*